Methanocaldococcus jannaschii and the Recycling of *S*-Adenosyl-L-methionine (SAM)

Danielle V. Miller

Dissertation submitted to the faculty of the Virginia Polytechnic Institute and State University in partial fulfillment of the requirements for the degree of

Doctor of Philosophy
In
Biochemistry

Robert H. White, Chair
Pablo Sobrado
Timothy J. Larson
David R. Bevan

March 16th, 2017
Blacksburg, VA

Keywords: *S*-adenosyl-L-methionine, SAM, recycling, 6-deoxy-5-ketofructose 1-phosphate, aromatic amino acids, methionine salvage, 5'-deoxyadenosine, *S*-adenosylhomoysteine, methylthioadenosine

Methanocaldococcus jannaschii and the recycling of *S*-Adenosyl-L-methionine (SAM)

Danielle V. Miller

ABSTRACT

S-Adenosyl-L-methionine (SAM) is an essential metabolite for all domains of life. SAM-dependent reactions result in three major metabolites: *S*-adenosyl-L-homocysteine (SAH), methylthioadenosine (MTA), and 5'-deoxyadenosine (5'-dA). Each of these has been demonstrated to be feedback inhibitors of SAM dependent enzymes. Thus, each metabolite has a pathway to prevent inhibition through the salvage of nucleoside and ribose moieties. However, these salvage pathways are not universally conserved. In the anaerobic archaeal organism *Methanocaldococcus jannaschii*, the salvage of SAH, MTA, and 5'-dA, proceeds first via deamination to *S*-inosylhomocysteine (SIH), methylthioinosine (MTI), and 5'-deoxyinosine (5'-dI). The annotated SAH hydrolase from *M. jannaschii* is specific for SIH and the hydrolyzed product homocysteine is then methylated to methionine. The salvage of MTA is known to proceed through the methionine salvage pathway, however, an anaerobic route for the salvage of MTA is still mostly unknown. Only two enzymes from the methionine salvage pathway are annotated in *M. jannaschii*'s proteome, a methylthioinosine phosphorylase (MTIP) and methylthioribose 1-phosphate isomerase (MTRI). These enzymes were shown to produce methylthioribulose 1-phosphate from MTI. Unfortunately, how MTI is converted to either 2-keto-(4-methylthio)butyrate or methionine remains unknown. The two enzymes involved in the salvage of MTI have also been demonstrated to be involved in the salvage of 5'-dI. Interestingly, there is little information on how 5'-dA or 5'-dI is recycled and it is proposed here to be the source of deoxysugars for the production methylglyoxal, a precursor for aromatic amino acids. MTIP and MTRI were demonstrated to produce 5-deoxyribulose 1-phosphate from 5'-dI. Additionally, two enzymes annotated as part of the pentose phosphate pathway, ribulose 5-phosphate 3-epimerase and transketolase, were able to convert 5-deoxyribulose 1-phosphate to lactaldehyde. Lactaldehyde was then reduced to methylglyoxal by an essential enzyme in methanogenesis, N^5, N^{10}-methylenetetahydromethanopterin reductase with NADPH. These results further demonstrate a novel route for the biosynthesis of methylglyoxal. Lastly, hypoxanthine produced from phosphorolysis of inosine, MTI, and 5'-dI was demonstrated to be reincorporated through the hypoxanthine/guanine phosphoribosyltransferase (Hpt) to IMP. Together these reactions represent novel pathways for the salvage of the SAM nucleoside and ribose moieties in *M. jannaschii*.

GENERAL AUDIENCE ABSTRACT

In the anaerobic methanogenic archaea *Methanocaldococcus jannaschii* traditional metabolic pathways are often missing or incomplete and are substituted by unique ones. *M. jannaschii* is deeply rooted on the phylogenetic tree and serves as a model organism for the study of primitive metabolism. Discussed here are the recycling pathways of the essential cofactor *S*-adenosyl-L-methionine (SAM). SAM recycling pathways in *Archaea* have not been investigated prior to this work. Two of the universal pathways responsible for recycling SAM to methionine were found to be modified and unique. A third pathway was proposed that would be responsible for generating an essential precursor for the biosynthesis of aromatic amino acids. The identification of the pathways and enzymes from *M. jannaschii* will give insight into the biochemical reactions that were occurring when life originated. Eight enzymes are discussed here that demonstrate how the recycling pathways in *M. jannaschii* are interconnected and the enzymes are shared between them. This work further describes the importance of understanding these unique microorganisms and the metabolic pathways they utilize to help understand primitive life.

Acknowledgments

I would like to thank Dr. Robert H. White for the time and effort he has put into the development of my scientific abilities. He has been instrumental in shaping the scientist I have become and will continue to be. He is always challenging the norm, which has opened my mind about the type of reactions that enzymes and nature are capable of performing. His passion and enthusiasm for science and research has left a lasting impression on me that I hope to pass on to my own students one day.

I would additionally like to thank my committee members, Dr. Bevan, Dr. Sobrado, and Dr. Larson for challenging me and always being supportive of my career objectives. I also want to thank everyone in the department of Biochemistry for all their help and support over the years.

Lastly, I would like to thank my friends and family for their support and encouragement these past five years of graduate school.

Table of Contents

Attributions

Abbreviations of authors:

DVM: Danielle V. Miller

HX: Huimin Xu

RHW: Robert H. White

WKR: W. Keith Ray

KH: Kim Harich

MR: Michelle Ruhlin

BJR: Benjamin J. Roach

JJP: John J. Perona

AMB: Anne M. Brown

DRB: David R. Bevan

Chapter 1: *S*-Inosylhomocysteine Hydrolase: A novel enzyme involved in SAM recycling

Danielle V. Miller, Huimin Xu, and Robert H. White

Miller, D., Xu, H., & White, R. H. (2015). S-Inosyl-L-Homocysteine Hydrolase, a Novel Enzyme Involved in S-Adenosyl-L-Methionine Recycling. *Journal of Bacteriology*, *197*(14), 2284–91. https://doi.org/10.1128/JB.00080-15

HX performed the cloning of *M. jannaschii* enzyme into *Escherichia coli* for recombinant overexpression. DVM performed all purification, biochemical experiments, and analysis of the recombinant protein's activity. The manuscript was written by DVM with edits and discussions about the analyzed data with RHW.

Chapter 2: Promiscuity of the Methionine Salvage Pathway Enzymes in *Methanocaldococcus jannaschii* and *Methanosarcina acetivorans*

Danielle V. Miller, Benjamin J. Rauch, Kim Harich, Huimin Xu, John J. Perona, and Robert H. White

HX performed the cloning of *M. jannaschii* enzymes into *Escherichia coli* for recombinant overexpression. DVM performed all purification, biochemical experiments, and analysis of the recombinant protein's activity. BJR performed all growth complementation experiments with the provided intermediates from DVM and RHW.

KH performed all the mass spectrometry and helped DVM interpret and analyze the results. The manuscript was written by DVM with edits and discussions about the analyzed data with RHW and JJP.

Chapter 3: Characterization of the ribulose 5-phosphate 3-epimerase and transketolase from *Methanocaldococcus jannaschii*

Danielle V. Miller, Kim Harich, Anne M. Brown, Huimin Xu, and Robert H. White.

HX cloned the *M. jannaschii* enzymes into *Escherichia coli* for recombinant overexpression. DVM performed all purification and analysis of the recombinant proteins. KH performed all mass spectrometry while DVM analyzed the data. DVM wrote the manuscript and RHW helped develop experimental design and edit the final manuscript. AMB made the molecular models and helped write/discuss the results of the molecular docking.

Chapter 4: Catalytic Promiscuity of N^5, N^{10}-methylenetetrahydromethanopterin reductase from *Methanocaldococcus jannaschii* as a methylglyoxal reductase

Danielle V. Miller, Michelle Ruhlin, W. Keith Ray, Huimin Xu, and Robert H. White

MR performed the biochemical assays to identify the fraction that contained the desired activity with help from DVM for method development and data interpretation. HX cloned the *M. jannaschii* enzyme into *Escherichia coli* for recombinant overexpression. DVM performed all purification and analysis of the recombinant protein. WKR performed all the mass spectrometry experiments and DVM analyzed the data. WKR also helped edit the manuscript written by DVM. RHW helped to edit the manuscript and discuss the results.

Chapter 5: Purine Salvage in *Methanocaldococcus jannaschii*: Elucidating the Role of a Conserved Cysteine in Adenine Deaminase

Danielle V. Miller, Anne M. Brown, Huimin Xu, David R. Bevan, and Robert H. White

Miller, D. V., Brown, A. M., Xu, H., Bevan, D. R., & White, R. H. (2016). Purine salvage in *Methanocaldococcus jannaschii*: Elucidating the role of a conserved cysteine

in adenine deaminase. *Proteins: Structure, Function and Bioinformatics*, *84*(6), 828–840. https://doi.org/10.1002/prot.25033

HX performed the cloning of *M. jannaschii* enzymes into *Escherichia coli* for recombinant overexpression. DVM performed all purification, biochemical experiments, and analysis of the recombinant protein's activity. Molecular dynamic analysis was performed by AMB. Analysis of molecular modeling, docking, and dynamic data was performed by AMB and DVM. DRB, AMB, and RHW helped editing the manuscript written by DVM.

Introduction

Charles Darwin, the forerunner in the search for the origin of species, observed "each species had not been independently created, but had descended, like varieties, from other species".(1) His seminal work established evolution as the method through which modern life has evolved. Through the advent of sequencing technology, we have been able to identify our ancestor and have been able to trace our origins through 16S ribosomal RNA (2) to an unknown organism denoted as the last universal common ancestor or LUCA.(3) Furthermore, all life has been classified as belonging to three domains(4), however, as science continues to progress the tree of life is still evolving.(5) Even with this a new version of the tree of life we know little about the biochemistry that started it all.

In order to address these questions, it is essential to think about the environment on Earth in which life originated. It is widely accepted by the scientific community that Earth started to form 4.568 billion years ago (6), was rich in carbon dioxide (7) and hot.(8) This primordial environment also contained Fe(II), hydrogen (H_2), and hydrogen sulfide (H_2S), which made it anaerobic. Carbon isotopic analysis of sedimentary rocks predicted that LUCA thrived 3.8 billion years ago.(9, 10) The first forms of respiration, occurred approximately 1 billion years after LUCA first emerged at the end of the Archaean era. Methanogenesis and methanotrophy, were predicted and dated based on microfossils found at ancient hydrothermal vents and ^{13}C isotope depletion in ancient rocks.(10, 11) Methanogenesis is a form of respiration that involves the reduction of carbon dioxide to methane (Figure 1) and still exists today in anaerobic environments, such as hydrothermal vents.

Today, hydrothermal vent systems are rich in CH_4, CO_2, H_2S, and nitrous oxide that are dissolved in the vent fluid and expelled at temperatures up to 380 ^oC and are rapidly cooled in the surrounding water.(12) Additionally, black smoker hydrothermal vents have been shown to be rich in Fe(II), Mn(II), and have dissolved H_2, CO_2, and H_2S in the area surrounding these vents.(11) These compounds are all essential for methanogenesis. One such organism that was isolated in 1982 from a white smoker hydrothermal vent found on the East Pacific Rise in the Pacific Ocean off the coast of California 2,600 m under the ocean's surface was *Methanocaldococcus jannaschii*.(12) *M. jannaschii* was the first archaeal organism to have its genome sequenced (1996) and has served as a model organism for studying Archaeal

metabolism. *M. jannaschii* is an exemplary tool for study for several important reasons: 1) It is autotrophic with a small genome of 1.66-megabase pair which encodes about 1800 proteins.(13) 2) *M. jannaschii* is an anaerobic hyperthermophile. 3) *M. jannaschii* uses methanogenesis for respiration. These traits demonstrate that *M. jannaschii* thrives in a niche environment that is reminiscent of early Earth, making *M. jannaschii* an important tool for the study of primitive metabolism.

Additionally, *M. jannaschii* only incorporates CO_2, H_2, H_2S, PO_4^{-3}, nitrogen, and minerals from the environment, demonstrating that *M. jannaschii*'s de novo synthesizes every metabolite from scratch. This would indicate that recycling pathways in *M. jannaschii* are important for energy conservation and survival. One metabolite that is critical to metabolism is *S*-adenosyl-L-methionine (SAM), which is used only secondarily to ATP as either a cofactor or co-substrate (Figure 2).(14) SAM is a universally used cofactor that is biosynthesized from methionine and ATP by an enzyme known as a SAM synthetase (Figure 2).(15) Some of the reactions using SAM include: methylation of DNA through transfer of the methyl group to a nucleophilic substrate (Figure 2, red), decarboxylation and transfer of the amino propyl group (Figure 2, green) for polyamine biosynthesis, and the generation of radicals through the reductive cleavage of SAM to methionine and 5'-deoxyadenosine (Figure 2, blue).(16)

Utilization of SAM for the generation of radicals for many specialized reactions is done by formation of a radical through reductive cleavage of SAM to form methionine and a 5'-deoxyadenosyl radical (5'-dA·) (Figure 3).(17) The enzymes involved in the reductive cleavage of SAM are known as radical SAM enzymes and require a [4Fe-4S] cluster that uniquely binds to the carboxyl and amino moieties of SAM to transfer an electron for the reductive cleavage of SAM and producing the 5'-dA·(Figure 3).(17) These enzymes can readily be identified by a conserved CX_3CX_2C motif in their amino acid sequence.(18) Utilizing the occurrence of this motif in protein sequences from *M. jannaschii*, we performed bioinformatic searches to determine the abundance of radical SAM enzymes present in *M. jannaschii*'s proteome as 1.5% (Table 1). This result was both unexpected and intriguing. When compared to abundances in *Escherichia coli* (0.5%) or anaerobic bacteria, such as *Clostridium difficile* (0.82%), methanogens contained the highest percentage of proteins with the radical SAM motif (Table 1, boxed). Of the radical SAM enzymes that were identified in this search, only nine of the 28 have a known or predicted function.

The discovery of *M. jannaschii*'s proteome encoding for 28 radical SAM enzymes makes it important to discern how *M. jannaschii* is able to recycle the SAM- derived products of these enzymatic reactions: 5'-deoxyadenosine (5'-dA), methylthioadenosine (MTA), and *S*-adenosyl-L-homocysteine (SAH) (Figure 2). Each of these metabolites are well known to be feedback inhibitors of SAM-dependent enzymes(19) and as such enzymes and pathways need to be present for the salvage of these metabolites.(20, 21) Typically, a MTA/SAH nucleosidase (MtnN) is the enzyme responsible for removing adenine from 5'-dA, MTA, and SAH to render them inactive as inhibitors of the essential SAM dependent enzymes.(19, 20, 22) The MtnN is not the only enzyme proposed to be responsible for the removal of SAM derived enzymatic products; SAH hydrolase is the other main enzyme responsible for maintaining the low concentration of SAM derived enzymatic products. However, unlike MtnN, which will work with all three SAM dependent enzyme products, the hydrolase only uses SAH and is limited to *Archaea* and *Eukyara*.(23) These two enzymes belong to pathways that are responsible for the salvage of methionine from SAH and MTA (Figure 4).

SAM dependent enzymes that produce these SAM-derived metabolites are expected to occur in *M. jannaschii*. Due to the expected feedback inhibition of the SAM dependent enzymes by 5'-dA, MTA, and SAH(19, 20), it is proposed that enzymes and associated pathways are present in *M. jannaschii* will recycle them. A homolog of MtnN has not been identified in the *M. jannaschii* proteome, so another enzyme must be present to prevent inhibition of SAM dependent enzymes. Recently, I identified a deaminase encoded by MJ1541, which I named a 5'-dA deaminase (DadD) and proposed it to be responsible for preventing the inhibition of SAM dependent enzymes. It was shown to be highly specific for 5'-dA over MTA, SAH, and adenosine, Table 2.(24) The deamination products, 5'-deoxyinosine (5'-dI), methylthioinosine (MTI), and S-inosylhomocysteine (SIH) (Figure 5) are expected to be integrated back into *M. jannaschii*'s metabolism in a manner that has yet to be established and is the focus of this dissertation, Figure 2. Furthermore, DadD was determined to deaminate adenosine to inosine (Table 2)(24), which catalyzes another important reaction for the salvage of purines.

S-Adenosyl-L-homocysteine (SAH) is produced from SAM dependent methyltransfereases (Figure 2). SAH is known to be salvaged by either cleavage of the glyosidic bond by a nucleosidase or by its hydrolysis to homocysteine and adenosine (Figure 4A).(20) In the former case, the resulting product, *S*-ribosyl-homocysteine, is used in the production of

autoinducer 2, which is a signaling molecule in plants.(25) However, due to the lack of a homologue of the nucleosidase in *M. jannaschii*, this pathway is unlikely. Instead, *M. jannaschii* contains a homologue of the SAH hydrolase encoded by MJ1388. However, I have established that *M. jannaschii* first deaminates SAH to SIH (Figure 5). Thus, the annotated SAH hydrolase is proposed to use SIH instead.(26) The resulting homocysteine product following hydrolysis of SIH is then re-methylated to methionine and the inosine can be re-incorporated into purine metabolism.(26)

An additional methionine salvage pathway starts with the methylthioribose moiety of MTA, Figure 4B.(27, 28) Of the seven to eight enzymes involved in this pathway, only two are annotated in the *M. jannaschii* proteome: methylthioadenosine phosphorylase (MtnP) and methylthioribose isomerase (MtnA). Additionally, the canonical methionine salvage pathway requires molecular oxygen to form 2-keto-(4-methylthio)butyrate (KMTB), a precursor to methionine. The methionine salvage pathway is likely not occurring in the same manner in anaerobic organisms, even though some of the enzymes for the methionine salvage pathway are found in anaerobic organisms.(27) Instead of cleavage of the MTA by a nucleosidase, it was first demonstrated that DadD deaminates MTA to MTI, representing a novel first step in the anaerobic methionine salvage pathway (Figure 5).(24) MTI is proposed to then undergo phosphorolysis and the product isomerized to methylthioribulose 1-phosphate (MTRu 1P) by the only two annotated methionine salvage pathway enzymes in *M. jannaschii*: methylthioinosine phosphorylase (MtnP or MTIP) encoded by MJ0060 and methylthioribose 1-phosphate isomerase (MtnA or MTRI) encoded by MJ0454. However, the remaining enzymes and intermediates responsible for the conversion of methylthioribulose 1-phosphate (MTRu 1P) to methionine remain unknown (Figure 4B).

Lastly, there is little information in the literature on how 5'-dA is recycled in any organism. With nearly 1.5% of *M. jannaschii*'s proteome being radical SAM enzymes, there is going to be significant amount of 5'-dA produced. It is hypothesized that 5'-dA enters the nucleotide pool. However, 5'-dA could also provide *M. jannaschii* with the necessary deoxysugar for an alternative source of the necessary C5 and C6 carbohydrates that are needed for other essential metabolic processes. In recent years, our laboratory has shown that erythrose 4-phosphate is not produced in *M. jannaschii* indicating the canonical pathway for production of 3-dehydroquinate (DHQ) (Figure 6A) is not occurring. Instead our laboratory has demonstrated

that the precursors for DHQ in *M. jannaschii* are L-aspartate semialdehyde and 6-deoxy-5-ketofructose 1-phosphate (DKFP) (Figure 6B).(29) The enzymes that are involved in this series of chemical conversions have been identified to be 2-amino-3,7-dideoxy-D-threo-hept-6-ulosonate synthase (encoded by MJ0400) and 3-dehydroquinate synthase (encoded by MJ1249) (Figure 6B).(29)

The biosynthesis of DKFP remains a mystery, with only one intermediate in this biosynthetic pathway having been confirmed, methylglyoxal. Methyglyoxal was shown to condense with a dihydroxyacetone-phosphate fragment that comes from fructose 1,6-bisphosphate via the enzyme encoded by MJ1585 (Figure 6B).(30) The MJ1585 gene is bifunctional and encodes fructose-bisphosphate aldolase and 6-deoxyketofructose 1-phosphate synthase that are necessary to produce DKFP and glyceraldehyde 3-phosphate from fructose 1,6-bisphosphate and methylglyoxal.(30) Interestingly, there are several enzymes that are annotated to be functioning as part of the non-oxidative half of the pentose phosphate pathway, the ribulose 5-phosphate 3-epimerase (RPE) encoded by MJ0680 and transketolase (TK) encoded by MJ0679 and MJ0681 (Figure 6A). I propose that these enzymes are instead apart of a novel pathway for the conversion of 5'-dA to methylglyoxal.

The overall goal of this work is to determine how SAM is recycled in *M. jannaschii*. In all recycling pathways the three major metabolites, 5'-dA, MTA, and SAH are first deaminated by DadD to 5'-dI, MTI, and SIH. In the following pages of this dissertation I will present data on how each of these metabolites are recycled in *M. jannaschii*. SIH and MTI are proposed to be salvaged into SAM through individual pathways that represent novel modifications on the established canonical SAM salvage pathways. Additionally, I will present data for a new pathway for the recycling of 5'-dA in *M. jannaschii* to serve as the source of deoxysugars for aromatic amino acid biosynthesis.

References

1. **Darwin C**. 1972. On the origins of species by means of natural selection (1859). Murray, London.
2. **Lane DJ**, **Pace B**, **Olsen GJ**, **Stahl DA**, **Sogin ML**, **Pace NR**. 1985. Rapid determination of 16S ribosomal RNA sequences for phylogenetic analyses. Proc Natl Acad Sci **82**:6955–6959.
3. **Woese C**. 1998. The universal ancestor. Proc Natl Acad Sci **95**:6854–6859.
4. **Woese CR**, **Kandler O**, **Wheelis ML**. 1990. Towards a natural system of organisms: proposal for the domains Archaea, Bacteria, and Eucarya. Proc Natl Acad Sci **87**:4576–4579.
5. **Hug LA**, **Baker BJ**, **Anantharaman K**, **Brown CT**, **Probst AJ**, **Castelle CJ**, **Butterfield CN**, **Hernsdorf AW**, **Amano Y**, **Ise K**. 2016. A new view of the tree of life. Nat Microbiol **1**:16048.
6. **Bouvier A**, **Blichert-Toft J**, **Moynier F**, **Vervoort JD**, **Albarède F**. 2007. Pb–Pb dating constraints on the accretion and cooling history of chondrites. Geochim Cosmochim Acta **71**:1583–1604.
7. **Walker JCG**. 1985. Carbon dioxide on the early Earth. Orig Life Evol Biosph **16**:117–127.
8. **Chyba CF**. 1993. The violent environment of the origin of life: Progress and uncertainties. Geochim Cosmochim Acta **57**:3351–3358.
9. **Rosing MT**. 1999. 13C-depleted carbon microparticles in> 3700-Ma sea-floor sedimentary rocks from West Greenland. Science (80-) **283**:674–676.
10. **Brocks JJ**, **Buick R**, **Summons RE**, **Logan GA**. 2003. A reconstruction of Archaean biological diveristy based on molecular fossils from the 2.78 to 2.45 billion-year-old Mount Bruce Supergroup, Hamersley Basin, Western Australia. Geochim Cosmochim Acta **67**:4321–4335.
11. **Martin W**, **Baroos J**, **Kelley D**, **Russell MJ**. 2008. Hydrothermal vents and the origin of life. Nat Rev Microbiol **6**:805–814.
12. **Jones WJ**, **Leigh JA**, **Mayer F**, **Woese CR**, **Wolfe RS**. 1983. Methanococcus jannaschii sp. nov., an extrememely thermophilic methanogen from a submarine hydrothermal vent.

Arch Microbiol **136**:254–261.

13. **Bult CJ**, **White O**, **Olsen GJ**, **Zhou L**, **Fleischmann RD**, **Sutton GG**, **Blake JA**, **Fitzgerald LM**, **Clayton RA**, **Gocayne JD**, **Kerlavage AR**, **Dougherty BA**, **Tomb J**, **Adams D**, **Reich C**, **Overbeek R**, **Kirkness EF**, **Weinstock KG**, **Merrick JM**, **Glodek A**, **Scott JL**, **Geoghagen NSM**, **Weidman JF**, **Fuhrmann JL**, **Nguyen D**, **Utterback TR**, **Kelley JM**, **Peterson JD**, **Sadow PW**, **Hanna MC**, **Cotton MD**, **Roberts KM**, **Hurst MA**, **Kaine BP**, **Borodovsky M**, **Klenk H**, **Fraser CM**, **Smith H**, **Woese CR**, **Venter JC**, **Gene MJ**. 1996. Complete Genome Sequence of the Methanogenic Arc haeon , Me thanococcus jannaschii nome sequence for a representative of the The Genome of Methanococcus jannaschii. Science (80-) **273**:1058–1073.
14. **Cantoni GL**. 1975. Biological methylation: selected aspects. Annu Rev Biochem **44**:435–451.
15. **Graham DE**, **Bock CL**, **Schalk-Hihi C**, **Lu ZJ**, **Markham GD**, **Markam GD**. 1999. Identification of a Highly Diverged Class of S-Adenosylmethionine Synthetases in the Archaea. J Biol Chem **275**:4055–4059.
16. **Fontecave M**, **Atta M**, **Mulliez E**. 2004. S-adenosylmethionine: Nothing goes to waste. Trends Biochem Sci **29**:243–249.
17. **Booker SJ**, **Grove TL**. 2010. Mechanistic and functional versatility of radical SAM enzymes. F1000 Biol Rep **2 (52)**.
18. **Sofia HJ**, **Chen G**, **Hetzler BG**, **Reyes-Spindola JF**, **Miller NE**. 2001. Radical SAM, a novel protein superfamily linking unresolved steps in familiar biosynthetic pathways with radical mechanis: functional characterization using new analysis and information visualization methods. Nucleic Acids Res **29**:1097–1106.
19. **Challand MR**, **Ziegert T**, **Douglas P**, **Douglas P**, **Wood RJ**, **Kriek M**, **Shaw NM**, **Roach PL**. 2009. Product inhibition in the radical S-adenosylmethionine family. FEBS Lett **583**:1358–1362.
20. **Parveen N**, **Cornell KA**. 2011. Methylthioadenosine/S-adenosylhomocysteine nucleosidase, a critical enzyme for bacterial metabolism. Mol Microbiol **79**:7–20.
21. **Albers E**. 2009. Metabolic Characteristics and Importance of the Universal Methionine Salvage Pathway Recycling Methionine from 5'-Methylthioadenosine. IUBMB Life2009/12/01. **61**:1132–1142.

22. **Hiscox MJ**, **Driesener RC**, **Roach PL**. 2012. Enzyme catalyzed formation of redicals from S-adenosylmethionin and inhibition of enzyme activity by the cleavage products. Biochem Biophys Acta **1824**:1165–1177.
23. **Knudsen RC**, **Yall I**. 1972. Partial Purification and Characterization of S-Adenosylhomocysteine Hydrolase Isolated from Saccharomyces cerevisiae. J Bacteriol **112**:569–575.
24. **Miller D**, **O'Brien K**, **Xu H**, **White RH**. 2014. Identification of a 5′-Deoxyadenosine Deaminase in Methanocaldococcus jannaschii and its Possible Role in Recycling the Radical SAM Enzyme Reaction Product 5′-Deoxyadenosine. J Bacteriol **196**:1064–1072.
25. **Sun J**, **Daniel R**, **Wagner-Dobler I**, **Zeng A-P**. 2004. Is autoinducer-2 a universal signal for interspecies communication: a comparative genomic and phylogentic analysis of the synthesis and signal transduction pathways. BMC Evol Biol **4**:36.
26. **Miller D V**, **Xu H**, **White RH**. 2015. S-Inosylhomocysteine Hydrolase: A novel enzyme involved in SAM recycling. J Bacteriol **197**:1-8 JB – 00080.
27. **Sekowska A**, **Dénervaud V**, **Ashida H**, **Michoud K**, **Haas D**, **Yokota A**, **Danchin A**. 2004. Bacterial variations on the methionine salvage pathway. BMC Microbiol2004/04/23. **4**:9.
28. **Furfine ES**, **Abeles RH**. 1988. Intermediates in the Conversion of 5'-S-Methylthioadenosine to Methionine in Klebsiella pneumoniae. J Biol Chem **263**:1988–9598.
29. **White RH**. 2004. L-aspartate semialdehyde and a 6-deoxy-5-ketohexose 1-phosphate are the precursors to the aromatic amino acids in Methanocaldococcus jannaschii. Biochemistry **43**:7618–7627.
30. **White RH**, **Xu H**. 2006. Methylglyoxal is an intermediate in the biosynthesis of 6-deoxy-5-ketofructose-1-phosphate: A precursor for aromatic amino acid biosynthesis in Methanocaldococcus jannaschii. Biochemistry **45**:12366–12379.

Tables

Table 1. Percentage of proteins containing the radical SAM motif per proteome in different microorganisms

Organism	Percent of encoded proteins with radical SAM motif (CX_3CX_2C)
Methanocaldococcus jannaschii	1.5%
Methanocaldococcus fervens	1.5%
Methanococcus maripaludis S2	1.3%
Methanosarcina acetivorans C2A	1.0%
Methanothermobacter thermautotrophicus ΔH	1.2%
Anaerobic Methanotrophic Archaea-1	1.4%
Clostridium difficile st. 630	0.82%
Bacteroides fragilis YCH46	0.73%
Methylobacterium extorquens AM1	0.41%
Escherichia coli K12	0.44%
Saccharomyces cerevisiae (Baker's yeast)	0.05%

Table 2. Kinetic parameters of DadD with 5'-dA, MTA, SAH, and Ad

Substrate	K_M (mM)	k_{cat} (s^{-1})	k_{cat}/K_M ($M^{-1}s^{-1}$)
5'-dA	0.014 ± 0.0012	1.2×10^5	9.1×10^9
MTA	0.11 ± 0.028	1.6×10^2	1.1×10^6
SAH	1.1 ± 1.3	1.3×10^3	4.4×10^6
Ad	0.15 ± 0.0047	1.1×10^2	7.5×10^5

Figures

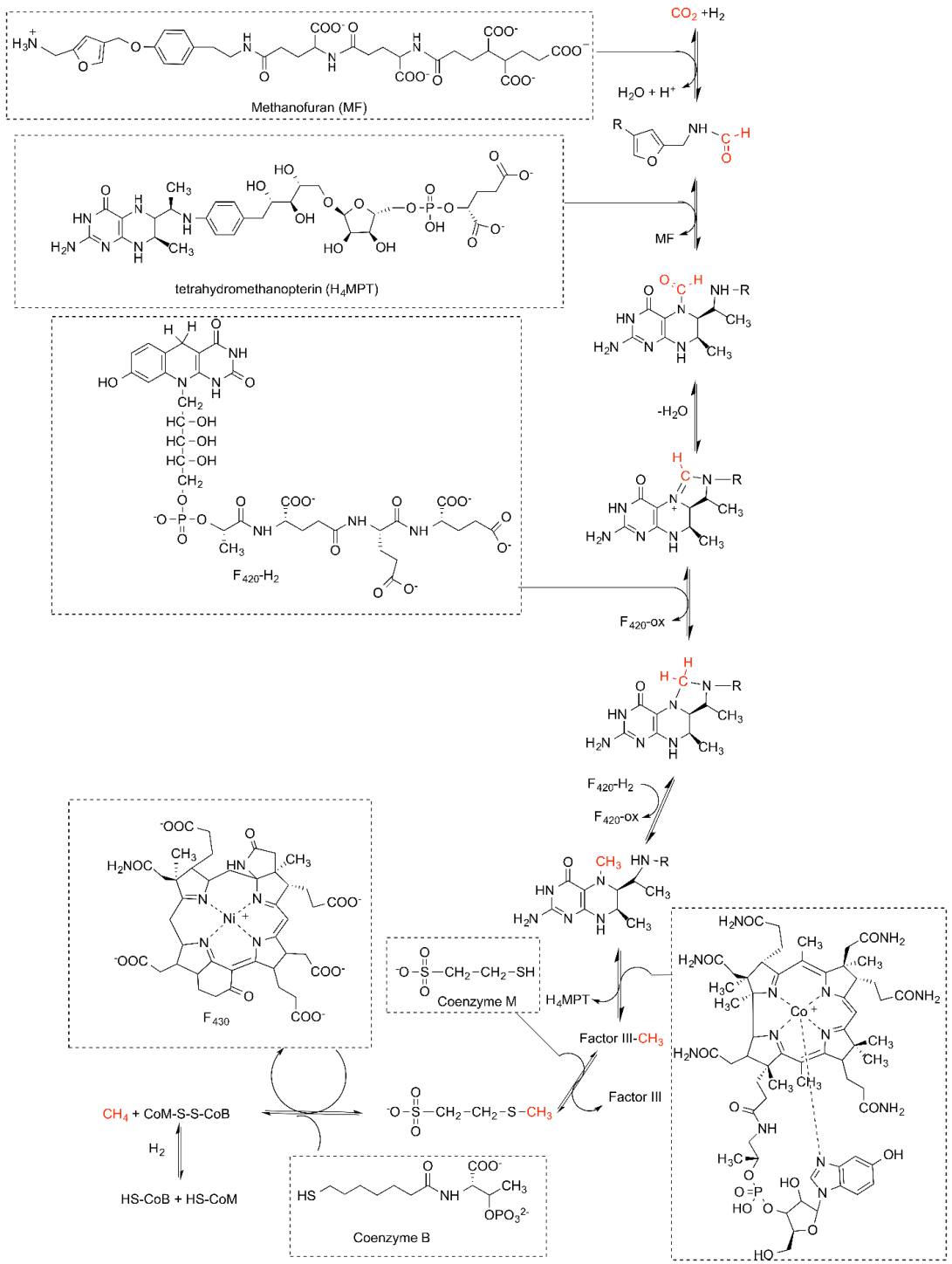

Figure 1. Methanogenesis

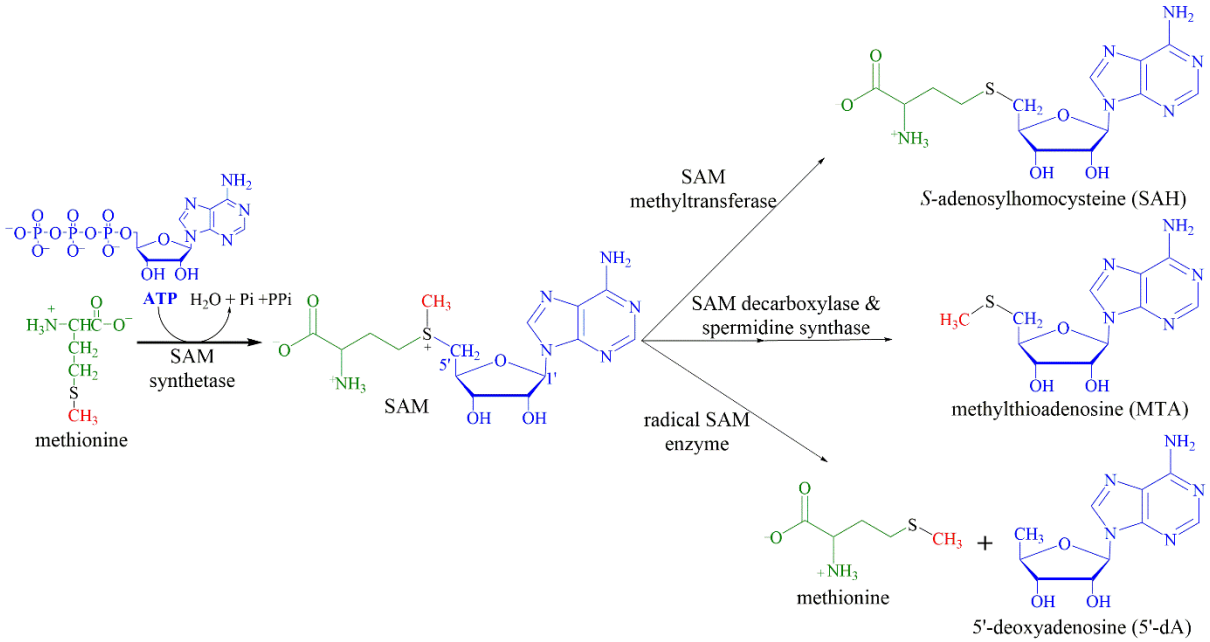

Figure 2. SAM biosynthesis and utilization

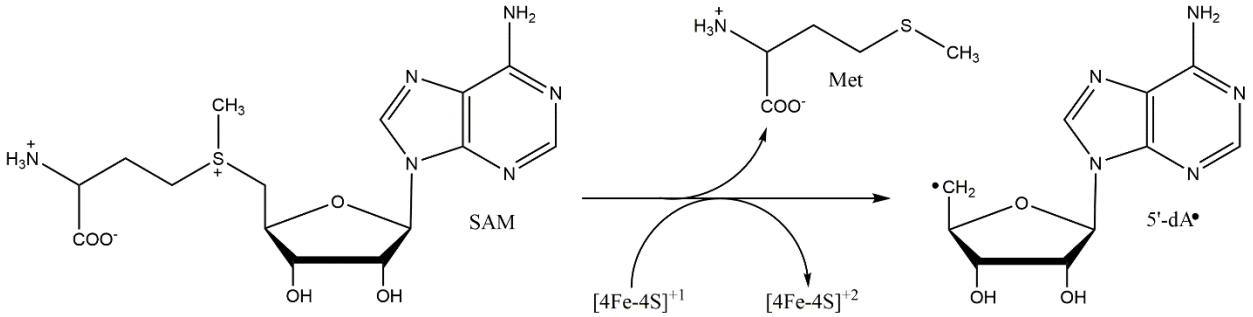

Figure 3. Reductive cleavage of SAM to Met and 5’-dA.

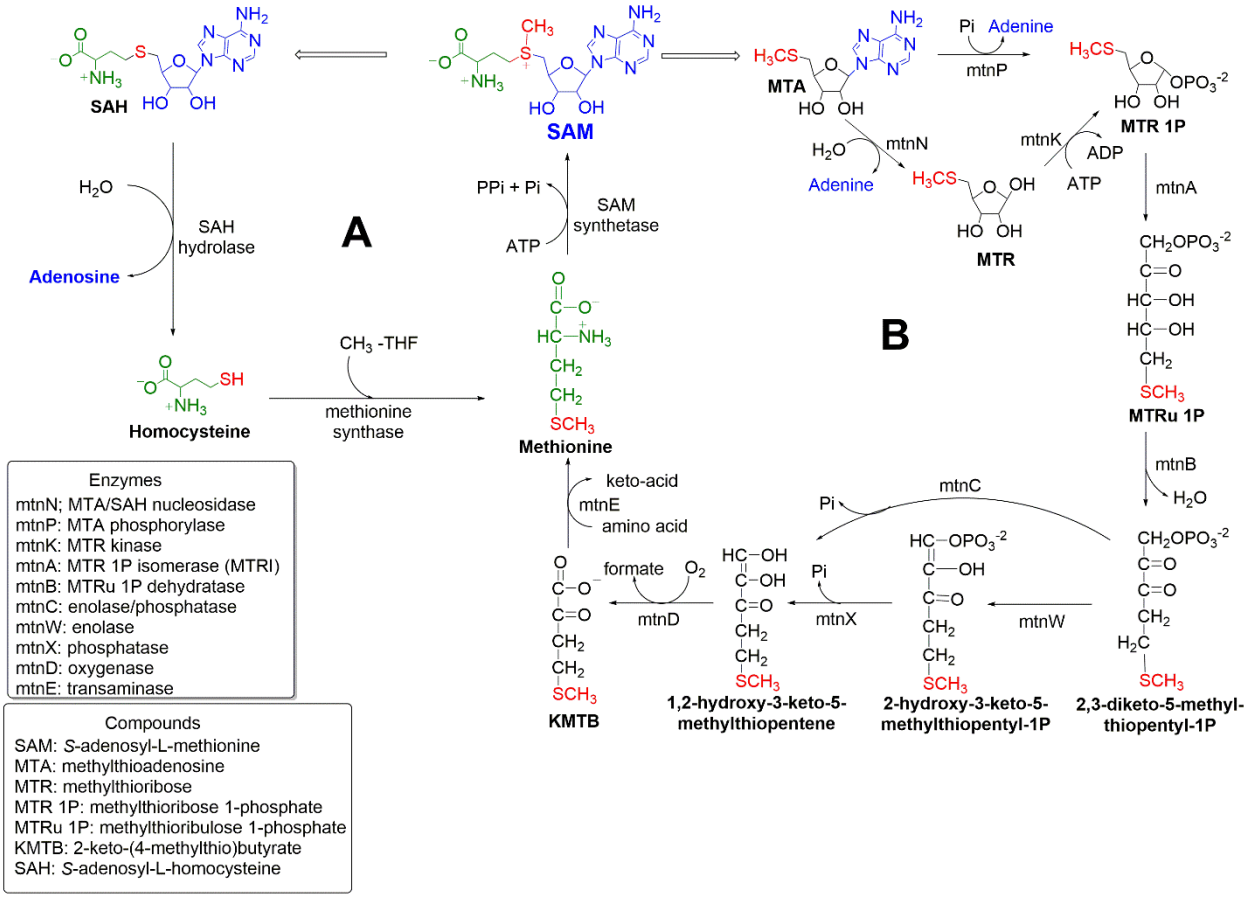

Figure 4. Canonical methionine salvage pathways of SAH (A) and MTA (B)

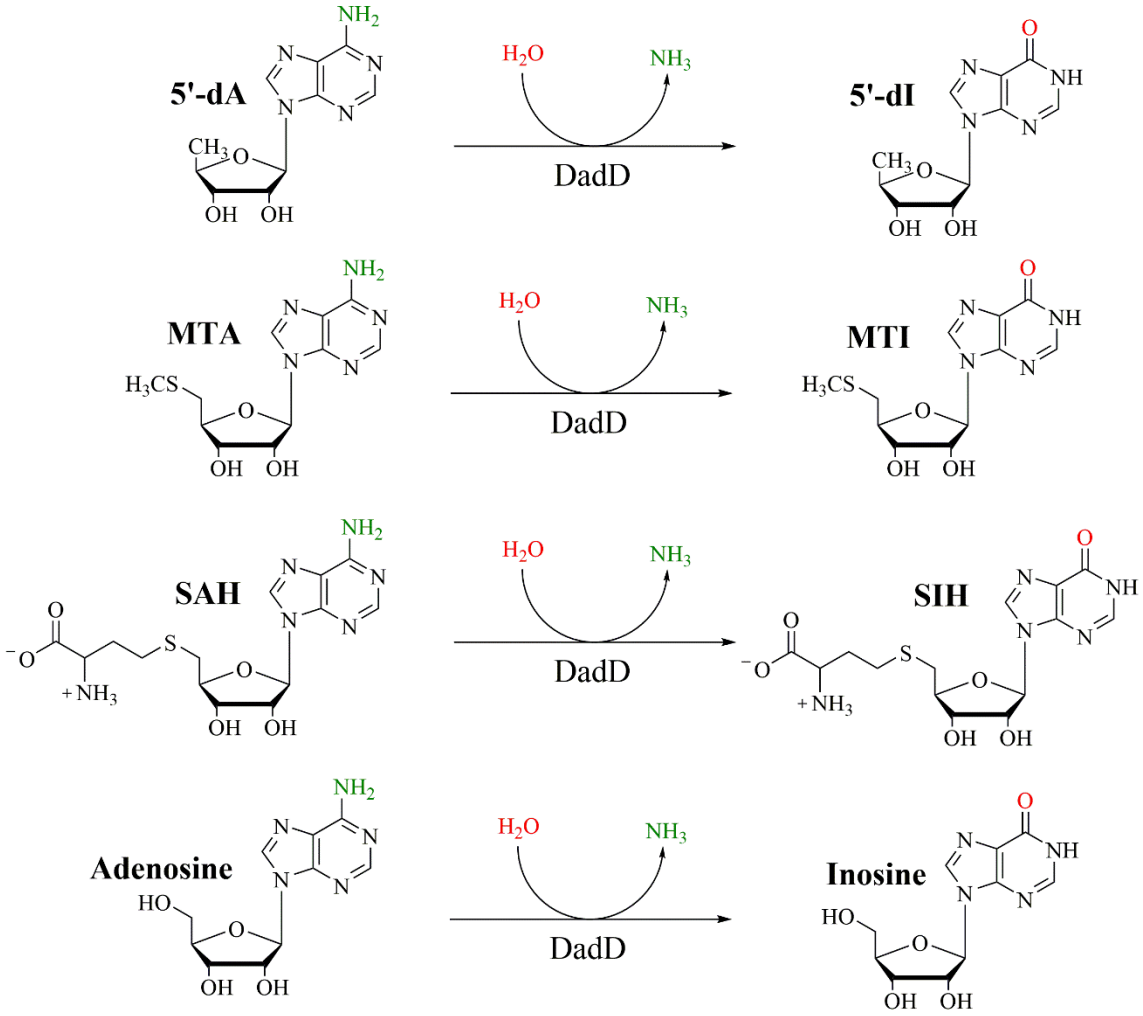

Figure 5. Deamination reactions performed by DadD

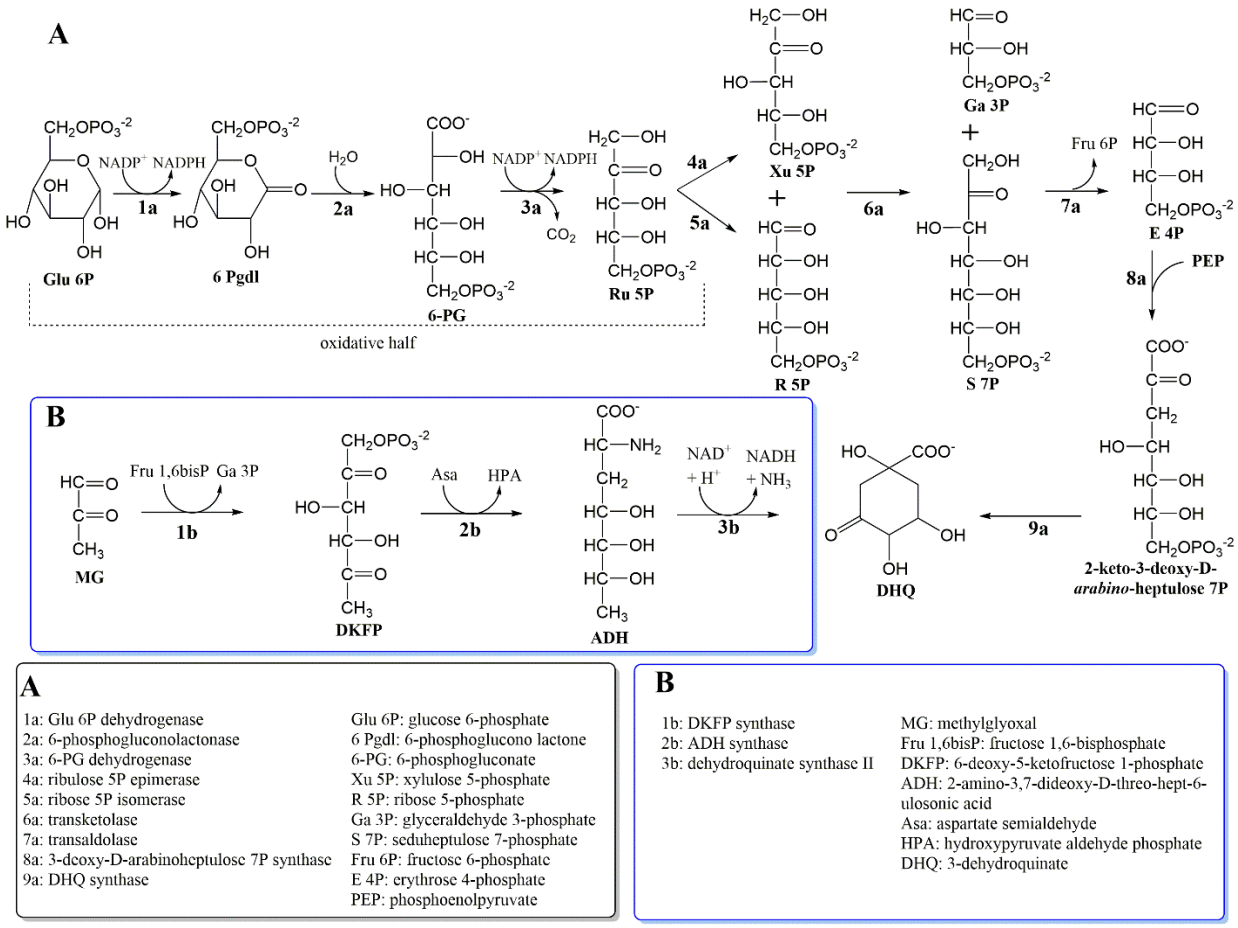

Figure 6. Comparison of the canonical route for DHQ biosynthesis (A) and the DHQ biosynthesis in *M. jannaschii* (B, blue box).

Chapter 1: *S*-Inosylhomocysteine Hydrolase: A novel enzyme involved in SAM recycling

Danielle Miller, Huimin Xu, and Robert H. White[#]

Department of Biochemistry, Virginia Polytechnic Institute and State University, Blacksburg, VA 24061

#To whom correspondence should be addressed. Telephone: (540) 231-6605, Fax: (540) 231-9070, e-mail: rhwhite@vt.edu

Running title: *S*-inosylhomocysteine hydrolase
Key words: *S*-inosylhomocysteine hydrolase, *S*-inosyl-L-homocysteine, SAM recycling

Miller D V, Xu H, White RH. 2015. S-Inosylhomocysteine Hydrolase: A novel enzyme involved in SAM recycling. *J Bacteriol* **197**:1-8 JB – 00080.

ABSTRACT

S-Adenosyl-L-homocysteine, the product of *S*-adenosyl-L-methionine (SAM) methyltransferases, is known to be a strong feedback inhibitor of these enzymes. A hydrolase specific for *S*-adenosyl-L-homocysteine produces L-homocysteine, which is re-methylated to methionine and can be used to regenerate SAM. Here, we show that the annotated *S*-adenosylhomocysteine hydrolase in *Methanocaldococcus jannaschii* is specific for the hydrolysis and synthesis of *S*-inosyl-L-homocysteine, not *S*-adenosyl-L-homocysteine. This is the first report of an enzyme specific for *S*-inosyl-L-homocysteine. As with *S*-adenosyl-L-homocysteine hydrolase, which shares greater than 45% sequence identity with the *M. jannaschii* homologue, the *M. jannaschii* enzyme was found to co-purify with bound NAD^+ and has a K_M of 0.64 ± 0.4 mM, 0.0054 ± 0.006 mM, and 0.22 ± 0.11 mM for inosine, L-homocysteine, and *S*-inosyl-L-homocysteine, respectively. No enzymatic activity was detected with *S*-adenosyl-L-homocysteine as the substrate in either the synthesis or hydrolysis direction. These results prompted us to re-name the *M. jannaschii* enzyme as an *S*-inosylhomocysteine hydrolase (SIHH). Identification of SIHH demonstrates a modified pathway in this methanogen for the regeneration of SAM from *S*-adenosyl-L-homocysteine that uses the deamination of *S*-adenosyl-L-homocysteine to form *S*-inosyl-L-homocysteine.

Importance

In strictly anaerobic methanogenic archaea, such as *Methanocaldococcus jannaschii*, canonical metabolic pathways are often not present and instead unique pathways are utilized by these organisms which are deeply rooted on the phylogenetic tree. Here we discuss the recycling pathway for *S*-adenosylhomocysteine, produced from *S*-adenosyl-L-methionine (SAM)-dependent methylation reactions, that uses a hydrolase specific for *S*-inosylhomocysteine, an uncommon metabolite. Identification of the pathways and enzymes involved in the unique pathways in the methanogens will give insight into the biochemical reactions that were occurring when life originated.

Abbreviations

S-adenosyl-L-methionine (SAM), 5'-deoxyadenosine deaminase (DadD), *S*-adenosylhomocysteine (SAH), *S*-adenosylhomocysteine hydrolase (SAHH), *S*-inosylhomocysteine (SIH), *S*-inosylhomocysteine hydrolase (SIHH), *N*-[tris(hydroxymethyl)methyl]-2-aminoethanesulfonic acid (TES), dithiothreitol (DTT), tris(hydroxymethyl)aminomethane (Tris), sodium dodecyl-sulfate polyacrylamide gel electrophoresis (SDS-PAGE), L-homocysteine (Hcy), cobalamin-dependent methionine synthase (metH), cobalamin-independent methionine synthase (metE), N^5-methyltetrahydrofolate (THF), methyltetrahydromethanopterin (MPT), and hypoxanthine (HX).

Introduction

The recycling of *S*-adenosyl-L-methionine (SAM)-derived metabolites in *Methanocaldococcus jannaschii* was recently shown to use a novel enzyme, 5'-deoxyadenosine deaminase (DadD) (1). DadD deaminates three SAM-derived enzymatic products (5'-methylthioadenosine, 5'-deoxyadenosine, and *S*-adenosylhomocysteine) to produce the inosine analogs (Figure 1) (1). The canonical pathway for recycling *S*-adenosyl-L-homocysteine (SAH) produced from SAM-dependent methyltransferases (2-4) proceeds in a three step recycling pathway back to SAM (Figure 2A). SAH is first hydrolyzed to produce adenosine and homocysteine using *S*-adenosylhomocysteine hydrolase (SAHH). Homocysteine is then methylated by methionine synthase to produce methionine (5). The last step in the pathway is the generation of SAM by combining the adenosyl moiety of ATP with methionine to produce SAM, pyrophosphate, and phosphate (Figure 2), catalyzed by SAM synthase (6). A similar pathway has been established in *M. jannaschii* but with the addition of one extra step involving the deamination of SAH to form *S*-inosylhomocysteine (SIH), catalyzed by DadD (Figure 2B).

The production of SIH prompted our search for an enzyme able to metabolize this uncommon metabolite. An annotated SAHH encoded by MJ1388, which shares greater than 45% sequence identity with other characterized SAHH's (Figure 3) was identified as possibly metabolizing SIH based on the structural similarities between SAH and SIH (Figure 2). Here, we show that the annotated SAHH from *M. jannaschii* is specific for SIH and failed to either hydrolyze or synthesize SAH, prompting the naming of the MJ1388 encoded enzyme as an *S*-inosylhomocysteine hydrolase (SIHH).

Materials and methods

Chemicals. All chemicals were purchased from Sigma/Aldrich unless otherwise noted.

Enzymatic Production of *S*-Inosyl-L-homocysteine. The enzymatic preparation of *S*-inosylhomocysteine was done by incubating 1 mM of *S*-adenosyl-L-homocysteine with 18.2 ng of DadD (MJ1541 gene product) overnight at 25 ^{o}C in 1 mL of 50 mM 1,3-bis[tris(hydroxymethylmethylamino]propane (BIS TRIS propane) buffer (pH 9.0) (1). Under these conditions 1 mM SAH was completely converted to 1 mM SIH as measured by HPLC.

Cloning, Overexpression, and Purification of *M. jannaschii* MJ1388 Gene Product in *E. coli*. The MJ1388 gene (UniProt accession number Q58783) was amplified by PCR from genomic DNA using oligonucleotide primers MJ1388- Fwd: 5'-

GGTCATATGTATGAAGTTAGGGAC-3' and MJ1388-Rev: 5'-GCTGGATCCTTAAGTT-CCTTCTC-3'. PCR amplification was performed as described previously (7) using a 55 ^{o}C annealing temperature. Purified PCR product was digested with Nde1 and BamH1 restriction enzymes and ligated into compatible sites in vector pT7-7. The sequence of the resulting plasmid, pMJ1388, was verified by DNA sequencing. pM1388 was transformed into *E. coli* strain BL21-CodonPlus(DE3)-RIL cells (Stratagene). The transformed cells were grown in LB medium (200 mL) supplemented with 100 µg/mL ampicillin at 37 ^{o}C with shaking until they reached an OD_{600} of 1.0. Recombinant protein production was induced by addition of lactose to a final concentration of 28 mM (7). After an additional 2 hours of culture, the cells (200 mL) were harvested by centrifugation (4,000 x *g*, 5 min) and frozen at -20 ^{o}C. Induction of the desired protein was confirmed by SDS-polyacrylamide gel electrophoresis (SDS-PAGE) analysis of total cellular proteins.

The frozen *E. coli* cell pellet containing the desired protein (~0.4 g wet wt) was suspended in 3 mL of extraction buffer (50 mM *N*-[tris(hydroxymethyl)methyl]-2-aminoethanesulfonic acid (TES), (pH 7.0), 10 mM $MgCl_2$, 20 mM dithiothreitol (DTT)) and lysed by sonication. After centrifugation (14,000 × *g* for 10 min), the resulting recombinant protein was found to remain soluble in the cell extract after heating for 10 min at 80 ^{o}C followed by centrifugation (8,100 × *g* for 20-30 min). This heating step allowed for the purification of the recombinant enzymes from the majority of *E. coli* proteins, which denature and precipitate under these conditions. Purification of the desired protein was performed by anion-exchange chromatography of the 80 ^{o}C soluble fractions on a MonoQ HR column (1 x 8 cm; Amersham Bioscience) using a linear salt gradient from 0 to 1 M NaCl in 25 mM tris(hydroxymethyl)aminomethane **(**Tris) buffer (pH 7.5) over 55 min at a flow rate of 1 mL/min. 1 mL fractions were collected and fractions containing the desired protein were identified through SDS-PAGE analysis of the individual fractions. MALDI-MS was used to confirm the identity of the MJ1388 gene product as previously described (1). Protein concentration was determined by Bradford analysis (8).

Measurement of Native Molecular Weight of SIHH. The native molecular weight of SIHH was determined by size exclusion chromatography as described previously using a Superose 12 HR column (9) using the following standards: blue dextran (2000 kDa), alcohol dehydrogenase (150 kDa), conalbumin (77.5 kDa), bovine serum albumin (66 kDa), carbonic

anhydrase (29 kDa), and cytochrome c (14 kDa).

Initial Characterization of the SIHH catalyzed reaction. All assays were done in a 100 μL reaction volume with the final concentrations of reagents indicated. The linear dependence of the reaction rate with the amount of enzyme was determined by incubating varying amounts of SIHH (0 to 11 μg) with 0.2 mM DL-homocysteine and inosine in 25 mM Tris buffer, pH 7.5, for 10 min at 70 ^{o}C and measuring the amount of SIH produced. The effect of temperature on SIHH (5.5 μg) activity was tested at 37, 70, and 80 ^{o}C by pre-incubating SIHH at each temperature for 10 min in 25 mM Tris, pH 7.5, prior to adding 0.2 mM inosine and 0.2 mM DL-homocysteine followed by incubation of the reaction at each fixed temperature for another 10 min. The results for the pre-incubated SIHH assays were compared with control assays (no pre-incubation) at the indicated temperatures. This allowed for determination of temperature activation through the comparison of enzymatic activity with and without pre-incubation at the indicated temperatures. A time course of the SIHH-catalyzed condensation of 0.2 mM inosine and 0.2 mM DL-homocysteine was performed at 70 ^{o}C in 25 mM Tris, pH 7.5, using 5.5 μg of enzyme in a 500 μL assay volume. Aliquots (100 μL) were removed after 0, 10, 20, 30, and 40 min and assayed for SIH formation.

After about two weeks of daily freeze/thaw cycles (-20 ^{o}C to room temperature (RT)) of the purified SIHH-containing solution, it was found that SIHH became less active. The addition of a final concentration of 20 mM DTT to the solution was found to fully restore the activity of the enzyme and, thus, DTT was included in the assay.

The specificity of the enzyme for the D versus the L configuration of homocysteine was determined by incubating SIHH with 0.2 mM inosine and either 0.2 mM DL-homocysteine or 0.2 mM L-homocysteine in the standard assay. The pH optimum of SIHH (1.1 μg) was determined over the pH range of 6.5 to 11.5 using 50 mM sodium phosphate buffer in 0.5 pH unit increments for both directions of the reaction. In the synthesis direction the assay contained 0.2 mM inosine, 0.2 mM L-homocysteine, and 20 mM DTT and in the hydrolysis direction the assay contained 0.2 mM SIH, 0.23 mM NAD^{+}, and 20 mM DTT. All reactions were stopped with the addition of 5 μL 2 M HCl and after a brief centrifugation (~7500 × *g*, 2 min), the supernatant was then analyzed by HPLC.

The HPLC analysis of substrates and products were performed on a Shimadzu HPLC System equipped with a photodiode array detector and a C18 reverse phase column (Kromasil

250 × 4.6 mm, 5 μm particle size) operated at RT. The elution profile consisted of 5 min at 95% sodium acetate buffer (25 mM, pH 6.0, 0.02% NaN_3) and 5% methanol followed by a linear gradient to 50% sodium acetate buffer/50% methanol over 25 min at 0.5 mL/min. Under these conditions SIH eluted at 15.3 min, inosine at 16.8 min, SAH at 18.8 min, and adenosine at 21.8 min. Quantitation was based on absorbance at 260 nm for the adenosine and 248 nm for the inosine containing compounds using $\varepsilon_{260} = 14900\ M^{-1}cm^{-1}$ for adenosine and $\varepsilon_{248} = 12300\ M^{-1}cm^{-1}$ for inosine (10). Quantitation was based on peak areas.

Standard Assays for SIHH Activity. The standard enzymatic assay used to measure the synthesis of SIH contained 1.1 μg SIHH, 0.2 mM inosine, 0.2 mM L-homocysteine (Hcy), and 20 mM DTT in a 100 μL total volume of 50 mM sodium phosphate buffer (pH 7.0). The reactions were incubated at 70 ºC for 20 min and stopped with the addition of 5 μL 2 M HCl. After brief centrifugation (~2 min, ~7500 x *g*) the samples were then analyzed by HPLC. The standard assay for measurement of the hydrolysis of SIH is the same as described here, but with the addition of 0.23 mM NAD^+.

Determining Substrate Specificity of SIHH. The activity of SIHH for the synthesis of SIH was tested with either inosine or adenosine and L-homocysteine (Hcy) using an equal molar concentration of adenosine or inosine and Hcy (each at 0.2 mM) with 1.1 μg of SIHH, 20 mM DTT, and in 100 μL total volume of 50 mM sodium phosphate buffer, pH 7.0, with 0.23 mM NAD^+ when added. The assay was then incubated at 70 ºC for 20 min followed by addition of 5 μL 2 M HCl to stop the reaction and by a brief centrifugation (~2 min, ~7500 x *g*) before HPLC analysis.

The hydrolysis of SIH or SAH was tested under varying conditions (Table 2). The equilibrium constant between SAH and adenosine and Hcy for SAHH has been previously reported to favor the synthesis of SAH *in vitro* and, as a result, the hydrolysis of SAH was only able to be observed upon the addition of an adenosine deaminase to remove the adenosine (2). The removal of adenosine was required to measure the hydrolysis of SAH; however, for SIHH the hydrolysis of SIH was able to be monitored without removal of inosine. The assay was performed with a final concentration of 0.1 mM SIH or SAH, 1.1 μg SIHH, 20 mM DTT, with or without 0.1 mM NAD^+ in 100 μL total volume of 50 mM sodium phosphate buffer at pH 7.0. The assay was incubated at 70 ºC for 20 min and stopped with the addition of 5 μL 2 M HCl,

followed by brief centrifugation and then analyzed for adenosine, SAH, inosine, and SIH by HPLC.

Determination of the Kinetic Parameters for SIHH. The kinetic parameters of the SIHH catalyzed condensation of inosine with Hcy were determined by using the standard assay parameters while varying concentrations of inosine (0, 0.2, 0.4, 0.6, and 0.8 mM) at 0.04, 0.06, and 0.08 mM Hcy. The kinetics of SIH hydrolysis was determined with an excess of NAD^+ (0.23 mM) and 20 mM DTT in 100 μL 50 mM sodium phosphate buffer, pH 7.0, and concentrations of SIH from 0, 0.05, 0.07, 0.1, and 0.2 mM. The kinetic experiments were then incubated at 70 ^oC for 20 min followed by 5 μL 2 M HCl, followed by brief centrifugation (7500 × *g*, 2 min) then analyzed by HPLC.

Determination of the Amount of NAD^+/NADH Bound to SIHH. In an effort to determine the amount of NAD^+ or NADH that was bound to the purified SIHH, the methods described by Yuan *et al.* (11) were used. To 400 μL of the MonoQ fraction containing 1.4 mg of SIHH, 1.2 mL 97% ethanol was added to precipitate the protein, which was pelleted by centrifugation (7500 × *g*, 10-15 min). The supernatant was evaporated to dryness with a stream of N_2 gas while being heated in a water bath of ~100 ^oC. The resulting residue was dissolved in 200 μL water and analyzed by HPLC as described above. Known concentrations of NAD^+, eluting at 13.3 min with a λ_{max} of 260 nm, and NADH, eluting at 14.3 min with a λ_{max} of 340 nm, were used to determine the ratio of NAD^+ and/or NADH that was bound to the recombinantly expressed and purified SIHH.

Preparation of Apo SIHH. The generation of apo SIHH was done by modifying the methods outlined by Yuan, *et al (12).* Saturated ammonium sulfate (2 mL) was gradually added to 100 μL of a stirred solution of 1.4 mg/mL SIHH in 25 mM Tris 0.45 M NaCl buffer (pH 7.5) from purification and continued stirring at RT for 30 min. After centrifugation (8,100 × *g*, for 10 min), the supernatant was removed and the precipitated protein was re-dissolved in 100 μL of 25 mM potassium phosphate, pH 7.2, buffer containing 1 mM EDTA and 5 mM DTT and the above steps repeated. Following centrifugation, the protein was re-dissolved in 100 μL of 25 mM potassium phosphate, pH 7.2, buffer containing 1 mM EDTA. The amount of protein recovered was determined by Bradford analysis (8).

The synthesis activity of the generated apo SIHH was performed by incubating 0.2 mM inosine, 0.2 mM Hcy, 0.42 μg apo-SIHH, or untreated SIHH with and without 0.2 mM NAD^+ in

100 μL volume of 50 mM sodium phosphate, pH 7.0, with 20 mM DTT for 20 min at 70 ºC. The hydrolysis activity of the apo SIHH was performed under the same conditions but with the substitution of the 0.2 mM inosine and 0.2 mM Hcy with 0.1 mM SIH. The reactions were stopped with the addition of 5 μL 2 M HCl, followed by brief centrifugation and analysis by HPLC.

Results

Cloning, Overexpression, and Purification of *M. jannaschii* MJ1388 Gene Product in *E. coli*. The MJ1388 derived protein was efficiently expressed in *E. coli* as measured from the SDS-PAGE analysis of the total proteins present in the *E. coli* cells after expression. A single new band was identified with a molecular weight of ~46 kDa that was not observed in the control cells. MALDI-MS analysis of the tryptic peptides derived from this band showed five unique peptides expected to arise from SIHH, confirming the presence of the desired protein in this band. After sonication and centrifugation of the *E. coli*, SDS-PAGE analysis of the soluble and insoluble material demonstrated that most of the expressed MJ1388 protein was found in the soluble extract. Heating portions of the resulting crude soluble extract at different temperatures indicated that SIHH remained soluble up to 80 °C based on SDS-PAGE analysis. Thus, the first step in purification of the native enzyme was heating of the sonicated cell extract to 80 °C for 20 min prior to purification of the SIHH on MonoQ. This separation produced one peak of MJ1388 activity eluting at 0.4 M NaCl. MALDI-MS analysis of the tryptic peptides showed four of the same five unique peptides reported above from analysis of the excised band of the SDS-PAGE of the crude extract of SIHH.

Native Molecular Weight of SIHH. The monomeric molecular mass of SIHH was measured to be 49 kDa by SDS-PAGE analysis, agreeing with the predicted molecular weight of 46 kDa. Using size exclusion chromatography, two peaks were identified that contained SIHH on the basis of their elution volumes; the major peak was the tetrameric form and the minor peak was the dimeric form of SIHH. The ratio of the tetramer to dimer form of SIHH was 4:1 based on their 280 nm absorbance.

Initial Characterization of the SIHH Catalyzed Reaction. SIHH was 25% more active in 50 mM, pH 7.5, sodium phosphate buffer than in 25 mM Tris, pH 7.5, buffer. Phosphate buffer was tested because it has been shown that the presence of phosphate can have an effect on SAHH's activity and it is the buffer most often used in characterizing SAHH in

other organisms (13). SIHH activity was activated when incubated at 10 min for 70 ^{o}C prior to being assayed. The activity of SIHH without pre-incubation retained only 35% of the pre-incubated activity (Table 1). This indicates that pre-incubation at 70 ^{o}C increased the observed activity. SIHH activity at 37 ^{o}C and 80 ^{o}C pre-incubated for 10 min versus just assayed at 37 ^{o}C and 80 ^{o}C demonstrated minimal change when compared with the SIHH activity following pre-incubation at 70 ^{o}C (Table 1). These results suggest that 70 ^{o}C is the optimal temperature to measure SIHH activity. A time course of the enzymatic activity at 70 ^{o}C was measured showing a linear increase in product formation up to 20 min.

SIHH did show a slight preference for L-homocysteine in the synthesis direction; however, it retained 94% activity when assayed with the same concentration of DL-homocysteine. This indicates that the D-isomer present in the DL-homocysteine is either not a strong inhibitor of SIHH or was a substrate. SIHH had no measurable activity at either pH 6.5 or 11 and showed maximal activity at pH 7.0 and pH 9.6 (Figure 4, blue squares). The activity of SIHH in the hydrolysis direction showed essentially the same activity over the same pH range (Figure 4, green triangles).

Substrate Specificity of SIHH. The activity of SIHH was found to be specific for Hcy and inosine versus Hcy and adenosine. No activity was observed for the synthesis of SAH from adenosine and Hcy. SIHH was found to only use Hcy and inosine as substrates and the addition of excess NAD^{+} (0.2 mM) increased enzymatic activity by ~2 fold (Table 2). Hydrolysis of SAH with and without the addition of excess NAD^{+} in the presence of SIHH was not successful. However, the hydrolysis of SIH was dependent upon the addition of excess NAD^{+} in the assay (Table 2). At this point, we are unable to explain why the addition of excess NAD^{+} allowed for the hydrolysis of SIH.

Determination of the Kinetic Parameters of SIHH. Our kinetic data are summarized in Table 3. During the analysis of the kinetic constants it was found that at high concentrations of Hcy (above 0.2 mM) and inosine (K_i = 2.0 ± 0.5 mM) non-linear kinetics was demonstrated (data not shown), which was most likely due to substrate inhibition. It has been previously shown in rat liver that L-Hcy concentrations above 0.6 mM inhibited SAHH (3). The non-linear kinetics that was seen at high concentrations of substrates also suggests cooperative binding between the four subunits of SIHH. Human SAHH was shown to go through conformational changes upon substrate binding that cause a dimer-dimer rotation to make the entire tetrameric structure more

compact (14). The kinetic constants for SIH were only able to be determined after the addition of excess NAD^+ (Table 3). The k_{cat} for the hydrolysis of SIH (25 min^{-1}) is similar to the reported k_{cat} for SAH hydrolysis (31.8 min^{-1}) by the human enzyme (4). The equilibrium constant (K_{eq}) of SIHH was calculated using the Uni-Bi Haldane-K_{eq} relationship with product inhibition equation (A) (15).

$$K_{eq} = \frac{v_{maxf} K_{ip} K_{Mq}}{v_{max\,r} K_{Ma}} \qquad \text{(A)}$$

For the above equation v_{maxf} represents the forward reaction and v_{maxr} represents the reverse reaction: where, v_{maxf} is 0.55 µmol min^{-1} mg^{-1}, inosine K_{ip} is 2.0 x 10^{-3} M, Hcy K_{Mq} is 5.4 x 10^{-6} M, , K_{Ma} is 2.2 x 10^{-4} M, and v_{maxr} is 0.27 µmol min^{-1} mg^{-1}. The K*eq* was determined to be 2.5 x 10^{-5} M. This is similar to the previously reported value from rat liver of 1.4 x 10^{-6} M (2).

NAD^+/NADH Bound to Purified SIHH. The ratio of NAD^+ bound per monomer of purified SIHH was measured at 0.62 ± 0.02. The ratio of NAD^+ per monomer of SIHH is in agreement with the reported ratio of 0.65 of NAD^+ per monomer of the human enzyme (16). NADH was not detected, suggesting that SIHH purifies only with NAD^+ bound to the enzyme.

Preparation of Apo SIHH. The creation of apo SIHH was determined by the loss of either the synthesis or hydrolysis activity of SIHH with and without the addition of NAD^+ to the assay. The results are summarized in Table 1. Apo SIHH had no activity without addition of NAD^+, suggesting that there was no bound NAD^+ following our procedure. The activity of the apo SIHH was restored upon addition of NAD^+ to the assay mixture. In both the synthesis and hydrolysis of SIH, apo SIHH only regained ~60% of the activity compared to untreated SIHH.

Discussion

S-Adenosyl-L-homocysteine (SAH) is a product of *S*-adenosyl-L-methionine (SAM) methyltransferases and is known to be a feedback inhibitor of these enzymes (17-20). As a result of this inhibition, organisms have evolved efficient enzymes to metabolize SAH. There are two established pathways to prevent inhibition of the methyltransferase reactions by SAH. In the first pathway, found only in *Bacteria*, a methylthioadenosine/S-adenosylhomocysteine nucleosidase cleaves the nucleotide to produce adenine and *S*-ribosylhomocysteine (5, 21, 22). *S*-ribosylhomocysteine is recycled by an *S*-ribosylhomocysteine lyase to produce homocysteine and 4,5-dihyroxy-2,3-pentanedione (5, 21). 4,5-Dihydroxy-2,3-pentanedione is an important precursor for autoinducer-2, which is involved in quorum sensing (5). In the second pathway, an S-adenosylhomocysteine hydrolase (SAHH) hydrolyzes off the nucleoside to produce

homocysteine and adenosine (5, 21) (Figure 2A). SAHH homologues are almost ubiquitously found in *Eukarya* and *Archaea* leading to the conclusion that the direct conversion of SAH to Hcy is occurring in these organisms (5).

M. jannaschii is a strict anaerobic methanogenic archaeal organism that is deeply rooted on the phylogenetic tree and has been a source for the identification of novel pathways and enzymes involved in its metabolism (23-25). Establishment of these pathways and the enzymes involved has given insight into the biochemical reactions that were occurring when life first originated. Annotation of an SAHH homolog in the *M. jannaschii* genome would indicate direct hydrolysis of SAH to Hcy and adenosine; however, we have recently shown that a different pathway must proceed due to the lack of an adenosine deaminase in methanogens. In *M. jannaschii,* 5'-deoxyadenosine deaminase (DadD), was found to deaminate SAH to *S*-inosylhomocysteine (SIH) with a k_{cat}/K_M of 4.4 x 10^6 $M^{-1}s^{-1}$ (1) (Figure 1). SIH is not a typical metabolite and has only been identified in *Streptomyces flocculus* (26). Here we show that the annotated SAHH in *M. jannaschii* (MJ1388) does not accept SAH as a substrate and instead exclusively uses SIH. In this reaction, SIH is hydrolyzed to Hcy and inosine for SAM recycling and purine metabolism (Figure 2B). This suggests that SIH is a central metabolite for SAM recycling in *M. jannaschii*.

SIHH is the first of two enzymes we have identified that are responsible for recycling the Hcy moiety of SAH into methionine. The generated Hcy is then methylated to form methionine (27, 28). The C- terminal portion of the cobalamin-independent methionine synthase (MetE) is encoded in the *M. jannaschii* (MJ1473) and the activity of the homologous enzyme from *Methanobacterium thermautotrophicus* has been demonstrated (29) (Figure 2). Therefore the Hcy generated from SIHH can be methylated to generate methionine.

Our characterization of *M. jannaschii* SIHH indicates that its mechanism is the same as the established mechanism for SAHH. Here, NAD^+ oxidizes the 3' hydroxyl to a carbonyl and the active site base then abstracts the C4' hydrogen eliminating Hcy. Conjugate addition of hydroxide to the resulting α,β-unsaturated ketone followed by rearrangement and protonation of the enolate ion generates the 3'-keto compound that is reduced by the NADH to inosine (17, 30-33). The general base has been established in *Mycobacterium tuberculosis* as H363 (H293 in *M. jannaschii*) (31), which is found to be highly conserved (Figure 3, asterisk). In addition to conservation of the general base, other residues involved in substrate and cofactor binding were

found to be conserved (Figure 3), further supporting that the mechanism is the same for SIHH and SAHH. Sequence alignments of SIHH and SAHH's show that the active site residues involved with binding of the substrate are highly conserved (Figure 3, blue). As a result, there is no clear indication as to what residues may be involved in causing SIHH to be specific for SIH rather than SAH. Further studies of the active site to determine what residues confer the differences in specificity for SIH versus SAH would be interesting.

Interestingly, a group of three threonine residues (T159-161, *M. jannaschii* numbering) involved in cofactor binding are also highly conserved (Figure 3, red brackets) and in *M. tuberculosis* SAHH, the conserved threonines were identified to be a site of post translational modification by phosphorylation and were required for enzymatic activity (34). Phosphorylation of the conserved threonines, in the NAD^+ binding pocket, generated an inactive enzyme by preventing NAD^+ binding (34). The conservation of these threonines could indicate a site of post translational modification by phosphorylation in *M. jannaschii*.

In the characterization of SIHH we found that there are two pH maxima for activity in synthesis of SIH activity (Figure 4, blue squares). The pH profile for the hydrolysis of SIH did not show a clear optima and instead showed activity across the whole pH range tested (Figure 4, green triangles). It has been shown in the SAHH from *Plasmodium falciparum* and human enzymes for the synthesis of SAH activity was found to be maximal between a pH of 7 and 8 (16); however, the maximal pH for SAHH was found between 8.0 and 10.5 for both the synthesis and hydrolysis of SAH for the SAHH from *Alicaligenes faecalis* (35). Interestingly, rat liver SAHH was found to have two different pH optimums depending on the direction of the reaction: the hydrolysis of SAH had a pH optimum between 6.4 and 7.2 and the synthesis of SAH had an optimum pH above 7.8 (36).

Identification of SIHH in *M. jannaschii* represents a reoccurring theme in *M. jannaschii* purine salvage pathways. Salvage of the nitrogen-rich purine ring, in this case hypoxanthine (HX), is carried out by several enzymes in *M. jannaschii*: DadD, which deaminates adenosine, 5'-deoxyadenosine, methylthioadenosine, SAH (1) (Figure 1), an adenine deaminase that deaminates adenine to HX (Miller, unpublished), a purine nucleoside phosphorylase that phosphorolyzes the HX base from methylthioinosine, 5'-deoxyinosine, inosine, 2'-deoxyinosine (Miller, unpublished), and now SIHH, which hydrolyzes SIH to produce inosine and Hcy. Recently, Armenta-Medina *et al* have postulated that inosine may have served as the original

base to guanosine (37), which is supported by 1) the widespread conservation of the *de novo* IMP biosynthetic pathway in all three domains of life (37), 2) an RNA polymerase II from *E. coli* that retains activity with IMP (38), and 3) an acetyl-CoA synthetase (ADP forming) from *Pyrococcus furiosus* that is twofold and threefold more active with IDP and ITP as substrates than ADP and ATP, respectively *(39).* Taken together, this suggests that HX-containing nucleosides and nucleotides potentially predated guanine-containing nucleotides and nucleosides. This is also supported by the annotated adenine phosphoribosyltransferase (encoded by MJ1655) and its homologous from *M. thermautotrophicus* and *Methanococcoccus voltae* were all demonstrated to be specific for HX and guanine showing no activity towards adenine (Miller unpublished) (40, 41). The presence of these enzymes demonstrates that in *M. jannaschii*, and possibly other methanogens, are unable to use adenine for the salvage of purines and requires conversion to HX prior to salvage of the nitrogen rich purine ring.

In summary, we demonstrate that SIHH in *M. jannaschii* is required for the recycling of SAH produced from SAM-dependent methyltransferases in a four step process (Figure 2B) versus the canonical three step pathway (Figure 2A). This is only the second report of SIH serving as a metabolite and likely represents a primitive pathway for SAM-recycling in methanogens.

Acknowledgements. The authors thank Dr. W. Keith Ray for performing the mass spectrometry experiments and Dr. Kylie Allen for her assistance in editing the manuscript. The mass spectrometry resources are maintained by the Virginia Tech Mass Spectrometry Incubator, a facility operated in part through funding by the Fralin Life Science Institute at Virginia Tech and by the Agricultural Experiment Station Hatch Program (CRIS Project Number: VA-135981). This work was supported by the National Science Foundation Grant MCB1120346. Funding for this work was also provided in part, by the Virginia Agricultural Experiment Station and the Hatch Program of the National Institute of Food and Agriculture, U.S. Department of Agriculture.

References

1. **Miller D, O'Brien K, Xu H, White RH.** 2014. Identification of a 5′-Deoxyadenosine Deaminase in *Methanocaldococcus jannaschii* and its Possible Role in Recycling the Radical SAM Enzyme Reaction Product 5′-Deoxyadenosine. J. Bacteriol. **196:**1064-1072.
2. **Haba GDl, Cantoni GL.** 1958. The Enzymatic Synthesis of *S*-adenosyl-L-homocysteine from Adenosine and Homocysteine. J. Biol. Chem. **234:**603-608.
3. **Walker RD, Duerre JA.** 1974. *S*-Adenosylhomocysteine Metabolism in Various Species. Can. J. Biochem. **53:**312-319.
4. **Nakanishi M, Iwata A, Yatome C, Kitade Y.** 2000. Purification and Properties of Recombinant *Plasmodium falciparum S*-Adenosyl-L-Homocysteine Hydrolase. J. Biochem. **129:**101-105.
5. **Sun J, Daniel R, Wagner-Dobler I, Zeng A-P.** 2004. Is autoinducer-2 a universal signal for interspecies communication: a comparative genomic and phylogentic analysis of the synthesis and signal transduction pathways. BMC Evol. Biol. **4:**36.
6. **Graham DE, Bock CL, Schalk-Hihi C, Lu ZJ, Markam GD.** 2000. Identification of a Highly Diverged Class of *S*-Adenosylmethionine Synthetases in the Archaea. J. Biol. Chem. **275:**4055-4059.
7. **Graham DE, Xu H, White RH.** 2002. Identification of coenzyme M biosynthetic phosphosulfolactate synthase: a new family of sulfonate biosynthesizing enzymes. J. Biol. Chem. **277:**13421-13429.
8. **Bradford MM.** 1976. A rapid and sensitive method for the quantitation of microgram quantities of protein utilizing the principle of protein dye-binding. Anal. Biochem. **72:**248-257.
9. **Miller DV, Xu H, White RH.** 2012. A new subfamily of agmatinases in methanogenic Archaea is Fe(II) dependent. Biochemistry **51:**3067-3078.
10. **Volkin E, Cohn WE.** 1954. Estimation of nucleic acids. Methods Biochem. Anal. **I:**287-305.

11. **Yuan C-S, Borchardt RT.** 1995. Photoaffinity Labeling of Human Placental *S*-Adenosylhomocysteine Hydrolase with [2-^{3}H]8-Azido-adenosine. J. Biol. Chem. **270:**16140-16146.

12. **Yuan C-S, Yeh J, Liu S, Borchardt RT.** 1993. Mechanism of Inactivation of *S*-Adenosylhomocysteine Hydrolase by (*Z*)-4',5'-Didehydro-5'-deoxy-5'-Fluoroadenosine. J. Biol. Chem. **268:**17030-17037.

13. **Ueland PM.** 1982. *S*-Adenosylhomocysteinase from Mouse Liver. Inactivation of the Enzyme in the Presence of Metabolites. Int. J. Biochem. **14:**207-213.

14. **Lee Y, Jeong LS, Choi S, Hyeon C.** 2011. Link between Allosteric Signal Transduction and Functional Dynamics in a Multisubunit Enzyme: *S*-adenosylhomocysteine Hydrolase. J. Am. Chem. Soc. **133:**10807-19815.

15. **Segel IH.** 1975. Enzyme Kinetics: Behavior and Analysis of Rapid Equilibrium and Steady-State Enzyme Systems. John Wiley & Sons, Inc., New York, USA.

16. **Nakanishi M, Iwata A, Yatome C, Kitade Y.** 2001. Purification and Properties of Recombinant *Plasmodium falciparum S*-Adenosyl-L-homocysteine Hydrolase. J. Biochem. **129:**101-105.

17. **Ueland PM.** 1982. Pharmacological and Biochemical Aspects of S-Adenosylhomocysteine and S-Adenosylhomocysteine Hydrolase. Pharmacol. Rev. **34:**223-253.

18. **Gibson KD, Wilson JD, Udenfriend S.** 1961. The Enzymatic Conversion of Phospholipid Ethanolamine to Phospholipid Choline in Rat Liver. J. Biol. Chem. **236:**673-679.

19. **Zappia V, Zydek-Cwick CR, Schlenk F.** 1969. The Specificity of *S*-adenosylmethionine Derivatives in Methyl Transfer Reactions. J. Biol. Chem. **244:**4499-4509.

20. **Growchowski LL, White RH.** 2008. Promiscuous Anaerobes: new and unconventional metabolism in methanogenic archaea. Ann. N.Y. Acad. Sci. **1125:**190-214.

21. **Parveen N, Cornell KA.** 2011. Methylthioadenosine/S-adenosylhomocysteine nucleosidase, a critical enzyme for bacterial metabolism. Mol. Microbiol. **79:**7-20.

22. **Crooks PA, Dreyer RN, Coward JK.** 1979. Metabolism of *S*-Adenosylhomocysteine and *S*-Tubercidinylhomocysteine in Neuroblastoma Cells. Biochemistry **18:**2601-2609.

23. **White RH.** 2004. L-Aspartate Semialdehyde and 6-Deoxy-5-ketofructose 1-Phosphate Are the Precursors to the Aromatic Amino Acids in *Methanocaldococcus jannaschii*. Biochemistry **43:**7618-7627.

24. **Grochowski L, Xu H, White RH.** 2005. Ribose-5-phosphate biosynthesis in *Methanocaldococcus jannaschii* occurs in the absence of a pentose phosphate pathway. J. Bacteriol. **187:**7382-7389.

25. **Miller D, Wang Y, Xu H, Harich K, White RH.** 2014. Biosynthesis of the 5-(Aminomethyl)-3-furanmethanol Moiety of Methanofuran. Biochemistry **53:**6220-6230.

26. **Zulty JJ, Speedie MK.** 1989. Purification and Characterization of *S*-adenosylhomocysteine Deaminase from Streptonigrin-Producing *Streptomyces flocculus*. J. Bacteriol. **171:**6840-6844.

27. **Weissbach H, Peterkofsky A, Redfield BG, Dickerman H.** 1963. Studies on the Terminal Reaction in the Biosynthesis of Methionine. J. Biol. Chem. **238:**3318-3324.

28. **Rosenthal S, Smith LC, Buchanan JM.** 1965. Enzymatic Synthesis of the Methyl Group of Methionine. J. Biol. Chem. **240:**836-843.

29. **Schroder I, Thauer RK.** 1999. Methylcobalamin:homocysteine methyltransferase from *Methanobacterium thermoautotrophicum*. Eur. J. Biochem. **263:**789-796.

30. **Palmer JL, Abeles RH.** 1976. Mechanism for the enzymatic thioether formation. Mechanism of action of *S*-adenosylhomocysteinase. J. Biol. Chem. **251:**5817-5819.

31. **Reddy MCM, Kuppan G, Shetty ND, Owen JL, Ioerger TR, Sacchettini JC.** 2008. Cyrstal structures of *Mycobacterium tuberculosis* S-adenosyl-L-homocysteine hydrolase in ternary complex with substrate and inhibitors. Protein Sci. **17:**2134-2144.

32. **Takata Y, Yamada T, Huang Y, Komoto J, Gomi T, Ogawa H, Fujioka M, Takusagawa F.** 2002. Catalytic Mechanism of *S*-adenosylhomocysteine Hydrolase. J. Biol. Chem. **277:**22670-22676.

33. **Yamada T, Takata Y, Komoto J, Gomi T, Ogawa H, Fujioka M, Takusagawa F.** 2005. Catalytic mechanism of *S*-adenosylhomocysteine hydrolase: Roles of His 54, Asp 130, Glu 155, Lys 185, and Asp 189. Int. J. Biochem. Cell Biol. **37:**2417-2435.

34. **Singhal A, Arora G, Sajid A, Maji B, Bhat A, Virmani R, Upadhyay S, Nandicoori VK, Sengupta S, Singh Y.** 2013. Regulation of homocysteine metabolism by *Mycobacterium tuberculosis S*-adenosylmomocysteine hydrolase. Sci. Rep. **3**.

35. **Shimizu S, Shiozaki S, Ohshiro T, Yamada H.** 1984. Occurence of S-adenosylhomocystine hydrolase in prokaryote cells: Characterization of the enzyme from *Alcaligenes faecalis* and role of the enzyme in the activated methyl cycle. Eur. J. Biochem. **141:**385-392.

36. **Fujioka M, Takata Y.** 1981. *S*-Adenosylhomocysteine Hydrolase from Rat Liver. J. Biol. Chem. **256:**1631-1635.

37. **Armenta-Medina D, Segovia L, Perez-Rueda E.** 2014. Comparative genomics of nucleotide metabolism: a tour to the past of the three cellular domains of life. BMC Genomics **15:**1-16.

38. **Thomas MJ, Platas AA, Hawley DK.** 1998. Transcriptional Fidelity and Proofreading by RNA Polymerase II. Cell **93:**627-637.

39. **Glasemacher J, Bock A-K, Schmid R, Schonheit P.** 1997. Purification and properties of acetyl-CoA synthetase (ADP-forming), an archaeal enzyme of acetate formation and ATP synthesis, from the hyperthermophile *Pyrococcus furiosus*. Eur. J. Biochem. **244:**561-567.

40. **Sauer J, Nygaard P.** 1999. Expression of the *Methanobacterium thermoautotrophicum hpt* Gene, Encoding Hxypoxanthine (Guanine) Phosphoribosyltransferase, in *Escherchia coli*. J. Bacteriol. **181:**1958-1962.

41. **Bowen TL, Lin WC, Whitman WB.** 1996. Characterization of Guanine and Hypoxanthine Phosphoribosyltransferase in *Methanococcus voltae*. J. Bacteriol. **178:**2521-2526.

Tables

Table 1. Activation of SIHH with temperature

Temperature	Condition	% Relative Activity
37 °C	Pre-incubated[a]	75
	No pre-incubation[b]	81
70 °C	Pre-incubated[a]	100
	No pre-incubation[b]	35
80 °C	Pre-incubated[a]	72
	No pre-incubation[b]	65

[a]SIHH and buffer were pre-incubated at the indicated temperatures for 10 min prior to being assayed at the same temperature for 10 min.

[b]Assay at the indicated temperature for 10 min.

Table 2. Comparison of activity of apo SIHH and holo SIHH with and without excess NAD^+

	Specific Activity (μmol min^{-1} mg^{-1})	
	Apo SIHH[a]	Holo SIHH[a]
Synthesis of SIH[b]		
No NAD^+	N.d.[d]	0.48
+ NAD^+ (0.2 mM)	0.63	1.1
Hydrolysis of SIH[c]		
No NAD^+	N.d.[d]	N.d.[d]
+ NAD^+ (0.1 mM)	0.33	0.55

[a]each sample contained 0.4 μg of SIHH

incubated with 0.2 mM Inosine and 0.2 mM Hcy

[c]incubated with 0.1 mM SIH

[d]no detectable activity

Table 3. Kinetic Parameters of SIHH

Substrate	K_M ± SD (mM)	k_{cat} ± SD (s^{-1})	k_{cat}/K_M ($s^{-1}M^{-1}$)
Inosine[a]	0.64 ± 0.4	0.83 ± 0.21	1.3×10^3
Hcy[a]	5.4×10^{-3} ± 0.006	0.83 ± 0.21	1.52×10^5
SIH[b]	0.22 ± 0.11	0.42 ± 0.06	1.9×10^3

[a] this was determined without the addition of NAD^+ in the assay

[b] this was determined in the presence of 0.23 mM NAD^+

Figures

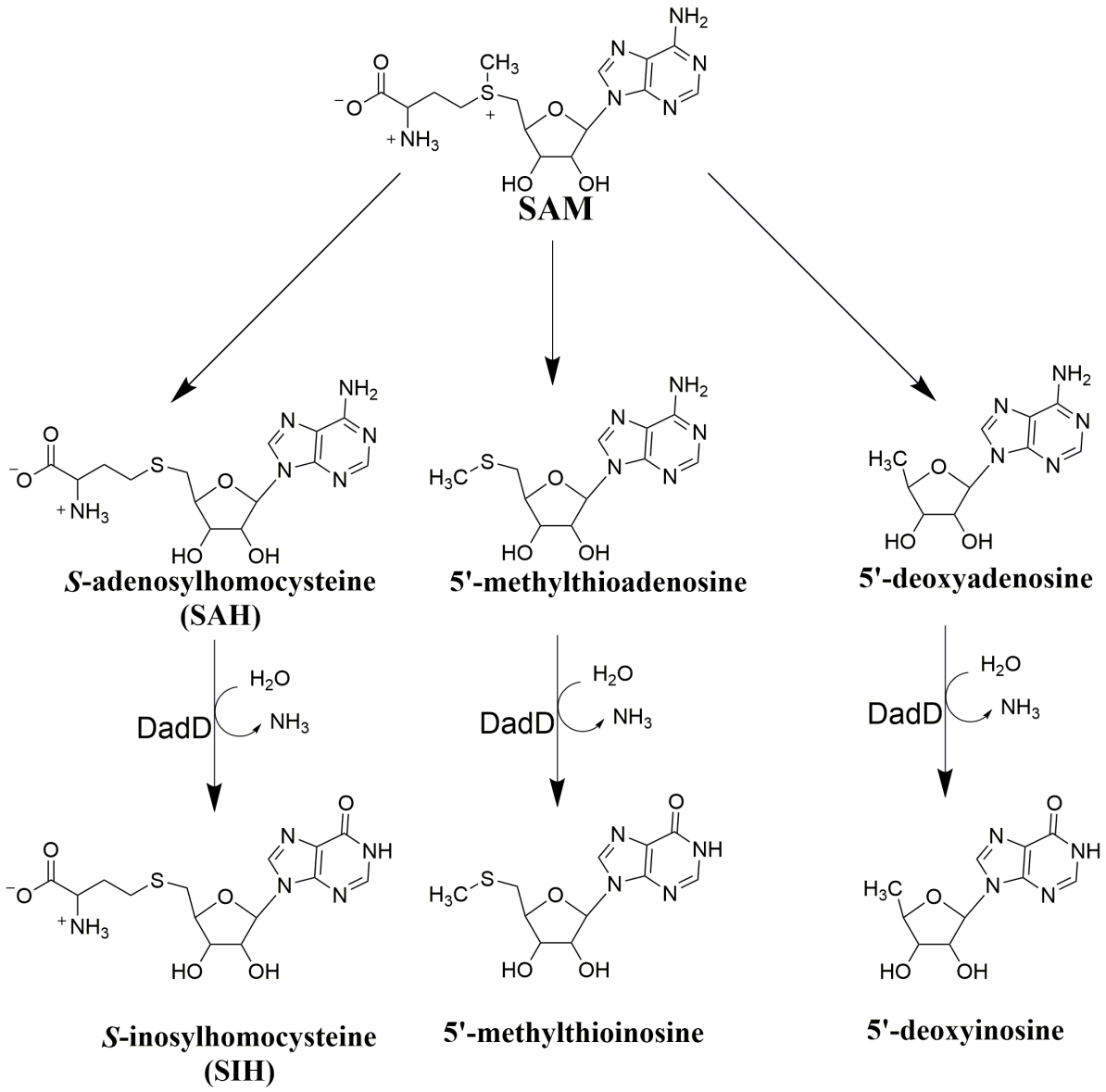

Figure 1. First step in recycling SAM derived enzymatic products in *M. jannaschii.*

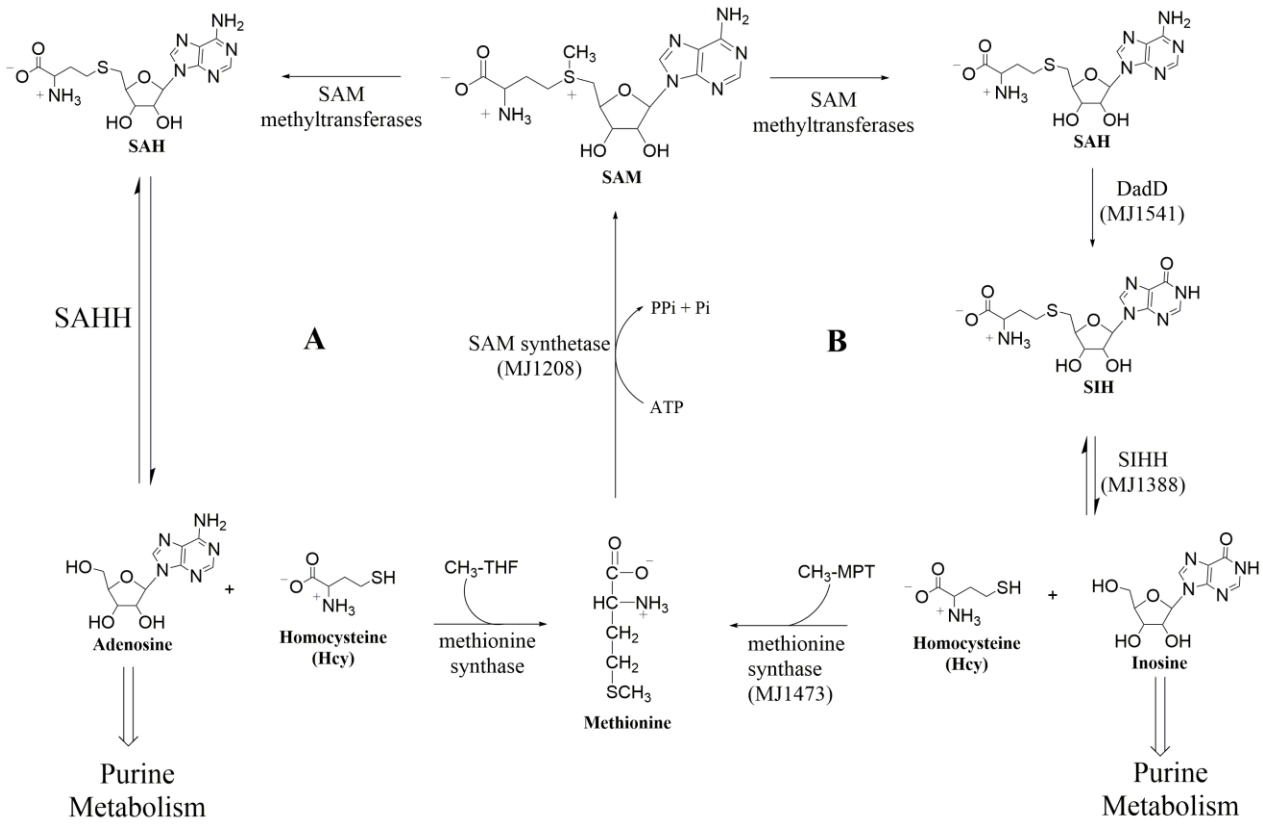

Figure 2. Canonical (A) versus methanogenic (B) pathways for the recycling of SAH to SAM.


42 91
M. jannaschii GITIGMALHLEAKTAVLAETLMEGGAEIAITGCNPLSTQDDVAAACA---------K-KG
M. fervens GITIGMALHLEAKTAVLAETLMEGGAKIAITGCNPLSTQDDVAATCA---------K-KG
M. thermautotrophicus GVTIGSCLHLEPKTINLGLTLQAGGAEVAMTGCNPLSTQDDATAAGA---------K-MG
M. maripaludis GLTIGMALHLEAKTAILAETLLEGGAKIVITGCNPLSTQDDVAAACV---------E-KG
M. vulcanius GITIGMALHLEAKTAVLAETLMEGGAKIAITGCNPLSTQDDVAAACA---------K-KG
A. fulgidus GFTVGMALHVEAKTAVLVRTLVDAGAEVAITGCNPMSTQDDVADALR---------E-SG
S. acidocaldarius GIRIGAVLHVTKETAVLVETLKAGGAEIALAGSNPLSTQDDVAAGLA---------K-NG
P. furiosus GVRIAATLHLEMKTAFLLLTLKAGGAEVSAAASNPLSTQDDVVAALA---------K-AG
A. aeolicus GKKISACLHVTTETANLMRTLKEGGAEVYLTASNPLSTQDDVAAALV---------KYFE
M. tuberculosis GARISGSLHMTVQTAVLIETLTALGAEVRWASCNIFSTQDHAAAAVVVGPHGTPDEP-KG
L. major GAKIAGCLHMTVQTAVLIETLKALGAELRWSSCNIFSTQDNAAAAIA---------K-TG
H. sapiens GARIAGCLHMTVETAVLIETLVTLGAEVQWSSCNIFSTQDHAAAAIA---------K-AG
92 133
M. jannaschii MHVYAWRGETVEEYYENLNKVL-----DHKPDIVIDDGCDLIFLLHT----------
M. fervens MHVYAWRGETVEEYYANLNKVL-----DHKPDIVIDDGCDLIFLLHT----------
M. thermautotrophicus LNMYGWRGETNEEYYENIHRVL-----DHEPEILIDDGADMIFLVHR----------
M. maripaludis MEVYAWRGETNEEYYENLNKVL-----DSNPDIIIDDGADLIFLIHT----------
M. vulcanius MHVYAWRGETVEEYYENLNKVL-----DHKPDIVIDDGCDLIFLLHT----------
A. fulgidus IACYAKRGMDVEEYYEALRNVI-----RAEPDIVIDDGADLIFLLHG----------
S. acidocaldarius IHVYAWRGETEKDYYDNIREIL-----KYEPHVIMDDGGDLHAYVHE----------
P. furiosus VKVYAIRGESREQYYEFMHKAL-----DIRPNIIIDDGADMISLVHK----------
A. aeolicus IPVFAIRGEDRETYYKHLRAVI-----EKEPDVVIDDGADLISTLHK----------
M. tuberculosis VPVFAWKGETLEEYWWAAEQMLTWPDPDKPANMILDDGGDATMLVLRGMQYEKAGVVPPA
L. major VPVFAWKGETDEEYEWCIAQTVKGFSGDGLPNMILDDGGDLTNLVID----------
H. sapiens IPVYAWKGETDEEYLWCIEQTL--YFKDGPLNMILDDGGDLTNLIHT----------
134 169
M. jannaschii ----------KRTELLDNIMGGCEETTTGIIRLKAMEKEGALKFPV
M. fervens ----------KRTELLDNIMGGCEETTTGIIRLKAMEKEGALKFPV
M. thermautotrophicus ----------ERPELLDGIIGACEETTTGINRLRAMAADGALKFPV
M. maripaludis ----------ERTELIGKIMGGCEETTTGIIRLKSMAEEGALKFPV
M. vulcanius ----------KRTELLDNIMGGCEETTTGIIRLKAMEREGALKFPV
A. fulgidus ----------EMESYAEKVKGASEETTTGVIRLRAMEREGVLKFPV
S. acidocaldarius ----------N--NLTSKIVGGTEETTTGVIRLKAMEEEKVLKYPV
P. furiosus ----------ERQEMLDEIWGGSEETTTGVIRLRAMEKAGILKFPV
A. aeolicus ----------EYPGLAEKVLGGMEETTTGVIRLRAMAEQGVLKFPI
M. tuberculosis EEDDPAEWKVFLNLLRTRFETDKDKWTKIAESVKGVTEETTTGVLRLYQFAAAGDLAFPA
L. major ----------RYPELVPKIFGISEETTTGVKNLYKRLSKGNLPISA
H. sapiens ----------KYPQLLPGIRGISEETTTGVHNLYKMMANGILKVPA
170 229
M. jannaschii MDVNDAYTKHLFDNRYGTGQSALDGILRATNLLIAGKTVVVAGYGWCGRGVAMRAKGLGA
M. fervens MDVNDAYTKHLFDNRYGTGQSALDGILRATNLLIAGKTVVVAGYGWCGRGVAMRAKGLGA
M. thermautotrophicus MAVNDAYTKYLFDNRYGTGQSTFDSIMGTTNMLIAGKTVVVCGYGWCGRGIAMRAEGLGA
M. maripaludis VNVNDAYTKHLFDNRYGTGQSAMDGIIRTTNLLIAGKNVVVGGYGWCGRGVASRAAGHGA
M. vulcanius MDVNDAYTKHLFDNRYGTGQSALDGILRSTNLLIAGKTVVVAGYGWCGRGVAMRAKGLGA
A. fulgidus IAVNDAYTKYLFDNRYGTGQSAIDGVIRATNLLMAGKIVVVAGYGWCGRGIAMRARGMGA
S. acidocaldarius IAVNNAFTKYLFDNRIGTGQSTIDGILRATNILIAGKVAVVIGYGWVGRGIASRFKGMGA
P. furiosus IAVNDAYTKHMFDNRYGTGQSTIDGILRATNRLLAGSYFVVAGYGWCGKGVAQRARGMGA
A. aeolicus IAVNDAYTKHMFDNRYGTGQSTIDGILRATNRLLAGSYFVVAGYGWCGKGVAQRARGMGA
M. tuberculosis INVNDSVTKSKFDNKYGTRHSLIDGINRGTDALIGGKKVLICGYGDVGKGCAEAMKGQGA
L. major INVNDSVTKSKFDNLYGCRESLVDGIKRATDVMIAGKTCCVCGYGDVGKGCAAALRAFGA
H. sapiens INVNDSVTKSKFDNLYGCRESLIDGIKRATDVMIAGKVAVVAGYGDVGKGCAQALRGFGA
230 289
M. jannaschii EVVVTEVNPIRALEARMDGFRVMKMEKAAEIGDIFITTTGCKDVIRKEHILKMRNGAILA
M. fervens EVVVTEVNPIRALEARMDGFRVMKMEKAAEIGDIFITTTGCKDVIRKEHMLKMKNGAILA
M. thermautotrophicus SVIVTEVDPIRALEARMDGFRVMKVSDAVKEADILITATGNTDVVSESEFMNMKDGCVMA
M. maripaludis NVIITEVNPIRALEAKMDGFTVLKMEEAAKIGDIFVTTTGCKDILRMEHFLLMKDGAVLS
M. vulcanius EVVITEVNPIRALEARMDGFRVMKMEKAAEIGDIFITTTGCKDVIRKEHILKMKDGAILS
A. fulgidus SVVVTEVDEIRALEAVMDGFRVMRMEDAAKIGDIFITATGNRDIIREEHIRLMKDGAILA
S. acidocaldarius RVIVVESSPFRALEALMDGFDVMTMNRASEIGDIFVTATGNLNVVSRDHILRMKDGAVLA
P. furiosus TVIVVEVDPIKALEARMDGFLVMDMKEAAKIGDIFVTATGNIKCIRREHFELMKDGAIMA
A. aeolicus IVIVTEVDPIKALEARMDGFLVMPMEEAAKLGDFFVTVTGNIHVIRREHFEVMKDGAIVA
M. tuberculosis RVSVTEIDPINALQAMMEGFDVVTVEEAIGDADIVVTATGNKDIIMLEHIKAMKDHAILG
L. major RVVVTEVDPINALQASMEGYQVALVEDVMADAHIFVTTTGNDDIITSDHFPHMRDDAIVC
H. sapiens RVIITEIDPINALQAAMEGYEVTTMDEACQEGNIFVTTTGCIDIILGRHFEQMKDDAIVC
290 345
M. jannaschii NAGHFDNEINKKHLEELAKSIKEVRNCVTEYDLG--NKKIYLLGEGRLVNLACA--DGHP
M. fervens NAGHFDNEINKKHLEELAKSIKEVRNCVTEYDLG--DKKLYLLGEGRLVNLACA--DGHP
M. thermautotrophicus NSGHFNVEINREALEELSRETGKVKEDIEVFIMP-DGRKIYLLAEGRLVNLASERGQGHP
M. maripaludis NAGHFDNEINKNDLKELSKSVKEARFNIEEYDLG--NKKIYLLGEGRLVNLACA--DGHP
M. vulcanius NAGHFDNEINKKELSEMAKSVKEVRKCITEYDLG--DKKIYLLGEGRLVNLACA--DGHP
A. fulgidus NAGHFNVEIDIPALERMAKAKREARKYVTEYDLG--DKRVYLLAEGRLVNLVAA--DGHP
S. acidocaldarius NSGHFNVEIDVKGLKEISVETREVRQNLEEYKLR-NGKRIYLLADGRLVNLVAA--EGHP
P. furiosus NAGHFDVEIWKPDLEKLAVEINNPRPNVTEYKLK-DGRRLYLLADGRLVNLVAA--DGHP
A. aeolicus NSGHFNVEIDIPALEEMAVEKREIRKEVTEYKLK-DGRRIYLLAEGRLVNLAAA--EGHP
M. tuberculosis NIGHFDNEIDMAGLERSGATRVNVKPQVDLWTFGDTGRSIIVLSEGRLLNLGNA--TGHP
L. major NIGHFDTEIQVGWLEANAKEHVEIKPQVDRYTME-NGRHIILLAKGRLVNLGCA--SGHP
H. sapiens NIGHFDVEIDVKWLNENAVEKVNIKPQVDRYRLK-NGRRIILLAEGRLVNLGCA--MGHP
346 399
M. jannaschii CEVMDMSFANQALAAEYILKNHEK--L----EPRVYNIPYEQDLMIASLKLKAMGIEIDE
M. fervens CEVMDMSFANQALAAEYILKNHDK--L----EPRVYNIPYEQDLMIASLKLKSMGIEIDE
M. thermautotrophicus AEIMDMSFAMQALSARHLLQ--EK--P----DPGVYRAPDEIDLMVARMKLDAMGIEIDE
M. maripaludis CEVMDMSFANQALSAKFIKENKGK--L----ENEVYEIPYEQDFKIALLKLHSMGADIDE
M. vulcanius CEVMDMSFANQALSAEYILKNHEK--L----EPRVYRIPYEQDLMIASLKLNAMGIEIDE
A. fulgidus VEVMDMSFANQALAAKYIAENWQK--L----ERKVYRLPEELDRMVARMKLESMGVEIDQ
S. acidocaldarius SEVMDLSFCNQALSVEHLIKNKGK--L----ENKVYNVPIEIDEQVARLKLKALGIEIEE
P. furiosus AEIMDMSFALQAKAAEYIKDNHER--L----EPKVYILPREIDEMVARIKLESMGIKIEE
A. aeolicus ASVMDMSFSNQALSAEYIVKHHKE--L----EKKVYRVPREIDEAVARLKLNALGIKIDE
M. tuberculosis SFVMSNSFANQTIAQIELWTKNDE--Y----DNEVYRLPKHLDEKVARIHVEALGGHLTK
L. major SFVMSNSFTNQVLAQIELWSNRDNGKYPRGDKAGVFFLPKALDEKVAALHLAHVGAKLTK
H. sapiens SFVMSNSFTNQVMAQIELWTHPDK--Y----PVGVHFLPKKLDEAVAEAHLGKLNVKLTK
400 415
M. jannaschii LTKEQKKYLEDWREGT--------
M. fervens LTEEQKRYLEDWREGT--------
M. thermautotrophicus LTEKQRLYLENWEEGT--------
M. maripaludis LSPEQRKYLSDWKEGT--------
M. vulcanius LTEEQKRYLEDWKEGT--------
A. fulgidus LTEEQVRYLSDWRCGT--------
S. acidocaldarius LTIEQKEYIKQWKYGT--------
P. furiosus LTEEQKKYLESWEHGT--------
A. aeolicus LTEEQKKYLSSWEMGT--------
M. tuberculosis LTKEQAEYLGVDVEGPYKPDHYRY
L. major LTPKQAEYINCPVNGPFKPDHYRY
H. sapiens LTEKQAQYLGMSCDGPFKPDHYRY

Figure 3. Sequence alignment of SIHH with homologs. Blue highlighted residues are those involved in substrate binding, green highlighted residues are those involved in binding the NAD^+, and the bolded residues are not highly conserved for either substrate or NAD^+ binding. The general base histidine is indicated by an asterisk and the threonines implicated in phosphorylation are highlighted by red brackets. The accession numbers for the sequence alignment are as follows in order from top down: Q58783 *M. jannaschii,* C7P826 *Methanocaldococcus fervens,* O27673 *Methanothermobacter thermautotrophicus,* Q6LYR8 *Methanococcus maripaluids,* C9RID4 *Methanocaldococcus vulcanius,* O28279 *Archaeoglobus fulgidus,* Q4JAZ7 *Sulfolobus acidocaldarius,* P50251 *Pyrococcus furiosus,* O67240 *Aquifex aeolicus,* P9WGV3 *Mycobacterium tuberculosis* (pdb 2ZIZ), Q4Q124 *Leishmania* (pdb 3G1U), P23526 *Homo sapiens* (pdb 2NJ4).

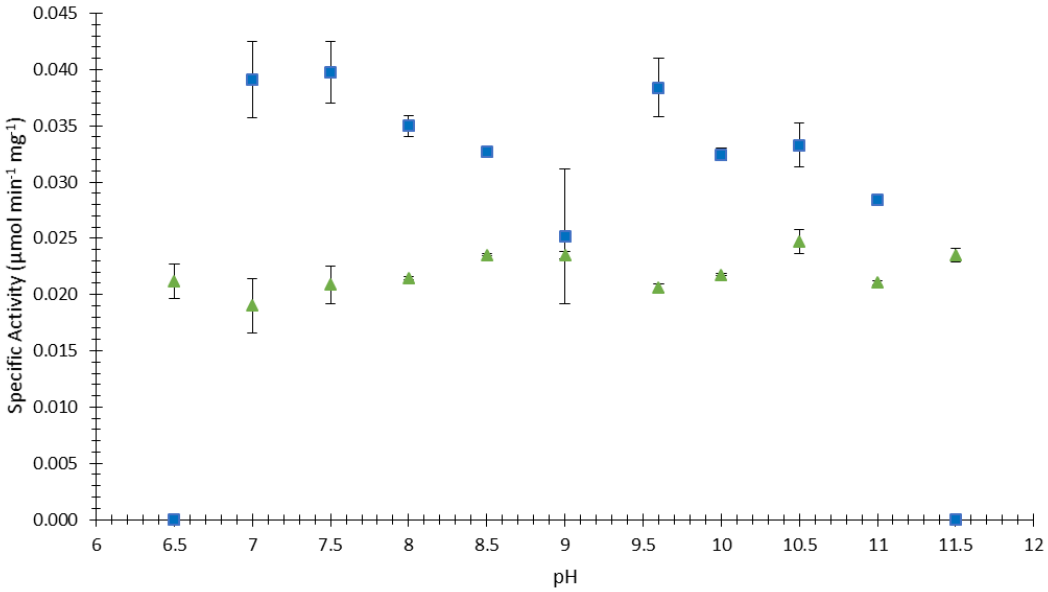

Figure 4. pH profile of SIHH activity. The blue squares represent the pH profile in the synthesis of SIH and the green triangles in the hydrolysis of SIH in the presence of 0.23 mM NAD^+.

Chapter 2: Promiscuity of Methionine Salvage Pathway Enzymes in *Methanocaldococcus jannaschii* and *Methanosarcina acetivorans*

Danielle V. Miller[a], Benjamin J. Rauch[b]*, Kim Harich[a], Huimin Xu[a], John J. Perona[bc], and Robert H. White[a]#

Department of Biochemistry, Virginia Polytechnic Institute and State University, Blacksburg, Virginia, USA[a]; Department of Chemistry, Portland State University, Portland, Organ, USA[b]; Department of Biochemistry and Molecular Biology, Oregon Health and Science University, Oregon, USA[c]

Running Head: Methionine Salvage Pathway in Methanogens

#Address correspondence to Robert H. White, rhwhite@vt.edu

*Present address: Department of Microbiology and Immunology, University of California, San Francisco, San Francisco, CA, USA; Quantitative Biosciences Institute, QBI, University of California, San Francisco, San Francisco, CA, USA.

Abstract

The methionine salvage pathway (MSP) is critical for regeneration of *S*-adenosyl-L-methionine (SAM), which is a widely used cofactor involved in many essential metabolic reactions. In aerobic organisms the MSP has been completely elucidated, however it relies on oxygen. Since anaerobic organisms would not be exposed to oxygen an alternative pathway must be present. Here we sought to establish if the two annotated MSP genes from *Methanocaldococcus jannaschii*: methylthioinosine phosphorylase (MTIP) encoded by MJ0060 and methylthioribose 1-phosphate isomerase (MTRI) encoded by MJ0454 indeed function in the MSP. Recombinant MTIP is shown to be active with six different purine nucleosides, and is postulated to function as a general purine nucleoside phosphorylase involved in both the anaerobic MSP (AnMSP) and in purine salvage. Recombinant MTRI demonstrated activity with methylthioribose 1-phosphate generated from phosphorolysis of methylthioinosine (MTI) by MTIP. Additionally, MTIP and MTRI are proposed to be functioning in a novel pathway for recycling the 5-deoxyadenosine moiety of SAM for the biosynthesis of 6-deoxy-5-ketofructose 1-phosphate, and essential intermediate in aromatic amino acid biosynthesis. We also utilized a strain of *Methanosarcina acetivorans* dependent on either methionine or homocysteine for growth to identify potential intermediates in the AnMSP. Growth recovery experiments of the *M. acetivorans* homocysteine auxotroph Δma1821-22Δoahs (HcyAux) were performed with methylthioadenosine (MTA), MTI, methylthioribose, 2-keto-(4-methylthio)butyric acid, 2-hydroxy-4-methylthiobutyric acid, methioninol, 3-(methylthio)propanoic acid, and 3-mercaptopropanoic acid. Among these metabolites, only 2-keto-(4-methylthio)butyric acid allowed growth of M. *acetivorians* HcyAux in the absence of homocysteine. These data suggest that the known enzymes involved in the MSP are promiscuous for alternative substrates that implicates in the salvage of 5'-deoxyadenosine and purines.

Importance

In the anaerobic methanogenic archaea *Methanocaldococcus jannaschii* and *Methanosarcina acetivorians* canonical metabolic pathways are often missing or incomplete and substituted by unique pathways. Here the methionine salvage pathway for methylthioadenosine, produced from *S*-adenosyl-L-methionine, for which more than half of the steps are unknown in methanogens is discussed. The only two annotated enzymes from this pathway are not specific for methionine salvage pathway metabolites, suggesting that the enzymes are involved in additional metabolic routes. Growth recovery experiments of *M. acetivorans* establish that methylthioadenosine is inhibitory to growth and identify an intermediate of the methionine salvage pathway. Identification of the pathways and enzymes involved in the unique pathways in the methanogens will give insight into the biochemical reactions that were occurring when life originated.

Introduction

S-Adenosyl-L-methionine (SAM) is an essential cofactor for life. Specifically SAM is required for the production of polyamines following decarboxylation to *S*-adenosylmethioninamine and transfer of the propylamine moiety to putrescine generating methylthioadenosine (MTA) (Figure 1)(1–3). MTA has been shown in many organisms to be a strong feedback inhibitor of SAM dependent enzymes (4). MTA is salvaged to methionine, which prevents feedback inhibition of polyamine biosynthesis (5). The salvage of MTA to methionine is known as the methionine salvage pathway (MSP) and was first identified in rat liver(6) and *Candida utilis*(7) in the early 1980s.

The salvage of methionine typically proceeds either by removal of the nucleobase followed by phosphorylation producing methylthioribose 1-phosphate (MTR 1P) by a MTA nucleosidase (MtnN) and methylthioribose (MTR) kinase (Figure 1, black top)(8). Alternatively, MTA can be directly transformed to MTR 1P by phosphorolysis by a MTA phosphorylase (MtnP) (Figure 1, black middle)(9). MTR 1P is then isomerized to methylthioribulose 1-phosphate (MTRu 1P) by an MTR 1P isomerase (MTRI or MtnA) (Figure 1)(10). The subsequent conversion of MTRu 1P to methionine proceeds by dehydration at C4 catalyzed by MtnB(11), enolization, and de-phosphorylation at C1 to form 1,2-hydroxy-3-keto-5-methylthiopentene (Figure 1, bottom black)(12, 13). The final two steps proceed via a dioxygenase (MtnD)(14) forming the keto-acid of methionine followed by transamination to methionine (Figure 1)(15). Though this pathway is considered to be operating in aerobic organisms with slight variations, the MSP in anaerobic organisms is doubtful given the explicit requirement for molecular oxygen by MtnD(16).

Determining the anaerobic pathway for methionine salvage is of further interest because many anaerobic bacteria and archaea lack the final genes: *mtnB, mtnW, mtnX, mtnC*, and *mtnD*, (Figure 1, bottom black). The lack of the final genes from the aerobic MSP indicate the anaerobic MSP proceeds through different intermediates and may utilize different enzymes. Recently it has been demonstrated that the facultative anaerobic bacterium *Rhodospirillum rubrum* utilizes a isoprenoid shunt pathway for the anaerobic MSP (isoprenoid shunt MSP, Figure 1, green)(17, 18). The proposed isoprenoid shunt MSP in *R. rubrum* is proposed to function with two enzymes described as an isomerase and a sulfurylase. The isomerase is homologous to ribulose 1,5-bisphosphate carboxylase/oxygenase (RuBisCO)-like protein and

isomerizes the shared intermediate of all three proposed pathways, MTRu 1P (Figure 1, green). RuBisCO-like proteins belong in the RuBisCO class IV family and lack essential residues for it to be a classical RuBisCO protein and have instead been found to function as the enolase (MtnW) in the MSP in *B. subtilis*(19). *M. jannaschii* and *M. acetivorans* contain type III RuBisCOs in their genomes, which have recently proposed to be involved in an AMP catabolism pathway(20). Additionally, disruption of the RuBisCO gene in *Thermococcus kodakarensis* did not demonstrate a phenotype that required methionine and the authors concluded it was not involved in the MSP in archaea(20). The second enzyme, a cupin protein or sulfurylase(17, 18), is proposed to be involved in the isoprenoid shunt MSP, but shares no homologue to proteins in either *M. jannaschii* or *M. acetivorans*. Furthermore, neither *M. jannaschii* nor *M. acetivorans* utilize the non-mevalonate pathway(21) for the production of isoprenoids and thus, would not have the necessary enzymes to metabolize 1-deoxyxylulose 5-phosphate (DXP) (Figure 1, green). These differences between *R. rubrum, M. jannaschii*, and *M. acetivorans* metabolism make it unlikely that methanogens proceed through the proposed isoprenoid shunt (17, 18) to anaerobically salvage MTA.

To determine the AnMSP in *M. jannaschii* the annotated enzymes were investigated. Here we characterize the only two annotated enzymes involved in the AnMSP; a methylthioinosine phosphorylase (MTIP) encoded by MJ0060 and a methylthioribose 1-phosphate isomerase (MTRI) encoded by MJ0454 (Figure 1). Furthermore to identify potential intermediates in the AnMSP various postulated intermediates were fed to *M. acetivorians* homocysteine auxotrophs (HcyAux) that require either homocysteine or methionine for growth(22). Feeding of various intermediates to the *M. acetivorians* HcyAux demonstrated that only 2-keto-(4-methylthio)butyrate (KMTB) was able to restore the growth and that MTA is inhibitory. These data suggest that methylthioinosine (MTI), methylthioribulose 1-phosphate (MTRu 1P) and KMTB are intermediates of the AnMSP in methanogens (Figure 1).

Additionally, the MTIP and MTRI enzymes were examined for their ability to utilize the 5-deoxyribose sugar moieties of SAM. Previous work from our laboratory has demonstrated that the first enzyme involved in the recycling of SAM is a 5'-deoxyadenosine deaminase (DadD) that was able to utilize MTA, 5'-deoxyadenosine (5'-dA) and *S*-adenosylhomocysteine(23). Data is presented here that suggest the recycling of MTA and 5'-dA utilize the same initial enzymes, DadD, MTIP, and MTRI (Figure 2). The recycling of 5'-dA is another essential

metabolic route to prevent the inhibition of radical SAM enzymes. Radical SAM enzymes are well known to be inhibited by the 5'-dA, which is produced from the reductive cleavage of SAM generating methionine and the 5'-dA radical(2, 24). Transfer of the 5'-dA radical to the substrate generates 5'-dA, which has been demonstrated to be a substrate of MtnN(24). However, there is little information in the literature as to how the 5'-dA moiety of SAM is recycled. We have proposed that the 5'-deoxyribose moiety could be a source of deoxysugars for the production of 6-deoxy-5-ketofructose 1-phosphate (DKFP) (Figure 3) (23).

Materials and methods

Chemicals. All chemicals were obtained from Sigma/Aldrich unless otherwise noted. Methioninol and 2-hydroxy-4-methylthiobutyric acid were obtained from Santa Cruz. 2-Mercaptopropanoic acid and 3-(methylthio)propanoic acid were both obtained from Alfa Aesar.

Synthesis of 5'-deoxyinosine. 5'-Deoxyinosine (5'-dI) was prepared from inosine via of 5'-deoxy-2',3'-*O*-(1-methylethylidene)inosine as previously described(25). The final product was deprotected by hydrolysis in 50% formic acid for 16 hr at room temperature and purified by preparative thin layer chromatography (TLC). Liquid chromatography-electrospray ionization-mass spectrometry (LC-ESI-MS) showed the product to consist of one single peak having the absorbance spectrum of inosine, λ_{max} = 250 nm, with a MH^+ = 253.3 *m/z*, $(M + Na)^+$ = 275.3 *m/z*, $(M + K)^+$ = 275.3 *m/z*, $(M - H)^-$ = 251.3 *m/z* and a base peak ion at 137 *m/z* for protonated hypoxanthine $(HX + H)^+$. LC-ESI-MS was performed on an AB Sciex 3200 Q Trap mass spectrometer attached to an Agilent 1200 series liquid chromatograph with a Kromasil 100-5-C18 column (4.6 x 250 mm) was used for the identification of 5'-dI. Buffer A was 25 mM ammonium acetate and buffer B was methanol. The flow rate was set at 0.7 mL/min and the elution profile consisted of a 3 min wash at 100% A, followed by a 15 min linear gradient to 65% B. The injection volume was 15 µl. MS and MS-MS data were acquired in negative enhanced resolution and enhanced product ion mode with electrospray ionization set at -4500 V at a temperature of 400°C. The curtain gas was set at 35, and ion source gas 1 and ion source gas 2 were 60 and 50, respectively. Analyst software (Applied Biosystems/MDS SCIEX) was used for system operation and data processing.

Enzymatic synthesis of 5'-deoxyinosine and methylthioinosine. The enzymatic preparation of 5'-dI and MTI was done as previously described by the enzymatic deamination of 5'-deoxyadenosine (5'-dA) and MTA (23). Reaction mixtures containing 5'-dA or MTA at a

concentration of 1 to 10 mM were incubated with 18 ng of 5'-deoxyadenosine deaminase (DadD) overnight at 25 ^{o}C in 50 mM 1,3-bis[tris(hydroxymethylmethylamino]propane (BIS TRIS propane) buffer (pH 9.0) (23). 5'-dA or MTA were completely converted to 5'-dI or MTI as measured by HPLC (described below).

Preparation of methylthioribose from MTA. Preparation of MTR was done by heating MTA in acid to hydrolyze the adenine moiety from the methylthioribose. MTA (20 mg) was heated in 2 mL 1 M HCl for 10 min at 100^{o}C. Following heating the sample was completely evaporated to dryness to remove the HCl. The remaining sample was then re-suspended in 2 mL water (pH adjusted to 7 with 1 M NaOH) and filtered. The concentration of MTR was calculated to be 27 mM on the basis of the amount of MTA used. The production of MTR was verified by reduction of a portion of the sample with 1-2 mg of sodium borohydride (NaBH4) and at room temperature for 1-2 hours. To desalt the sample, it was first passed through a column of Dowex-50W-X8 (H+) 200-400 mesh (2 x 0.5 cm). The borate was removed by dissolving the samples in methanol and then evaporated to dryness under a stream of N_2 while being heated in a water bath at ~100 ^{o}C. Next the samples were run through a column of Dowex-1-X10 (OAc-) 200-400 mesh (2 x 0.5 cm) to remove sodium. After drying the samples by evaporation with a stream of nitrogen gas while being heated at 100 ^{o}C in a water bath, the resulting residue was reacted with 60 µL of a mixture of pyridine, hexamethyldisilazane, and chlorotrimethylsilane (9:3:1, vol/vol/vol) for 1-2 min at 100 ^{o}C to generate the TMS derivative. TMS derivatives were separated on a Phenomenex Zebron ZB-5MS plus (30 m x 0.32 mm x 0.25 µm) film capillary column installed in a HP5890 gas chromatograph. The oven temperature was programmed from 80 ^{o}C to 270 ^{o}C at 8 ^{o}C per minute. A 7 psi helium carrier gas was supplied and split-less injection (200 ^{o}C) was employed. The column effluent was introduced into the electron impact ion source (200 ^{o}C) of a VG70S mass spectrometer, which was scanned from 50 to 400 amu at 1 second per decade. Mass spectral data was acquired and processed with a VG Opus data system.

Cloning, overexpression, and purification of *M. jannaschii* MJ0060 and MJ0454 gene products in *E. coli*. The MJ0060 gene (UniProt accession number Q60367) and the MJ0454 gene (UniProt accession number Q57896) were amplified by PCR from genomic DNA using oligonucleotide primers for MJ0060 and MJ0454 are shown in Table S1. PCR amplification was performed as described previously (26) using a 55 ^{o}C annealing temperature

for both. Purified PCR products were digested with Nde1 and BamH1 restriction enzymes and ligated into compatible sites in vector pT7-7. The sequence of the resulting plasmids pMJ0060 and pMJ0454, were verified by DNA sequencing. The plasmids, pMJ0060 and pMJ0454, were then transformed into *E. coli* strain BL21-CodonPlus(DE3)-RIL cells (Stratagene). The transformed cells were grown in LB medium (200 mL) supplemented with 100 µg/mL ampicillin at 37 ^{o}C with shaking until they reached an OD600 of 1.0. Recombinant protein production was induced by addition of lactose to a final concentration of 28 mM (27). After an additional 2 hours of culture, the cells were harvested by centrifugation (4,000 *x g*, 5 min) and frozen at -20 ^{o}C. Induction of the desired protein was confirmed by SDS-polyacrylamide gel electrophoresis (SDS-PAGE) analysis of total cellular proteins.

The frozen *E. coli* cell pellet containing the desired protein (~0.4 g wet wt) was suspended in 3 mL of extraction buffer (50 mM N-[tris(hydroxymethyl)methyl]-2-aminoethanesulfonic acid (TES), pH 7.0, 10 mM $MgCl_2$, 20 mM dithiothreitol (DTT)) and lysed by sonication. The resulting expressed proteins were found to remain soluble after heating the resulting cell extracts containing the MJ0060 and MJ0454 gene products for 20 min at 80 ^{o}C and 70 ^{o}C, respectfully, followed by centrifugation (16,000 *x g* for 10 min) to remove denatured and insoluble *E. coli* proteins. Purification was performed by anion-exchange chromatography of the heated soluble fractions on a MonoQ HR column (1 x 8 cm; Amersham Bioscience) using a linear gradient from 0 to 1 M NaCl in 25 mM Tris buffer (pH 7.5), over 55 min at a flow rate of 1 mL/min. Fractions of 1 mL were collected and the desired protein was identified through SDS-PAGE. The protein bands corresponding to the predicted molecular mass of the MJ0060 gene product (~28 kDa) and MJ0454 gene product (~36 kDa) were excised from the polyacrylamide gel and prepared for matrix assisted laser desorption ionization-mass spectrometry (MALDI-MS) as previously described (23). Protein concentrations were determined by Bradford analysis (28).

The MTIP (encoded by MJ0060) and MTRI (encoded by MJ0454) derived proteins were efficiently expressed in *E. coli* as measured from the SDS-PAGE analysis of the total proteins in the *E. coli* cells after expression. MALDI analysis of the tryptic peptides recovered from the hydrolysis of the expressed protein band confirmed the presence and purity of each desired protein. After sonication of the *E. coli* cell pellet (~1 g wt weight suspended in 2 mL of extraction buffer) and centrifugation (14,000 $\times$ *g*, 5 min), SDS-PAGE analysis of the soluble

material and the pellet demonstrated that most of the expressed MJ0060 and MJ0454 proteins were found in the soluble extracts. Heating 200 µl portions of the resulting crude soluble extract for 10 min at different temperatures indicated that MJ0060 and MJ0454 remained soluble up to 80 °C and 70 °C, respectively, based on SDS-PAGE analysis. Thus the first step in the purification of each protein from the cell extracts involved heating the MJ0060 cell extracts at 80 °C for 20 min and the MJ0454 at 70 °C for 20 min followed by centrifugation (14,000 $\times g$, 10 min) prior to purification of soluble proteins on MonoQ. This purification produced one peak of activity eluting at 0.4 M NaCl for each gene product that contained a single band upon SDS-PAGE analysis. MALDI analysis of the tryptic digests of the excised bands from the SDS-PAGE gel identified MTIP from six identified unique peptides and MTRI from eight identified unique peptides.

Measurement of native molecular weight of MTIP and MTRI. The native molecular weight of MTIP and MTRI were determined by size exclusion chromatography (SEC) as described previously using a Superose 12 HR column (29). The following standards were used to generate the standard curve for MTRI: blue dextran (2000 kDa), conalbumin (77.5 kDa), bovine serum albumin (66 kDa), carbonic anhydrase (29 kDa), and cytochrome c (14 kDa). The same standards where used with MTIP but with the addition of β-amylase (200 kDa).

Standard assay, pH optima, and substrate specificity for MTIP. The standard enzymatic assay for MTIP measured the release of the purine base and consisted of 0.4 µg of MTIP with 0.2 mM nucleoside, 40 mM sodium phosphate in 100 µL 0.1 M TES buffer at pH 7.0. The mixture was incubated at 37 ^{o}C for 15 min to assay the phosphorolysis of the nucleoside. It was found that when assayed at 70 ^{o}C the reaction came to equilibrium between substrate and product formation within 5 min. The use of lower concentrations of substrate did not adjust the observed equilibrium, so a lower temperature was used to slow the reaction. The pH optimum was determined over the pH range 6.5 to 11.5 using 25 mM piperazine-*N, N'*-bis(2-ethanesulfonic acid), *N*-tris(hydroxymethyl)methyl-3-aminopropanesulfonic acid, and *N*-cyclohexyl-3-aminopropanesulfonic acid (PIPES, TAPS, CAPS) buffer system with 50 mM phosphate, using the standard assay with a final concentration of 0.2 mM MTI in 100 µL. The activity of MTIP was examined with the following nucleosides in the standard assay: MTA, 5'-dA, adenosine, MTI, 5'-dI, inosine, 2'-deoxyinsoine, guanosine, and 2'-deoxyguanosine. The

reaction was stopped upon addition of 5 μL of 2 M perchloric acid, briefly centrifuged (~7500 × g, ~2 min), then analyzed by HPLC as described below.

To determine substrate specificity of MTIP, the kinetic parameters of MTIP were determined using 4 μg MTIP with 5'-dI (0 to 0.4 mM), MTI (0 to 0.3 mM), inosine (0 to 0.1 mM), 2'-deoxyinosine (0 to 0.2 mM), guanosine (0 to 1 mM), or 2'-deoxyguanosine (0 to 2 mM). The buffer used was 0.5 M sodium phosphate buffer (pH 7.0) for MTI and 5'-dI, 0.1 M sodium phosphate buffer (pH 7.0) for inosine, guanosine, 2'-deoxyinosine, and 2'-deoxyguanosine. The reactions were all incubated at 37 °C for 15 min, quenched 5 μL of 2 M perchloric acid or hydrochloric acid, and analyzed by HPLC.

Identification of sugar containing products from the MTIP catalyzed reactions. To establish the production of 5-deoxyribose 1-phosphate (5-dR 1P) and methylthioribose 1-phosphate (MTR 1P) as the enzymatic product of the MTIP reaction they were derivatized with NBHA which allowed for their detection by UV-HPLC and LC-UV-ESI-MS. Following the standard assay for MTIP with 5'-dI or MTI (0.4 mM) the reactions were titrated to pH 4.0 with 10 M acetic acid and a 10-fold molar excess (~4 mM) of *O*-(4-nitrobenzyl)hydroxylamine (NBHA) was added over substrate. After incubation at 100 °C for 30 min the samples were cooled to room temperature then briefly centrifuged (~7500 × *g*, 2 min) prior to HPLC and LC-UV-ESI-MS analysis (described below).

Characterization of MTRI substrate specificity and mechanism. To assay for MTRI activity, the MTIP reaction was coupled to the MTRI reaction. The products were derivatized with NBHA and analyzed by HPLC and LC-UV-ESI-MS (see below). The standard assay used for the MTIP/MTRI coupled assay was 0.4 μg MTIP, 5 μg of MTRI in 100 μL 0.1 M TES (pH 7.0) with a final concentration of 0.4 mM 5'-dI or MTI, 40 mM phosphate and 20 mM DTT followed by incubation at 60 °C for 50 min. MTRI reaction was found to be dependent on DTT (20 mM) for activity and thus was included in all assays. The substrate specificity of MTRI was determined using the coupled assay as described with varying concentrations of 5'-dI (0 to 1 mM) and MTI (0 to 0.6 mM). The ability of MTRI to use 5-deoxyribose (5-dR) and ribose 5-phosphate (ribose 5P) was also analyzed. The reactions were titrated to pH 4.0 with 10 M acetic acid and 4 mM NBHA was added for derivatization followed by incubation at 100 °C for 30 min. The samples were cooled to RT then briefly centrifuged (~7500 *x g*, 2 min) prior to HPLC and LC-UV-ESI-MS analysis.

The mechanism of MTRI catalyzed reaction was probed by following the incorporation deuterium from the D_2O included in the reaction solvent into the product of MTRI, 5-dRu 1P. This was done by incubation of 0.4 μg MTIP, 5 μg of MTRI in 100 μL 0.1 M TES (pH 7.0), with a final concentration of 0.4 mM 5'-dI, 40 mM phosphate and 20 mM DTT followed by incubation at 60 ^oC for 50 min in 20% D_2O. The reactions were derivatized with NBHA as described above and then analyzed by LC-UV-ESI-MS analysis of the resulting derivatives looking for deuterium incorporation or by HPLC described below.

HPLC and LC-UV-ESI-MS analysis. Chromatographic analysis of each substrate and product of the MTIP catalyzed reactions were performed on a Shimadzu HPLC System with a C18 reverse phase column (Shimadzu 50 × 4.6 mm, 5 μm particle size) equipped with photodiode array detector and operated at room temperature (RT). The elution profile consisted of 5 min at 95% sodium acetate buffer (25 mM, pH 6.0, 0.02% NaN_3) and 5% methanol followed by a linear gradient to 50% sodium acetate buffer/50% methanol over 9 min at 0.5 mL/min. The nucleotide and nucleoside elution times can be found in Table S2. The absorbance at 260 nm for adenine and adenosine containing compounds, 250 nm for hypoxanthine and inosine containing compounds, 246 nm for guanine, and 253-254 nm for guanosine analogues using ε_{260} = 14.9 x 10^3 $M^{-1}cm^{-1}$ for adenosine, ε_{260} = 13.4 x 10^3 $M^{-1}cm^{-1}$ for adenine, ε_{250} = 12.3 x 10^3 $M^{-1}cm^{-1}$ for inosine, ε_{250} = 10.7 x 10^3 $M^{-1}cm^{-1}$ for HX, ε_{246} = 10.7 x 10^3 $M^{-1}cm^{-1}$ for guanine, ε_{253} = 13.6 x 10^3 $M^{-1}cm^{-1}$ for guanosine, and ε_{254} = 13.0 x 10^3 $M^{-1}cm^{-1}$ for 2'-deoxyguanosine (30) was used for peak identification. Quantitation was based on peak areas.

HPLC analysis of the NBHA derivatized samples was done on the same HPLC system but using a C18 reverse phase column (Kromasil 250 × 4.6 mm, 5 μm particle size). The elution profile consisted of 5 min at 100% sodium acetate buffer (25 mM, pH 6.0, 0.02% NaN_3) followed by a linear gradient to 100% methanol over 50 min at 0.5 mL/min. Under these chromatographic conditions the NBHA derivatized sugars, measured at 270 nm, eluted with the retention times indicated in Table S2. Each derivatized sugar produced two chromatographic peaks, one for the cis and one for the trans oximine derivative. For clarity only data for the major peak was reported in Table S2. Quantitation was based on the peak areas at 270 nm for the NBHA derivative (ε_{270} = 9490 $M^{-1}cm^{-1}$)(30).

Analysis of the NBHA derivatives was also done by LC-UV-ESI-MS (Agilent 1200 HPLC series in combination with an AB Sciex 3200 Q TRAP) using a Waters XTerra reverse

phase C18 column (5 μM, 3.9 x 150 mm) with an injection volume between 5-25 μL. Elution of the derivatives was done using 25 mM ammonium acetate (solvent A) and methanol (solvent B) with a total flow of 0.5 mL per min and the following gradient profile: (t (min), %B): (0.01, 0), (10.00, 65), (10.01-13.00, 95), (13.01-15.00, 0). Electrospray ionization was employed at 4500 volts and a temperature of 600 ^{o}C. Curtain gas, gas 1, and gas 2 flow pressures were 40, 60 and 50 psi, respectively. Desolvation, entrance, and collision cell potentials were 35, 12, and 10 volts, respectively. Mass analysis was performed in the Enhanced MS (EMS) mode, and positive ions were measured in the mass range 100-500 Da.

Growth recovery of homocysteine auxotrophs from *Methanosarcina acetivorans*. All cellular cultures were conducted with high salt (HS) growth media to promote single-cell growth (31, 32). Methanol was used throughout as the methanogenic growth substrate. Cultures were maintained at 37 °C in 18 mm aluminum-sealed Balch tubes, containing 5-10 ml liquid growth media. Optical density measurements were taken by directly inserting the culture tubes into a spectrophotometer (Turner model 330). Prior to individual growth experiments, homocysteine-prototrophic (WWM75)(33) and homocysteine-auxotrophic (BJR10)(22) *Methanosarcina acetivorans* strains were grown to high optical density (0.5 < A600 < 1.2) on HSMet, a sulfide-rich, methionine-containing growth medium(22). To initiate growth experiments, HSMet cultures were diluted 50-fold into culture tubes containing the HSDTT growth medium.(22) Since the HSDTT medium lacks a viable sulfur sources, it was supplemented with sodium sulfide (0.2-2 mM) and the proposed intermediates for methionine salvage to support growth, prior to inoculation. The eight potential methionine salvage intermediates included were MTA (0.2 and 0.02 mM), MTI (0.2 mM), MTR (2 mM), 2-keto-4-(methylthio)butyrate (KMTB, 2 mM), methioninol (4 mM), 2-hydroxy-4-methylthiobutyric acid (HMTB, 2 mM), 3-mercaptopropanoic acid (SP, 2 mM), and 3-(methylthio)propanoic acid (MeSP, 2 mM).

Results and discussion

MTIP functions as an enzyme in the AnMSP and purine salvage. The first phosphorylase specific for MTI was described from *Pseudomonas aeruginosa*(34), which was demonstrated to be active with both inosine and adenosine (34). Unlike *P. aeruginosa* MTIP, the *M. jannaschii* enzyme preferred hypoxanthine (HX)-containing nucleosides and was unable to utilize MTA or adenosine as substrates (Table 1). MTI in *P. aeruginosa* is proposed to be

produced via deamination of MTA by an adenosine deaminase (34), similar to *M. jannaschii* where MTI is the deamination product of MTA catalyzed by DadD, which is proposed to be functioning in place of an adenosine deaminase in *M. jannaschii* (Figure 2A)(23).

The *M. jannaschii* MTIP catalyzed reaction came to equilibrium with ~70% conversion of substrate to product within 5 min at 70 ^{o}C with 0.2 mM 5'-dI with excess sodium phosphate (pH 7) and 0.4 µg MTIP. The equilibrium constant of the nucleoside phosphorylase catalyzed reaction is known to favor the formation of the nucleoside (35, 36). Thus, in order to monitor the reaction in the phosphorolysis direction the temperature was decreased to 37 ^{o}C where a steady increase in product formation was observed over 35 min at 37 ^{o}C (Figure S1A). The pH optimum of MTIP was found to be pH 7.0-8.0 in PIPES, TAPS, CAPS buffer system. At pH 11 MTIP retained approximately 20% of the activity compared to pH 7 (Figure S1B). The molecular mass of MTIP was measured to be 90 kDa using size exclusion chromatography (SEC). This is consistent with the enzyme being a trimer with a monomeric subunit mass of 30 kDa. Determination of the MTIP as a trimer indicates that it is a member of the nucleoside phosphorylase-I family of nucleoside phosphorylases(37).

The purine nucleoside phosphorylase superfamily are known to accept a wide range of substrates(37) and we sought to determine if MTIP would function with alternate purine nucleosides. MTIP from *M. jannaschii* was found to utilize MTI, 5'-dI, inosine, 2'-deoxyinosine, guanosine, and 2'-deoxyguanosine, as assayed by following formation of the nucleobase by HPLC (Table 1). Steady state kinetics indicate that MTI is the preferred substrate (k_{cat}/K_M of 1.2 x 10^4 $s^{-1}M^{-1}$), which was only 1.5 fold higher than 5'-dI (Table 1). However, there was a 10-fold higher k_{cat}/K_M for MTI than inosine and guanosine (Table 1). This suggests that MTIP is involved in both the AnMSP and general salvage of purine nucleosides. The role of MTIP acting as a general purine nucleoside phosphorylase is further supported by the fact that the *M. jannaschii* genome is only annotated to encode three other phosphorylases (from UniProt (38)). Of the three annotated phosphorylases none are annotated as a general purine nucleoside phosphorylase likely to correspond to a non-specific enzyme involved in the salvage of diverse purines (36, 37). The other phosphorylases are annotated as a thymidine/AMP phosphorylase encoded by MJ0667, a ribulose 1,5-bisphosphate isomerase encoded by MJ0122, and a glycogen phosphorylase encoded by MJ1631. To date only the MJ0667 derived enzyme has been examined and neither annotated activity was observed (Miller unpublished). Furthermore, it has

been demonstrated that a purine nucleoside phosphorylase from *Plasmodium falciparum* used MTI as well as inosine as a substrate (39). Thus, MTIP is likely serving as the general purine nucleoside phosphorylase in *M. jannaschii*. This enzyme would be serving to salvage HX and guanine nucleotides for regeneration of IMP, GMP, and AMP through the HX/guanine phorphoribosyltransferase(40).

Analysis by HPLC and LC-ESI-MS for the sugar product moieties of the MTIP reaction was done through derivatization with NBHA. All of the sugars discussed were analyzed as the NBHA derivative, but for clarity they are only referred to as the sugar and the *m/z* for the NBHA adducts. The results demonstrated that MTR and 5-dR were products of the MTIP phosphorolysis of MTI and 5'-dI, respectively (Figure 2). Figure 4 is a representative HPLC chromatograph of the MTIP (Figure 4, red) and MTIP/MTRI coupled reaction demonstrating formation of the new 5-dRu 1P (Figure 4, blue). When MTRI was included in the reaction, 5-deoxyribulose 1P (5-dRu 1P, retention time of 27.5 min) (Figure 4, blue) and the methylthioribulose 1P (MTRu 1P, retention time of 29.5 min) were detected. LC-ESI-MS was used to further confirm the 5-dR 1P (MH^+ = 363.2 *m/z*) and MTR 1P (MH^+ = 409.2 *m/z*) products of the MTIP and MTRI reaction (Figure 2). Under the procedures used to derivatize the ribose product moieties with NBHA it would not be expected to detect the 1-phosphate ribose product moieties. Ultimately, these data indicate that 5-dR 1P and MTR 1P are produced by MTIP since the subsequent isomerization reaction products (5-dRu 1P and MTRu 1P) contained the phosphate at the C1 position of the ketose sugar product. These data would suggest that MTI and MTR 1P are intermediates of the AnMSP with MTIP catalyzing the phosphorolysis.

MTRI catalyzes the third step in AnMSP. MTRI is responsible for isomerization of MTR 1P to MTRu 1P and is the first well conserved enzyme of the MSP (16). This enzyme shares close sequence homology with eukaryotic translation initiation factor 2B α family (41). Only two other MTRI's have been studied in detail, one from *Bacillus subtilis* (10, 41) and one from yeast (42), both of whom have had their structures determined to contain an N-terminal domain fold of three-stranded antiparallel β-sheets and a C-terminal domain Rossmann fold that binds the substrate (41). MTRI from *M. jannaschii* was found to be predominantly a dimer with a monomeric subunit mass of ~40 kDa as measured by SEC. The tetrameric form was also observed but to a lesser extent. The ratio of tetramer to dimer was 1:4 based on UV absorbance at 280 nm of each peak. Interestingly, this is the first report of this enzyme as a dimer; it was

found to be a tetramer of two dimers in the homologues from *Bacillus subtilis* (10) and yeast (42).

The MTRI in *M. jannaschii* was demonstrated to use MTR 1P and 5-dR 1P equally well (Table 2). Neither ribose, ribose 5P, nor ribose 1P were found to be substrates of MTRI from *M. jannaschii*. Interestingly, MTRI demonstrated a four-fold higher K_M for 5dR 1P than for 5-dR, suggesting that the 1-phosphate moiety of 5-dR 1P is a substrate binding determinant. Furthermore, without the 1-phosphate moiety the turnover (k_{cat}) was 15-fold slower with 5-dR than 5-dR 1P (Table 2). This data would indicate that the 1-phosphate moiety of MTR 1P plays an important role in the binding of the substrate to MTRI. The mechanism of MTRI is still largely unclear and even after analysis the *B. subtilis* X-ray crystal structure(41) and had been postulated to proceed via a metal dependent 1,2-hydride shift or through a *cis*-enediol intermediate(41).

The mechanism of the *M. jannaschii* MTRI was briefly investigated to establish if it proceeded either via a metal dependent 1,2-hydride shift or a *cis*-endiol mechanism. First, MTRI was analyzed for the presence of metals and the results (Table S3) did not indicate the presence of any specific metal bound to the recombinantly produced purified protein. Sequence alignments of MTRI's further distanced the mechanism from a metal dependent 1,2-hydride shift because MTRI's lack any conserved metal binding residues with known isomerases like the xylose isomerase(43). Next, the MTRI reaction was followed in the presence of 20% D_2O, because there should be an incorporated deuterium into the product from the solvent if a *cis*-endiol mechanism is followed. The results from this experiment showed no incorporation of deuterium into the product, which might suggest that the *cis*-endiol mechanism is not followed as the expected labeled product (5-dRu 1P, MH^+ = 364.1 *m/z*) was not observed (Figure S2). A similar analysis of isotope exchange experiment for the *B. subtilis* MTRI also demonstrated no deuterium incorporation(10). Unfortunately, our results could not distinguish between the two proposed mechanisms for MTRI.

AnMSP and 6-deoxy-5-ketofructose 1-phosphate biosynthesis. The ability of MTIP and MTRI to utilize 5-dR 1P and 5-dRu 1P (Figure 2B) as substrates is particularly important for our understanding of how aromatic amino acids are biosynthesized in Archaea. It has been clearly demonstrated in *M. jannaschii* and *Halobacterium solinarum* that the canonical precursors, erythrose 4-phosphate and phosphoenoyl pyruvate (PEP), are not used for the

production of aromatic amino acids (44, 45). Alternatively, 6-deoxy-5-ketofructose 1-phosphate (DKFP) and L-aspartate semialdehyde are used to generate 3-dehydroquinate(44, 45), which is an essential intermediate for the shikimic acid pathway (46). However, the biosynthesis of DKFP remains largely unknown. Only a single enzyme has been identified to be responsible for formation of DKFP from fructose 1,6-bisphosphate and methylglyoxal (Figure 3)(47). Methylglyoxal is known to be toxic metabolite and is not traditionally utilized as an intermediate, but is instead quickly degraded through detoxifying enzymes(48–51). Thus, to be utilized as an intermediate for the production of DKFP methylglyoxal is likely to be enzymatically produced instead of just being a degradation product of glyceraldehyde 3-phosphate(52, 53).

As has been proposed by earlier work from our laboratory, 5'-dA derived from radical SAM enzymatic reactions could be the source of deoxysugars for the production of methylglyoxal and DKFP(23). 5'-dA is known to be deaminated to 5'-dI by DadD and here we have demonstrated that MTIP and MTRI converts 5'-dI to 5-dRu 1P (Figure 3). The results of these experiments demonstrated that MTIP and MTRI functioned with both substrates and in the case of the isomerase there was near equal specificity for either MTR 1P or 5-dR 1P (Table 2). 5-dRu 1P is then hypothesized to be further metabolized to methylglyoxal by the annotated ribulose 5-phosphate 3-epimerase and transketolase enzymes (Figure 3). Characterization of these enzymes and reactions is currently underway by our laboratory. Preliminary analysis does suggest that when MTIP, MTRI, ribulose 5-phosphate 3-epimerase, and transketolase enzymes are incubated together with 5'-dI, lactaldehyde is produced (Miller unpublished).

Possible AnMSP intermediates after MTRu 1P. In an effort to identify potential intermediates in the AnMSP an *M. acetivorians* HcyAux strain was utilized (22). *M. acetivorans* contains homologues to both MTIP and MTRI with 44% and 46% sequence identity to the *M. jannaschii* enzymes, respectively. This strain of *M. acetivorans* had previously been demonstrated to require either homocysteine or methionine for growth (22). Like *M. jannaschii, M. acetivorans* also lacks the genes of the aerobic MSP. Using the *M. acetivorians* HcyAux allowed us to test various intermediates that could potentially be taken up and converted to methionine by enzymes that have yet to be identified. Once an intermediate is identified that recovers the growth of the *M. acetivorians* HcyAux, then the types of biochemical reactions that might be used to connect the intermediate to methionine could be identified. This information

could be used to propose a list of enzymes that are either known or predicted based on bioinformatics searches, followed by examining the individual protein's *in vitro* function.

First we examined whether MTA was able to recover the growth of the *M. acetivorans* HcyAux and simultaneously compared its effect on growth of a wild type (wt) strain of *M. acetivorans* (Figure 5). These results demonstrated that MTA at low concentrations (0.2, but not 0.02 mM) was inhibitory to the growth of wt *M. acetivorians*, suggesting that like other bacterial and eukaryotic organisms (4, 54, 55), MTA inhibits growth by blocking the activity of SAM dependent enzymes. Next, we incubated the growing cultures with MTI, which did not inhibit growth of wt *M. acetivorans* (Figure 5A). However, MTI was unable to rescue growth of *M. acetivorians* HcyAux. This indicates that MTI is either unable to enter the cell or is not converted to methionine. Next, chemically generated methylthioribose (MTR) from the acid hydrolysis of MTA was fed to growing cultures of wt and HcyAux *M. acetivorians*. MTR did not rescue the growth of the HcyAux *M. acetivorians* (Figure 5B), but MTR fed to wt *M. acetivorians* had growth characteristics similar to the rescue effected by 0.2 mM methionine on the HcyAux *M. acetivorians* (Figure 5). These data suggest that MTR does enter the cell and is likely metabolized in some way to overcome the inhibition that is initially observed in the wt *M. acetivorans* when fed MTR. (Figure 5A).

The last known intermediate that was tested for growth recovery was the final intermediate before conversion to methionine, 2-keto-(4-methylthio)butyrate (KMTB) (Figure 5). These data demonstrated conversion of KMTB to methionine thus restoring the growth of the *M. acetivorians* HcyAux and no inhibition of wt *M. acetivorians*. Transamination of KMTB to methionine would be catalyzed by a PLP-dependent aminotransferase. *M. jannaschii* contains ten aminotransferases, and preliminary data suggests more than half are able to transaminate KMTB to methionine to some extent (Miller unpublished). It has been shown that in yeast transamination of KMTB was highly redundant, due to the mutant strains with the knocked out aminotransferases lacking any growth defect (56). The *M. jannaschii* aminotransferases are currently being investigated to further establish if KMTB is an intermediate of the AnMSP or if it is non-specifically transaminated to methionine.

Other intermediates from the aerobic MSP were not tested as they are not commercially available nor were they easily chemically synthesized. Instead, alternate intermediates with either a 3- or 4-methylthio moiety (Figure S3A) were investigated for their ability to be

converted to methionine and recover the growth of the *M. acetivorans* HcyAux (Figure S3B). The four intermediates were chosen because of their structural similarities to methionine (Figure S3A). Hydroxy-4-methylthiobutyric acid (HMTB) or methioninol could potentially be intermediates to methionine, but neither HMTB nor methioninol were successful at recovering the growth of the *M. acetivorans* HcyAux, suggesting that neither of these compounds are intermediates in the methanogenic AnMSP. 3-Mercaptopropanoic acid and 3-(methylthio)propanoic acid were examined as potential intermediates as it had been demonstrated that 3-mercaptopropanoic acid was methylated by *M. acetivorans* (White unpublished). Additionally, 3-mercaptopropanoic acid was recently found to be biosynthesized in *M. jannaschii* suggesting its potential as an intermediate (57). Carboxylation of 3-(methylthio)propanoic acid would generate KMTB which could then be transaminated to methionine. Interestingly, neither 3-mercaptopropanoic acid nor 3-(methylthio)propanoic acid were able to substitute for methionine and allow the *M. acetivorans* HcyAux to grow as the wt *M. acetivorians*. These data further suggest that the AnMSP proceeds through unique intermediates that cannot be readily predicted.

Conclusions

In conclusion we have demonstrated that the two annotated enzymes of the MSP are functioning as MTIP and MTRI. Furthermore, both of these enzymes were found to utilize alternative substrates suggesting that MTIP and MTRI are not specific for only the AnMSP. MTIP was able to utilize a wide variety of purine nucleosides (Table 1) indicating it functions as a purine nucleoside phosphorylase involved in the salvage of purines. Both MTIP and MTRI have also been implicated in the biosynthesis of DKFP as well. Taking this information we sought to determine potential intermediates in the AnMSP utilizing *M. aceitvorians* HcyAux, which require either homocysteine or methionine for normal growth (22). Of the eight compounds that were examined only KMTB was able to restore growth. MTA was demonstrated to be inhibitory of the wt *M. acetivorians* indicating that it functions as a feedback inhibitor of SAM dependent enzymes in methanogens. Neither MTI nor MTR were able to successfully restore growth, but nor did they inhibit the growth of wt *M. acetivorians*. The remaining four compounds that were postulated to be potential intermediates of the AnMSP were unable to restore growth. Ultimately, the last steps in the AnMSP still remains a mystery in

methanogens, but it is proposed that MTI, MTR 1P, MTRu 1P, and KMTB are intermediates of the AnMSP where MTIP and MTRI catalyze the second and third steps.

Acknowledgments. The authors thank Dr. W. Keith Ray for performing the mass spectrometry experiments. The mass spectrometry recourses are maintained by the Virginia Tech Mass Spectrometry Incubator, a facility operated in part through funding by the Fralin Life Science Institute at Virginia Tech and by the Agricultural Experiment Station Hatch Program (CRIS Project Number: VA-135981). This work was supported by the National Science Foundation Grant MCB1120346 and by the Agricultural Experiment Station Hatch Program (CRIS Project Number: VA-135981) awarded to R.H. White. This work was supported by NASA NNX15AP59G awarded to J. J. Perona.

References

1. **Fontecave M**, **Atta M**, **Mulliez E**. 2004. S-adenosylmethionine: Nothing goes to waste. Trends Biochem Sci **29**:243–249.
2. **Hiscox MJ**, **Driesener RC**, **Roach PL**. 2012. Enzyme catalyzed formation of redicals from S-adenosylmethionin and inhibition of enzyme activity by the cleavage products. Biochem Biophys Acta **1824**:1165–1177.
3. **Kozbial PZ**, **Mushegian AR**. 2005. Natural history of S-adenosylmethionine-binding proteins. BMC Struct Biol **5**:19–44.
4. **Avila MA**, **Garcıa-Trevijano ER**, **Lu SC**, **Corrales FJ**, **Mato JM**. 2004. Methylthioadenosine. Int J Biochem Cell Biol **36**:2125–2130.
5. **Albers E**. 2009. Metabolic Characteristics and Importance of the Universal Methionine Salvage Pathway Recycling Methionine from 5'-Methylthioadenosine. IUBMB Life2009/12/01. **61**:1132–1142.
6. **Backlund PS**, **Smith RA**. 1981. Methionine synthesis from 5'-methylthioadenosine in rat liver. J Biol Chem **256**:1533–1535.
7. **Shapiro SK**, **Schlenk F**. 1980. Conversion of 5′-methylthioadenosine into S-adenosylmethionine by yeast cells. Biochim Biophys Acta **633**:176–180.
8. **Nakano T**, **Saito Y**, **Yokota A**, **Ashida H**. 2013. Plausable Novel Ribose Metabolism Catalyzed by Enzymes of the Methionine Salvage Pathway in Bacillus subtilis. Biosc Biotechnol Biochem **77**:1104–1107.
9. **Buckoreelall K**, **Sun Y**, **Hobrath J V**, **Wilson L**, **Parker WB**. 2012. Identification of Rv0535 as methylthioadenosine phosphorylase from Mycobacterium tuberculosis. Tuberculosis **92**:139–147.
10. **Saito Y**, **Ashida H**, **Kojima C**, **Tamura H**, **Matsumura H**, **Kai Y**, **Yokota A**. 2007. Enzymatic Characterization of 5-Methylthioribose 1-Phosphate Isomerase from Bacillus subtilis. Biosc Biotechnol Biochem **71**:2021–2028.
11. **Ashida H**, **Saito Y**, **Kojima C**, **Yokota A**. 2008. Enzymatic Characterization of 5-Methylthioribose-1-phosphate Dehydratase of the Methionine Salvage Pathway in Bacillus subtilis. Biosc Biotechnol Biochem **72**:959–967.
12. **Saito Y**, **Ashida H**, **Sakiyama T**, **de Marsac NT**, **Danchin A**, **Sekowska A**, **Yokota A**. 2009. Structural and functional similarities between a ribulose-1, 5-bisphosphate

carboxylase/oxygenase (RuBisCO)-like protein from Bacillus subtilis and photosynthetic RuBisCO. J Biol Chem **284**:13256–13264.

13. **Myers RW**, **Wray JW**, **Fish S**, **Abeles RH**. 1993. Purification and characterization of an enzyme involved in oxidative carbon-carbon bond cleavage reactions in the methionine salvage pathway of Klebsiella pneumoniae. J Biol Chem **268**:24785–24791.
14. **Dai Y**, **Wensink PC**, **Abeles RH**. 1999. One protein, two enzymes. J Biol Chem1999/01/09. **274**:1193–1195.
15. **Backlund PS**, **Chang CP**, **Smith RA**. 1982. Identification of 2-keto-4-methylthiobutyrate as an intermediate compound in methionine synthesis from 5'-methylthioadenosine. J Biol Chem **257**:4196–4202.
16. **Sekowska A**, **Dénervaud V**, **Ashida H**, **Michoud K**, **Haas D**, **Yokota A**, **Danchin A**. 2004. Bacterial variations on the methionine salvage pathway. BMC Microbiol2004/04/23. **4**:9.
17. **Dey S**, **North JA**, **Sriram J**, **Evans BS**, **Tabita FR**. 2015. In Vivo Studies in Rhodospirillum rubrum Indicate That Ribulose-1, 5-bisphosphate Carboxylase/Oxygenase (Rubisco) Catalyzes Two Obligatorily Required and Physiologically Significant Reactions for Distinct Carbon and Sulfur Metabolic Pathways. J Biol Chem **290**:30658–30668.
18. **North JA**, **Sriram J**, **Chourey K**, **Ecker CD**, **Sharma R**, **Wildenthal JA**, **Hettich RL**, **Tabita FR**. 2016. Metabolic Regulation as a Consequence of Anaerobic 5-Methylthioadenosine Recycling in Rhodospirillum rubrum. MBio **7**:e00855-16.
19. **Ashida H**, **Saito Y**, **Kojima C**, **Kobayashi K**, **Ogasawara N**, **Yokota A**. 2003. A Functional Link Between RuBisCO-like Protein of Bacillus and Photosynthetic RuBisCO. Science (80-) **302**:286–290.
20. **Sato T**, **Atomi H**, **Imanaka T**. 2007. Archaeal type III RuBisCOs function in a pathway for AMP metabolism. Science (80-) **315**:1003–1006.
21. **Grochowski LL**, **Xu H**, **White RH**. 2006. Methanocaldococcus jannaschii uses a modified mevalonate pathway for biosynthesis of isopentenyl diphosphate. J Bacteriol **188**:3192–3198.
22. **Rauch BJ**, **Gustafson A**, **Perona JJ**. 2014. Novel proteins for homocysteine biosynthesis in anaerobic microorganisms. Mol Microbiol2014/10/16. **94**:1330–1342.
23. **Miller D**, **O'Brien K**, **Xu H**, **White RH**. 2014. Identification of a 5′-Deoxyadenosine

Deaminase in Methanocaldococcus jannaschii and its Possible Role in Recycling the Radical SAM Enzyme Reaction Product 5′-Deoxyadenosine. J Bacteriol **196**:1064–1072.

24. **Challand MR**, **Ziegert T**, **Douglas P**, **Douglas P**, **Wood RJ**, **Kriek M**, **Shaw NM**, **Roach PL**. 2009. Product inhibition in the radical S-adenosylmethionine family. FEBS Lett **583**:1358–1362.
25. **Davidson JG**, **Fiore PJ**. 1991. A Direct and Efficient Synthesis of 5′-Deoxy-2′, 3′. Nucleos Nucleot **10**:1477–1483.
26. **Graham DE**, **Xu H**, **White RH**. 2002. Identification of coenzyme M biosynthetic phosphosulfolactate synthase. A new family of sulfonate-biosynthesizing enzymes. J Biol Chem **277**:13421–13429.
27. **Kezmarsky ND**, **Xu H**, **Graham DE**, **White RH**. 2005. Identification and characterization of a L-tyrosine decarboxylase in Methanocaldococcus jannaschii. Biochim Biophys Acta **1722**:175–182.
28. **Bradford MM**. 1976. A rapid and sensitive method for the quantitation of microgram quantities of protein utilizing the principle of protein dye-binding. Anal Biochem **72**:248–257.
29. **Miller D V**, **Xu H**, **White RH**. 2012. A new subfamily of agmatinases in methanogenic Archaea is Fe(II) dependent. Biochemistry **51**:3067–3078.
30. **Sober HA**. 1970. Handbook of BiochemistrySelected Data for Molecular Biology. The Chemical Rubber Co., 18901 Cranwood Parkway, Cleveland, Ohio, 44128.
31. **Sowers KR**, **Boone JE**, **Gunsalus RP**. 1993. Disaggregation of Methanosarcina spp. and growth as single cells at elevated osmolarity. Appl Environ Microbiol **59**:3832–3839.
32. **Metcalf WW**, **Zhang J-K**, **Shi X**, **Wolfe RS**. 1996. Molecular, genetic, and biochemical characterization of the serC gene of Methanosarcina barkeri Fusaro. J Bacteriol **178**:5797–5802.
33. **Guss AM**, **Rother M**, **Zhang JK**, **Kulkkarni G**, **Metcalf WW**. 2008. New methods for tightly regulated gene expression and highly efficient chromosomal integration of cloned genes for Methanosarcina species. Archaea **2**:193–203.
34. **Guan R**, **Ho M-C**, **Almo SC**, **Schramm VL**. 2011. Methylthioinosine Phosphorylase from Pseudomonas aeroginosa. Structure and Annotaion of a Novel Enzyme in Quorum Sensing. Biochemistry **50**:1247–1254.

35. **Friedkin M**. 1950. Desoxyribose-1-phosphate II. The isolation of crystalline desoxyribose-1-phosphate. J Biol Chem **184**:449–460.
36. **Erion MD**, **Takabayashi K**, **Smith HB**, **Kessi J**, **Wagner S**, **Honger S**, **Shames SL**, **Ealick SE**. 1997. Purine Nucleoside Phosphoylase 1. Structure- Function Studies. Biochemistry **36**:11725–11734.
37. **Pugmire MJ**, **Ealick SE**. 2002. Structural analyses reveal two distinct families of nucleoside phosphorylases. Biochem J **361**:1–25.
38. **Consortium U**. 2014. UniProt: a hub for protein information. Nucleic Acids Res gku989.
39. **Shi W**, **Ting L-M**, **Kicska GA**, **Lewandowicz A**, **Tyler PC**, **Evans GB**, **Furneaux RH**, **Kim K**, **Almo SC**, **Schramm VL**. 2004. Plasmodium falciparum Purine Nucleoside Phosphorylase crystal structures, immucillin inhibitors, and dual catalytic function. J Biol Chem **279**:18103–18106.
40. **Miller D V**, **Brown AM**, **Xu H**, **Bevan DR**, **White RH**. 2016. Purine salvage in Methanocaldococcus jannaschii: Elucidating the role of a conserved cysteine in adenine deaminase. Proteins Struct Funct Bioinforma **84**:828–840.
41. **Tamura H**, **Saito Y**, **Ashida H**, **Inoue T**, **Kai Y**, **Yokota A**, **Matsumura H**. 2008. Cyrstal structure of 5-methylthioriobse 1-phosphate isomerase product complex from Bacillus subtilis: Implications for catalytic mechanism. Protein Sci **17**:126–135.
42. **Bumann M**, **Djafarzadeh S**, **Oberholzer AE**, **Bigler P**, **Altmann M**, **Trachsel H**, **Baumann U**. 2004. Crystal Structure of Yeast Ypr118w, a Methylthioribose-1-phosphate Isomerase Related to Regulatory eIF2B Subunits. J Biol Chem **279**:37087–37094.
43. **Fenn TD**, **Ringe D**, **Petsko GA**. 2004. Xylose isomerase in substrate and inhibitor michaelis states: atomic resolution studies of a metal-mediated hydride shift. Biochemistry **43**:6464–6474.
44. **White RH**. 2004. L-aspartate semialdehyde and a 6-deoxy-5-ketohexose 1-phosphate are the precursors to the aromatic amino acids in Methanocaldococcus jannaschii. Biochemistry **43**:7618–7627.
45. **Gulko MK**, **Dyall-Smith M**, **Gonzalez O**, **Oesterhelt D**. 2014. How do haloarchaea synthesize aromatic amino acids? PLoS One **9**:e107475.
46. **Pittard J**, **Yang J**. 2008. Biosynthesis of the aromatic amino acids. EcoSal Plus **3**:1–75.
47. **White RH**, **Xu H**. 2006. Methylglyoxal is an intermediate in the biosynthesis of 6-deoxy-

5-ketofructose-1-phosphate: A precursor for aromatic amino acid biosynthesis in Methanocaldococcus jannaschii. Biochemistry **45**:12366–12379.

48. **Thornalley PJ**. 1996. Pharmacology of methyglyoxal: formation, modification of proteins and nucleic acids, and enzymatic detoxification--a role in pathogenesis and antiproliferative chemotherapy. Gen Pharmacol **27**:565–573.
49. **Misra K**, **Banerjee AB**, **Ray S**, **Ray M**. 1995. Glyoxalase III from Escherichia coli: a single novel enzyme for the conversion of methyglyoxal into D-lactate without reduced glutathione. Biochem J **305**:999–1003.
50. **Booth IR**, **Ferguson GP**, **Miller S**, **Li C**, **Gunasekera B**, **Kinghorn S**. 2003. Bacterial production of methylglyoxal: a survival strategy or death by misadventure? Biochem Soc Trans **31**:1406–1408.
51. **Greig N**, **Whllie S**, **Patterson S**, **Fairlamb AH**. 2009. A comparative study of methyglyoxal metabolism in trypanosomatids. FEBS J **276**:376–386.
52. **Richard JP**. 1984. Acid-base catalysis of the elimination and isomerization reactions of triose phosphates. J Am Chem Soc **106**:4926–4936.
53. **Richard JP**. 1991. Kinetic parameters for the elimination reaction catalyzed by triosephosphate isomerase and an estimation of the reaction's physiological significance. Biochemistry **30**:4581–4585.
54. **Pajula R-L**, **Raina A**. 1979. Methylthioadenosine, a potent inhibitor of spermine synthase from bovine brain. FEBS Lett **99**:343–345.
55. **Raina A**, **Tuomi K**, **Pajula R-L**. 1982. Inhibition of the synthesis of polyamines and macromolecules by 5′-methylthioadenosine and 5′-alkylthiotubercidins in BHK21 cells. Biochem J **204**:697–703.
56. **Pirkov I**, **Norbeck J**, **Gustafsson L**, **Albers E**. 2008. A complete inventory of all enzymes in the eukaryotic methionine salvage pathway. FEBS J **275**:4111–4120.
57. **Allen KD**, **White RH**. 2016. Occurrence and Biosynthesis of 3-Mercaptopropionic acid in Methanocaldococcus jannaschii. FEMS Microbiol Lett **363**:fnw217.

Tables

Table 1. Apparent kinetic parameters of MTIP at 37 °C

Substrate	K_M ± SD (mM)	k_{cat} ± SD (s^{-1})	k_{cat}/K_M ($s^{-1}M^{-1}$)
MTI	0.13 ± 0.08	1.5 ± 0.12	1.2×10^4
5'-dI	0.86 ± 0.17	6.6 ± 0.61	7.6×10^3
inosine	0.93 ± 0.75	1.30 ± 0.72	1.4×10^3
2'-deoxyinosine	0.86 ± 0.09	4.2 ± 0.8	4.9×10^3
guanosine	0.61 ± 0.50	0.92 ± 0.38	1.5×10^3
2'-deoxyguanosine	15 ± 5	64 ± 22	4.3×10^3
MTA	N.d.[a]		
5'-dA	N.d.[a]		
adenosine	N.d.[a]		

[a] No detectable activity with 0.2 mM MTA, 5'-dA, or adenosine

Table 2. Apparent kinetic parameters of MTRI at 60 °C

Substrate	K_M ± SD (mM)	k_{cat} ± SD (s^{-1})	k_{cat}/K_M ($s^{-1}M^{-1}$)
MTR 1P[a]	0.53 ± 0.11	0.14 ± 0.021	2.5×10^2
5-dR 1P[a]	0.41 ± 0.09	0.067 ± 0.0037	1.7×10^2
5-dR[b]	1.6 ± 0.8	0.0043 ± 0.0013	2.6
Ribose 5P[b]	N.d.[c]		

[a] Coupled assay through MTIP

[b] Substrate added directly to MTIR

[c] No detectable activity with 0.2 mM ribose 5P and 5 µg MTRI

Figures

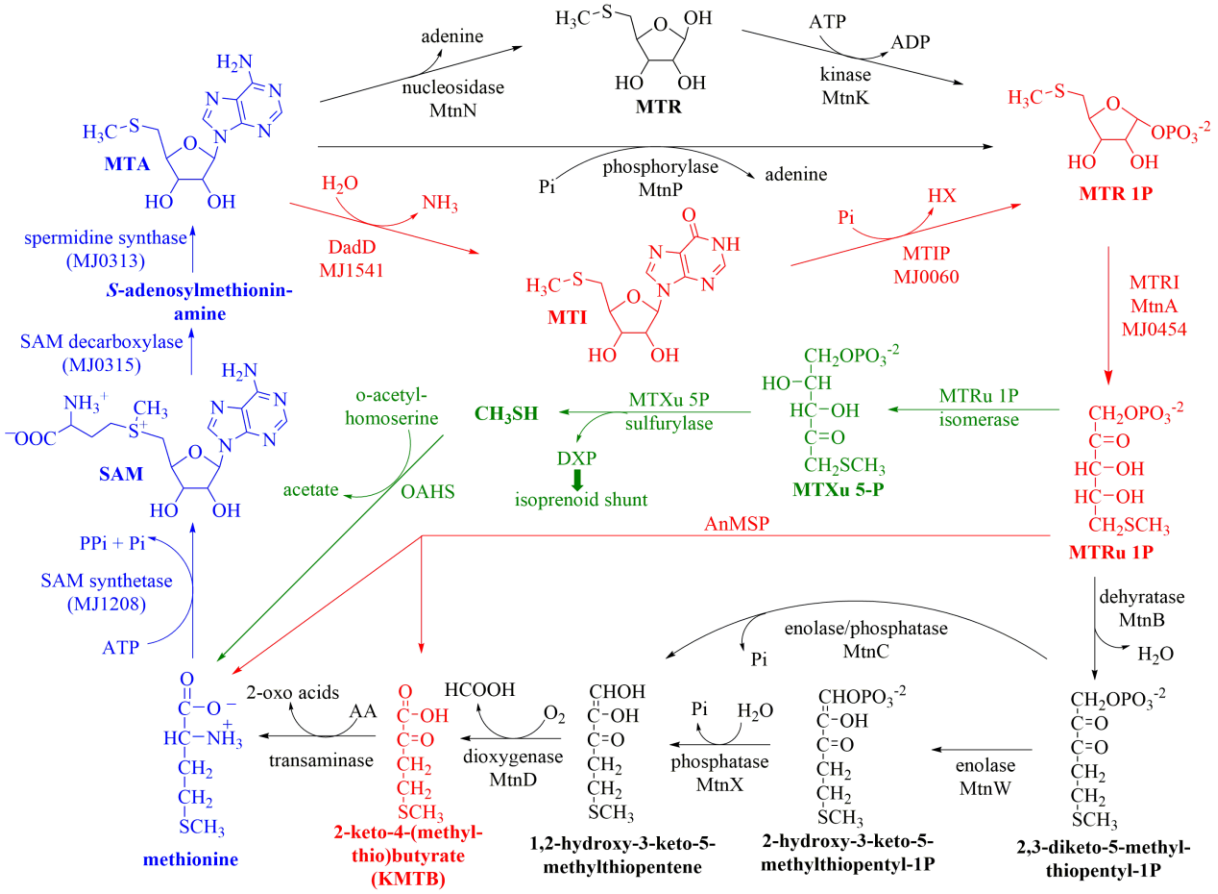

Figure 1. Different methionine salvage pathways. Highlighted in blue are the known intermediates shared with the MSP, red is the AnMSP proposed in methanogens, green is the isoprenoid shunt AnMSP, and shown in black are the intermediates and enzymes missing from the MSP pathway in anaerobic organisms.

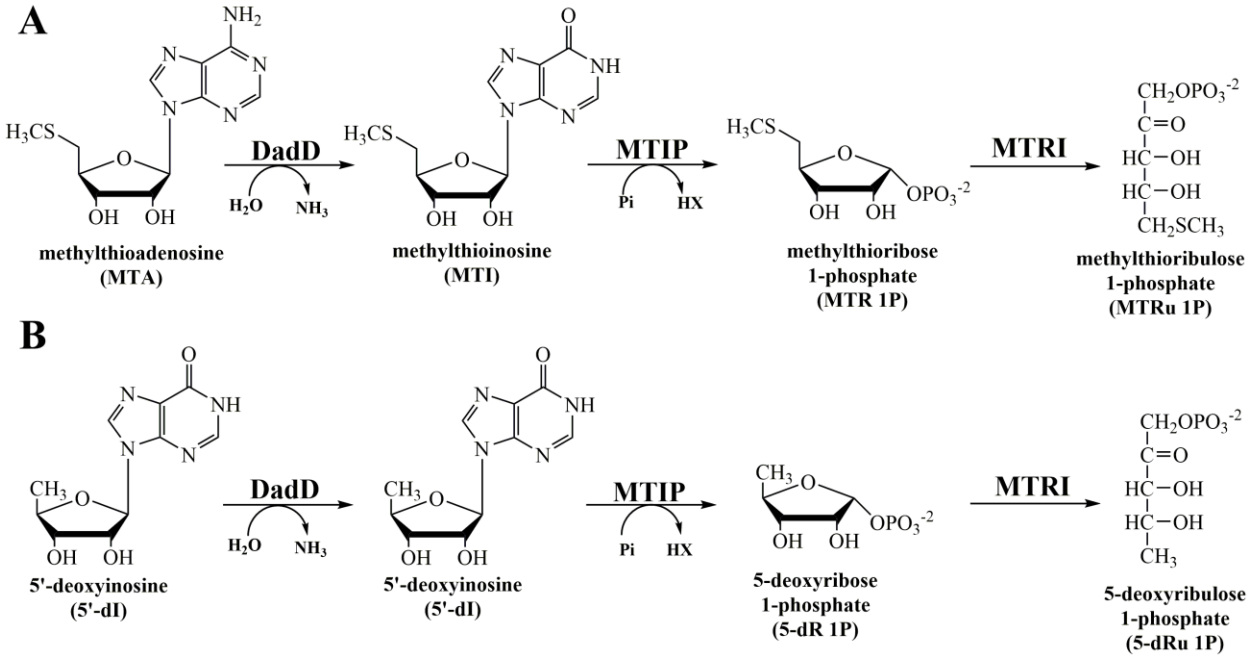

Figure 2. Comparison of substrates for first three steps of MTA (A) and 5'-dA (B) salvage pathways with DadD, MTIP, and MTRI.

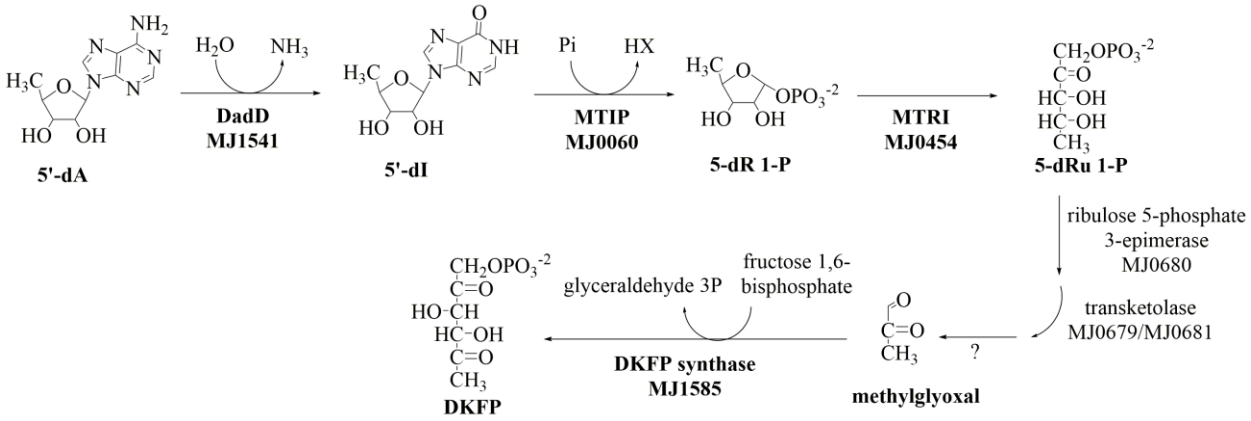

Figure 3. Proposed pathway for the biosynthesis of DKFP from 5'-dA.

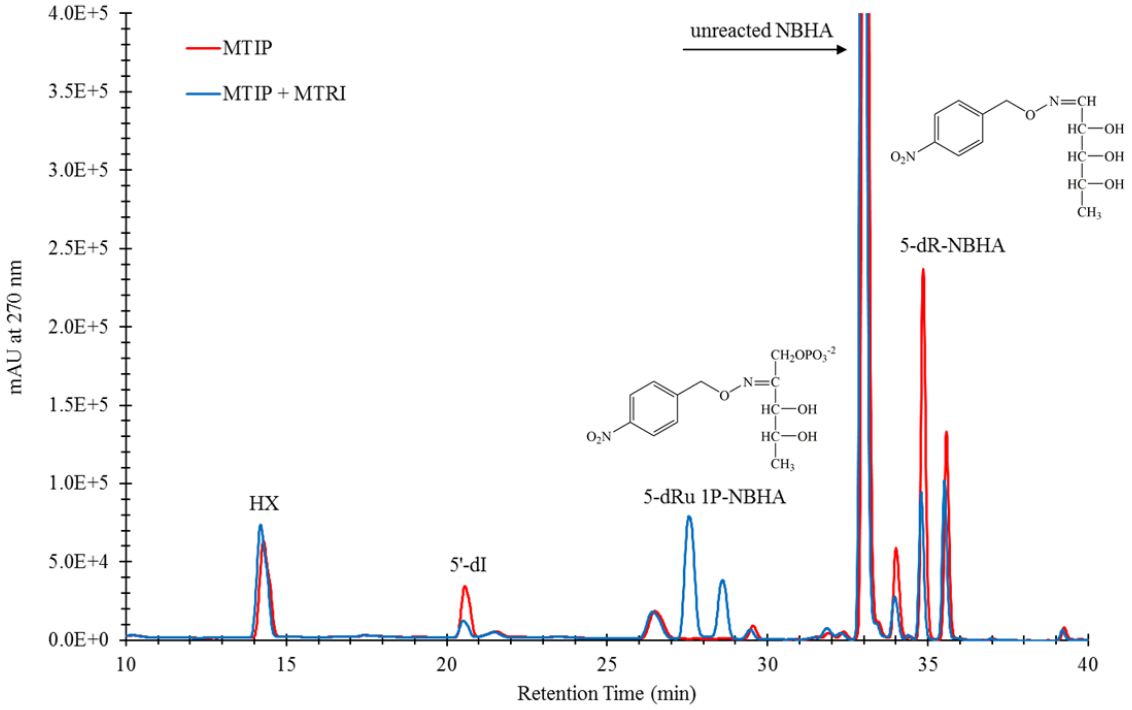

Figure 4. HPLC analysis of the products from the coupled assay of MTIP and MTRI with 5'-dI and excess Pi. The red line indicates the MTIP control without addition of MTRI and the blue is when the MTRI is added to the reaction. The peaks are labeled and the absorbance is measured at 270 nm. The secondary peaks seen with the NBHA derivatives is due to the different isomers of the oxime derivative.

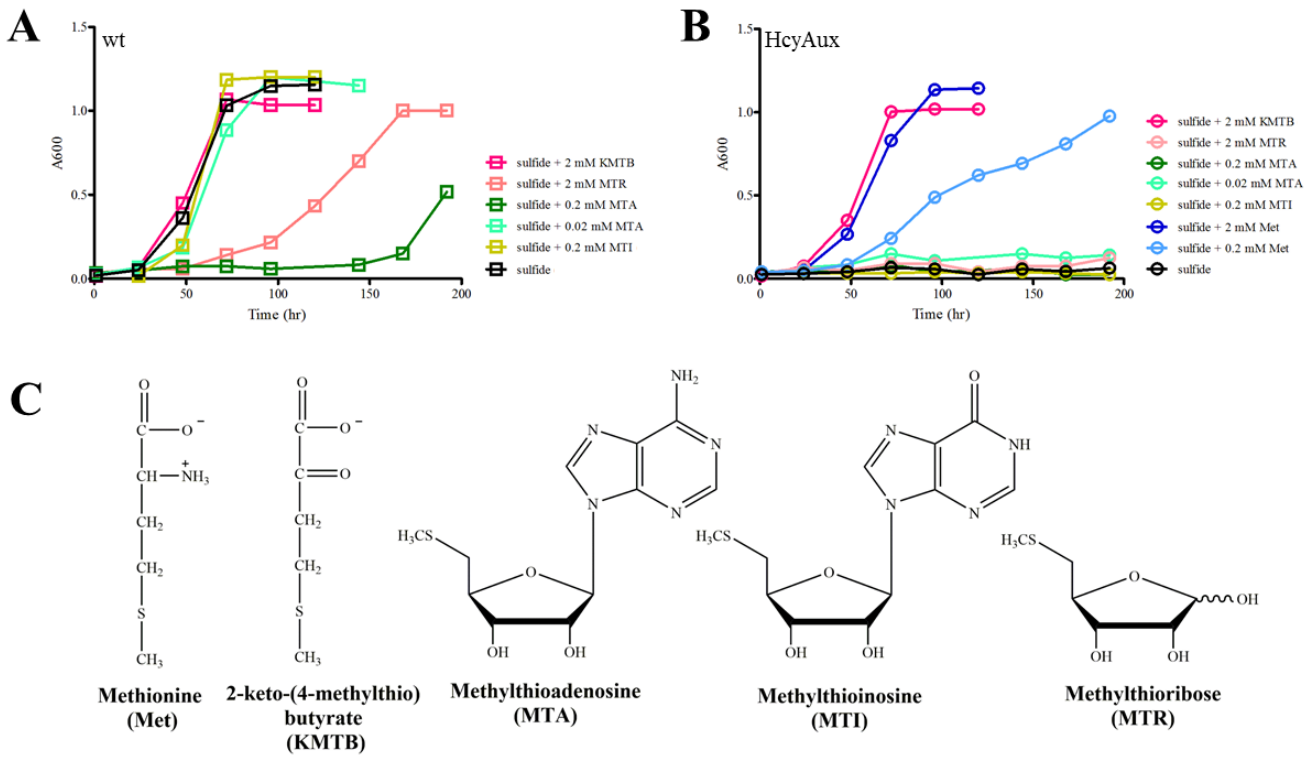

Figure 5. Growth recovery of M. acetivorans wt (A) and homocysteine auxotrophs (HcyAux) (B) with possible MSP intermediates (C).

Supporting Information for Promiscuity of Methionine Salvage Pathway Enzymes in *Methanocaldococcus jannaschii* and *Methanosarcina acetivorans*

Danielle V. Miller[a], Benjamin J. Rauch[b]*, Kim Harich[a], Humin Xu[a], John J. Perona[bc], and Robert H. White[a]#

Department of Biochemistry, Virginia Polytechnic Institute and State University, Blacksburg, Virginia, USA[a]; Department of Chemistry, Portland State University, Portland, Organ, USA[b]; Department of Biochemistry and Molecular Biology, Oregon Health and Science University, Oregon, USA[c]

Running Head: Methionine Salvage Pathway in Methanogens

#Address correspondence to Robert H. White, rhwhite@vt.edu

*Present address: Department of Microbiology and Immunology, University of California, San Francisco, San Francisco, CA, USA; Quantitative Biosciences Institute, QBI, University of California, San Francisco, San Francisco, CA, USA.

Tables

Table S1. Oligonucleotide primers for MJ0060 (MTIP) and MJ0454 (MTRI) gene products

Gene	Primers
MJ0060	Fwd : 5'-GGTCATATGATTGGTATAATAGGAGGGAC-3'
	Rev : 5'-GCTGGATCCTTACCCAATAACAGCATG-3'
MJ0454	Fwd : 5'-GGTCATATGACAAAAGATTTAAGAC-3'
	Rev : 5'-GCTGGATCCCTACCTAAAGAGCTTTAAAATC-3'

Table S2. Elution times of analyzed standards on the two different C18 columns used for HPLC analysis.

Standard	Elution Time (min)	
	Shimadzu C18[b]	Kromasil C18[c]
Adenine	3.4	16.0
Hypoxanthine (HX)	2.2	14
Guanine	2.1	12.2[d]
5'-Deoxyadenosine (5'-dA)	5.5	--
5'-Deoxyinsoine (5'-dI)	4.4	19.9
Methylthioadenosine (MTA)	7.2	--
Methylthioinosine (MTI)	5.9	24.2
Adenosine	4.6	--
Inosine	3.2	--
Guanosine	3.4	--
2'-Deoxyinosine	3.5	17.6[d]
2'-Deoxyguanosine	3.7	18.4[d]
5-Deoxyribose 1-phosphate (5-dR 1P)[a]	--	32.7
5-Deoxyribulose 1-phosphate (5-dRu 1P)[a]	--	25.4
Methylthioribose 1-phosphate (MTR 1P)[a]	--	37.0
Methylthioribulose 1-phosphate (MTRu 1P)[a]	--	29.5
5-Deoxyribose (5-dR)[a]	--	32.8
5-Deoxyribulose (5-dRu)[a]	--	25.5
Ribose[a]	--	28.6
Ribose 5-phosphate[a]	--	24.6

[a]These were assayed as their NBHA derivatives and measured by their UV absorbance at 270 nm
[b]Elution profile of 0.1 min at 95% sodium acetate buffer (25 mM, pH 6.0, 0.02% NaN3) and 5% methanol followed by a linear gradient to 50% sodium acetate/50% methanol over 9 min at 0.5 mL/min.
[c]Elution profile of 5 min at 100% sodium acetate buffer followed by a linear gradient to 100% methanol over 50 min at 0.5 mL/min.
[d]Elution profile of 5 min at 95% sodium acetate buffer followed by a linear gradient to 50% methanol over 30 min at 0.5 mL/min.

Table S3. Metal analysis of MTRI by ICP-MS

	Cobalt	Iron	Magnesium	Manganese	Nickel	Zinc
Detection Limit (mg/L)	0.002	0.005	0.04	0.0003	0.002	0.0005
Detected (µM)	0.071	0.25	<0.04	<0.0003	<0.002	0.024
Metal/MTRI[a]	0.035	0.128	<0.04	<0.0003	<0.002	0.012

[a]2µM MTRI

Figures

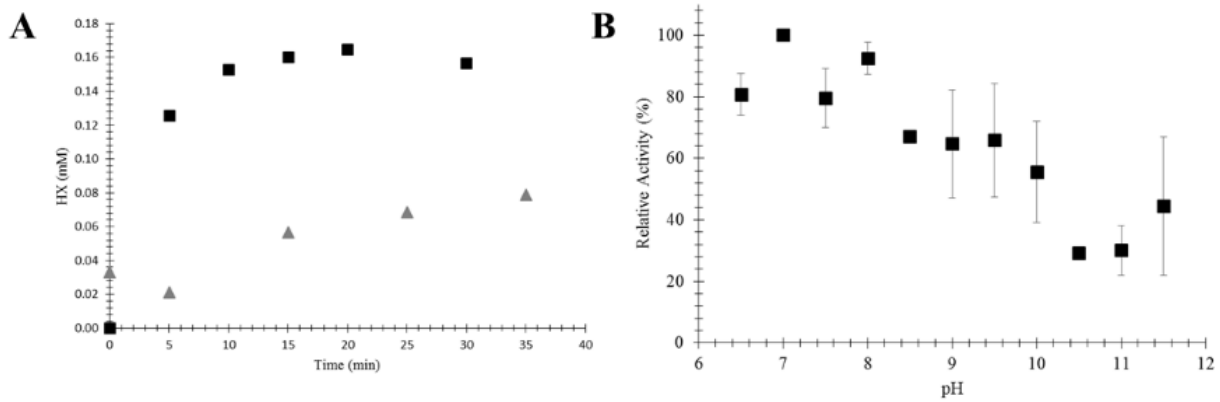

Figure S1. Time course of MTIP catalyzed reaction at 70 ^{o}C (squares) and 37 ^{o}C (triangles) (A) and pH profile of MTIP activity (B).

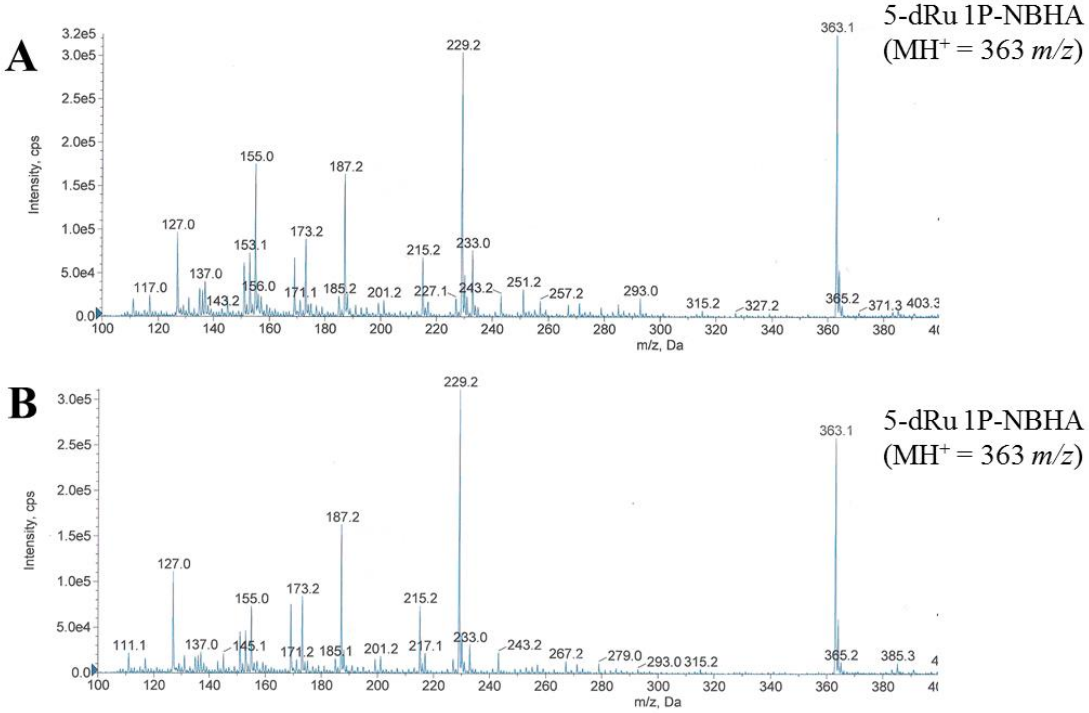

Figure S2. LC-ESI-MS spectrum to the NBHA derivative of 5-dRu 1P product of the MTIP/MTRI catalyzed reaction in the absence (A) and presence of 20% D_2O (B).

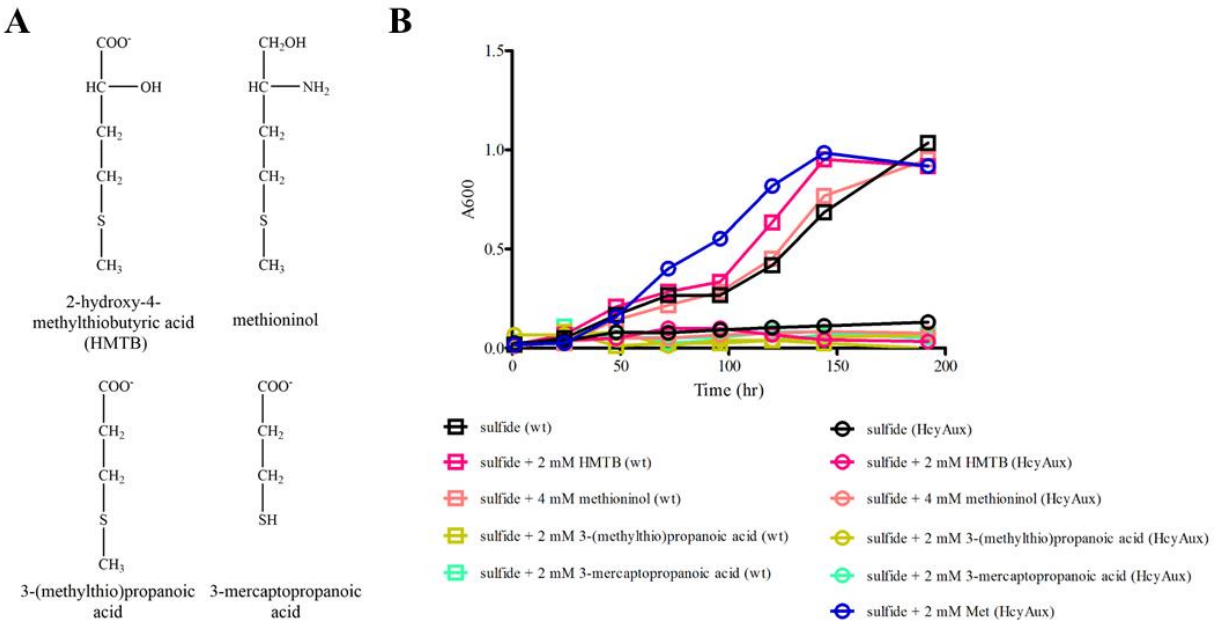

Figure S3. Growth recovery of *M. acetivorans* wt and HcyAux with fed methionine analogues. (A) the structures of HMTB, methioninol, 3-(methylthio)propanoic acid, and 3-mecaptopropanoic acid fed and (B) growth recovery data of HMTB (pink), methioninol (light pink), 3-(methylthio)propanoic acid (olive), 3-mercaptopropanoic acid (light green) and the controls Met (blue) and sulfide (black).

Chapter 3: Characterization of the ribulose 5-phosphate 3-epimerase and transketolase from *Methanocaldococcus jannaschii*

Danielle V. Miller, Kim Harich, Anne M. Brown, Huimin Xu, and Robert H. White#

Department of Biochemistry, Virginia Polytechnic Institute and State University, Blacksburg, VA 24061

#To whom correspondence should be addressed. Telephone: (540)231-6605, Fax: (540)231-9070, e-mail: rhwhite@vt.edu

Running title: *M. jannaschii* epimerase and transketolase
Key words: transketolase, ribulose 5-phosphate epimerase, deoxysugar biosynthesis, methanogens

Abstract

In the hyperthermophilic autotrophic anaerobe, *Methanocaldococcus jannaschii*, many of the canonical biosynthetic pathways are replaced with novel routes. Such is the case with the pentose phosphate pathway, which is replaced with the ribulose monophosphate pathway. Though the pentose phosphate pathway is absent, three enzymes are annotated as belonging to the pentose phosphate pathway in *M. jannaschii.* Our aim was to determine the role of the two of these enzymes, ribulose 5-phosphate 3-epimerase (RPE) and transketolase (TK) in *M. jannaschii* metabolism. In our analysis of *M. jannaschii* metabolism we have proposed a new route for deoxysugar metabolism that is responsible for recycling the 5-deoxyribose 1-phosphate, produced by radical *S*-adenosyl-L-methionine enzymes, to methylglyoxal. An enzyme coupled assay was developed using the phosphorylase and isomerase from the methionine salvage pathway for the conversion of 5'-deoxyinosine to 5-deoxyribulose 1-phosphate, the proposed substrate for RPE in *M. jannaschii*. When RPE was included in the coupled assay, 5-deoxyxylulose 1-phosphate was detected by GC-MS of the reduced TMS derivatized sugar. These results were further validated by molecular docking studies that suggest 5-deoxyxyluse 1-phosphate binds the active site in a similar conformation as xylulose 5-phosphate. Additionally, when the TK and erythrose were included in another coupled assay, lactaldehyde was produced (0.23 μmol min^{-1} mg^{-1} TK) and confirmed by the addition of the $NADP^+$ dependent alcohol dehydrogenase. Furthermore, the *M. jannaschii* TK, which is encoded by two genes representing the C-terminus and N-terminus, was demonstrated to only be active when the two genes were recombinantly co-expressed in *Escherichia coli*. This work demonstrates a novel role for RPE and TK in a novel route for deoxysugar metabolism.

Introduction

In this post genomic era, the annotation of encoded proteins based on sequence identity (1) has led to enzyme functional annotations that are often misleading or inaccurate.(2) However, though in error, the predicted chemistry can be utilized to hypothesize and establish the *in vivo* function. This approach has been used to identify the enzymes involved in multiple pathways in *Methanocaldococcus jannaschii*.(3) One pathway that has several annotated enzymes belonging to it, but is absent in *M. jannaschii* and several other archaeal organisms, such as *Thermococcus kodakarensis*(4), is the pentose phosphate pathway (PPP, Figure 1A).(4–6) *M. jannaschii* is a deeply rooted thermophilic autotrophic archaeal organism that does not use the PPP for the generation of ribose 5P.(6) The three annotated enzymes from the PPP are ribulose 5-phosphate 3-epimerase (RPE, EC 5.1.3.1), transketolase (TK, EC 2.2.1.1), and transaldolase (EC 2.2.1.2). The transaldolase from *M. jannaschii* has been demonstrated to be active with erythrose 4-phosphate and fructose 6-phosphate.(7)

The PPP is responsible for the conversion of glucose 6-phosphate (Glu 6P) to erythrose 4P through seven enzymes (Figure 1A) and is split into the oxidative and non-oxidative sections (Figure 1A). The PPP is responsible for the production of ribose 5P for nucleotide biosynthesis, the production of NADPH for redox homeostasis, and erythrose 4P for aromatic amino acid biosynthesis.(8) The non-oxidative branch of the PPP is made up of four enzymes: RPE, ribulose 5-phosphate isomerase, TK, and transaldolase (Figure 1A). The epimerase and isomerase are responsible for epimerizing ribulose 5-phosphate to xylulose 5P and the isomerization of ribulose 5P to ribose 5P (Figure 1, steps 4a and 5a). These two enzymes serve as the first two enzymes in the non-oxidative half of the pentose phosphate pathway. Xylulose 5P is subsequently combined with ribose 5P by TK to produce sedoheptulose 7P and glyceraldehyde 3-phosphate (Ga 3P) (Figure 1, step 6a). Sedoheptulose 7P and Ga 3P are then reassembled by a transaldolase to form fructose 6P and erythrose 4P (Figure 1, step 7a). However, it has been well established in several Archaeal organisms, such as *T. kodarkarensis*(4), that the oxidative branch of the PPP is replaced by the ribulose monophosphate pathway (Figure S1) for the production of ribose 5P.(4, 6)

M. jannaschii and *Halobacterium salinarum* do not utilize the oxidative PPP for the production erythrose 4P required for 3-dehydroquinate (DHQ) biosynthesis. Instead, *M.*

jannaschii and *H. salinarum* use aspartate semialdehyde and 6-deoxy-5-ketofructose 1-phosphate (DKFP) for the biosynthesis of DHQ (Figure 1B).(9) DHQ is universally required for the biosynthesis of aromatic amino acids via the shikimate pathway.(10, 11) Analysis of carbohydrates in *M. jannaschii* revealed the absence of erythrose 4P, seduheptulose 7P, and xylulose 5P, suggesting that they are not biosynthesized.(6) These results are consistent with ^{13}C labeling studies in *Methanospirillum hungatei*(12), suggesting an inoperable PPP. Thus, though annotated as RPE and TK, these enzymes are not likely using their canonical substrates (Figure 2A). Additionally, we demonstrate that the *M. jannaschii* TK, which is encoded from two separate genes, MJ0679 (C-MjTK) and MJ0681 (N-MjTK), is only active when the two genes are recombinantly co-expressed. Here we propose potential *in vivo* substrates for the annotated RPE and TK in *M. jannaschii* (Figure 2B) and their involvement in the recycling of 5-deoxyribose (5-dR) moiety produced from *S*-adenosyl-L-methionine (SAM) dependent enzymes.

Materials and Methods.

Chemicals. All chemicals were obtained from Sigma/Aldrich unless otherwise noted. The pRSFDuet-1 plasmid was generously provided by the laboratory of Dr. Dennis Dean from Virginia Tech.

Enzymatic production of 5'-deoxyinosine. The enzymatic preparation of 5'-deoxyinosine (5'-dI) was done as previously described by the enzymatic deamination of 5'-deoxyadenosine (5'-dA).(13) Reaction mixtures containing 5'-dI at a concentration of 1 to 10 mM were incubated with 18 ng of 5'-deoxyadenosine deaminase (DadD) overnight at 25 ^{o}C in 50 mM 1,3-bis[tris(hydroxymethylmethylamino]propane (BIS TRIS propane) buffer (pH 9.0).(13) 5'-dA were completely converted to 5'-dI as measured by HPLC previously described.(13)

Cloning, Overexpression, and Purification of *M. jannaschii* MJ0680, MJ0679, and MJ0681 Gene Products in *E. coli*. The encoded enzymes from MJ0680 (Swiss Prot accession number Q58093), MJ0679 (Swiss Prot accession number Q58092), and MJ0681 (Swiss Prot accession number Q58094) were amplified by PCR from genomic DNA using oligonucleotide primers shown in Table S1. PCR amplification was performed as described previously(14) using a 55 ^{o}C annealing temperature for all genes products. Purified PCR product was digested with Nde1 and BamH1 restriction enzymes and ligated into compatible sites in vector pT7-7. Sequence of the resulting plasmids pMJ0680, pMJ0679, and pMJ0681 were verified by DNA

sequencing prior to transformation into *E. coli* strain BL21-CodonPlus(DE3)-RIL cells (Stratagene). The transformed cells were grown in LB medium (200 mL) supplemented with 100 µg/mL ampicillin at 37 ^{o}C with shaking until they reached an OD_{600} of 1.0. Recombinant protein production was induced by the addition of lactose to a final concentration of 28 mM.(14) After an additional 2 hours of culture, the cells (200 mL) were harvested by centrifugation (4,000 x *g*, 5 min) and frozen at -20 ^{o}C. Induction of the desired protein was confirmed by SDS-polyacrylamide gel electrophoresis (SDS-PAGE) analysis of total cellular proteins.

The frozen *E. coli* cell pellet containing the desired protein (~0.4 g wet wt) was suspended in 3 mL of extraction buffer (50 mM *N*-[tris(hydroxymethyl)methyl]-2-aminoethanesulfonic acid (TES), pH 7.0, 10 mM $MgCl_2$, 20 mM dithiothreitol (DTT)) and lysed by sonication. The resulting expressed proteins were found to remain soluble after heating the MJ0680 gene product at 60 ^{o}C for 20 min and the MJ0679 and MJ0681 gene products for 20 min at 70 ^{o}C for 20 min followed by centrifugation (16,000 x *g* for 10 min). This heating step allowed for the purification of the recombinant enzymes from the majority of *E. coli* proteins, which denature and precipitate under these conditions. The next step of purification was performed by anion-exchange chromatography of the heated soluble fractions on a MonoQ HR column (1 x 8 cm; Amersham Bioscience) using a linear gradient from 0 to 1 M NaCl in 25 mM Tris buffer (pH 7.5), over 55 min at a flow rate of 1 mL/min. Fractions of 1 mL were collected and the desired protein was identified through SDS-PAGE analysis of the fractions and subsequent sequencing by MALDI-MS of the excised protein bands. The protein bands corresponding to the predicted molecular mass of the MJ0680 gene product (~25 kDa), MJ0679 gene product (~34 kDa), and MJ0681 gene product (~30 kDa) were excised from the polyacrylamide gel and prepared for MALDI-MS as previously described.(13) Protein concentrations were determined by Bradford analysis.(15)

Dual Cloning, Overexpression, and Purification of *M. jannaschii* MJ0679 and MJ0681 Gene Products together in *E. coli*. In order to determine if production of an active TK enzyme requires the overexpression of the two proteins together, two approaches were performed. First, the plasmids containing the MJ0679 and MJ0681 genes (described above) were transformed into *E. coli* strain BL21-CodonPlus(DE3)-RIL cells (Stratagene) and overexpressed as described above. Randomly selected colonies were screened following extraction of the proteins from the *E. coli* cell pellet for both proteins (Figure 3A). A single

colony was found to contain both proteins expressed at approximately equal quantities as judged by SDS-PAGE and to be thermally stable up to 80 ^{o}C (Figure 3B). The observed bands were verified by MALDI-MS of the excised bands as previously described (Figure 3, red boxes).(16) The two proteins were then co-purified by SEC (described below) using the following standards: Blue dextran (2000 kDa), bovine serum albumin (66 kDa), conalbumin (77.5 kDa), carbonic anhydrase (29 kDa), and cytochrome C (14 kDa).

Additionally, the two proteins were also cloned directly and amplified by PCR from the genomic DNA as the template with oligonucleotide primers described in Table S1 into the pRSFDuet-1 plasmid, which allows for the cloning of two genes in the same vector.(17, 18) PCR amplifications were performed as described previously(14) using 50 ^{o}C annealing temperature. The purified MJ0679 PCR product was digested with Nco 1 and Bam H1 restriction enzymes and ligated into compatible multiple cloning site (MCS) 1 site in plasmid pRSFDuet-1. The purified MJ0681 PCR product was digested with Nde 1 and Bg1 11 restriction enzymes and ligated into compatible MCS2 site in plasmid pRSFDuet-1 for the final combined pRSFDuet-1. MCS1 and MCS2 sequences of the plasmid DNA verified by DNA sequencing and the resulting pRSFDuet-1 was transformed into *E. coli* BL21-CodonPlus (DE3)-RIL cells (Stratagene). The transformed cells were grown in LB Broth Miller medium (200 mL) supplemented with 50 µg/mL kanamycin at 37 ^{o}C with shaking at 300 rpm until they reached an OD_{600} of 1.0. Recombinant protein productions were induced by the addition of IPTG to a final concentration of 1 mM. After an additional 6 hours of culture, the cells were harvested by centrifugation (4,000 x g, 5 min) and frozen at -20 C. Induction of the desired proteins were confirmed by SDS-polyacrylamide gel electrophoresis (SDS-PAGE) analysis of total cellular proteins.

Metal analysis of MjRPE and MjTK. Metal analysis of the recombinant purified *M. jannaschii* RPE (MjRPE), C-MjTK, and N-MjTK was performed at the Virginia Tech Soil Testing Laboratory using inductively coupled plasma emission spectrophotometry. Instrumentation included a Spectro CirOS VISION made by Spectro Analytical Instruments equipped with a Crossflow nebulizer with a Modified Scott spray chamber, nebulizer rate was 0.75 L/min. A 50 mg/L yttrium internal standard was introduced by peristaltic pump. Samples were analyzed for calcium, cobalt, iron, magnesium, manganese, nickel, and zinc.

Size exclusion chromatographic analysis of MjRPE, C-MjTK and N-MjTK. The native molecular weight of the recombinantly purified MjRPE, N-MjTK, and C-MjTK were

determined by size exclusion chromatography (SEC) as described previously using a Superose 12 HR column(16) with the following standards used to generate the standard curve for MjREP and TK analysis: Blue Dextran (2000 kDa), alcohol dehydrogenase (150 kDa, only for MjRPE SEC), conalbumin (77.5 kDa), bovine serum albumin (66 kDa), carbonic anhydrase (29 kDa), and cytochrome C (14 kDa). The native molecular weight of the TK was determined for the C-MjTK, N-MjTK, and a 1:1 ratio of C-MjTK and N-MjTK.

Molecular modeling of *M. jannaschii* RPE and TK. Homology models for both MjRPE and full length *M. jannaschii* TK (MjTK) were generated using Molecular Operating Environment (MOE)(19). The MjRPE homology model was based on the template structure from *Streptococcus pyrogenes* (PDB ID: 2FLI)(20), which shares an overall sequence identity of 44% with MjRPE. Additionally, the *S. pyrogenes* structure was further chosen as the template structure because it has a resolution of 1.8 Å and contains D-xylitol 5-phosphate and Zn^{2+} bound in the active site with an active site conservation of 94% (Figure S2). The presence of D-xylitol 5-phosphate and Zn^{2+} were important for subsequence docking studies and active site analysis. A combined, full-length structure was modeled for *M. jannaschii* TK (MjTK) gene products C-MjTK and N-MjTK. The full-length, combined sequence model of MjTK was generated using human transketolase (HsTK), PDB ID: 3OOY, as a template. The combined sequence of C-MjTK and N-MjTK have 35.9% identity and 55.4 % similarity to HsTK. Both models, MjRPE and full-length MjTK, were energy minimized in MOE using the Amber12EHT force field.(21) Models were assessed and validated before and after energy minimization using Anolea(22, 23), QMEAN(24), Verify 3D(25, 26), and ProCheck(27). Models after energy minimization showed more favorable energy and were deemed acceptable per assessment standards (Figures S3 and S4). The energy minimized models for both MjRPE and MjTK were further used for either docking or overlay analysis.

Molecular docking into the homology model of MjRPE and *S. pyrogenes* RPE (SpRPE – PDB ID: 2FLI) was done with xylulose 5-phosphate (Xu 5P) and 5-deoxyxylulose 1-phosphate (5-dXu 1P). 5-dXu 1P structure files were generated using the PRODRG server.(28) The Xu 5P structure utilized is the bound product in the SpRPE structure.(20) The MjRPE and SpRPE structures and Xu 5P and 5-dXu 1P ligands were prepared for docking using AutoDock Tools 1.5.6.(29) and AutoDock Vina(30) was used to perform the molecular docking for each product substrate into both *M. jannaschii* and *S. pyrogenes* RPE. The MjRPE and SpRPE were overlaid

prior to docking experiments in order to use the same box and coordinate parameters. Parameters for docking included using a box size of 10 Å x 10 Å x 10 Å for both structures. The *M. jannaschii* and *S. pyrogenes* RPE box was centered within the coordinates of (60.609, 96.956, 54.938). The position of the box was relative to the active site in each structure based on overlay coordinates. Re-docking of Xu 5P into the *S. pyrogenes* RPE demonstrated successful re-docking of Xu 5P into the active with an RMSD of 1.216 Å (Figure 4A) and suggests molecular docking as a viable method for studying 5-dXu 1P in *M. jannaschii*.

Assay of MjRPE via a coupled enzyme assay. The activity of MjRPE was assayed using several methods. First, MjRPE was analyzed for its canonical activity with Ru 5P. This was done by incubating the enzyme with 4.4 units phosphoribose isomerase from Spinach, 4 µg transketolase from *E. coli*, 3.8 units of triosephosphate isomerase from rabbit muscle, 2.7 units of glycerolphosphate dehydrogenase from rabbit muscle, 2.4 µg RPE, 10 mM $MgCl_2$, 0.13 mM TPP, 0.18 mM NADH, 0.41 mM erythrose, 0.45 mM $ZnCl_2$, and 0.41 mM ribose 5P in 110 µL 50 mM glycine-glycine buffer (pH 7.6). The reaction was initiated by the addition of ribose 5P and monitored at 340 nm and 25 ^oC for 10 minutes. The reaction was done with and without MjRPE in the reaction to confirm MjRPE activity.

In order to observe the proposed activity with 5-dRu 1P as the substrate, an enzyme coupled reaction using multiple enzymes, believed to be involved in the production of DKFP from 5'-dI, was developed (Figure S5). The activity of RPE was analyzed by GC-MS analysis of the dephosphorylated and reduced sugars as their TMS derivatives. This was done by incubation of MjRPE with methylthioinosine phosphorolase (MTIP) and methylthioribose 1-phosphate isomerase (MTRI) (Figure S5, brackets) and 5'-dI as the starting substrate. The assays were performed in a 100 µL of 50 mM glycine-glycine buffer (pH 7.6) with 0.4 µg of MTIP, 6 µg MTRI, 5 µg MJ0680, and a final concentration of 1 mM 5'-dI, 40 mM phosphate, 20 mM DTT, and 0.5 mM $ZnCl_2$ or $Fe(NH_4)_2(SO_4)_2$. The reaction mixture was incubated at 60 ^oC for 50 min then cooled on ice before addition of 2 mg *E. coli* alkaline phosphatase and 0.1 M glycine buffer (pH 10.4) with 1 mM ZnOAc and 1 mM $MgCl_2$ for a total volume of 127 µL and incubated at 37 ^oC for 1 hour for removal of the phosphate from the phosphorylated sugars. The samples were then heated at 100 ^oC for 5-10 min to precipitate the proteins and quench the reaction. The reaction mixtures were centrifuged to remove the precipitated proteins and the resulting supernatant was reduced by dissolving 0.5 mg of sodium borohydride ($NaBH_4$) in the sample and

allowing the reaction to proceed for 1-2 hours at room temperature. To desalt the sample, it was passed first through a column of Dowex-50W-X8 (H^+) 200-400 mesh (2 x 0.5 cm). The excess borohydride was removed by washing the evaporated samples with methanol and then evaporated to dryness under a stream of N_2 while being heated in a water bath at ~100 ^oC. The samples were run through a column of Dowex-1-X10 (OAc^-) 200-400 mesh (2 x 0.5 cm) followed by evaporation of the water. The resulting dried residue was reacted with 30-60 µL of a mixture of pyridine, hexamethyldisilazane, and chlorotrimethylsilane (9:3:1, vol/vol/vol) for 2-5 min at 100 ^oC. The samples were than analyzed by GC-MS as described below.

Assay of the *M. jannaschii* transketolase. The activity of the MjTK was tested with lithium hydroxypyruvate (HPA) as the donor ketose for all analysis. The use of HPA as the donating ketose results in the release of CO_2 from HPA, which blocks the reverse reaction.(31) Several different acceptor aldose sugars were tested for activity: glyceraldehyde, 5'-deoxyribose (5-dR, Waterstone), and erythrose. The assay was done in 100 µL of 50 mM TES (pH 7.4) with a final concentration of 0.5 mM HPA, 0.5 mM acceptor aldose, and 0.5 mM thiamine pyrophosphate (TPP), 0.5 mM $MgCl_2$ and 3 µg MjTK and incubated at 70 ^oC for 30 min. The reactants and products were then derivatized with NBHA by adjusting the reaction to pH 4 with 5 µL 1 M sodium acetate buffer (pH 4) and adding 2-fold excess of *O*-(4-nitrobenzyl)hydroxylamine (NBHA) (2.5 µL of 0.1 M) over the total aldose/ketose concentration. The samples were then incubated at 100 ^oC for 30 min, cooled to RT and then centrifuged for (2-4 min at 6,700 *x g*). The resulting soluble NBHA-derivitized sugars were analyzed by LC-ESI-MS as described below. Reference standards (Table S2) were prepared and analyzed in the same manner. To determine if the addition of cofactors to C-MjTK and N-MjTK prior to the standard assay (described above) would create an active enzyme, TPP and Mg^{2+} was incubated with C-MjTK and N-MjTK. Using the same methods described above the C-MjTK and N-MjTK, 3 µg of each, were pre-incubated with 0.5 mM TPP and $MgCl_2$ for 30 min at 70 ^oC prior to the addition of 0.5 mM erythrose and HPA.

Coupled assay to confirm production of lactaldehyde. In order to confirm that lactaldehyde is produced when 5'-dI is incubated with all the enzymes involved in DKFP biosynthesis (Figure S5) a coupled assay was performed with the alcohol dehydrogenase (ADH) from *Thermoanaerobium brockii* (Sigma, 100 units). ADH was chosen because it has been demonstrated to use utilize lactaldehyde as substrate and is used routinely as a method to monitor

enzyme activities.(32–34) In this assay, 3.2 µg MTIP, 5.3 µg MTRI, 5 µg RPE, and 4 µg TK were incubated in 1 mL 50 mM glycine-glycine buffer (pH 7.6) with a final concentration of 1 mM 5'-dI, 40 mM phosphate, 20 mM DTT, 0.5 mM $Fe(NH_4)_2(SO_4)_2$, 0.5 mM erythrose, 0.5 mM TPP, and 0.5 mM $MgCl_2$ overnight at 37 ^oC in vials made anaerobic by flushing with a stream of Ar. A control was done as described above without the addition of 5'-dI. The next day the samples were transferred to a warmed (40 ^oC) cuvette with the addition of 0.5 mM $NADP^+$ and 0.22 units of ADH (added last and mixed by rapid pipetting). The change in absorbance was followed at 340 nm for 5 min at 40 ^oC for the formation of NADPH when lactaldehyde is converted to 1,2-propanediol by the added ADH. The activity was calculated based on the NADPH extinction coefficient ($\varepsilon_{340\ nm}$ = 6.22 $mM^{-1}cm^{-1}$), where 1 µmol of NADPH is formed per min at 40 ^oC at pH 7.6.

LC-ESI-MS analysis of NBHA derivatized sugars and GC-MS analysis of reduced sugars. Analysis of the NBHA derivatives was also done by LC-ESI-MS (Agilent 1200 HPLC series in combination with an AB Sciex 3200 Q TRAP) using a Kromasil reverse phase C18 column (5 µM, 250 x 4.6 mm) and an AxxiChrom reverse phase C18 column (5 µm, 150 x 4.6 mm) with an injection volume between 5-25 µL. Two columns were used as the Kromasil C18 column was replaced with the AxxiChrom column over the course of time the experiments were being performed. Elution of the derivatives was done using 25 mM ammonium acetate (solvent A) and methanol (solvent B) with a total flow of 0.5 mL per min and the following gradient profile: (t (min), %B): (0.01, 0), (10.00, 65), (10.01-13.00, 95), (13.01-15.00, 0). Electrospray ionization was employed at 4500 volts and a temperature of 600 ^oC. Curtain gas, gas 1, and gas 2 flow pressures were 40, 60 and 50 psi, respectively. Desolvation, entrance, and collision cell potentials were 35, 12, and 10 volts, respectively. Mass analysis was performed in the Enhanced MS (EMS) mode, and positive ions were measured in the mass range 100-500 Da. The respective retention times and observed *m/z* for the analyzed NBHA-derivitized sugars are in Table S2. Only the major isomer for the NBHA-derivitized sugar is reported for clarity.

GC-MS spectra of standards and samples were obtained using a HP5890 gas chromatograph and VG-70-70EHF mass spectrometer. TMS derivatives were separated on a Phenomenex Zebron ZB-5MS plus 30 M x 0.32 mm 0.25 µm film capillary column. The oven temperature was programmed from 80 to 270 ^oC at 8 ^oC per minute. A 7 psi helium carrier gas was supplied and splitless injection (200 ^oC) was employed. The column effluent was introduced

into the electron impact ion source (200 ^{o}C) of the mass spectrometer, which was scanned from 50 to 400 amu at 1 second/decade. Mass spectral data was acquired and processed with a VG Opus data system.

Results

Cloning, Overexpression, and Purification of *M. jannaschii* MjRPE, C-MjTK, and C-MjTK Gene Products in *E. coli*. MjRPE, C-MjTK, and N-MjTK derived proteins were highly expressed in *E. coli* as measured from the SDS-PAGE analysis of the total proteins in the *E. coli* cells after expression. After sonication of the *E. coli* cells suspended in extraction buffer and centrifugation (14,000 × *g*, 5 min), SDS-PAGE analysis of the soluble material and the pellet demonstrated that most of the expressed MjRPE, C-MjTK, and N-MjTK proteins were found in the soluble extracts. Heating portions of the resulting crude soluble extract for 10 min at different temperatures indicated that MjRPE was only soluble up to 60 ^{o}C while C-MjTK and N-MjTK remained soluble up to 70 °C based on SDS-PAGE analysis. The first step in the purification of the MjRPE, C-MjTK, and N-MjTK was heating of the sonicated cell extracts at 60 and 70 °C for 20 min prior to purification of the desired soluble enzymes via MonoQ, respectfully. Under the conditions used, MjRPE eluted at 0.48 M NaCl, C-MjTK at 0.48 M NaCl, and N-MjTK at 0.4 M NaCl as measured by SDS-PAGE. MALDI analysis of the tryptic digests of the excised bands from SDS-PAGE identified MjRPE gene product with six unique tryptic peptides.

Dual Cloning, Overexpression, and Purification of *M. jannaschii* C-MjTK and N-MjTK Gene Products together in *E. coli*. Two attempts were made to overexpress C-MjTK and N-MjTK simultaneously. In the first attempt, the two plasmids containing C-MjTK and N-MjTK were cloned separately into *E. coli* at the same time and random colonies were screened for both proteins by SDS-PAGE. Using this method, a single colony was found to contain both proteins (Figure 3A), which was further verified by MALDI-MS analysis of the cut and excised bands where eight and nine peptides were identified for C-MjTK and N-MjTK, respectfully. Unlike in the single expression of the two proteins the dual expression demonstrated C-MjTK and N-MjTK (further denoted MjTK) was found to be thermally stable to temperatures above 80 ^{o}C (Figure 3B). The observed bands were sequenced by MALDI-MS and confirmed to be C-MjTK and N-MjTK, by identification of ten and nine peptides for C-MjTK and N-MjTK, respectfully, in the 80 ^{o}C heated MjTK. In order to prevent separation of the two TK halves, MjTK was purified by SEC (Figure 3C) following heating at 80 ^{o}C for 20 min to remove a

majority of the *E. coli* proteins. Unfortunately, successful overexpression of both proteins using the pRSFDuet-1 vector was unsuccessful. Only C-MjTK was overexpressed as determined by SDS-PAGE and LC-ESI-MS/MS (see supplemental information). Further attempts to clone the two genes together were not attempted.

Metal and SEC analysis of *M. jannaschii* RPE. Interestingly, when MjRPE was analyzed for metals by ICP-MS, no metal was found to be present (Table 1). The presence of a divalent metal, such as Zn(II) or Fe(II), is required for catalysis, where it stabilizes the endiolate intermediate through electrostatic interactions with the O_2 and O_3 of Ru 5P or Xu 5P.(20) When analyzing for activity both Zn^{2+} and Fe^{2+} were used and MjRPE was active with both metals. The human and *E. coli* RPE have both been shown to be Fe^{2+} dependent(35, 36); however, many RPEs are Zn^{2+} dependent.(20) In experiments mimicking the Archaean ocean, which had a high concentration of Fe(II), the metabolites from glycolysis and PPP were shown to interconvert without any organism or enzyme present to catalyze the reactions.(37) The presence of Fe(II) in the experiments demonstrated stabilization of the sugar-phosphates and specificity for the interconversion of metabolites.(37) These experiments further suggest that due to the abundance of Fe(II) in the Archaean oceans that ancient enzymes were Fe(II) dependent.(38) These data would support that MjRPE is likely Fe(II) dependent, but Zn(II) is able to substitute for Fe(II) and generate an active enzyme. The details of this metal dependence were not further examined given assay conditions used to examine the MjRPE activity contain excess phosphate, which is required for the upstream MTIP enzyme in the developed assay for phosphorolysis of 5'-dI to 5-dR 1P (Figure S5). The excess phosphate reacts with the added Fe(II), zinc, nickel, or cobalt forming an insoluble metal-phosphate precipitate. Unfortunately, at this time, MjRPE was not able to be assayed separately of the upstream enzymes as the substrate, since 5-dRu 1P is difficult to organically synthesize and is not commercially available.

The native molecular weight of MjRPE was determined to be a dimer with a monomeric weight of 36 kDa. The RPE from human has also been described as a dimer (36); however, it is most often described as a hexamer from potato chloroplasts(39), *E. coli*(35), and *S. pyrogenes*(20). The MjRPE shares no more than 45% sequence identity with known RPE enzymes, yet the active site and metal ligands are well conserved (Figure S2). The two aspartate residues that have been identified to be the general acid (Asp172, *M. jannaschii* numbering) and base (Asp34) are conserved in *M. jannaschii* as well as those residues that coordinate the

divalent metal (either Zn^{2+} or Fe^{2+}). The conservation of these residues (Figure S2) suggest that the mechanism would proceed in the same manner has been well established for RPE (Figure 4A).(20, 36, 39–41) In the mechanism, Asp34 abstracts of a proton from the C3 of Ru 5P forming a enediolate intermediate, which is then protonated by Asp172 from the opposite side resulting in a change in the stereochemistry at C3 generating Xu 5P (Figure 4A). The mechanism of MjRPE would proceed in an identical manner with 5-dRu 1P as a substrate to generate 5-dXu 1P (Figure 4B).

Molecular modeling and docking of products into MjRPE. In order to assess if the position of the phosphate at C1 instead of C5 and if methyl moiety at C5 instead of phosphate would alter the binding capacity of the substrate or product, molecular modeling and docking studies were performed. SpRPE was chosen because it shared 44% sequence identity with the MjRPE, has Zn(II) and D-xylitol-5-phosphate bound in the active site of the crystal structure.(20) Several approaches were used to assess the ability of 5-dXu 1P and Xu 5P to dock into the active site of SpRPE and MjRPE. First, Xu 5P was re-docked into the active site to confirm that the molecular docking techniques were able to generate the same results as the X-ray crystal structure (Figure 5A). The re-docked, lowest energy pose of Xu 5P (-6.5 kcal mol^{-1}) had an RMSD of 1.216 Å compared to the originally bound product, D-xylitol 5P, in the crystal structure. Second, the lowest energy pose of 5-dXu 1P (-6.4 kcal mol^{-1}) docked into the active site of SpRPE (Figure 5B) showed it was able to orient in the active site similar to Xu 5P (Figure 5C). These results suggest that Xu 5P and 5-dXu 1P can bind into the active site with distances to key residues that are similar to Xu 5P to suggest catalysis is possible with 5-dXu 1P (Table 2 and Figure 4A). The molecular docking of Xu 5P and 5-dXu 1P were then examined in the MjRPE model.

The MjRPE model was generated and assessed using Anolea(22, 23), QMEAN(24), Verify 3D(25, 26), and ProCheck(27). Validation using these metrics show that a majority of the model is energetically favorable (Figure S3B). An overlay of the MjRPE model and SpRPE structures (Figure S3A) demonstrates that the modeled MjRPE shares a high degree of structural similarity in major secondary structure as well as in conservation in active site residue placement (Figure 5). As predicted based on sequence homology, the lowest energy pose of Xu 5P docked (-6.5 kcal mol^{-1}) into the MjRPE active site oriented correctly for catalysis (Figure 5D) as compared with SpRPE (Figure 5A). The measured distances from Xu 5P to the Zn(II), general

acid, and general base residues are slightly longer than for SpRPE (Table 2), but are still within 5 Å, which is the maximum distance for electrostatic interactions to occur. The lowest energy pose of 5-dXu 1P (-4.6 kcal mol^{-1}) docked into MjRPE also bound in the active site in a similar orientation to that of SpRPE with 5-dXu 1P (Figure 5B and E). The measured distances of 5-dXu 1P to Zn(II), the general acid, and general base (Table 2) and observed docked pose in the MjRPE modeled structure all support 5-dXu 1P as a catalytically competent substrate for both SpREP and MjRPE and that the mechanism would be identical with 5-dRu 1P as the substrate (Figure 4B).

Analysis of MjRPE activity. Analysis of MjRPE activity was analyzed by several methods. The canonical activity was examined using several enzymes from the pentose phosphate pathway and glycolysis to confirm that Ru 5P is a substrate (Figure 2A). The results demonstrated that when MjRPE was included in the assay, there was a decrease the absorbance at 340 nm indicating that Xu 5P was produced. Xu 5P is then converted to fructose and Ga 3P by the transketolase. Ga 3P was then isomerized to dihydroxyacetone phosphate and hydrogenated to glycerol 3P by triosephosphate isomerase and glycerol phosphate dehydrogenase. Using this assay, a specific activity of 9.38 µmol min^{-1} mg^{-1} for MjRPE was measured. No change in absorbance was observed when MjRPE was excluded. These results demonstrate that MjRPE is able to catalyze the epimerization of Ru 5P to Xu 5P (Figure 2A).

In order to analyze the ability of MjRPE to use 5-dRu 1P as a substrate (Figure 2B), MjRPE was coupled with MTIP and MTRI from *M. jannaschii* to generate this substrate (Figure S5). In this assay, 5'-dI was enzymatically transformed to 5-dRu 1P by MTIP and MTRI by phosphorolysis and isomerization (Figure S5). MTIP and MTRI were demonstrated to be catalytically efficient with 5'-dI and 5-dR 1P as substrates (k_{cat}/K_M of 7.6 x 10^3 $s^{-1}M^{-1}$ and 1.7 x 10^2 $s^{-1}M^{-1}$, respectively) in previous work by our laboratory.(42) The analysis of the epimerization reaction was done with and without the addition of MjRPE to the assay and analyzed by GC-MS of the TMS derivatives (Figure 6). A standard of 5-dR was used to verify the observed 5-deoxyribitol peak produced from MTIP and MTRI, by comparison of elution time and mass spectra. Upon inclusion of MjRPE, to the coupled assay a new peak was observed on the GC trace eluted before 5-dR (Figure 6A). The mass chromatogram confirmed that the new peak contained fragments suggesting that it was a deoxysugar, either 5-dR or 5-deoxyxylitol (5-dX) (Figure 6B and C). In analysis of ribitol and xylitol $(TMS)_5$ derivatives, the same elution

pattern was observed, with xylitol eluting prior to ribitol. These results suggest that the new peak eluting before 5-dR is 5-dX (Figure 6). Additionally, when the phosphatase step was excluded in the methods, no peak was detected by GC-MS when MjRPE was both absent in present from the assay suggesting that the MjRPE substrate and product are both phosphorylated. Together, these results suggest that MjRPE is active with 5-dRu 1P as a substrate and 5-dXu 1P is the product. Unfortunately, the data was not quantified at this time so the efficiency of 5-dRu 1P as a substrate was not determined. It will be of further interest to compare the activity of MjRPE with Ru 5P and 5-dRu 1P.

Structure and metal analysis *M. jannaschii* TK. The molecular mass of the C-MjTK was measured to be ~410 kDa, N-MjTK ~320 kDa using size exclusion chromatography (Table 3), suggesting that C-MjTK is a dodecamer and N-MjTK is a decamer. Alternatively, these results could indicate that the individual subunits C-MjTK and N-MjTK are large protein aggregates. Since neither C-MjTK nor N-MjTK were found to be active it would suggest that the proteins are aggregates and not a dodecamer or decamer. When a 1:1 ratio of C-MjTK and N-MjTK was analyzed by SEC, a heptamer (~450 kDa) was observed (Table 3). These data suggest the N-MjTK and C-MjTK are unable to form an active enzyme, which is presumably because the two halves are unable to form a structural conformation that is catalytically competent.

The TK is a well characterized enzyme and has been determined to be a homodimer from numerous organism such as human TK(43), *E. coli* TK(44), and the yeast TK(45). However, in human, *E. coli,* and yeast, the TK is encoded by a single gene. In contrast, *M. jannaschii* and other methanogens, the TK enzyme is encoded by at least two, separate genes. It is well known that a single gene can encode multiple enzymes(46–48), but the reverse has not been described. Since, the *M. jannaschii* TK is encoded by two genes, it would suggest that formation of a functionally active enzyme might be more complicated. The MjTK is encoded by two genes: MJ0681 encoding the *N*-terminus (N-MjTK) and MJ0679 encoding the *C*-terminus (C-MjTK) (Figure 7, blue and green, respectfully). Analysis of the quarternary structure by SEC of the co-expressed MjTK determined a native molecular weight of 171 kDa, which with a heterodimeric mass of 64 kDa suggests a dimer for MjTK. The quartnary structure of MjTK would be described as a dimer of heterodimers, where this structure is only formed when the two genes are co-expressed. Co-expression of two genes for an active enzyme has been demonstrated before,

with several enzymes involved in macrolide antibiotic biosynthesis.(49) However, in this case, the two genes did not encode a whole protein, instead one of the two proteins enhanced the activity of the other protein.(49) This is the first report of a single, active enzyme being encoded by two gene products to the author's knowledge.

Metal analysis of N-MjTK and C-MjTK demonstrate that the *M. jannaschii* uses magnesium for stabilization of TPP (Table 1). The TK has been shown previously from other organisms to coordinate either magnesium or calcium.(50, 51) Coordination of the divalent metal, either Mg^{2+} or Ca^{2+} have been shown to be essential for stabilization of the pyrophosphate moiety of TPP and reconstitution of apo-TK, from yeast, with divalent metals showed dependence with TPP binding.(44) The Mg^{2+} was found in N-MjTK, which is in agreement with the metal binding domain being located in the N-terminal region of TK as has been shown with the TK from human and *Mycobacterium tuberculosis*.(51)

Molecular modeling of the full length MjTK was done to determine the similarities and differences of the MjTK and canonical TK structures. The model is mostly energetically favorable based on validation metrics, with some small sections of positive energy in loop regions, an expected result given loop variability (Figure S4). The full-length model of MjTK compared to the HsTK structure shows two domain regions, with the active site in a region joining them (Figure 7, grey). Molecular modeling of the MjTK clearly demonstrates that the fully length protein overlays with the HsTK (Figure 7) and that the C-MjTK and N-MjTK regions overlay with the two domain regions of the HsTK (Figure 7). The molecular modeling and co-expression data indicates that modern TK enzymes merged into a single gene over time and likely originated with the enzyme being encoded by two separate halves, as is commonly found in the methanogenic genomes. This hypothesis is consistent with observed gene fusion events that have led to the formation of multifunctional proteins that are encoded from a single gene.(46, 52)

Analysis of *M. jannaschii* TK for activity. In order to determine if the TK from *M. jannaschii* shared the broad substrate usage that has been described in other TK's(53), several different aldose acceptors were tested for activity. These assays were performed with HPA as the donor ketose since HPA generates CO_2, which makes the TK reaction irreversible.(54) The results of our analysis demonstrate that the *M. jannaschii* TK (co-expressed MjTK) was active with erythrose, 5-deoxyribose, and glyceraldehyde as the and MH^+ and $(M^+Na)^+$ products,

fructose, 7-deoxysedoheptose, and xylulose (elutes the same as ribose) were confirmed by LC-ESI-MS (Table S2). HPA and erythrose were used regularly to confirm the TK was active as standards of the substrates and products could be used for controls. The separately assayed C-MjTK, N-MjTK and 1:1 mixture of C-MjTK: N-MjTK did not demonstrate activity under any of the assays conditions attempted. These results demonstrate that for an active enzyme, the TK from *M. jannaschii* must be co-expressed simultaneously to generate a properly folded protein. This is supported by SEC analysis of the recombinant C-MjTK and N-MjTK halves and MjTK (Table 3).

Confirmation of lactaldehyde production from 5'-dI. In order to assess if lactaldehyde was produced from 5'-dI, an enzyme coupled reaction was pursued. The enzymes from *M. jannaschii* proposed to be involved in this pathway (Figure S5) were coupled to an alcohol dehydrogenase (EC 1.1.1.2). Only upon the production of lactaldehyde from the coupled *M. jannaschi* enzymes, would the reduction of $NADP^+$ to NADPH be observed when lactaldehyde was oxidized to 1,2-propanediol. In order to allow for ample production of lactaldehyde from 5'-dI, the reaction was allowed to incubate at 37 ^oC overnight prior to the addition of $NADP^+$ and alcohol dehydrogenase. The results demonstrated that only when 5'-dI was present in the reaction, did the reduction of $NADP^+$ occur. Based on this observation, we concluded that lactaldehyde was produced from incubation of 5'-dI with MTIP, MTRI, MjRPE, and MjTK and all necessary cofactors. A specific activity of 0.23 μmol min^{-1} mg^{-1} MjTK was calculated for the MjTK with lactaldehyde and erythrose as substrates.

Discussion

The identification of enzyme function is a challenging task, but with functional characterization of homologous enzymes the functional assignment of unknown enzymes can begin to be revealed. The functional identification of enzymes can revel the metabolic pathways that these enzymes are involved, which includes new pathways or filling in the missing gaps of canonical pathways. Here we demonstrate that the annotated ribulose 5-phosphate 3-epimerase (RPE) and transketolase (TK) enzymes from *M. jannaschii* function as canonical RPE and TK enzymes (Figure 2A), but are unlikely using ribulose 5-phosphate and xylulose 5-phosphate as substrates. Instead, I have proposed that these enzymes are involved in a related biochemical pathway for the salvage of the 5-deoxyribose moiety of 5'-dA for deoxysugars in *M. jannaschii* (Figure 8).

The salvage of 5'-dA is an essential process across all organisms. 5'-dA is one of the major products of radical *S*-adenosyl-L-methionine (SAM) catalyzed reactions; however, there is little information in the literature about what happens to 5'-dA. 5'-Deoxyadenosine has been shown to be a substrate by a methylthioadenosine/*S*-adenosylhomocysteine nucleosidase to produce 5-deoxyribose and adenine in bacteria.(55, 56) However, *Archaea* and *Eukaryotes* do not typically have this nucleosidase present in their genomes as they typically salvage the SAM derived metabolites, methylthioadenosine and *S*-adenosylhomocysteine through alternative routes.(57, 58) *S*-Adenosylhomocysteine is hydrolyzed by a specific hydrolase(59) to homocysteine and adenosine while methylthioadenosine is phosphorolyzed to methytlhioribose 1-phosphate and adenine.(60) In spite of these well-studied enzymes, our laboratory has demonstrated that in *M. jannaschii* the initial steps for the salvage of methylthioadenosine, *S*-adenosylhomocysteine, and 5'-deoxyadenosine is different.(13) Each of these metabolites have been demonstrated to be first deaminated by a 5'-deoxyadenonsine deaminase to methylthioinosine, *S*-inosylhomocysteine, and 5'-deoxyinosine (5'-dI).(13) Furthermore, the annotated *S*-adenosylhomocysteine hydrolase was demonstrated to be specific for *S*-inosylhomocysteine, further establishing that the salvage of SAM metabolites proceed through alternative pathways.(61)

The discovery of MTIP and MTRI's ability to use multiple substrates, including 5'-dI and 5-deoxyribose 1-phosphate (5-dR 1P)(42) suggest a new route for 5'-dA salvage. A possible route for the production of lacaldehyde from 5'-dI was proposed based on the observed production of 5-dXu 1P and lactaldehyde when MjRPE and MjTK were assayed with MTIP and MTRI. Confirmation of lactaldehyde production when all four enzymes from *M. jannaschii* incubated together with 5'-dI (Figure S5) was demonstrated when an alcohol dehydrogenase was included. The observed reduction of $NADP^+$ to NADPH by the alcohol dehydrogenase would only be observed if lactaldehyde was present in the analyzed samples. These results further suggest that the proposed pathway is feasible. Unfortunately, the enzymatic rates were unable to be determined for MjRPE and MjTK with 5-dRu 1P and 5-dXu 1P as substrates at this time, but will be of further interest to determine if the proposed pathway would be feasible *in vivo*.

Once lactaldehyde has been generated, it is known that *M. jannaschii* cell extracts are able to oxidize lactaldehyde to methylglyoxal with $F_{420}H_2$.(62) Until recently, the enzyme responsible for the oxidation of lactaldehyde had been unknown.(63) The enzyme was identified

to be N^5, N^{10}-methylenetetrahydromethanopterin reductase (Mer), which was purified from *M. jannaschii* cell extracts based on activity.(63) Mer is an essential enzyme involved in methanogensis and has been well studied from other methanogens.(64–67) Methylglyoxal is then utilized by the DKFP synthase along with fructose 1,6-bisphosphate to generate DKFP and Ga 3P (Figure 8).(68)

In conclusion, these experiments support the production of lactaldehyde from 5'-dI when MTIP, MTRI, MjRPE, and MjTK are incubated together. The observed production of intermediates, 5-dXu 1P and lactaldehyde, support the role of RPE and TK in the production of the deoxysugar necessary for the production methylglyoxal (Figure 8). However, if the proposed pathway is the sole source of DKFP remains to be determined. Interestingly, it is well known that in mammals cysteine is made primarily from methionine via SAM(69), which could indicate that there is enough flux through SAM to allow 5'-dA be the major source of deoxysugars for aromatic amino acid biosynthesis in methanogens.

Acknowledgements. The authors thank Dr. W. Keith Ray for performing the mass spectrometry experiments. The mass spectrometry resources are maintained by the Virginia Tech Mass Spectrometry Incubator, a facility operated in part through funding by the Fralin Life Science Institute at Virginia Tech and by the Agricultural Experiment Station Hatch Program (CRIS Project Number: VA-135981). This work was supported by the National Science Foundation Grant MCB1120346. Funding for this work was also provided in part by the Agricultural Experiment Station and Hatch Program of the National Institute of Food and Agriculture, U.S. Department of Agriculture.

References

1. **Tian W**, **Skolnick J**. 2003. How well is enzyme function conserved as a function of pairwise sequence identity? J Mol Biol **333**:863–882.
2. **Schnoes AM**, **Brown SD**, **Dodevski I**, **Babbitt PC**. 2009. Annotation error in public databases: misannotation of molecular function in enzyme superfamilies. PLoS Comput Biol **5**:e1000605.
3. **Grochowski LL**, **White RH**. 2008. Promiscuous anaerobes: New and unconventional metabolism in methanogenic archaea. Ann N Y Acad Sci **1125**:190–214.
4. **Orita I**, **Sato T**, **Yurimoto H**, **Kato N**, **Atomi H**, **Imanaka T**, **Sakai Y**. 2006. The Ribulose Monophosphate Pathway Substitutes for the Missing Pentose Phosphate Pathway in the Archaeon Thermococcus kodakaraensis. J Bacteriol **188**:4698–4704.
5. **Soderberg T**. 2005. Biosynthesis of ribose-5-phosphate and erythrose-4-phosphate in arcaea: a phylogenetic analysis of archaeal genoes. Archaea **1**:347–352.
6. **Grochowski LL**, **Xu H**, **White RH**. 2005. Ribose-5-phosphate biosynthesis in Methanocaldococcus jannaschii occurs in the absence of a pentose-phosphate pathway. J Bacteriol **187**:7382–7389.
7. **Soderberg T**, **Alver RC**. 2004. Transaldolase of Methanocaldococcus jannaschii. Archaea **1**:255–262.
8. **Kruger NJ**, **von Schaewen A**. 2003. The oxidative pentose phosphate pathway: structure and organisation. Curr Opin Plant Biol **6**:236–246.
9. **White RH**. 2004. L-aspartate semialdehyde and a 6-deoxy-5-ketohexose 1-phosphate are the precursors to the aromatic amino acids in Methanocaldococcus jannaschii. Biochemistry **43**:7618–7627.
10. **Pittard J**, **Yang J**. 2008. Biosynthesis of the aromatic amino acids. EcoSal Plus **3**:1–75.
11. **Bentley R**, **Haslam E**. 1990. The Shikimate Pathway — A Metabolic Tree with Many Branches. Crit Rev Biochem Mol Biol **25**:307–384.
12. **Ekiel I**, **Smith I a NCP**, **Sprott GD**. 1983. Biosynthetic pathways in Methanospirillum hungatei as determined by 13C Nuclear Magnetic Resonance. J Bacteriol **156**:316–326.
13. **Miller D**, **O'Brien K**, **Xu H**, **White RH**. 2014. Identification of a 5′-Deoxyadenosine Deaminase in Methanocaldococcus jannaschii and its Possible Role in Recycling the Radical SAM Enzyme Reaction Product 5′-Deoxyadenosine. J Bacteriol **196**:1064–1072.

14. **Graham DE**, **Xu H**, **White RH**. 2002. Identification of coenzyme M biosynthetic phosphosulfolactate synthase. A new family of sulfonate-biosynthesizing enzymes. J Biol Chem **277**:13421–13429.
15. **Bradford MM**. 1976. A rapid and sensitive method for the quantitation of microgram quantities of protein utilizing the principle of protein dye-binding. Anal Biochem **72**:248–257.
16. **Miller D V**, **Xu H**, **White RH**. 2012. A new subfamily of agmatinases in methanogenic Archaea is Fe(II) dependent. Biochemistry **51**:3067–3078.
17. **Shuman S**. 1990. Catalytic activity of vaccinia mRNA capping enzyme subunits coexpressed in Escherichia coli. J Biol Chem **265**:11960–11966.
18. **Li C**, **Schwabe JWR**, **Banayo E**, **Evans RM**. 1997. Coexpression of nuclear receptor partners increases their solubility and biological activities. Proc Natl Acad Sci **94**:2278–2283.
19. 2013. Molecular Operating Enviroment (MOE), 2013.08. 1010 Sherbooke St. West, Suite#910, Montreal, QC, Canada, H3A 2R7.
20. **Akana J**, **Fedorov AA**, **Fedorov E**, **Novak WRP**, **Babbitt PC**, **Almo SC**, **Gerlt JA**. 2006. D-Ribulose 5-Phosphate 3-Epimerase: Functional and Structural Relationships to Members of the Ribulose-Phosphate Binding (beta/alpha)8-Barrel Superfamily. Biochemistry **45**:2493–2503.
21. **Wang J**, **Wolf RM**, **Caldwell JW**, **Kollman PA**, **Case DA**. 2004. Development and testing of a general amber force field. J Comput Chem **25**:1157–1174.
22. **Melo F**, **Feytmans E**. 1998. Assessing Protein Structures with a Non-local Atomic Interaction Energy. J Mol Biol **277**:1141–1152.
23. **Melo F**, **Sali A**. 2007. Fold assessment for comparative protein structure modeling. Prot Sci **16**:2412–2426.
24. **Benkert P**, **Tosatto SCE**, **Schomburg D**. 2007. QMEAN: A comprehensive scoring function for model quality assessment. Proteins: Struct, Funct, Bioinf **71**:261–277.
25. **Luthy R**, **Bowie JU**, **Eisenberg D**. 1992. Asssessment of protein models with three-dimensional profiles. Nature **356**:83–85.
26. **Bowie JU**, **Luthy R**, **Eisenberg D**. 1991. A method to identify protein sequences that fold into a known three deminsional structure. Science (80-) **253**:164–170.

27. **Laskowski RA**, **MacArthur MW**, **Moss DS**, **Thornton JM**. 1993. PROCHECK: a program to check the stereochemical quality of protein structures. J Appl Crystallogr **26**:283–291.
28. **Schuttelkopf AW**, **Van Aalten DMF**. 2004. PRODRG: a tool for high-throughput crystallography of protein-ligand complexes. Acta Crystallogr Sect D Biol Crystallogr **60**:1355–1363.
29. **Morris GM**, **Huey R**, **Lindstrom W**, **Sanner MF**, **Belew RK**, **Goodsell DS**, **Olson AJ**. 2009. AutoDock 4 and AutoDock Tools 4: automated docking with selective receptor flexibility. J Comput Chem **16**:2785–2791.
30. **Trott O**, **Olson AJ**. 2010. AutoDock Vina: Improving the speed and accuracy of docking with a new scoring funcion, efficient optimization and multithreading. J Comput Chem **31**:455–461.
31. **Solovjeva ON**, **Kochetov GA**. 1999. Inhibition of transketolase by p-hydroxyphenylpyruvate. FEBS Lett **462**:246–248.
32. **Bosron WF**, **Prairie RL**. 1972. Triphosphopyridine nucleotide-linked aldehyde reductase I. Purification and properties of the enzyme from pig kidney cortex. J Biol Chem **247**:4480–4485.
33. **Wermuth B**, **Münch JD**, **Von Wartburg JP**. 1977. Purification and properties of NADPH-dependent aldehyde reductase from human liver. J Biol Chem **252**:3821–3828.
34. **Bryant FO**, **Wiegel J**, **Ljungdahl LG**. 1988. Purification and properties of primary and secondary alcohol dehydrogenases from Thermoanaerobacter ethanolicus. Appl Environ Microbiol **54**:460–465.
35. **Sobota JM**, **Imlay JA**. 2011. Iron enzyme ribulose-5-phosphate 3-epimerase in Escherichia coli is rapidly damaged by hydrogen peroxide but can be protected by manganese. PNAS **108**:5402–5407.
36. **Liang W**, **Ouyang S**, **Shaw N**, **Joachimiak A**, **Zhang R**, **Liu Z-JZ-J**. 2011. Conversion of D-ribulose 5-phosphate to D-xylulose 5-phosphate: new insights from structural and biochemical studies on human RPE. FASEB J **25.2**:497–504.
37. **Keller MA**, **Turchyn A V**, **Ralser M**. 2014. Non-enzymatic glycolysis and pentose phosphate pathway-like reactions in a plausible Archean ocean. Mol Syst Biol **10**:725.
38. **Belmonte L**, **Mansy SS**. 2016. Metal Catalysts and the Origin of Life. Elements **12**:413–

418.

39. **Kopp J**, **Kopriva S**, **Suss K-H**, **Shulz GE**. 1999. Structure and Mechanism of the Amphibolic Enzyme D-Ribulose-5-phosphate 3-Epimerase from Potato Chloroplasts. J Mol Biol **287**:761–771.
40. **Davis L**, **Lee N**, **Glaser L**. 1972. On the Mechanism of the Penotose Phosphate Epimerases. J Biol Chem **247**:5862–5866.
41. **McDonough MW**, **Wood WA**. 1961. The Mechanism of Pentose Phosphate Isomerization and Epimerization Studied with T2O and H2O18. J Biol Chem **236**:1220–1224.
42. **Miller D V**, **Rauch BJ**, **Harich K**, **Xu H**, **Perona JJ**, **White RH**. 2017. Uncovering the Anaerobic Methionine Salvage Pathway in Methanocaldococcus jannaschii and Methanosarcina acetivorans.
43. **Mitschke L**, **Parthier C**, **Schroder-Tittmann K**, **Coy J**, **Ludtke S**, **Tittmann K**. 2010. The Crystal Structure of Human Transketolase and New Insights into its Mode of Action. J Biol Chem **285**:31559–31570.
44. **Sprenger GA**, **Schorken U**, **Sahm H**. 1995. Transketolase A of Escherichia coli K12 Purification and properties of the enzyme from recombinant strains. Eurpean J Biochem **230**:525–532.
45. **Lindqvist Y**, **Schneider G**, **Ermler U**, **Sunstrom M**. 1992. Three-dimensional structure of transketolase, a thiamine diphosphate dependent enzyme, at 2.5 A resolution. EMBO J **11**:2373–2379.
46. **Kirschner K**, **Bisswanger H**. 1976. Multifunctional proteins. Annu Rev Biochem **45**:143–166.
47. **Gaertner FH**, **Cole KW**. 1977. A cluster-gene: evidence for one gene, one polypeptide, five enzymes. Biochem Biophys Res Commun **75**:259–264.
48. **Smith S**. 1994. The animal fatty acid synthase: one gene, one polypeptide, seven enzymes. FASEB J **8**:1248–1259.
49. **Charles E. Melancon III and Hung-wen Liu HT**. 2004. Characterization of tylM3/tylM2 and mydC/mycD Pairs Required for Efficient Glycosyltransfer in Macrolide Antibiotic Biosynthesis. J Am Chem Soc **126**:16726–16727.
50. **Kochetov GA**, **Sevostyanova IA**. 2005. Binding of the Coenzyme and Formation of the

Transketolase Active Center. IUBMB Life **57**:491–497.

51. **Fullam E**, **Pojer F**, **Bergfors T**, **Jones TA**, **Cole ST**. 2012. Structure and function of the transketolase from Mycobacterium tuberculosis and comparison with the human enzyme. Open Biol **2**:110026.
52. **Elleuche S**. 2015. Bringing functions together with fusion enzymes—from nature's inventions to biotechnological applications. Appl Microbiol Biotechnol **99**:1545–1556.
53. **Yi D**, **Devamani T**, **Abdoul-Zabar J**, **Charmantray F**, **Helaine V**, **Hecquet L**, **Fessner W-D**. 2012. A pH-based High Throughput Assay for Transketolase: Fingerprinting of Substrate Tolerance and Quantitative Kinetics. ChemBioChem **13**:2290–2300.
54. **De La Haba G**, **Leder IG**, **Racker E**. 1955. Crystalline Transketolase from Baker's Yeast: Isolation and Properties. J Biol Chem **214**:409–426.
55. **Choi-Rhee E**, **Cronan JE**. 2005. A nucleosidase required for in vivo function of the S-adenosyl-L-methionine radical enzyme, biotin synthase. Chem Biol **12**:589–593.
56. **Challand MR**, **Martins FT**, **Roach PL**. 2010. Catalytic activity of the anaerobic tyrosine lyase required for thiamine biosynthesis in Escherichia coli. J Biol Chem **285**:5240–5248.
57. **Sekowska A**, **Dénervaud V**, **Ashida H**, **Michoud K**, **Haas D**, **Yokota A**, **Danchin A**. 2004. Bacterial variations on the methionine salvage pathway. BMC Microbiol2004/04/23. **4**:9.
58. **Sauter M**, **Moffatt B**, **Saechao MC**, **Hell R**, **Wirtz M**. 2013. Methionine salvage and S-adenosylmethionine: essential links between sulfur, ethylene and polyamine biosynthesis. Biochem J **451**:145–154.
59. **Fujioka M**, **Takata Y**. 1981. S-Adenosylhomocysteine Hydrolase from Rat Liver. J Biol Chem **256**:1631–1635.
60. **Appleby TC**, **Mathews II**, **Porcelli M**, **Cacciapuoti G**, **Ealick SE**. 2001. Three-dimensional structure of a hyperthermophilic 5′-deoxy-5′-methylthioadenosine phosphorylase from Sulfolobus solfataricus. J Biol Chem **276**:39232–39242.
61. **Miller D V**, **Xu H**, **White RH**. 2015. S-Inosylhomocysteine Hydrolase: A novel enzyme involved in SAM recycling. J Bacteriol **197**:1-8 JB – 00080.
62. **White RH**. 2008. Biochemical Origins of Lactaldehyde and Hydroxyacetone in Methanocaldococcus jannaschii. Biochemistry **47**:5037–5046.
63. **Miller D V**, **Ruhliln M**, **Ray WK**, **Xu H**, **White RH**. 2017. N5,N10-

methylenetetrahydromethanopterin reductase from Methanocaldococcus jannaschii shows catalytic promiscuity as an NADPH dependent methylglyoxal reductase. Prep.

64. **MA K**, **THAUER RK**. 1990. Purification and properties of N5, N10-methylenetetrahydromethanopterin reductase from Methanobacterium thermoautotrophicum (strain Marburg). Eur J Biochem **191**:187–193.
65. **Ma K**, **Linder D**, **Stetter KO**, **Thauer RK**. 1991. Purification and properties of N 5, N 10-methylenetetrahydromethanopterin reductase (coenzyme F420-dependent) from the extreme thermophile Methanopyrus kandleri. Arch Microbiol **155**:593–600.
66. **Kunow J**, **Schworer B**, **Setzke E**, **Thauer RK**. 1993. Si-face stereospecificity at C5 of coenzyme F420 for F420-dependent N5, N10-methylenetetrahydromethanopterin dehydrogenase, F420-dependent N5, N10-methylenetetrahydromethanopterin reductase and F420H2: dimethylnaphthoquinone oxidoreductase. Eur J Biochem **214**:641–646.
67. **Shima S**, **Warkentin E**, **Grabarse W**, **Sordel M**, **Wicke M**, **Thauer RK**, **Ermler U**. 2000. Structure of coenzyme F 420 dependent methylenetetrahydromethanopterin reductase from two methanogenic archaea. J Mol Biol **300**:935–950.
68. **White RH**, **Xu H**. 2006. Methylglyoxal is an intermediate in the biosynthesis of 6-deoxy-5-ketofructose-1-phosphate: A precursor for aromatic amino acid biosynthesis in Methanocaldococcus jannaschii. Biochemistry **45**:12366–12379.
69. **Griffith OW**. 1987. Mammalian sulfur amino acid metabolism: An overview. Methods Enzymol **143**:367–376.

Tables

Table 1. Metal analysis of MjRPE, C-MjTK, and N-MjTK

	Calcium	Magnesium	Cobalt	Iron	Manganese	Nickel	Zinc
Detection Limit (mg/L)	0.047	0.04	0.002	0.005	0.0003	0.002	0.0005
Detected (µM)	Nd[b]	<0.04	0.049	0.38	0.009	0.1	0.19
Metal/MjRPE[a]			0.024	0.19	0.0045	0.053	0.097
Detected (µM)	<0.047	5.4	<0.002	0.44	<0.0003	0.26	0.94
Metal/C-MjTK[a]		2.57		0.22		0.13	0.47
Detected (µM)	<0.047	1.7	<0.002	0.24	0.034	0.25	0.54
Metal/N-MjTK[a]		0.87		0.12	0.017	0.128	0.27

[a]Ratio of metal over 2 µM protein
[b]Not determined

Table 2. Comparison of distances between MjRPE and SpRPE docked with Xu 5P and 5-dXu 1P

Measured distance (Å)	SpRPE		MjRPE	
	Xu 5P	5-dXu 1P	Xu 5P	5-dXu 1P
O3 to Zn(II)	3.0	3.5	3.6	4.7
O2/4 to Zn(II)	2.6	2.6	4.1	3.7
C3 to acid[a]	3.2	3.2	3.3	3.4
C3 to base[a]	3.5	3.8	4.2	3.6

[a]measurement was to the nearest oxygen atom of aspartate 176 and 36 for SpRPE and aspartate 172 and 37 for MjRPE to O3, O2/4, and C3 of Xu 5P or 5-dXu 5P

Table 3. Multiplicity of TK

Enzyme	Calculated MW	Observed Multiplicity
C-MjTK[a]	416 kDa	dodecamer
N-MjTK[b]	323 kDa	decamer
1:1 C-MjTK:N-MjTK[c]	457 kDa	heptamer
MjTK[c]	465, 230, and 171 kDa	heptamer, trimer, and dimer

[a] based off a predicted monomeric MW of 34 kDa
[b] based off a predicted monomeric MW of 30 kDa
[c] based off a combined predicted monomeric MW of 64 kDa

Figures

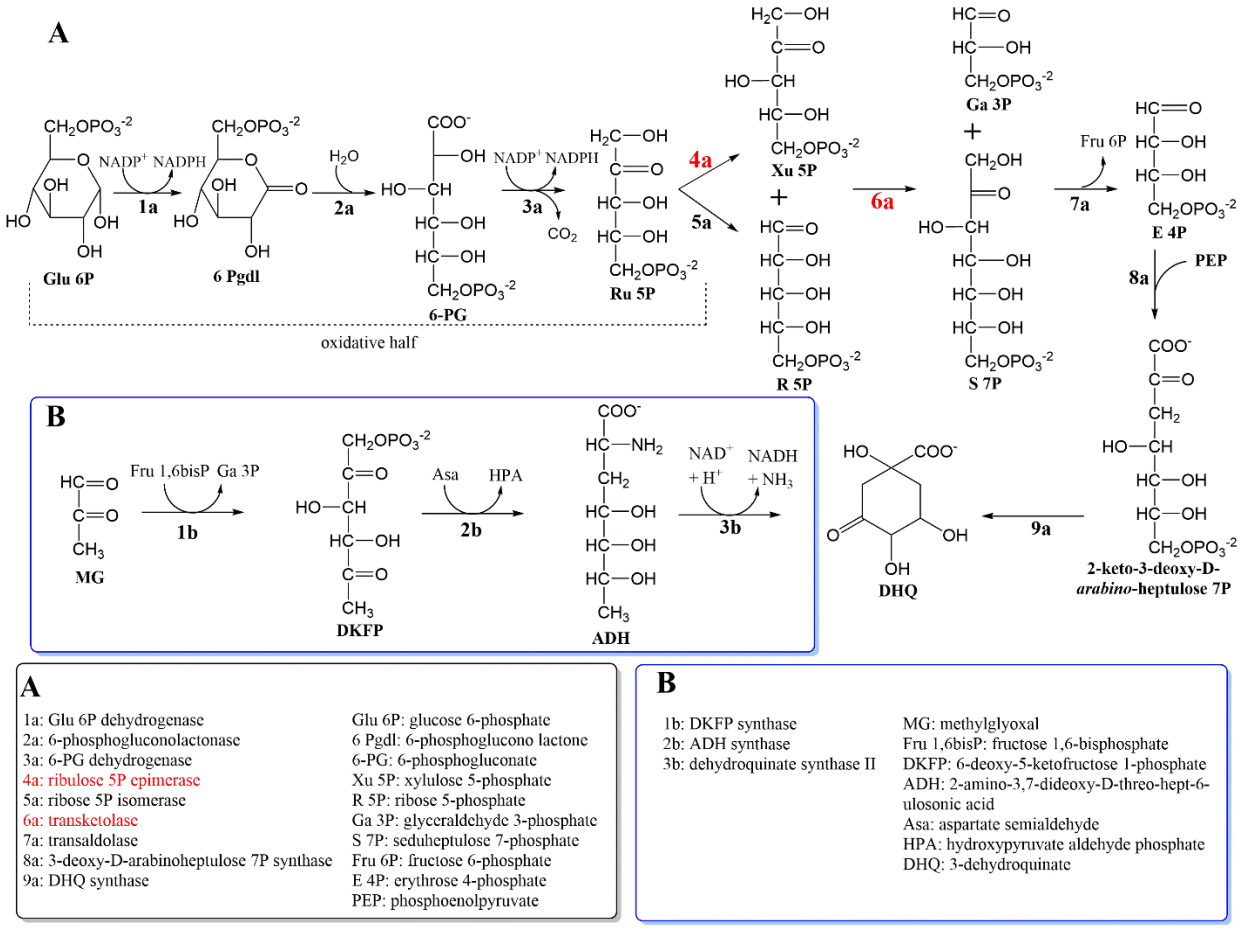

Figure 1. Comparison of the canonical route for DHQ biosynthesis (A) and the DHQ biosynthesis in *M. jannaschii* (B, blue box). Highlighted in red are the two enzymes that are the focus of this work.

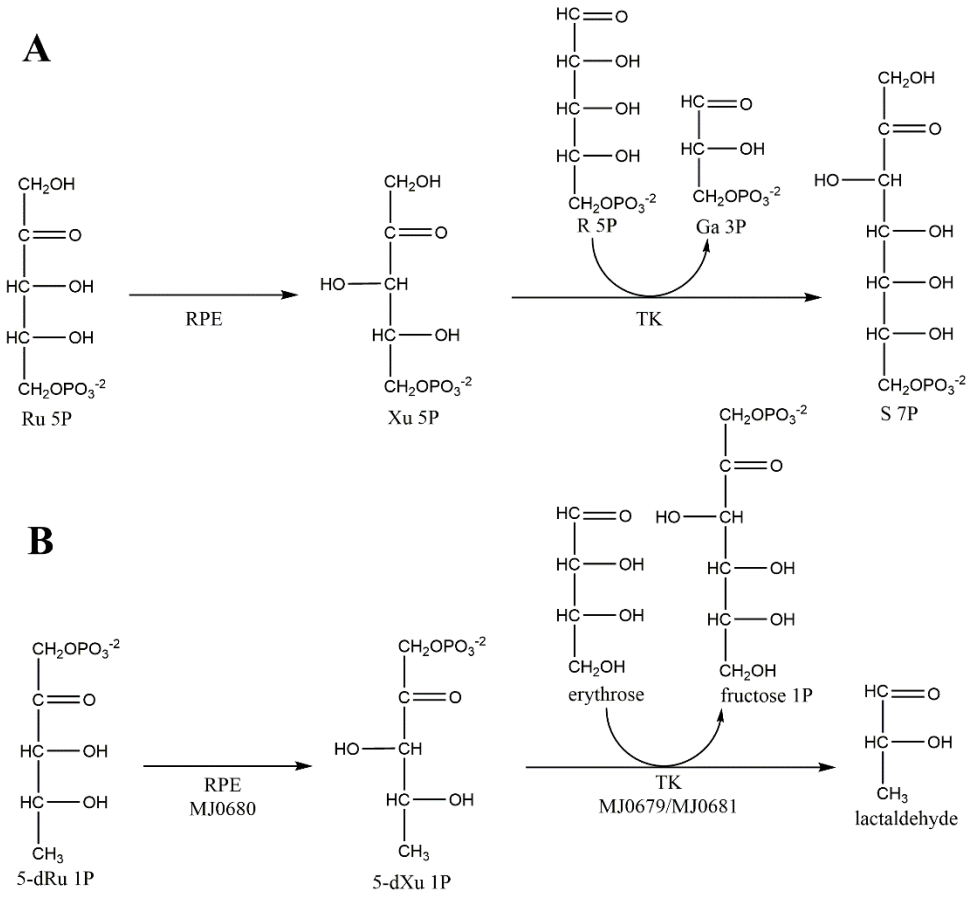

Figure 2. Canonical (A) and proposed (B) substrates for RPE and TK in *M. jannaschii*

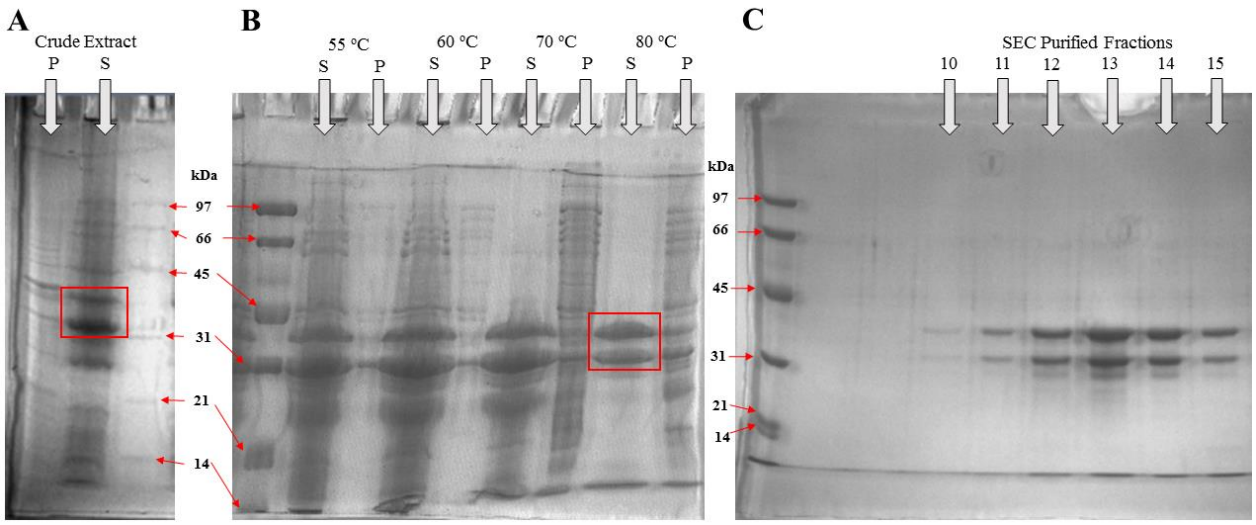

Figure 3. SDS-PAGE analysis of the dual expression of C-MjTK and N-MjTK crude extract (A) heat purification of crude extract (B) and purification of 80 °C heated extract by SEC (C). The bands indicated in the red boxes were sequenced by MALDI-MS and confirmed to be C-MjTK and N-MjTK at each successive step of purification. In all instances P denotes the pellet and S the soluble extracts.

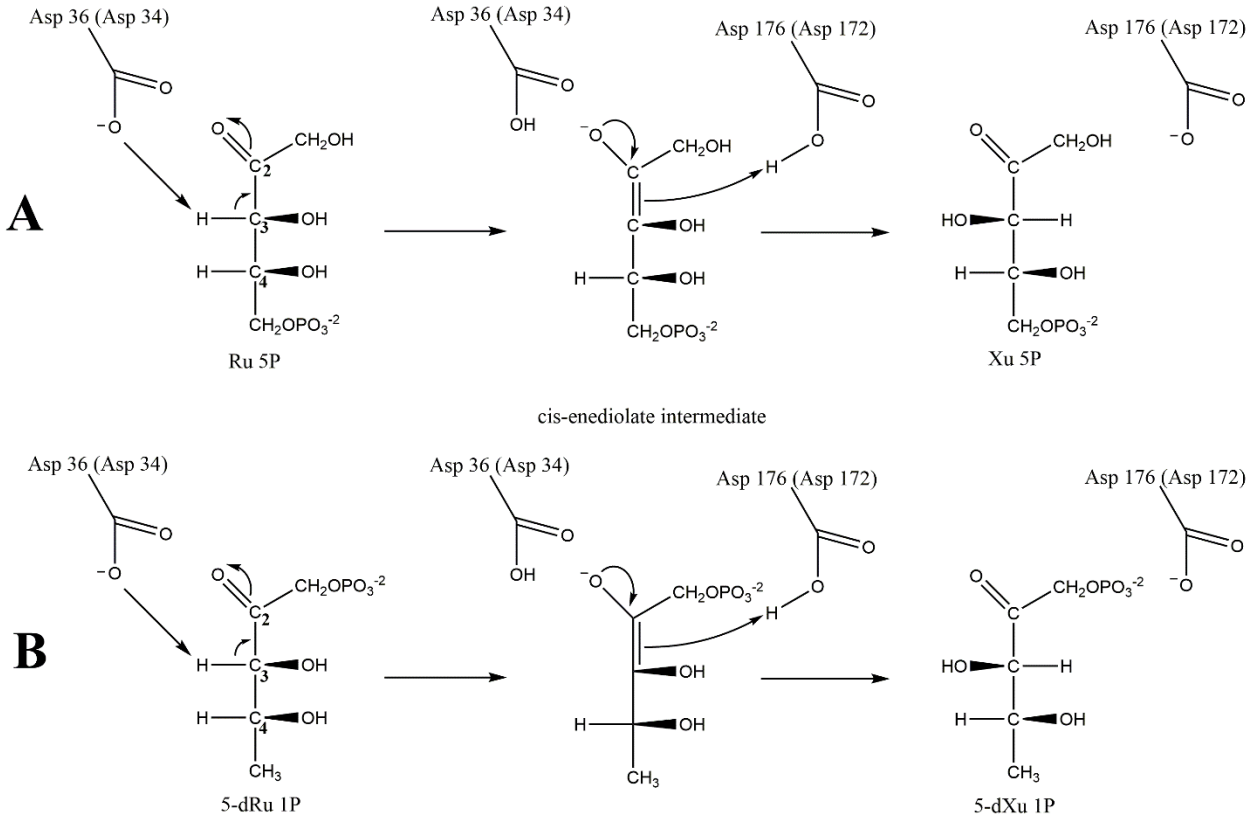

Figure 4. Comparison of RPE mechanism with Ru 5P (A) and 5-dRu 1P (B) as the substrate. The general acid and base for SpRPE are Asp36 and Asp176, respectively, with the corresponding residues for MjRPE shown in parenthesis.

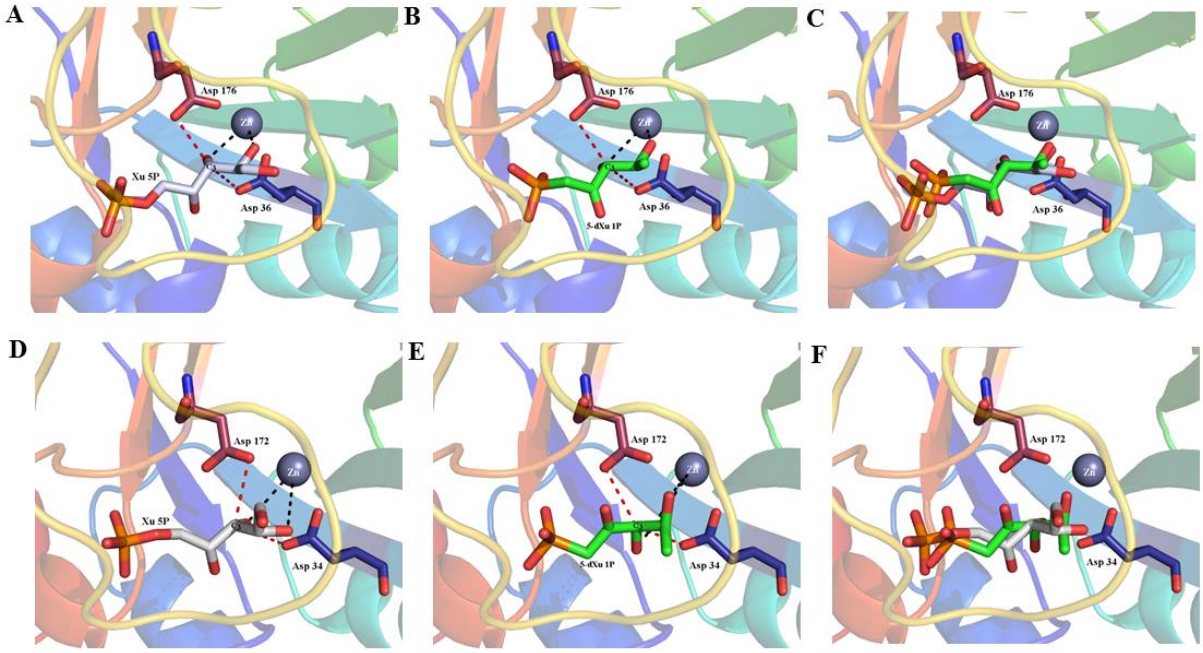

Figure 5. Molecular docking of Xu 5P and 5-dXu 1P into SpRPE (A-C) and into MjRPE (D-F). Asp 176 of *S. pyrogenes* and Asp 172 of *M. jannaschii* represents the general acid and Asp 36 and 34 the general base for *S. pyrogenes* and *M. jannaschii*, respectfully. Protein structures are shown as cartoon as colored as rainbow from N-(blue) to C-terminus (red). Xu 5P is shown as sticks colored by element with carbon atoms and 5-dXu 1P is shown as sticks colored by green carbon atoms, with all other atoms colored as follows: oxygen (red), phosphate (orange), and nitrogen (blue). Zn^{2+} is shown as a dark grey sphere.

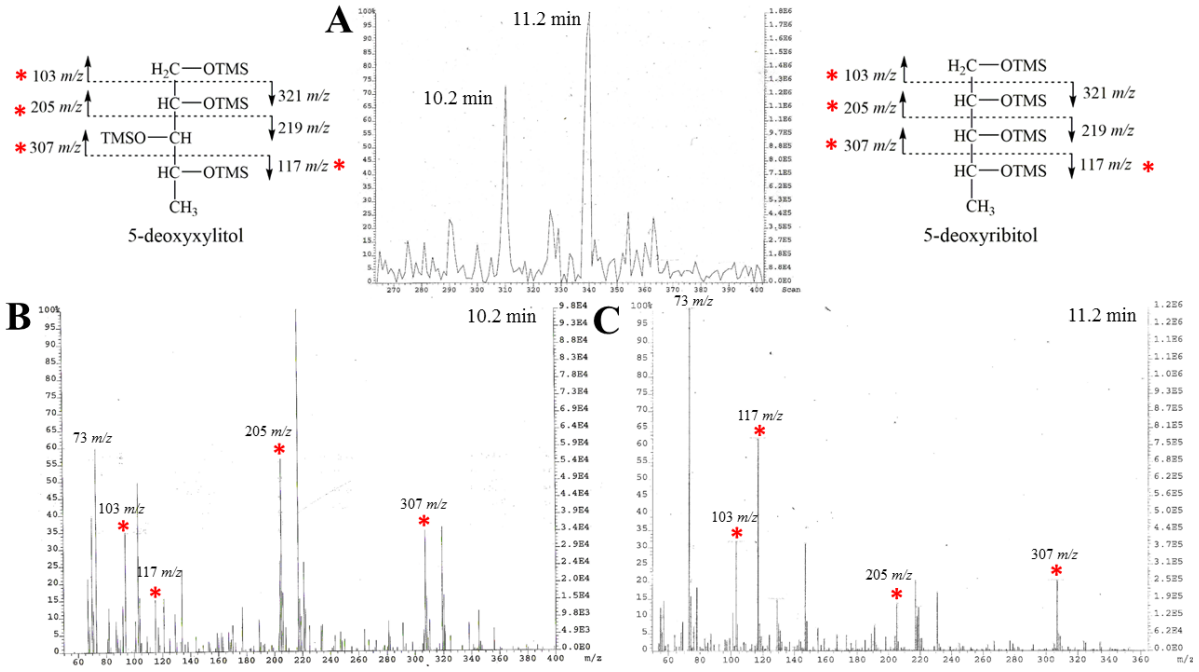

Figure 6. Assay of MjRPE activity by GC-MS of the reduced deoxysgurars as their TMS derivatives. The GC chromatograph scanning for the 117 *m/z* fragment (A) with the corresponding mass spectra for 10.2 min (5-deoxyxylitol) (B) and 11.2 min (5-deoxyribitol) (C). The identified fragments are highlighted with red asterisks for the corresponding deoxysugars shown above the mass spectra.

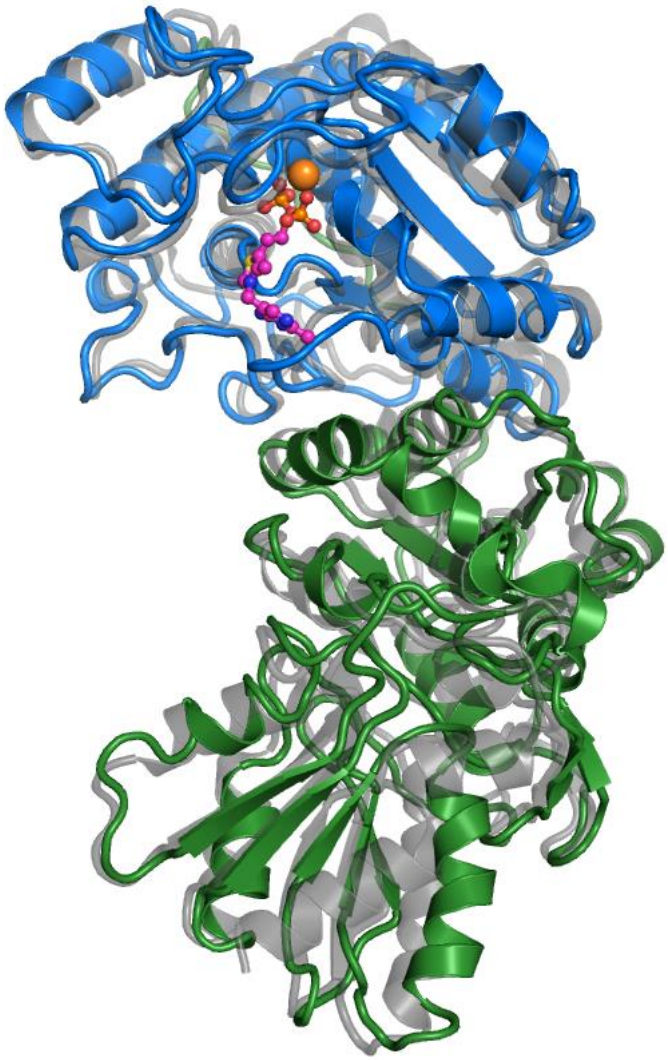

Figure 7. Overlay of modeled structure of MjTK (N-MjTK blue and C-MjTK green) and HsTK (grey). Bound TPP in the HsTK structure is shown with pink carbons, colored by element, and the calcium ion is shown as an orange sphere.

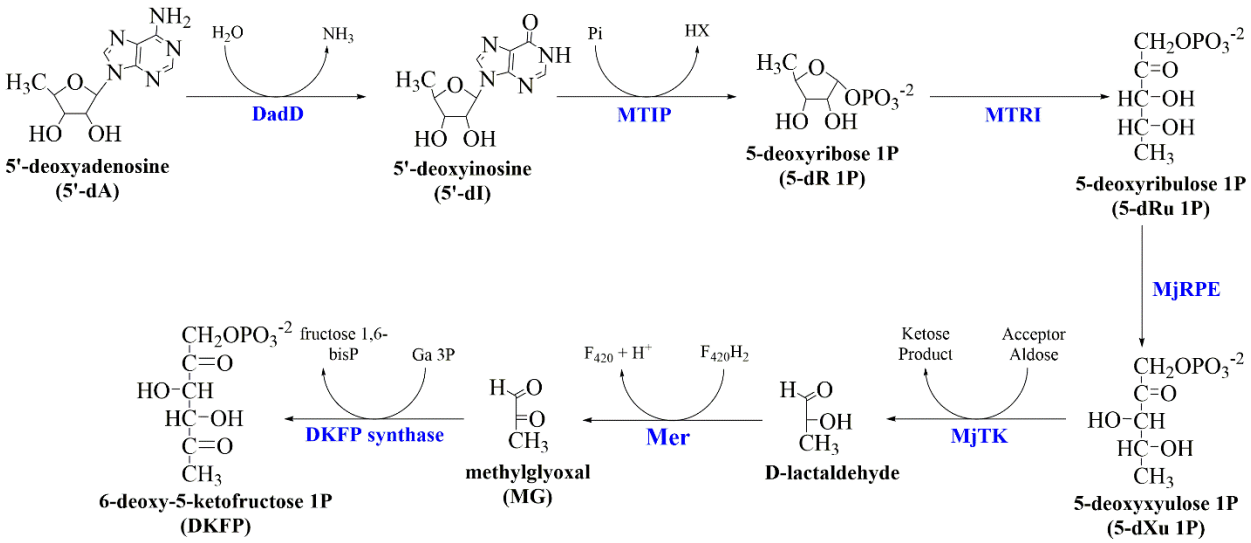

Figure 8. Proposed pathway for the biosynthesis of DKFP from 5'-dA in *M. jannaschii*.

Supplemental information for Characterization of ribulose 5-phosphate 3-epimerase and transketolase from *Methanocaldococcus jannaschii*

Danielle V. Miller, Kim Harich, Anne Brown, Huimin Xu, and Robert H. White#

Tables

Table S1. Oligonucleotide primers for MJ0680, MJ0679, and MJ0681 gene products

Gene	Plasmid	Primers
MJ0680	pT7-7	Fwd: 5'-GGTCATATGATTAAAATTGGAGCTTC-3'
		Rev: 5'-GCTGGATCCTTACTGTTTTTCTTCATTTG-3'
MJ0679	pT7-7	Fwd: 5'-GGTCATATGGTTAAGTTGAGTG-3'
		Rev: 5'-GCTGGATCCTTATTCTTTTTTC-3'
MJ0681	pT7-7	Fwd: 5'-GGTCATATGGATAATAACTTAG-3'
		Rev: 5'-GGTCATATGGATAATAACTTAG-3’
MJ0679	pRSFDuet-1	Fwd: 5’-GGTCCATGGTTAAGTTGAGTGGAG-3’
		Rev: 5’-GCTGGATCCTTATTCTTTTTTCATTTC-3’
MJ0681	pRSFDuet-1	Fwd: 5’-GGTCATATGGATAATAACTTAG-3’
		Rev: 5’-GCTAGATCTTTATTCACTTAATTC-3’

Table S2. Elution times of analyzed standards separated on the two different C18 columns used for LC-MS analysis of NBHA derivatized sugars

	Elution Time (min)		Observed *m/z*	
Standard	Kromasil	AxxiChrom	MH^+	M^+Na^+
glyceraldehyde	36.1	Nd[a]	240	262
hydroxypyruvate (HPA)	Nd	13.4	405	427
erythrose	34.2	15.2	271	293
ribose	32.8	15.3	301	323
xylose	32.8	Nd	301	323
5-deoxyribose (5-dR)	39.4	16.2	285	307
fructose	32.0	14.3	330	352
sedoheptulose	32.5	Nd	361	383
7-deoxyheptulose	Nd	24.3	345	367
NBHA	33.7	20.0	168	

[a]Not determined for the indicated column.

Figures

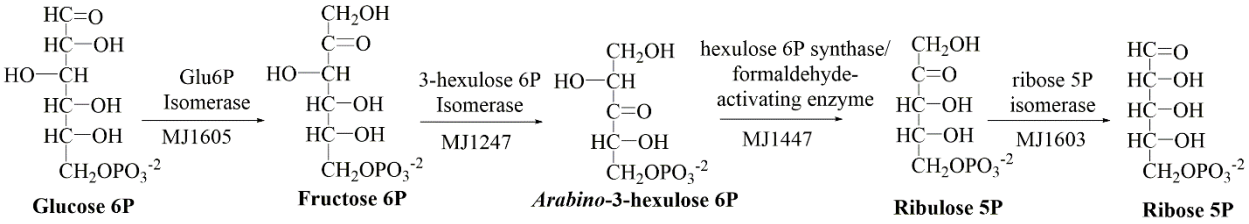

Figure S1. Ribulose monophosphate pathway in *M. jannaschii*

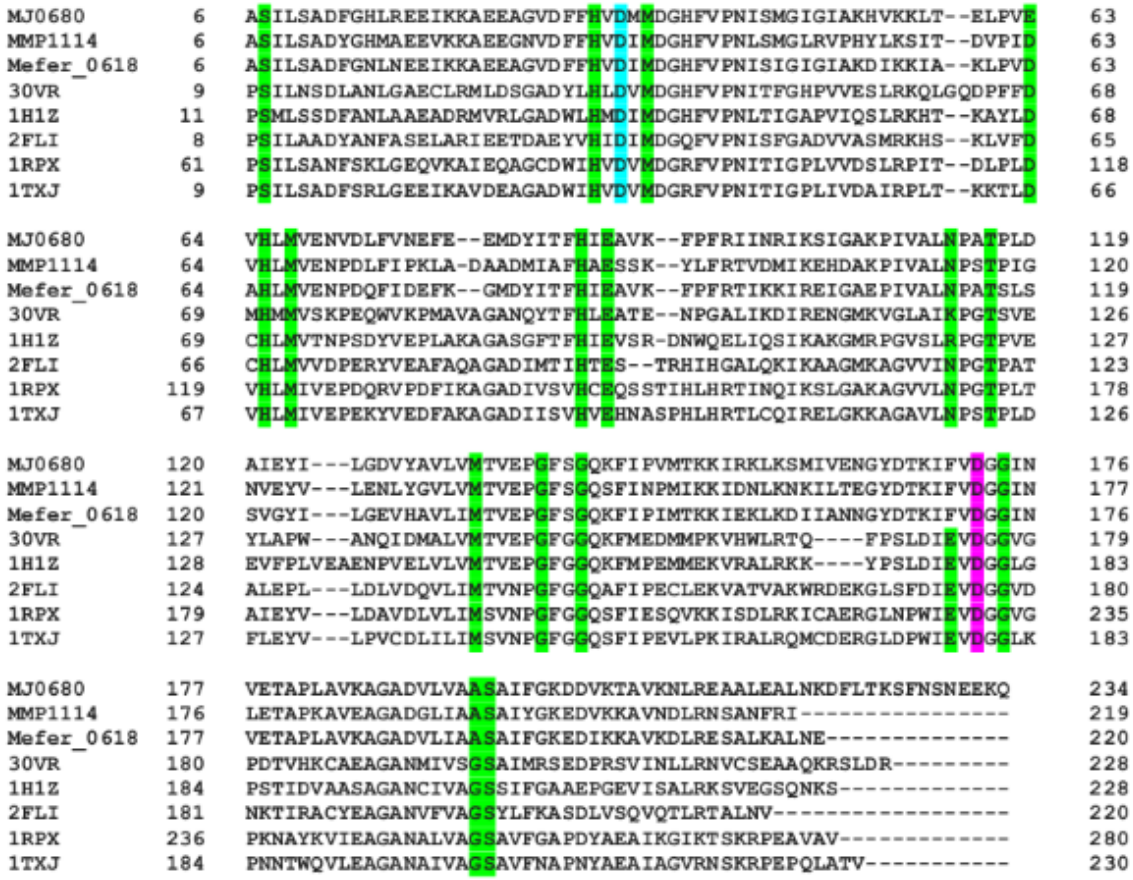

Figure S2. Truncated sequence alignment of *M. jannaschii* RPE with its homologues. The green highlighted residues are those highly conserved in the active site and include metal ligands, the blue and magenta highlighted aspartates represent the conserved general base and acid. The organisms in the alignment are denoted by either their locus tag for the first three or PDB ID. They are listed from top to bottom with the UniProt accession number and sequence identity to *M. jannashii* RPE (MJ0680) in parenthesis: *M. jannaschii* (Q58093), *Methanococcus maripaludis* (Q6LY77, 62%), *Methanocaldococcus fervens* (C7P7A7, 79%), Human (Q96AT9, 34%), Rice (Q9SE42, 39%), *S. pyrogenes* (Q9A1H8, 38%), Potato chloroplast (Q43843, 43%), and *Synechocystists sp.* (P74061, 40%).

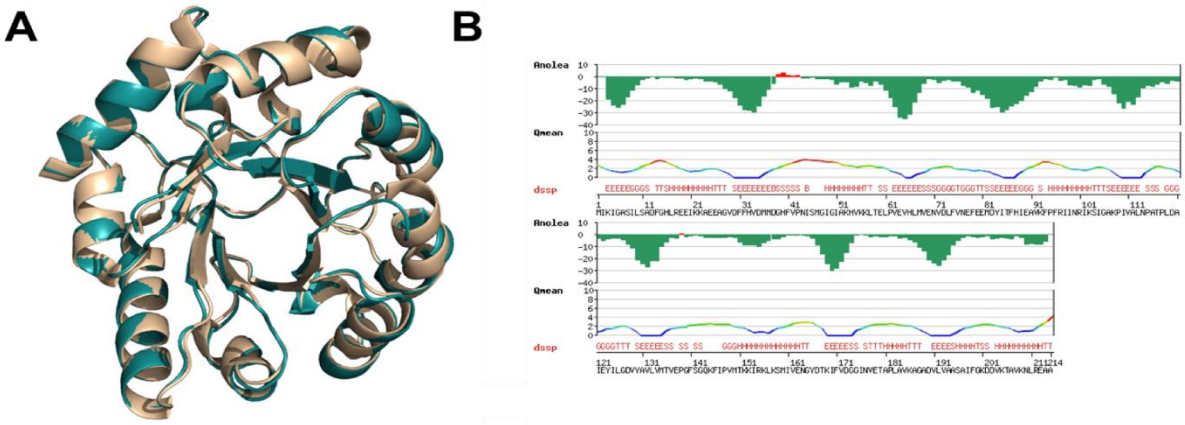

Figure S3. Model analysis of MjRPE. Overlay of SpRPE (PDB ID: 2FLI, tan) and MjRPE model (teal) (A) and Anolea, QMEAN, and DSSP analysis of MjRPE model (B).

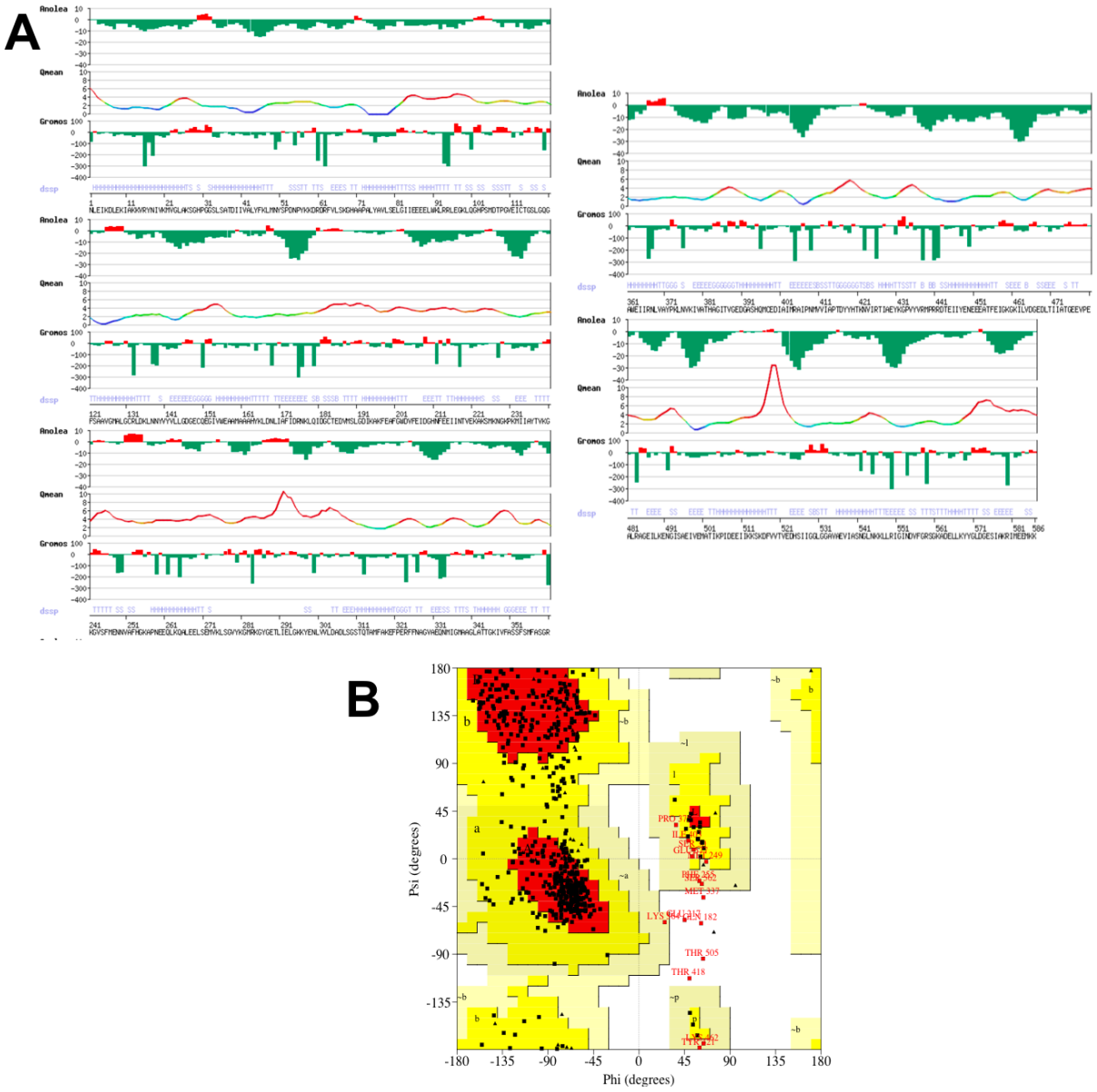

Figure S4. Model validation results for MjTK. Anolea, QMEAN, and DSSP analysis (A) and Ramachandran plot (B) indicate an energetically favorable structure with only few residues (in loop regions) in disallowed regions.

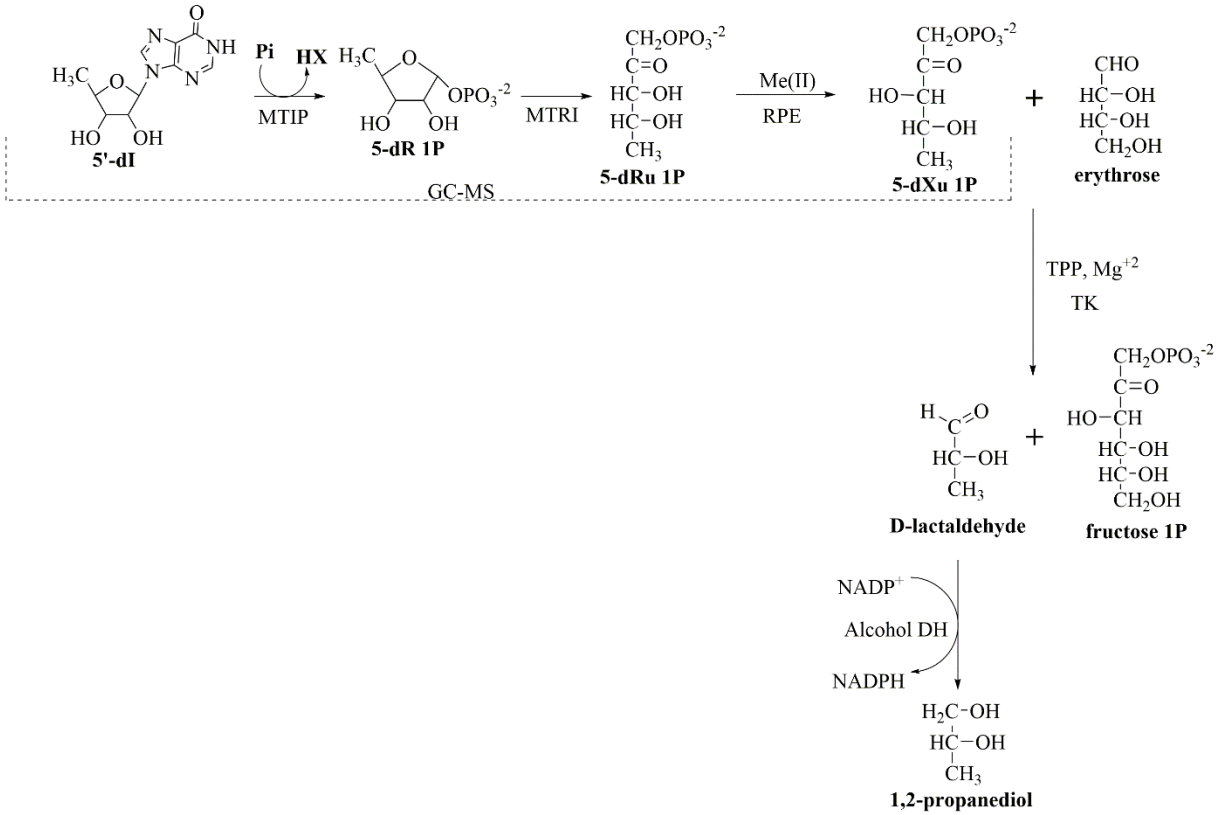

Figure S5. Coupled enzyme assays for detection of 5-dXu 1P using GC-MS of dephosphorylated and reduced sugar TMS derivatives (bracketed) and lactaldehyde from 5'-dI (whole figure). Me(II) was Zn(II) for the GC-MS assay and Fe(II) for detection of the lactaldehyde by reaction with NADP and alcohol dehydrogenase.

Chapter 4: Promiscuity of N^5, N^{10}-methylenetetrahydromethanopterin reductase from *Methanocaldococcus jannaschii* as a methylglyoxal reductase

Danielle V. Miller, Michelle Ruhlin, W. Keith Ray, Huimin Xu, and Robert H. White#

Department of Biochemistry, Virginia Polytechnic Institute and State University, Blacksburg, VA 24061

#To whom correspondence should be addressed. Telephone: +1 (540) 231- 6605, Fax: (540) 231- 9070, e-mail: rhwhite@vt.edu

Abstract

In *Methanocaldococcus jannaschii*, methylglyoxal is required for aromatic amino acid biosynthesis. Reduction of methylglyoxal to lactaldehyde in *M. jannaschii* extracts using either NADPH or $F_{420}H_2$ was demonstrated, but the responsible enzyme was unknown. Using NADPH as the reductant, the unknown enzyme was purified from cell extracts of *M. jannaschii* and determined to be the F_{420} dependent N^5, N^{10}-methylenetetrahydromethanopterin reductase (Mer). This is the first report of recombinant overexpression of Mer and its ability to utilize NADPH and methylglyoxal as substrates. Additionally, Mer did not catalyze the reduction of methylglyoxal to lactaldehyde in the presence of reduced Fo, precursor of F_{420}.

Introduction

Methylglyoxal (MG) is a well-known toxic metabolite that chemically modifies amino acids in proteins and binds DNA and RNA.(1) MG is produced through non-enzymatic elimination of phosphate from glyceraldehyde 3-phosphate and dihydroxyacetone phosphate(2) or enzymatically via a MG synthase with dihydroxyacetone phosphate as the substrate.(3, 4) In the established pathways, MG is converted to D- or L-lactate and ultimately to pyruvate (Figure 1).(5) In the glyoxalase system, MG non-enzymatically reacts with glutathione to form the hemithioacetal adduct which is then converted to D-lactate through the glyoxalase I and II enzymes (Figure 1A).(1) Alternatively, a glutathione independent glyoxalase III characterized from *Escherchia coli* metabolizes MG to D-lactate in a single step (Figure 1B).(5, 6) Complete conversion of MG without addition of D-lactate dehydrogenase (Figure 1C) to pyruvate was observed in *Pseudomonas putida*, but activity by the MG dehydrogenase (MG DH) was not conserved among other bacterial and eukaryotic organisms.(7) Reduction of MG to L-lactaldehyde by the NADPH dependent MG reductase (Figure 1E) was much more widely dispersed across bacteria and eukaryotes(7) where the conversion of L-lactaldehyde to pyruvate by the lactaldehyde dehydrogenase and lactate dehydrogenase is well established.(8, 9) However, no homologue of any of these well described enzymes exists in *Methanocaldococcus jannaschii* or in any other Archaeal organism. This suggests that MG is not detoxified in Archaea by any of the enzymes shown in black in Figure 1.

Discovery of an enzyme in *M. jannaschii*(10) and *Halobacterium salinarum*(11) that utilizes MG as a substrate for production of an essential metabolite suggests MG is not detoxified. Furthermore, cell extracts of *M. jannaschii* were determined to contain 70 µM MG(10), which is ~30 fold higher than has been detected previously in other organisms (0.1 to 2 µM).(1) The presence of a MG synthase and glyoxalase I have been predicted to be functioning in halophilic archaea.(12) However, since the presence of glyoxalase I activity was only observed in the presence of exogenously added glutathione, the observed glyoxalase I activity was likely an artifact of the assay, as glutathione is absent in Archaea.(13) Since glutathione is absent, this would further indicate that MG is not converted to pyruvate by this pathway (Figure 1A). Additionally, the annotated L-lactate dehydrogenase from *M. jannaschii* was determined to be a malate dehydrogenase(14, 15) suggesting once again that lactate is not converted to pyruvate (Figure 1). Instead, L-lactate is important for F_{420} biosynthesis in *M. jannaschii*(16),

where the reduction of MG to D-lactaldehyde was observed in the presence of either NADPH or $F_{420}H_2$ when incubated with *M. jannaschii* cell extracts(16, 17) confirming that MG is likely derived from D-lactaldehyde. However, the reduction of MG is not performed by the canonical MG reductase. Instead, analysis of the activity from cell extracts demonstrates that the enzyme(s) catalyzing the reduction of MG is either NADPH or F_{420} dependent.(17) F_{420} is a unique 5-deazaflavin cofactor that performs two-electron hydride transfers that are more similar to nicotinamides than flavins (Figure S2).(18) F_{420} is characteristic of methanogenic organisms, though it has been demonstrated to be utilized by aerobic actinobacteria as well.(18) Here we describe the isolation of an enzyme responsible for the oxidation of lactaldehyde to methylglyoxal, as the F_{420}-dependent N^5, N^{10}-methylenetetrahydromethanopterin reductase (Mer) (Figure 1D). Subsequently, recombinant expression and purification of this enzyme followed by *in vitro* characterization for its ability to catalyze the reduction of MG with NADPH, was performed.

Materials and methods

Chemicals. All chemicals were purchased from Sigma/Aldrich unless otherwise noted.

Preparation of *M. jannaschii* cell extracts and isolation of native enzyme. *M. jannaschii* cells grown as described previously(19) were suspended in 3-4 mL of extraction buffer (50 mM *N*-[tris(hydroxymethyl)methyl]-2-aminoethanesulfonic acid (TES), pH 7.0, 10 mM $MgCl_2$) and lysed by sonication followed by centrifugation (16,000 *x g* for 20 min at 3 ^oC). The resulting supernatant, containing the soluble proteins (3.2 mL from 2 g wet wt cells), was first separated by anion-exchange chromatography on a MonoQ HR column (1 x 8 cm; Amersham Bioscience) using a linear salt gradient from 0 to 1 M NaCl in 25 mM Tris buffer pH 7.5, over 55 min at a flow rate of 1 mL/min. Fractions of 1 mL were collected and tested for activity and analyzed for F_{420} by MALDI-MS (see below).

The fractions found to contain activity were further separated on a Shimadzu HPLC system equipped with a photodiode array using a Phenomenex BioSep SEC-s2000 column (300 x 7.8 mm, 5 µm particle size) equipped with a Phenomenex security guard cartridge and operated at room temperature (RT). The elution profile consisted of 20 min at an isocratic flow of buffer (50 mM TES, pH 7.2, 150 mM NaCl) at a flow rate of 1 mL/min. Fractions of 0.5 mL were collected every half minute and tested for the desired activity and analyzed for F_{420} by MALDI-MS (see below). Half of the collected fractions (250 µL) that contained the desired activity were

evaporated to dryness in glass vials under N_2 while being heated prior to analysis by LC-ESI-MS (see below) for the contained proteins.

Analysis for F_{420} by MALDI-MS. Collected fractions (10 µL) from the first separation (via MonoQ) were diluted 4-fold using solvent Y (98:2 LC/MS grade water: LC/MS grade acetonitrile containing 0.1% (v/v) TFA). One microliter of each fraction was then spotted onto a MALDI target plate (AB Sciex). Once dried, the sample was overlaid with one microliter of matrix solution. The matrix solution was 4 mg/ml alpha-cyano-4-hydroxycinnamic acid (Sigma) in solvent Z (50:50 LC/MS grade water: LC/MS grade acetonitrile containing 0.1% (v/v) TFA) supplemented with 10 mM ammonium chloride (Sigma). After the matrix solution dried, the samples were analyzed utilizing a 4800 MALDI Tof/Tof (AB Sciex). Data were collected utilizing the reflector positive ion acquisition method for the m/z range of 800 to 1200 summing the data from 4000 individual laser shots. Peak intensities were extracted utilizing the MALDI control software (AB Sciex) and exported to Excel (Microsoft) for analysis.

Identification of enzyme by LC-ESI-MS. The fractions from SEC that were identified to have the desired activity (250 µL) were evaporated to dryness before analysis by liquid chromatography electrospray ionization mass spectrometry (LC-ESI-MS). The fractions containing protein pellets were resuspended in 250 µl freshly-prepared 8 M urea in 100 mM ammonium bicarbonate (AmBic). Proteins were denatured and disulfides reduced by incubation of 1 hour at 37 ˚C after the addition of 4.5 mM dithiothreitol (DTT) in 100 mM AmBic. Free sulfhydryls were then alkylated by incubation for 30 minutes in the dark at room temperature after the addition of freshly-prepared 10 mM iodoacetamide (IA) in 100 mM AmBic. Unreacted IA was then neutralized by the addition of 10 mM DTT in 100 mM AmBic and urea content diluted to 4 M by bringing the final volume to 500 µl by the addition of 100 mM AmBic. One microgram of Endoproteinase LysC (Wako) was added and digestions incubated with shaking at 37 ˚C overnight. The following day, urea content was further diluted to 1.4 M by bringing the final volume to 1.43 ml by the addition of 100 mM AmBic. Proteomics-grade trypsin (Sigma-Aldrich) was added at 1 µg and the digestions incubated for four hours with shaking at 37˚C.

Digestions were desalted using solid phase extraction (SPE) after acidification by the addition of 0.2% (v/v) trifluoroacetic acid (TFA) and 1% (v/v) formic acid. SPE utilized OMIX C18 100 µl tips (Varian). Tips were conditioned and equilibrated using 2X200 µl LC/MS grade methanol followed by 2X200 µl solvent Y (98:2 LC/MS grade water: LC/MS grade acetonitrile

containing 0.1% (v/v) TFA). The sample was then applied to the tip followed by 5X200 µl washes of solvent Y and desalted peptides were finally recovered using 200 µl solvent Z. Peptide samples were concentrated to dryness using a centrifugal vacuum concentrator, resolubilized in 40 µl solvent Y by sonication and stored at -20°C.

Ten microliters of each resolubilized peptide sample were separated using an Acquity I-class UPLC system (Waters). The mobile phases were solvent A (0.1% (v/v) formic acid (Sigma) in LC/MS grade water (Spectrum Chemicals) and solvent B (0.1% (v/v) formic acid (Sigma) in LC/MS grade acetonitrile (Spectrum Chemicals). The separation was performed using a CSH130 C18 1.7 µm, 1.0 x 150 mm column (Waters) at 50 µL/min using a 110 minute gradient from 3-40% solvent B. The column temperature was maintained at 45˚C.

Column effluent was analyzed using a Synapt G2-S mass spectrometer (Waters) using an HDMSe (high-definition mass spectrometry with alternating scans utilizing low and elevated collision energies) acquisition method in continuum positive ion "resolution" MS mode. Source conditions were as follows: capillary voltage, 3.0 kV; source temperature, 120˚C; sampling cone, 60 V; desolvation temperature, 350˚C; cone gas flow, 50 L/hr; desolvation gas flow, 500 L/hr; nebulizer gas flow, 6 bar. Both low energy (4 V and 2 V in the trap and transfer region, respectively) and elevated energy (4 V in the trap and ramped from 20 to 50 V in the transfer region) scans were 1.2 seconds each for the m/z range of 50 to 1800. For ion mobility separation, the IMS and transfer wave velocities were 600 and 1200 m/sec, respectively. Wave height within the ion mobility cell was ramped from 10 to 40 V.

For lock-mass correction, a 1.2 second low energy scan was acquired every 30 seconds of a 100 fmol/µL [Glu1]-fibrinopeptide B (Waters) solution (50:50 acetonitrile: water supplemented with 0.1 % formic acid) infused at 10 µL/min introduced into the mass spectrometer through a different source which was also maintained at a capillary voltage of 3.0 kV. The data for lock-mass correction was collected but not applied to sample data until data processing.

Mass spectrometric data from 1-101 minutes of each chromatographic run were processed and analyzed utilizing ProteinLynx Global Server (PLGS) v. 3.0.2 (Waters). Average chromatographic and mass spectrometric peak width resolution were automatically determined by the software. Mass values were lock-mass corrected based on the exact *m/z* value of the +2 charge state of [Glu1]-fibrinopeptide B (785.842). Peaks were defined based on the low energy,

elevated energy and bin intensity thresholds of 250, 25 and 2000 counts, respectively. The final peak list for each sample was then searched against a protein database containing the complete *M. jannaschii* proteome including isoforms downloaded from Uniprot (10/08/15) and 3 randomized decoy entries for each real entry appended using PLGS. Workflow parameters for the protein identification searches were 2 possible missed cleavages utilizing Lys-C and trypsin as the protease combination, a fixed modification of carbamidomethylation of cysteine, and possible modifications of glutamine to pyroglutamate when glutamine is present at the N-terminus of a peptide and oxidation of methionine. The software automatically determined peptide and peptide fragment mass tolerances. Protein identification searches using PLGS had a false discovery rate of no more than 3%.

Cloning, Overexpression, and Purification of *M. jannaschii* MJ1534 in *Escherichia coli*. The MJ1534 gene (UniProt accession number Q58929) was amplified by PCR from genomic DNA using oligonucleotide primers for MJ1534-Fwd: 5'-GGTCATATGAAATTTGGTATCGAATTTG-3' and MJ1534-Rev: 5'-GCTGGATCCTTACTCTTTTAATGCTG-3'. PCR amplification was performed as described previously(20) using a 55 ^{o}C annealing temperature. Purified PCR product was digested with Nde1 and BamH1 restriction enzymes and ligated into compatible sites in vector pT7-7. The sequence of the resulting plasmid pMJ1534 was verified by DNA sequencing. The plasmid, pMJ1534 was then transformed into *E. coli* strain BL21-CodonPlus(DE3)-RIL cells (Stratagene). The transformed cells were grown in LB medium supplemented with 100 µg/mL ampicillin at 37 ^{o}C with shaking until they reached an OD_{600} of 1.0. Recombinant protein production was induced by addition of lactose to a final concentration of 28 mM.(20) After an additional 2 hours of culture, the cells (200 mL) were harvested by centrifugation (4,000 *x g*, 5 min) and frozen at -20 ^{o}C. Induction of the desired protein was confirmed by SDS-polyacrylamide gel electrophoresis (SDS-PAGE) analysis of total cellular proteins. Protein concentrations were determined by Bradford analysis.(21)

The frozen *E. coli* cell pellet containing the desired protein (~0.4 g wet wt) was suspended in 3 mL of extraction buffer (50 mM *N*-[tris(hydroxymethyl)methyl]-2-aminoethanesulfonic acid (TES), pH 7.0, 10 mM $MgCl_2$, 20 mM dithiothreitol (DTT)) and lysed by sonication. The resulting expressed proteins were found to remain soluble after heating. The resulting cell extracts were heated for 20 min at 80 ^{o}C for the MJ1534 gene product, followed by

centrifugation (16,000 *x g* for 30 min) to remove the insoluble *E. coli* proteins, which denature and precipitate under these conditions. The next step of purification was performed by anion-exchange chromatography of the heated soluble fractions on a MonoQ HR column (1 x 8 cm; Amersham Bioscience) using a linear gradient from 0 to 1 M NaCl in 25 mM Tris buffer (pH 7.5), over 55 min at a flow rate of 1 mL/min. Fractions of 1 mL were collected and the desired protein was identified through SDS-PAGE analysis of the fractions and subsequent sequencing by MALDI-MS of the excised protein bands. The protein bands corresponding to the predicted molecular mass of the MJ1534 gene product (~35 kDa) were excised from the polyacrylamide gel and prepared for MALDI-MS as previously described.(22) Protein concentrations were determined by Bradford analysis.(21) The molecular weight of the recombinant protein was determined using a Shimadzu HPLC system with a Phenomenex BioSep SEC-s2000 column (300 x 7.8 mm, 5 µm particle size) with a Phenomenex security guard cartridge equipped with a photodiode array and fluorescent detection was operated at RT. The elution profile consisted of 20 min at an isocratic flow of 50 mM TES, pH 7.2, and 150 mM NaCl at a flow rate of 1 mL/min. Fractions of 0.5 mL were collected every half minute.

Analysis for enzymatic activity of MG reduction with NADPH and FoH_2 as reductants. The activities of *M. jannaschii* whole cell extract and collected fractions from the two separations were accomplished in a total reaction volume of 100 µL with 25 mM Tris pH 7.0 and a final concentration of 0.4 mM NADPH and 0.2 mM methylglyoxal. *M. jannaschii* cell extract or fraction (10-30 µL) was added last and mixed by rapid pipetting. The reaction was monitored for 2.5 min at 340 nm at room temperature in a 100 µL cuvette with a 1 cm path length using a Shimadzu BioSpec-1601 UV-vis spectrophotometer. A control was run for every assay to account for background NADPH oxidation without methylglyoxal in the above assay. A positive activity was indicated when a larger decrease in absorbance was observed when MG was present than without the addition of MG at 340 nm for NADPH ($\varepsilon_{340\ nm}$ = 6.22 mM^{-1} cm^{-1}). The Bradford protein assay(21) was used for protein concentration determination of the active fraction(s). The same assay conditions were used to analyze the recombinant purified Mer using 5.3 µg of Mer for each assay plus and minus MG in the presence of NADPH. A shortened form of F_{420}, Fo, was used to test Mer's capability of catalyzing the reduction of MG (Figure S2A). Fo was synthesized as previously described(23) and reduced to FoH_2 using methods previously described.(17) Briefly, Fo (~0.7 mM in 100 µL 25 mM Tris buffer pH 7.5) was reduced with 0.7

mg sodium borohydride under argon in a sealed vial. After disappearance of yellow color, 1 M anaerobic HCl was added to a pH 4 to destroy the borohydride. The sample was neutralized to pH 7 with 1 M anaerobic NaOH. Fo was also included in the assay with NADPH to determine if NADPH would reduce Fo and increase activity. The reduced Fo was added to 5 µg Mer and 0.2 mM MG in 100 µL 25 mM Tris (pH 7.5) to make a 0.1 mM solution and the absorbance at 420 nm was monitored over 2.5 min at room temperature. An increase in absorbance indicates a positive activity.

Confirmation of lactaldehyde production. In order to establish that lactaldehyde was produced from the reduction of methylglyoxal with NADPH a second enzyme was included in the assay following completion of MG reduction. Completion of MG reduction was assumed when there was no longer an observed change in absorbance at 340 nm for at least 1 min. The standard assay described above was monitored for 2.5 min to completion, and then 0.5 mM NAD^+ and 8.7 µg lactaldehyde dehydrogenase from *M. jannaschii*(16) was added increasing the volume to 125 µL. This reaction was monitored for 5 min, looking for an increase in absorbance at 340 nm if lactaldehyde was produced by the reduction of methylglyoxal with NADPH and *M. jannaschii* cell extracts.

Results and discussion

Identification of the enzyme responsible for catalyzing the conversion of MG to lactaldehyde. A *M. jannaschii* cell extract was separated by anion exchange chromatography using a gradient from 0 to 1 M NaCl and collecting 1 mL fractions every minute. Analysis of every third fraction showed a peak (fraction 23, Figure 2) with the desired activity (specific activity of 0.21 µmol min^{-1} mg^{-1} total protein) eluting at 0.2 M NaCl. The desired activity was determined by a greater change in absorbance when MG and NADPH were incubated with the *M. jannaschii* fractions versus when the fractions were assayed only with NADPH (Figure 2A). These procedures were necessary for comparison of activity of the NADPH dependent enzymes and our enzyme of interest from *M. jannaschii*, so that only the desired enzyme was isolated. The same set of fractions were also analyzed by MALDI-MS for the presence of F_{420} with either 2 or 3 glutamates (903.2 and 1032.0 *m/z*, respectively). In our analysis only F_{420} with 2 glutamates (F_{420}-2) was detected and may signify that an F_{420}-2 dependent enzyme may be present in the fractions (Figure 2B). This is intriguing as F_{420}-3 had previously been demonstrated to be the most abundant form in *M. jannaschii*.(24) Fraction 23 contained F_{420}-2,

further supporting that this fraction could contain the protein of interest. Furthermore, fraction 23 was additionally confirmed to produce lactaldehyde by the addition lactaldehyde dehydrogenase, which demonstrated an increase in absorbance at 340 nm when added to the assay, which would only occur if lactaldehyde was produced from the reduction of MG.

Fraction 23 was further purified by SEC (Figure 3A) and each fraction was analyzed for activity plus or minus MG in the presence of NAPDH (Figure 3B). Two peaks of activity corresponding to a mass of ~80 kDa were observed (Figure 3, Fractions 17 to 19). The collected SEC fractions were also analyzed for F_{420} by MALDI-MS and though most of the F_{420} eluted earlier (Fractions 12 to 15, Figure 3B), there was a small peak that eluted with the active fractions (Figure 3B). Half of the collected 0.5 mL fractions (Fractions 17 to 19) containing activity were dried completely and the tryptic peptides were analyzed by LC-ESI-MS for the contained proteins. The only significantly identified protein in the three fractions exhibition activity was identified as N^5, N^{10}- methylenetetraphydromethanopterin reductase (Mer, encoded by MJ1534) with three peptides. Mer is an essential enzyme involved in the final steps of methanogenesis, performing the reversible F_{420} dependent reduction of N^5,N^{10}-methylenetetrahydromethanopterin (CH_2=H_4MPT) to N^5-methyltetrahydromethanopterin (CH_3-H_4MPT)(25–28) (Figure 4B).

Cloning, overexpression, and purification of MJ1534 gene product (Mer) in *E. coli*. The MJ1534 derived protein was efficiently expressed in *E. coli* as measured from the SDS-PAGE analysis of the total proteins in the *E. coli* cells after expression. MALDI-MS analysis of the tryptic peptides recovered from the excised expressed protein band confirmed the presence of the desired protein by the detection of ten unique peptides. Heating portions of the resulting crude soluble extract for 10 min at different temperatures indicated that Mer remained soluble up to 80 ^{o}C based on SDS-PAGE analysis. Thus, the first step in the purification involved heating cell extracts at 80 ^{o}C for 20 min followed by centrifugation (14,000 $\times$ *g*, 10 min) prior to purification of soluble proteins on MonoQ. This produced a peak of activity at 0.4 M NaCl using the same methods as described above for the *M. jannaschii* cell extracts. The *M. jannaschii* Mer was determined to be a dimer (~80 kDa) with a monomeric mass of 35-40 kDa as judged by isolation of the protein from *M. jannaschii* extracts and by SDS-PAGE and SEC of the recombinantly expressed protein. This is the first report of Mer being recombinantly produced and being a homodimer. Mer proteins isolated from various Archaea were determined to be

homotetrameric in *Methanosarcina bakeri*(28) and *Methanothemobacter thermautotrophicus*,(26) homopentameric in *Archaeoglobus fulgidus*,(29) and homoheptameric in *Methanopyrus kandleri*.(25)

Analysis of recombinant Mer for MG reductase activity. The recombinant pure Mer was tested for MG reductase activity. The results demonstrated that when Mer was incubated only with NADPH, no change in absorbance was observed, indicating no activity. However, upon addition of MG a decrease in absorbance at 340 nm was observed indicating the oxidation of NADPH to $NADP^+$ (Figure 5). A specific activity of 0.73 ± 0.07 μmol min^{-1} mg^{-1} protein was measured. Surprisingly, analysis demonstrated that Mer was unable to reduce MG with reduced Fo, as had been previously reported for *M. jannaschii* cell extracts.(17) However, the observed discrepancy could be due to the use of Fo instead of F_{420} (Figure S2A). Though Fo has been used successfully as a replacement for F_{420} for many F_{420} dependent enzymes(30), Mer appears to have never been tested with Fo as a cofactor. Thus, some specificity for the F_{420} might exist that was not examined here (Figure S2A). No previously studied Mer has been demonstrated to use NADPH as a cofactor, and Mer was reported to have a strict requirement for F_{420}.(25–29) Additionally, the recombinant enzyme lost activity after three weeks of freeze/thaw at -20 ºC. The instability of the recombinant Mer could be due to the lack of F_{420} in the active site, which could further suggest a specificity for F_{420} that was unknown before and will be of interest for future work on this enzyme. All previously characterized Mer's have been isolated from their respective organisms. The isolated Mer from *M. jannaschii* maintained activity for several months of freeze/thaw at -20 ºC and F_{420}-2 was determined to be present in the active fractions (Figures 2B and 3C). This is the first report of Mer functioning with NADPH as a cofactor and using MG as a substrate. The X-ray crystal structure of Mer from *Methanopyrus kandleri*, *Methanothermobacter marburgensis*, and *Methanosarcina barkeri* have been determined and analysis of the active site suggests that it is a large cleft capable of binding $F_{420}H_2$ and CH_2=H_4MPT.(28, 31) The large cleft region that this work identified does not rule out the possibility that a small molecule like MG or lactaldehyde may also bind within the active site for catalysis to occur. These conclusions suggest an additional role of Mer in *M. jannasachii* and other methanogens, indicating that Mer is catalytically promiscuous, where it is able to complete two distinctive reactions with two distinct cofactors (Figure 4). Both of these reactions are expected to be essential for *M. jannaschii*'s survival.

Catalytic Promiscuity of Mer in *M. jannaschii*. Catalytically promiscuous enzymes are defined by their ability to transform an alternate substrate through a different transition state than the canonical substrate.(32) Enzymes demonstrating catalytically promiscuous activity are often overlooked because their promiscuous activity is not probed due to its differences from the canonical activity. In this case, the promiscuous activity of Mer was identified by isolating Mer by following a different activity from *M. jannaschii* cell extracts. At the outset of this work, a unique enzyme was believed to be the source of the MG reductase activity, not a well characterized enzyme like Mer. Mer has been studied in three other methanogens and one sulfate reducing archaeal organism, *Archeaoglobus fulgidus*. In all previously studied Mer enzymes, Mer demonstrated a strict requirement for F_{420} when assayed with CH_2=H_4MPT as the substrate.(25–27, 29) Mer has not previously been investigated for an activity other than as a CH_2=H_4MPT reductase, and nothing indicates that the *M. jannaschii* Mer (MjMer) is not functioning as the CH_2=H_4MPT reductase. Thus, the ability of MjMer to function as a CH_2=H_4MPT reductase was not investigated here, but would be of further interest to study to see how the two activities compare in more detail.

The discovery that MjMer is catalytic promiscuous demonstrates that the second function of Mer is as essential as the initial reported function, which is unique since many enzymes catalytic promiscuities are believed to be nonessential.(33) MG is a required intermediate for the biosynthesis of 6-deoxy-5-ketofructose 1-phosphate (DKFP) in *M. jannaschii* and *Halobacterium soluniarum*(10, 11) (Figure 6) and as such is believed to be essential. DKFP is one of two necessary precursors for the biosynthesis of 3-dehydroquinate (DHQ) in methanogens and halobacterium(11, 34) (Figure 6), the ability of Mer to oxidize lactaldehyde to MG for the generation of DHQ, and thus aromatic amino acids, is an essential metabolic function in *M. jannaschii*.

Conclusions. This work indicates that Mer from *M. jannaschii* is able to catalyze the reduction of MG to lactaldehyde using NADPH. The ability of Mer to perform this reaction demonstrates a catalytically promiscuous activity when compared to its known function (Figure 4). The catalytically promiscuous activity of Mer may be responsible for the in vivo oxidation of lactaldehyde to MG, an essential metabolite for the biosynthesis of aromatic amino acids in many archaeal organisms.

Acknowledgements. The authors would like to thank Dr. Kevin Sowers from the University of Maryland for providing *Methanocaldococcus jannaschii* for this work. The mass spectrometry recourses are maintained by the Virginia Tech Mass Spectrometry Incubator, a facility operated in part through funding by the Fralin Life Science Institute at Virginia Tech and by the Agricultural Experiment Station Hatch Program (CRIS Project Number: VA-135981). This work was supported by the National Science Foundation Grant MCB1120346 and by the Agricultural Experiment Station Hatch Program (CRIS Project Number: VA-135981) awarded to R.H. White.

References

1. **Thornalley PJ**. 1990. The glyoxalase system: new develoments toward functional characterization of a metabolic pathway fundamental to biological life. Biochem J **269**:1.
2. **Richard JP**. 1991. Kinetic parameters for the elimination reaction catalyzed by triosephosphate isomerase and an estimation of the reaction's physiological significance. Biochemistry **30**:4581–4585.
3. **Hopper DJ**, **Cooper RA**. 1971. The regulation of Escherichia coli methylglyoxal synthase; a new control site in glycolysis? FEBS Lett **13**:213–216.
4. **Huang K**, **Rudolph FB**, **Bennett GN**. 1999. Characterization of Methylglyoxal Synthase fromClostridium acetobutylicum ATCC 824 and Its Use in the Formation of 1, 2-Propanediol. Appl Environ Microbiol **65**:3244–3247.
5. **Subedi KP**, **Choi D**, **Kim I**, **Min B**, **Park C**. 2003. Hsp31 of Escherichia coli K-12 is glyoxalase III. Mol Microbiol **81**:926–936.
6. **Misra K**, **Banerjee AB**, **Ray S**, **Ray M**. 1995. Glyoxalase III from Escherichia coli: a single novel enzyme for the conversion of methyglyoxal into D-lactate without reduced glutathione. Biochem J **305**:999–1003.
7. **Rhee H**, **Watanabe K**, **Murata K**, **Kimura A**. 1987. Metabolism of 2-ketoaldehydes in bacteria: oxidative conversion of methylglyoxal to pyruvate by an enzyme from Pseudomonas putida. Agric Biol Chem **51**:1059–1066.
8. **Baldoma L**, **Aguilar J**. 1987. Involvement of lactaldehyde dehydrogenase in several metabolic pathways of Escherichia coli K12. J Biol Chem **262**:13991–13996.
9. **Holbrook JJ**, **Liljas A**, **Steindel SJ**, **Rossmann MG**. 1975. 4 Lactate Dehydrogenase.
10. **White RH**, **Xu H**. 2006. Methylglyoxal is an intermediate in the biosynthesis of 6-deoxy-5-ketofructose-1-phosphate: A precursor for aromatic amino acid biosynthesis in Methanocaldococcus jannaschii. Biochemistry **45**:12366–12379.
11. **Gulko MK**, **Dyall-Smith M**, **Gonzalez O**, **Oesterhelt D**. 2014. How do haloarchaea synthesize aromatic amino acids? PLoS One **9**:e107475.
12. **Oren A**, **Gurevich P**. 1995. Occurrence of the methylglyoxal bypass in halophilic Archaea. FEMS Microbiol Lett **125**:83–87.
13. **Malki L**, **Yanku M**, **Borovok I**, **Cohen G**, **Mevarech M**, **Aharonowitz Y**. 2009. Identification and characterization of gshA, a gene encoding the glutamate-cysteine ligase

in the halophilic archaeon Haloferax volcanii. J Bacteriol **191**:5196–5204.

14. **Madern D**. 2000. The putative l-lactate dehydrogenase from Methanococcus jannaschii is an NADPH-dependent l-malate dehydrogenase. Mol Microbiol **37**:1515–1520.
15. **Graupner M**, **Xu H**, **White RH**. 2000. Identification of an archaeal 2-hydroxy acid dehydrogenase catalyzing reactions involved in coenzyme biosynthesis in methanoarchaea. J Bacteriol **182**:3688–3692.
16. **Grochowski LL**, **Xu H**, **White RH**. 2006. Identification of lactaldehyde dehydrogenase in Methanocaldococcus jannaschii and its involvement in production of lactate for F420 biosynthesis. J Bacteriol **188**:2836–2844.
17. **White RH**. 2008. Biochemical Origins of Lactaldehyde and Hydroxyacetone in Methanocaldococcus jannaschii. Biochemistry **47**:5037–5046.
18. **Greening C**, **Ahmed FH**, **Mohamed AE**, **Lee BM**, **Pandey G**, **Warden AC**, **Scott C**, **Oakeshott JG**, **Taylor MC**, **Jackson CJ**. 2016. Physiology, Biochemistry, and Applications of F420-and Fo-Dependent Redox Reactions. Microbiol Mol Biol Rev **80**:451–493.
19. **Mukhopadhyay B**, **Johnson EF**, **Wolfe RS**. 1999. Reactor-Scale Cultivation of the Hyperthermophilic MethanarchaeonMethanococcus jannaschii to High Cell Densities. Appl Environ Microbiol **65**:5059–5065.
20. **Graham DE**, **Xu H**, **White RH**. 2002. Identification of coenzyme M biosynthetic phosphosulfolactate synthase. A new family of sulfonate-biosynthesizing enzymes. J Biol Chem **277**:13421–13429.
21. **Bradford MM**. 1976. A rapid and sensitive method for the quantitation of microgram quantities of protein utilizing the principle of protein dye-binding. Anal Biochem **72**:248–257.
22. **Miller D**, **O'Brien K**, **Xu H**, **White RH**. 2014. Identification of a 5′-Deoxyadenosine Deaminase in Methanocaldococcus jannaschii and its Possible Role in Recycling the Radical SAM Enzyme Reaction Product 5′-Deoxyadenosine. J Bacteriol **196**:1064–1072.
23. **Ashton WT**, **Brown RD**. 1980. Synthesis of 8-demethyl-8-hydroxy-5-deazariboflavins. J Heterocycl Chem **17**:1709–1712.
24. **Graupner M**, **White RH**. 2003. Methanococcus jannaschii coenzyme F420 analogs contain a terminal α-linked glutamate. J Bacteriol **185**:4662–4665.

25. **Ma K**, **Linder D**, **Stetter KO**, **Thauer RK**. 1991. Purification and properties of N 5, N 10-methylenetetrahydromethanopterin reductase (coenzyme F420-dependent) from the extreme thermophile Methanopyrus kandleri. Arch Microbiol **155**:593–600.
26. **MA K**, **THAUER RK**. 1990. Purification and properties of N5, N10-methylenetetrahydromethanopterin reductase from Methanobacterium thermoautotrophicum (strain Marburg). Eur J Biochem **191**:187–193.
27. **Ma K**, **Thauer RK**. 1990. N5, N10-Methylenetetrahydromethanopterin reductase from Methanosarcina barkeri. FEMS Microbiol Lett **70**:119–124.
28. **Aufhammer SW**, **Warkentin E**, **Ermler U**, **Hagemeier CH**, **Thauer RK**, **Shima S**. 2005. Crystal structure of methylenetetrahydromethanopterin reductase (Mer) in complex with coenzyme F420: Architecture of the F420/FMN binding site of enzymes within the nonprolyl cis-peptide containing bacterial luciferase family. Protein Sci **14**:1840–1849.
29. **Schmitz RA**, **Linder D**, **Stetter KO**, **Thauer RK**. 1991. N 5, N 10-Methylenetetrahydromethanopterin reductase (coenzyme F420-dependent) and formylmethanofuran dehydrogenase from the hyperthermophile Archaeoglobus fulgidus. Arch Microbiol **156**:427–434.
30. **Livingston DJ**, **Fox JA**, **Orme-Johnson W**, **Walsh CT**. 1987. 8-hydroxy-5-deazaflavin-reducing hydrogenase from methanobacterium thermoautotrophicum: 2. Kinetic and hydrogen-transfer studies. Derivation of a steady-state rate equation for deazaflavin-reducing hydrogenase. Biochemistry **26**:4228–4237.
31. **Shima S**, **Warkentin E**, **Grabarse W**, **Sordel M**, **Wicke M**, **Thauer RK**, **Ermler U**. 2000. Structure of coenzyme F 420 dependent methylenetetrahydromethanopterin reductase from two methanogenic archaea. J Mol Biol **300**:935–950.
32. **Devamani T**, **Rauwerdink AM**, **Lunzer M**, **Jones BJ**, **Mooney JL**, **Tan MAO**, **Zhang Z-J**, **Xu J-H**, **Dean AM**, **Kazlauskas RJ**. 2016. Catalytic promiscuity of ancestral esterases and hydroxynitrile lyases. J Am Chem Soc **138**:1046–1056.
33. **Copley SD**. 2015. An evolutionary biochemist's perspective on promiscuity. Trends Biochem Sci **40**:72–78.
34. **White RH**. 2004. L-aspartate semialdehyde and a 6-deoxy-5-ketohexose 1-phosphate are the precursors to the aromatic amino acids in Methanocaldococcus jannaschii. Biochemistry **43**:7618–7627.

Figures

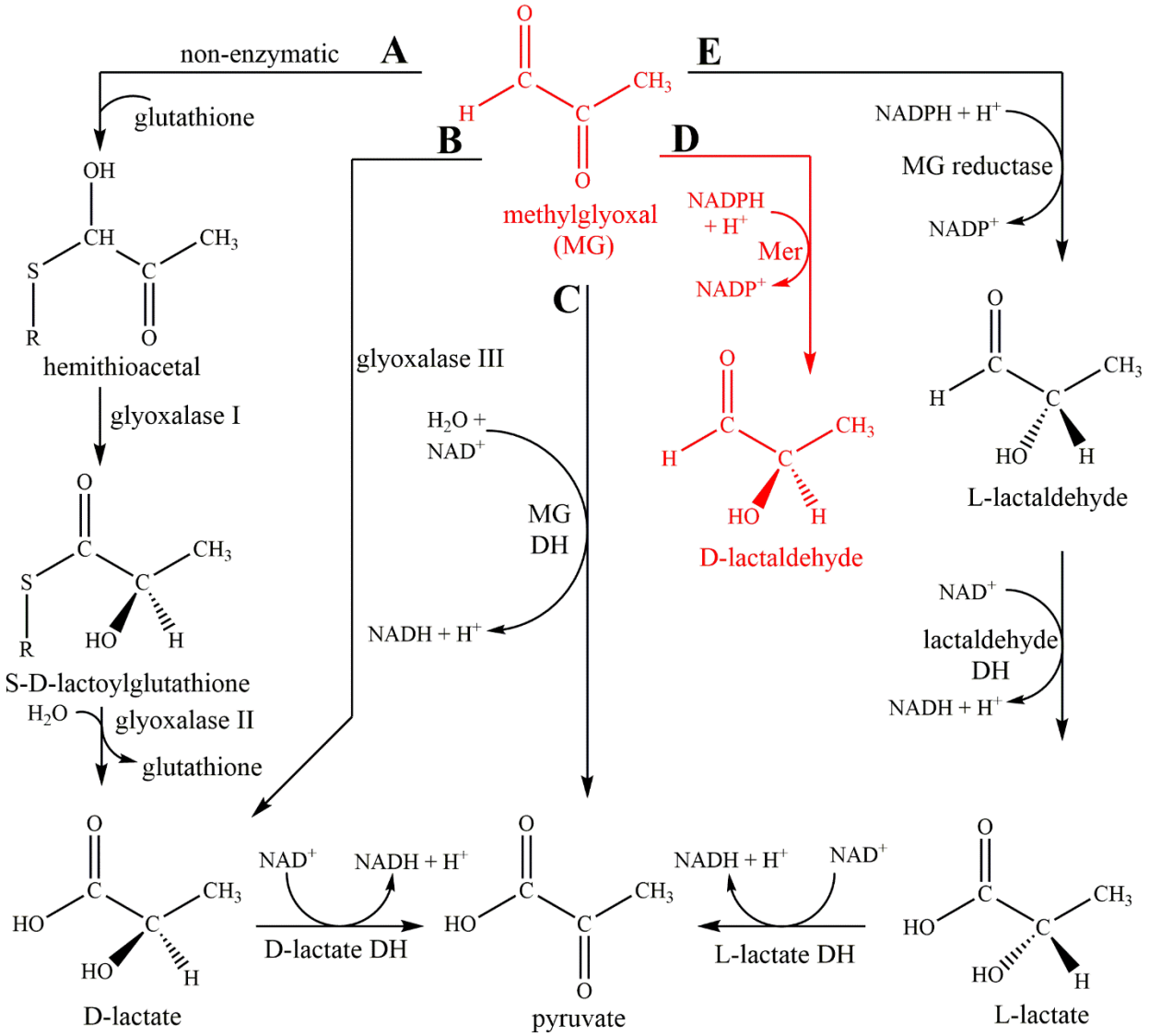

Figure 1. Methylglyoxal (MG) catabolic pathways. Highlighted in red is the new reaction identified in this work.

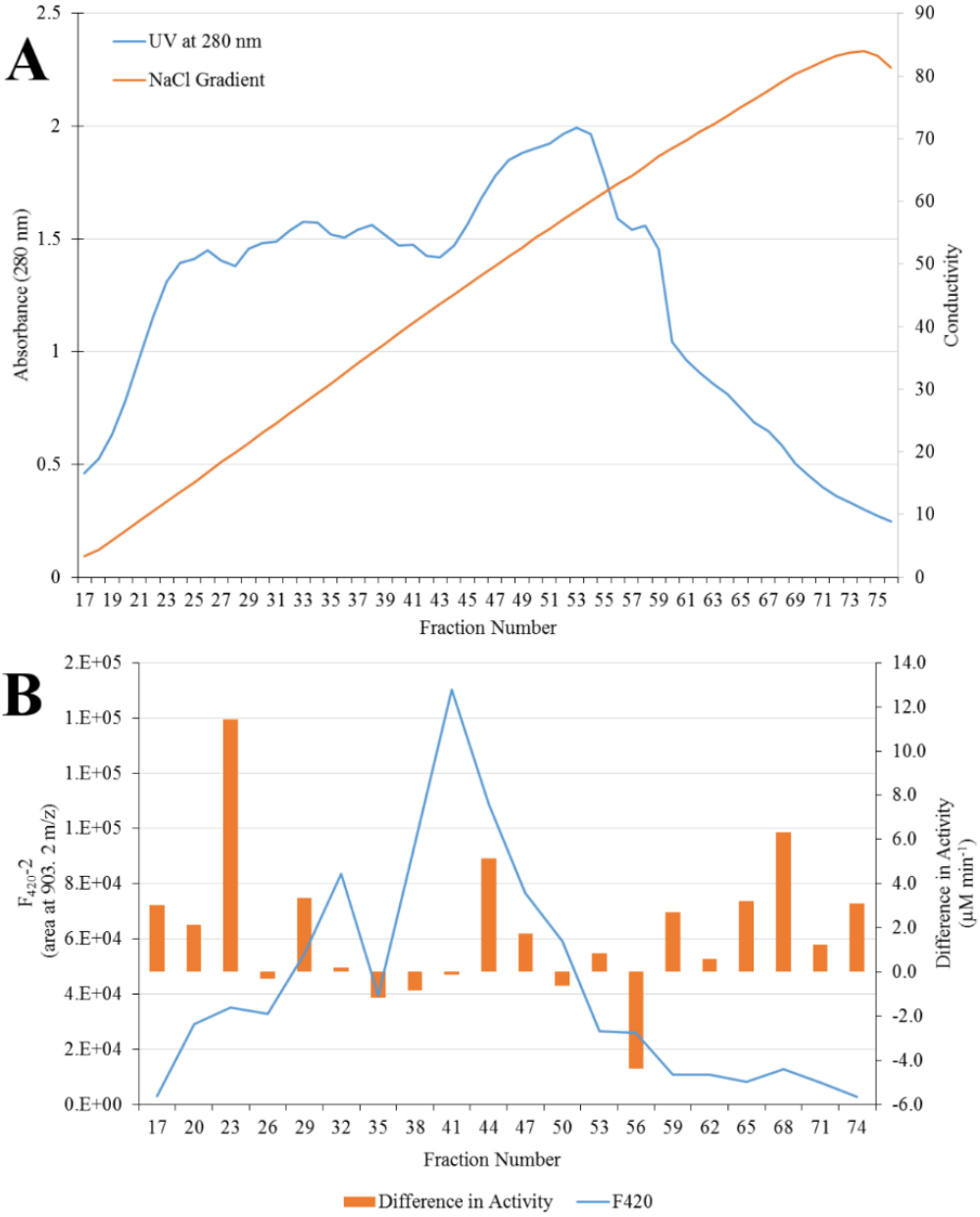

Figure 2. Separation *M. jannaschii* cell extract via MonoQ with a salt gradient and absorbance at 280 nm overlaid (A) and overlay of difference in activity (µM min^{-1}) of every third fraction with analysis of fractions for F_{420}-2 (B). The difference in activity was calculated by subtracting the NADPH plus MG activity from the NADPH alone activity for each analyzed fraction at 340 nm. Fraction 23 (0.21 µmol min^{-1} mg^{-1}) contained the most activity and was further separated by SEC (Figure 3).

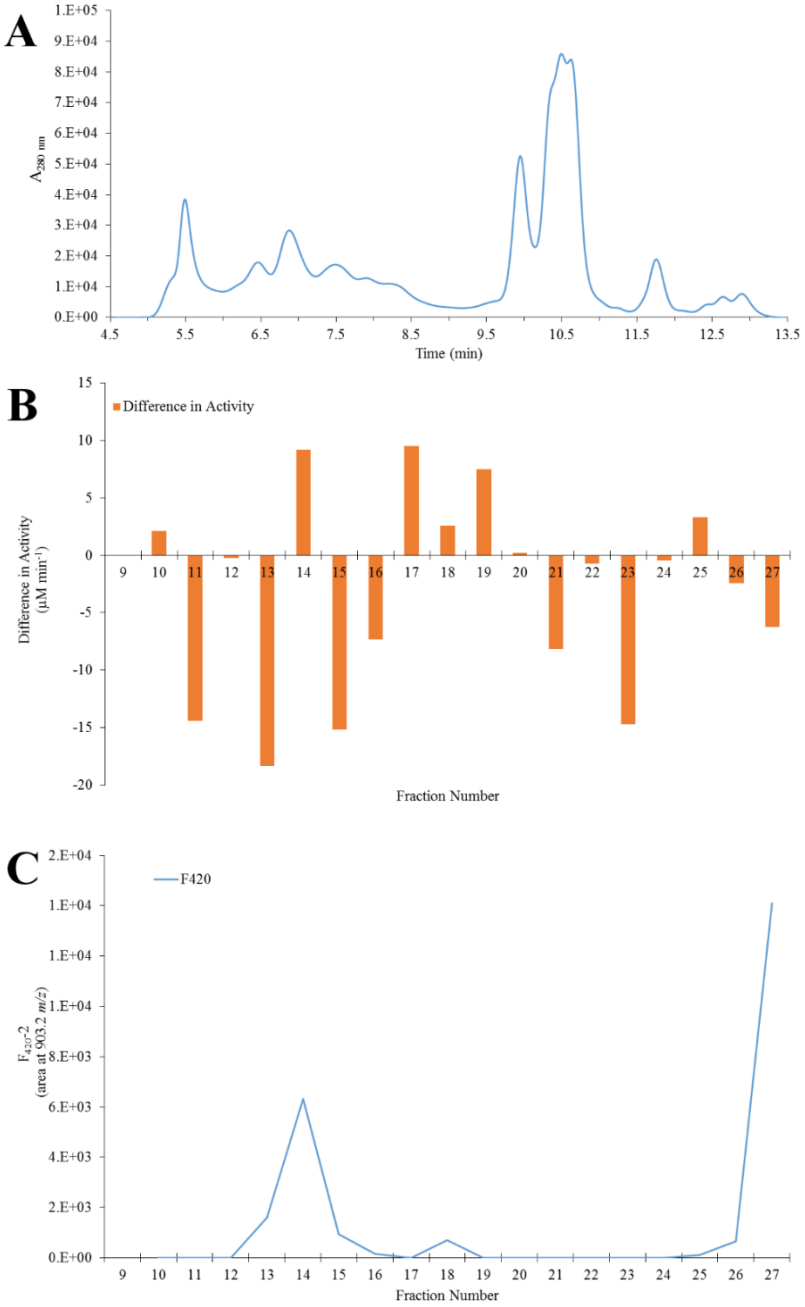

Figure 3. SEC separation of Fraction 23 from Figure 2. Absorbance at 280 nm of SEC separation (A), difference of activity for fractions 9 to 27 plus and minus MG (B), and F_{420}-2 analysis for fractions 9 to 27 (C). The time shown in (A) coordinates with the fraction numbers indicated in (B and C). The difference in activity was calculated by subtracting the NADPH plus MG activity from the NADPH alone activity for each analyzed fraction at 340 nm.

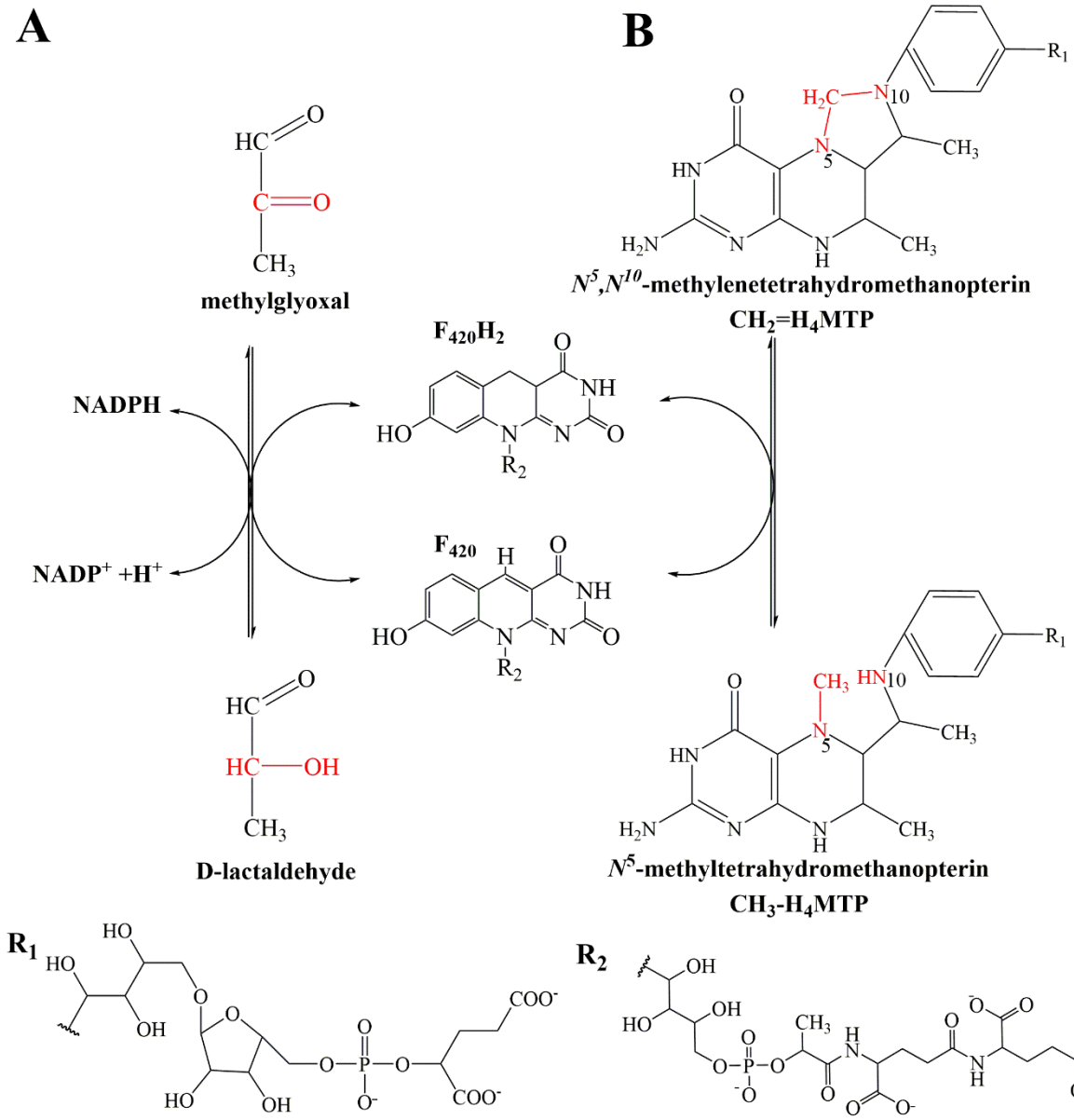

Figure 4. Comparison of reactions catalyzed by Mer from *M. jannaschii*. Methylglyoxal reduction to D-lactaldehyde with either NADPH or $F_{420}H_2$ (A) and $F_{420}H_2$ dependent reduction of CH_2=H_4MPT to CH_3-H_4MPT (B). The R groups for H_4MPT and F_{420} are shown at the bottom. Highlighted in red are where the reduction of each compound is performed.

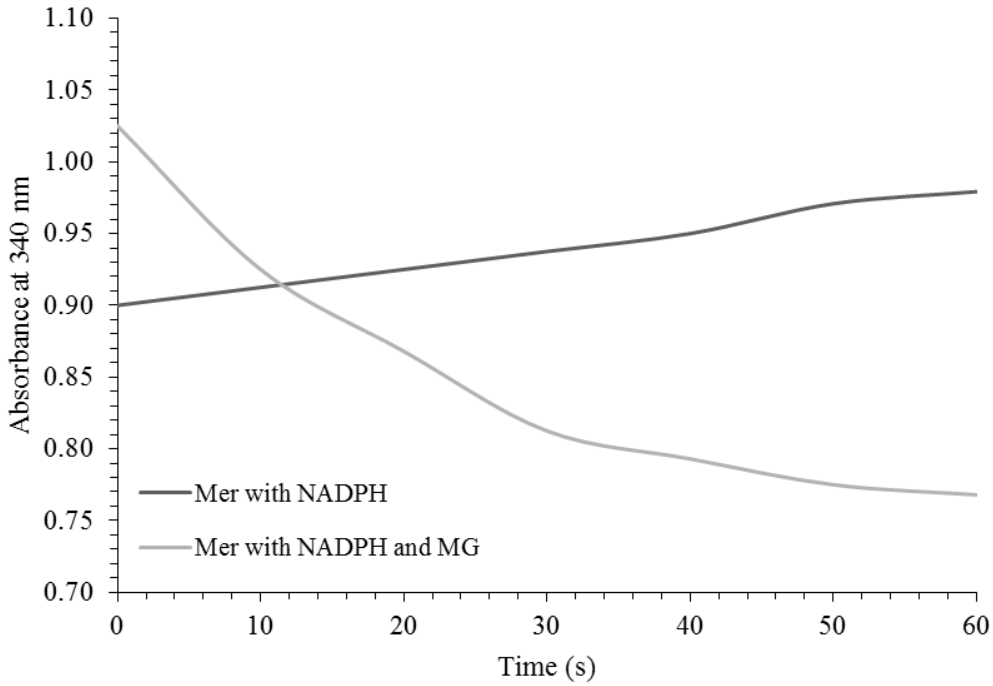

Figure 5. Kinetic profile of the reduction of MG with NADPH with recombinant Mer. Observed change in absorbance at 340 nm with time of Mer incubated with NADPH (black) or with NADPH and MG (grey). The specific activity was measured to be 1.3 μmol min^{-1} mg^{-1}.

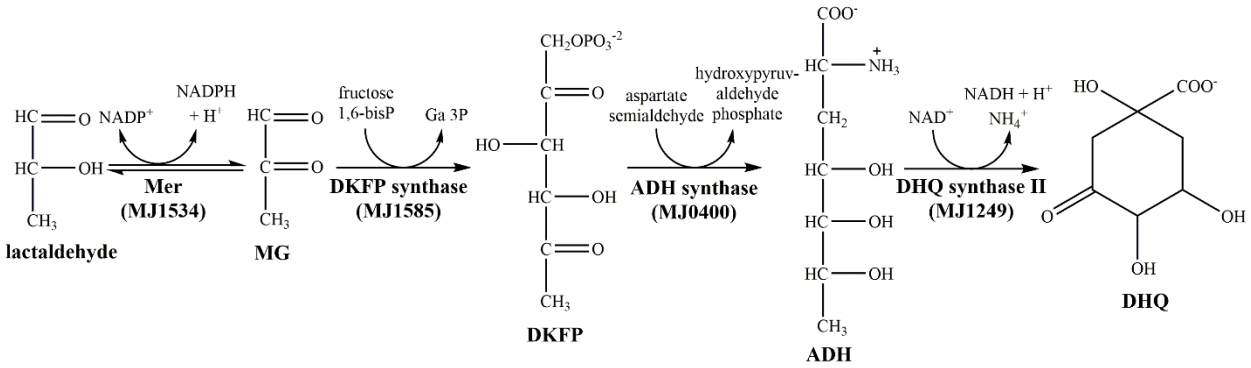

Figure 6. Biosynthetic pathway for 3-dehydroquinate (DHQ) production in *M. jannaschii*. ADH is the abbreviation for 2-amino-3, 7-dideoxy-D-*threo*-hept-6-ulosonic acid.

Supplemental information for Catalytic Promiscuity of N^5,N^{10}-methylenetetrahydromethanopterin reductase from *Methanocaldococcus jannaschii* as a methylglyoxal reductase

Danielle V. Miller, Michelle Ruhlin, W. Keith Ray, Huimin Xu, and Robert H. White

This work was supported by the National Science Foundation Grant MCB1120346.

Department of Biochemistry, Virginia Polytechnic Institute and State University, Blacksburg, VA 24061

Figures

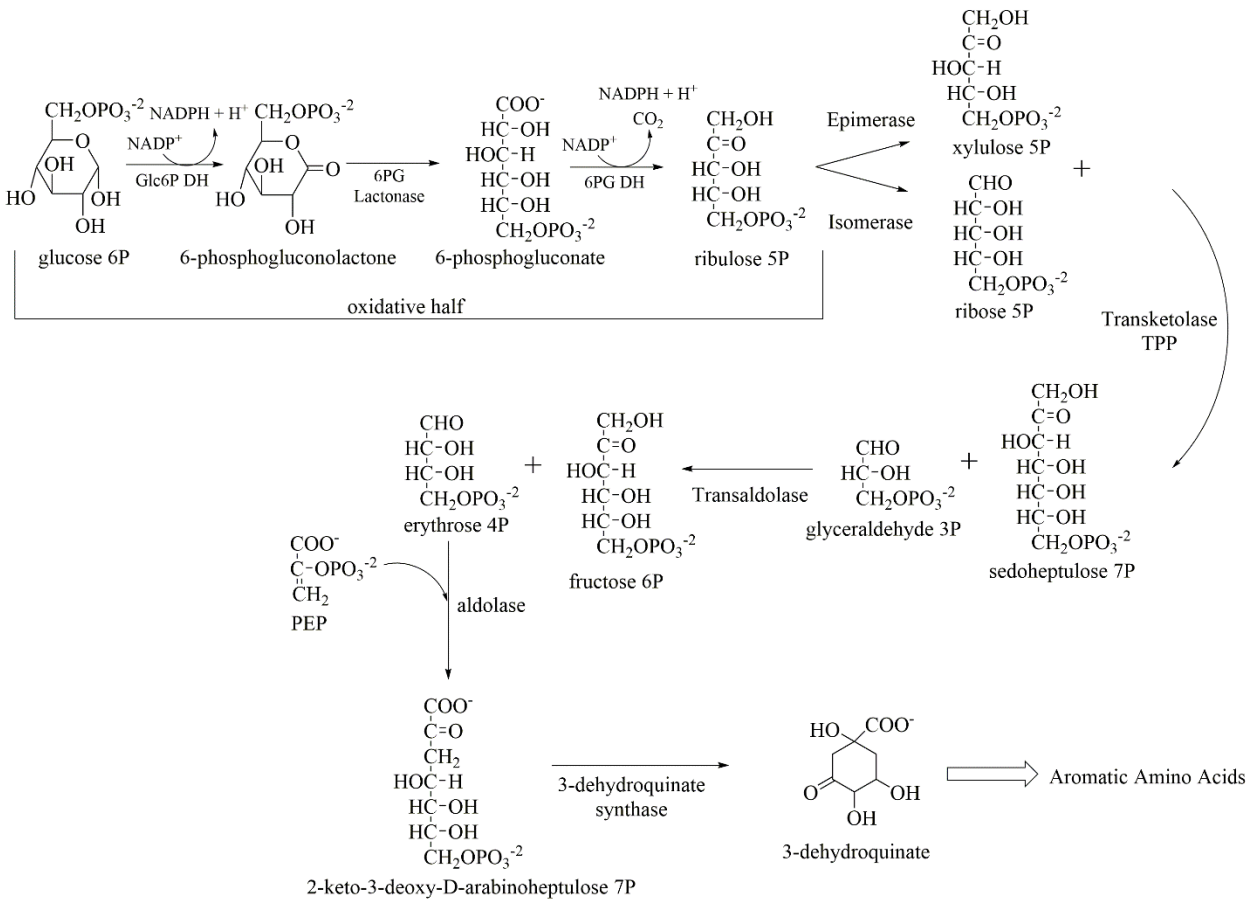

Figure S1. Canonical pentose phosphate pathway as the source of erythrose 4-phosphate

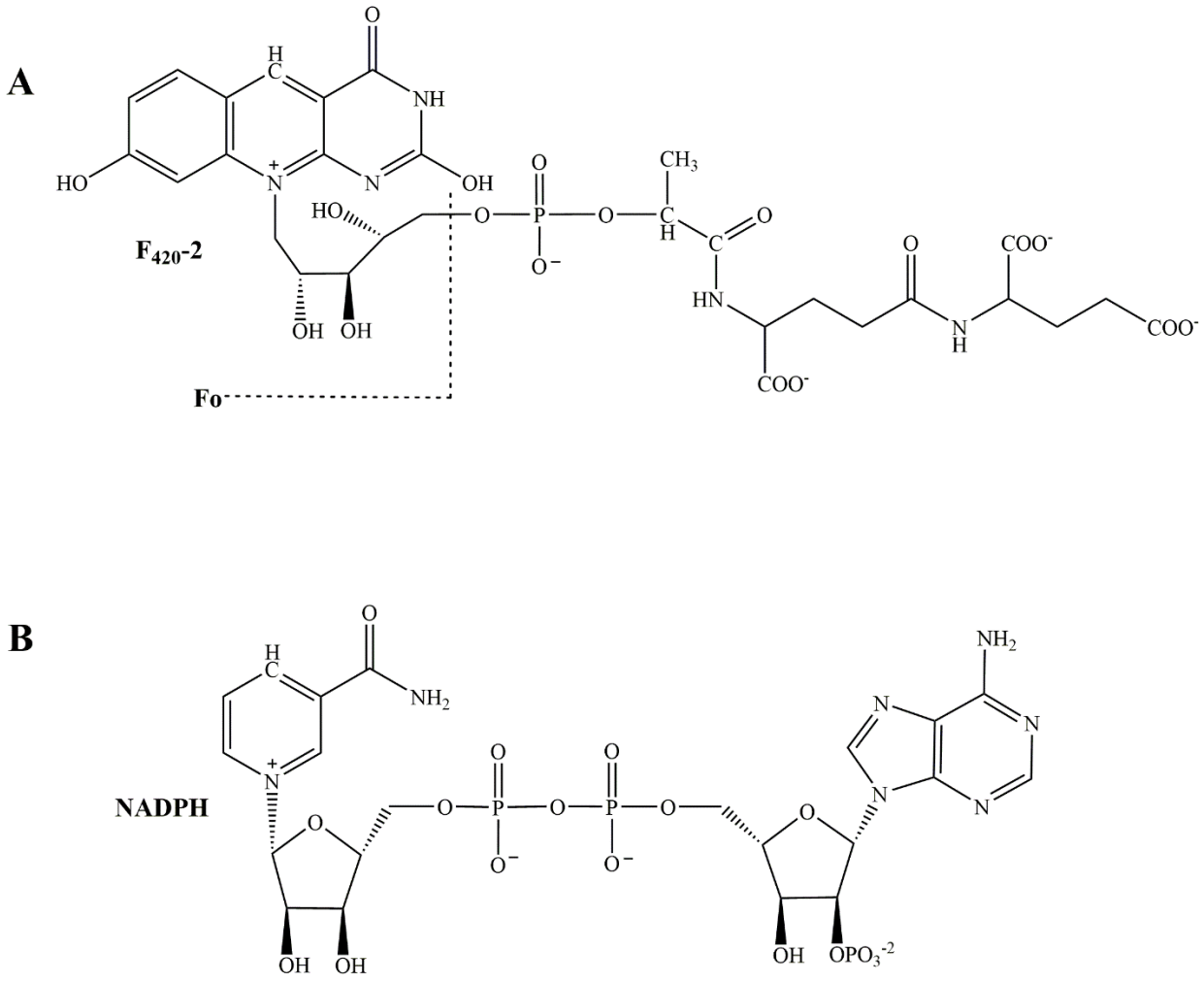

Figure S2. Comparison of F_{420}-2, Fo (A) and NADPH (B) structures.

Chapter 5: Purine Salvage in *Methanocaldococcus jannaschii*: Elucidating the Role of a Conserved Cysteine in Adenine Deaminase

Short Title: Purine Salvage in *M. jannaschii*

Danielle V. Miller, Anne M. Brown, Huimin Xu, David R. Bevan, and Robert H. White*

Department of Biochemistry, Virginia Polytechnic Institute and State University, Blacksburg, Virginia, USA 24061

*To whom correspondence should be addressed. Telephone: +1 (540) 231-6605, Fax: +1 (540) 231-9070, e-mail: rhwhite@vt.edu

Key words: methanogen, archaea, amino acid conservation, cysteine, molecular docking, and molecular dynamics

Miller D V, Brown AM, Xu H, Bevan DR, White RH. 2016. Purine salvage in *Methanocaldococcus jannaschii*: Elucidating the role of a conserved cysteine in adenine deaminase. *Proteins Struct Funct Bioinforma* **84**:828–840.

Abstract

Adenine deaminases (Ade) and hypoxanthine/guanine phosphoribosyltransferases (Hpt) are widely distributed enzymes involved in purine salvage. Characterization of the previously uncharacterized Ade (MJ1459 gene product) and Hpt (MJ1655 gene product) are discussed here and provide insight into purine salvage in *Methanocaldococcus jannaschii*. Ade was demonstrated to use either Fe(II) and/or Mn(II) as the catalytic metal. Hpt demonstrated no detectable activity with adenine, but was equally specific for hypoxanthine and guanine with a k_{cat}/K_M of 3.2 x 10^7 and 3.0 x 10^7 $s^{-1}M^{-1}$, respectively. These results demonstrate that hypoxanthine and IMP are the central metabolites in purine salvage in *M. jannaschii* for AMP and GMP production. A conserved cysteine (C127, *M. jannaschii* numbering) was examined due to its high conservation in bacterial and archaeal homologues. To assess the role of this highly conserved cysteine in *M. jannaschii* Ade, site directed mutagenesis was performed. It was determined that mutation to serine (C127S) completely abolished Ade activity and mutation to alanine (C127A) exhibited 10-fold decrease in k_{cat} over the wild type Ade. To further investigate the role of C127, detailed molecular docking and dynamics studies were performed and revealed adenine was unable to properly orient in the active site in the C127A and C127S Ade model structures due to distinct differences in active site conformation and rotation of D261. Together this work illuminates purine salvage in *M. jannaschii* and the critical role of a cysteine residue in maintaining active site conformation of Ade.

Introduction

The salvage of purine bases and nucleosides is thought to have emerged at the same time as the de novo pathway for purine biosynthesis, with the direct salvage of adenine to AMP occurring following the divergence of *Bacteria* and *Eukarya*, given the lack of an adenine phosphoryltransferase (Apt) and adenosine kinase in *Archaea*(1). The direct salvage of adenine would bypass the need for an adenine deaminase (Ade) and directly condense adenine with 5-phospho-α-D-ribosyl-1-pyrophosphate (PRPP) to produce AMP by an Apt. Alternatively, adenine could be salvaged directly by conversion to adenosine by a purine nucleoside phosphorylase then subsequent phosphorylation to AMP by an adenosine kinase. However, the possible purine nucleoside phosphorylase, annotated as a methylthioinosine phosphorylase, in *Methanocaldococcus jannaschii* does not utilize adenosine as a substrate (Miller unpublished) and no adenosine kinase homologue has been identified in the M. jannaschii genome. These findings suggest that adenine is not directly salvaged in *M. jannaschii*.

By lacking Apt and adenosine kinase, Archaea must salvage adenine through an alternative route, first by deaminating adenine to hypoxanthine followed by further conversion to AMP and GMP (Figure 1A). Therefore, it is proposed that *M. jannaschii* is able to salvage adenine using an enzyme annotated as adenine deaminase (EC 3.5.4.2, Ade)(2) and a hypoxanthine/guanine phosphoribosyltransferase (EC 2.4.2.8, Hpt). Ade's are members of the amidohydrolyase superfamily of enzymes with a (β/α)8-barrel structure (3, 4) and are ubiquitous enzymes that catalyze the deamination of adenine to hypoxanthine through attack on C6 of the purine ring by a nucleophilic water. The first indication that Archaea contained an Ade was reported in 1990 by the measurement of its enzymatic activity in cell extracts of *Methanobacterium thermoautotrophicum* (5). Hpt's catalyzed the condensation of purine nucleobases (hypoxanthine and guanine) with PRPP to form nucleosides IMP and GMP (Figure 1). Hpt has been described in *M. thermoautotrophicum* and *Methanococcus voltae* to be specific for hypoxanthine and guanine (6, 7). Characterizations of Ade and Hpt from *M. jannaschii,* encoded by the MJ1459 and MJ1655 gene products, respectively, are described here.

In investigating the Ade from *M. jannaschii*, a conserved cysteine at position 127 (*M. jannaschii* numbering) was identified to be present in archaeal and bacterial Ade's (Figure 2). The conserved cysteine in Ade, with no clear function, was noted and considered of interest due

to the low abundance of cysteine residues in proteins (8). In addition, this conserved cysteine was of interest given that it was not observed in a conserved motif commonly associated with either formation of disulfide bonds used in structure stabilization (9), iron-sulfur clusters (10), redox control (11), or nucleophilic activity, such as in cysteine proteases (12). Taken together, this information indicated that the conserved cysteine found at position 127 (*M. jannaschii* numbering) may have an important role in either the enzymatic activity or structure of Ade's and thus the role of this cysteine was investigated. A combination of experimental and computational approaches was used to provide insight into the potential role of the conserved cysteine at position 127 in *M. jannaschii.*

Materials and methods

Cloning, overexpression, and purification of the MJ1459 (Wt and C127S/A) and MJ1655 gene products in *E. coli*. The MJ1459 (UniProt accession number Q58854) and MJ1655 (UniProt accession number Q59094) gene products were amplified by PCR from genomic DNA using the oligonucleotide primers shown in Table S1. The MJ1459 mutants, C127A and C127S, were amplified by PCR of QuikChange Site-Directed Mutagenesis kit (Stratagene) using the cloned wild type pMJ1459 as the template and the used primers shown in Table S1. PCR amplification was performed as described previously (13) using a 50 ^{o}C annealing temperature. Purified PCR product was digested with Nde1 and Bam H1 restriction enzymes and ligated into compatible sites in plasmid pET 19b for MJ1459 and mutants (C127A and C127S) and in plasmid pT7-7 for MJ1655. The sequence of the resulting plasmids pMJ1459 and mutants C127A, C127S and pMJ1655 were verified by DNA sequencing and were transformed into *E. coli* BL21-CodonPlus (DE3)-RIL cells (Stratagene). The transformed cells containing pMJ1459, mutants (C127A and C127S), and pMJ1655 were individually grown in Luria-Bertani medium (200 mL) supplemented with 100 µg/mL ampicillin and were grown at 37o C with shaking until they reached an OD 600 of 1.0. A concentration of 1 mM $MnCl_2$ was supplemented in addition to the ampicillin for MJ1459 and C127S/A mutant cultures. Recombinant protein production was induced by the addition of lactose to a final concentration of 28 mM (13). After an additional 2 hours of culture, the cells were harvested by centrifugation (4,000 *x g*, 5 min) and frozen at -20 ^{o}C. Induction of the desired proteins was confirmed by SDS-polyacrylamide gel electrophoresis (SDS-PAGE) analysis of total cellular proteins.

E. coli cells expressing recombinant protein were re-suspended in 3 mL extraction buffer consisting of 50 mM extraction buffer (*N*-[tris(hydroxymethyl)methyl]-2-aminoethanesulfonic acid (TES-K+) pH 7.0, 10 mM $MgCl_2$, 20 mM dithiothreitol (DTT)) and lysed by sonication. After precipitating the majority of *E. coli* proteins by heating the cell lysate to 90 °C for 10 min for the Wt MJ1459-derived protein, 60 °C for 10 min for the C127S MJ1459-derived protein, and 80 °C for 10 min for the MJ1655-derived protein, they were purified by anion exchange chromatography on a MonoQ HR column (1 x 8 cm, Amersham Bioscience) with a linear gradient from 0 to 1 M NaCl in 25 mM tris(hydroxymethyl)aminomethane (Tris) pH 7.5 over 55 mL at 1 mL/min. Protein concentration was determined by Bradford analysis (14). The MonoQ fractions containing Wt MJ1459-, C127S MJ1459- and MJ1655-derived proteins were identified by SDS-PAGE analysis of the individual fractions. The protein bands corresponding to the predicted molecular mass of the MJ1459 gene product (~62 kDa) and MJ1655 (~20 kDa) were excised from the polyacrylamide gel, and the cut gel bands were prepared for matrix assisted laser desorption ionization mass spectrometry (MALDI-MS) as described previously (15).

C127A Ade was not efficiently recombinantly expressed in *E. coli* as judged by SDS-PAGE of the total cellular protein, and the C127A MJ1459-gene product was unable to be identified by MALDI-MS (Figure S2). Instead, the C127A Ade was purified based on activity using an *E. coli* extract overexpressing the MJ0100-gene product (referred to as the *E. coli* control from here on). The MJ0100 gene product was only produced in the insoluble pellet (Figure S2C). The activity of MJ0100 was demonstrated in *M. jannaschii* to catalyze the reaction of hydrogen sulfide with aspartate semialdehyde to form homocysteine (16). Thus, the *E. coli* extract from the recombinant expression of MJ0100 was used as a negative control for *E. coli* adenine deaminase activity to purify C127A Ade from the recombinant expression. The crude extracts of the C127A Ade and *E. coli* control were tested for activity using the standard enzyme assay described below following Bradford analysis of the total protein concentration. Successive steps of purification were done by heating the cell extracts at 60, 70, and 80 °C and MonoQ purification followed by the standard assay to determine where the protein eluted. The protein concentration was determined by Bradford analysis (17) . Results of the purification are summarized in Table S2.

Kinetic and physical characterization of Ade. Ade activity was measured in 100 µL of extraction buffer (50 mM TES-K^+ pH 7.0, 10 mM $MgCl_2$, 20 mM DTT) containing 0.5 mM

Mn(II) or Fe(II), 1 mM adenine, 1.0 µg of the Wt, C127S, C127A Ade, or *E. coli* control. To determine if there was a linear relationship between product formation and time, a standard assay was performed using Wt Ade except the incubation period was altered to 0, 10, 20, and 30 min. Kinetic parameters were determined using from 0 to 1 mM final concentrations of adenine in the standard assay with 22 ng Wt Ade and 5.6 µg C127A Ade and *E. coli* control. The samples were incubated at 60 ^{o}C for 20 min followed by the addition of 5 µL of 2 M hydrochloric acid and centrifugation (14000 *x g*, 2 min) to remove the precipitated proteins. The soluble material was separated from the pellet, and 10 µL was injected for HPLC analysis.

The chromatographic separation and analysis of adenine and hypoxanthine was performed on a Shimadzu HPLC System with a C18 reverse phase column (Varian Pursuit XRs 250 × 4.6 mm, 5 µm particle size) with photodiode array detection. The elution profile consisted of 5 min at 95% sodium acetate buffer (25 mM, pH 6.0, 0.02% NaN_3) and 5% methanol followed by a linear gradient to 20% sodium acetate buffer/80% methanol over 25 min at 0.5 mL/min. Under these conditions hypoxanthine eluted at 13 minutes and adenine at 19 minutes. Quantitation was based on absorbance at 260 nm for the adenine and 250 nm for the hypoxanthine using ε_{260} = 13400 $M^{-1}cm^{-1}$ for adenine and ε_{250} = 10700 $M^{-1}cm^{-1}$ for hypoxanthine (18).

The native molecular weight of Wt Ade was determined by size exclusion chromatography as described previously using a Superose 12 HR column (19). Protein standards used to generate the standard curve included: apoferritin (443 kDa), β-amylase (200 kDa), alcohol dehydrogenase (150 kDa), conalbumin (77.5 kDa), bovine serum albumin (66 kDa), carbonic anhydrase (29 kDa), cytochrome c (14.4 kDa), and B12 (1.4 kDa).

Metal analysis of Wt Ade was performed at the Virginia Tech Soil Testing Laboratory using inductively coupled plasma emission spectrophotometry. Instrumentation included a Spectro CirOS VISION made by Spectro Analytical Instruments equipped with a Crossflow nebulizer with a Modified Scott spray chamber; the nebulizer rate was 0.75 L/min. A yttrium internal standard (50 mg/L) was introduced by peristaltic pump. Samples were analyzed for cobalt, iron, manganese, nickel, and zinc.

Kinetic characterization of Hpt. Hpt activity was monitored in 100 µL of 25 mM tris buffer (pH 7.5) with a final concentration of 0.2 mM $MgCl_2$, 0.2 mM PRPP, 0.2 mM purine (adenine, guanine, or hypoxanthine (HX)), and 11.0 µg of the Hpt for 10 min at 70 ^{o}C. To

determine if there was a linear relationship of product formation with time the above assay was done at 0, 10, 20, 30, and 40 min. Kinetic parameters were determined using from 0 to 0.4 mM final concentrations of guanine and from 0 to 0.15 mM final concentrations of hypoxanthine with PRPP in excess (0.5 mM) with 0.53 μg Hpt in 100 μL 25 mM tris buffer (pH 7.5). The kinetics of PRPP was determined with guanine in excess (0.4 mM) and PRPP from 0 to 0.5 mM with 0.53 μg Hpt in 100 μL 25 mM tris buffer (pH 7.5). All assays were incubated at 70 ^{o}C for 10 min followed by the addition of 5 μL of 2 M hydrochloric acid and centrifugation (14000 *x g*, 2 min) to remove the precipitated proteins. The soluble material was separated from the pellet and 10 μL was injected for HPLC analysis (see above). Under these conditions GMP eluted at 6.3 minutes, IMP at 6.7 minutes, AMP at 9.9 minutes, and guanine at 12.3 minutes. Quantitation was based on absorbance at 260 nm for the AMP, 246 nm for guanine, 252 nm for GMP, and 250 nm for IMP using ε_{260} = 15400 $M^{-1}cm^{-1}$ for AMP, ε_{246} = 10700 $M^{-1}cm^{-1}$ for guanine, ε_{252} = 13700 $M^{-1}cm^{-1}$ for GMP, ε_{250} = 12300 $M^{-1}cm^{-1}$ for inosine (IMP) (18).

Generation of the Wt, C127A, and C127S Ade homology models. All MD and docking results were based on homology models built in MODELLER version 9v7 (20) and based on the template structure from *A. tumefaciens* (PDB ID:3NQB) (21). The Ade structure from *A. tumefaciens* was chosen as the template because it has a resolution of 2.21 Å, contains three bound Mn(II) ions, and the sequence identity between the whole *A. tumefaciens* and *M. jannaschii* protein sequences is 31% with the active site conservation of 99% (Figure 2). Model quality was assessed by Anolea (22, 23), QMEAN (24), and ProCheck (25) and the models were deemed acceptable per assessment standards. Models were also evaluated using the Verify 3D server (26, 27). The C127S and C127A model was generated by changing C127 to Ser or Ala in the Ade amino acid sequence and then building the homology model in MODELLER and assessing as described above. Energy minimization was performed using Molecular Operating Environment (MOE) (28) and the OPLS-AA force field (29).

Molecular docking of Wt, C127A, and C127S Ade with adenine. Wt, C217S, and C127A homology models from above were utilized for molecular docking and molecular dynamics (Figures 3 and S1). The adenine structure was acquired from the Protein Data Bank (Ligand ID: ADE). Wt and C127S/A Ade and adenine were prepared for docking using AutoDock Tools 1.5.6 (30). AutoDock Vina (31) was used to perform the molecular docking of adenine into the Wt and C127S/A Ade. Parameters for docking included using the same box size

of 15 Å x 15 Å x 15 Å for Wt and C127S/A docking experiments. The Wt Ade box was centered within the coordinates of (67.965, -21.471, 18.243), the C127S box was centered within the coordinates (-1.571, -7.302, 5.381), and the C127A, box was centered within the coordinates (-1.571, -7.302, -1.649). The position of the box was relative to the active site in each structure. Docking was done with the initial homology models and results were inconclusive. MD, as described below, was utilized to allow residues to position themselves in a more energetically favorable position, and RMSD clustering was performed over the last 50 ns of MD. The representative structure, which was the center structure of the dominant cluster (Table S3) for the last 50 ns of simulation time, was used for docking.

Molecular dynamics simulations of Wt, C127A, and C127S Ade. System construction and simulations were performed using the GROMACS software package, version 4.5.4 (32, 33). All protein parameters were from the AMBER99SB-IDLN force field (34). Wt, C127S, and C127A Ade were centered in a cubic box with a minimum solute-box distance of 1.0 nm. Systems were solvated with TIP3P water (35) and neutralized with Na+ counterions. Mn(II) parameters were taken from Bradbrook et al. (36), and crystal waters in the active site were retained by overlaying the model and template structures. To preserve the active site geometry, harmonic connections were added between all Mn(II) ions and heavy atoms of ligating water molecules and protein residues. The solvated system was energy-minimized using the steepest descent method and subsequently equilibrated in two steps, NVT and NPT. Three replicate simulations of Wt, C127S, and C127A Ade were produced, each with random starting velocities. NVT and NPT using the Berendsen weak coupling method (37) at 300 K was performed for 100 ps and 500 ps, respectively. Position restraints were imposed on all protein heavy atoms during equilibration and released during the molecular dynamics simulations.

MD simulations utilized three-dimensional periodic boundary conditions. P-LINCS (38) was used to constrain bond lengths to allow an integration time step of 2 fs. Nonbonded interactions were calculated within a short-range interaction cutoff of 0.8 nm. The smooth particle mesh Ewald (PME) method (39, 40) using cubic interpolation, and Fourier grid spacing of 0.12 nm was employed to calculate long-range electrostatic interactions. Simulations were conducted for 100 ns and found to be converged, based on backbone RMSD and backbone RMSD clustering employing a cutoff of 0.2 nm, using the method of Daura et al (41). Secondary structure was determined according to the DSSP algorithm (42) . All other analysis was

performed using programs in the GROMACS package. Structure visualization was performed with Pymol (43). Statistical analysis was carried out using a two-tailed t-test, with statistical significance determined if $p < 0.05$.

Results and discussion

Ade and Hpt's are ubiquitous enzymes and are predominantly involved in purine salvage. Purine incorporation and metabolism has been evaluated in three methanogens: *Methanobacterium thermautotrophicus*, *Methanococcus vannielii*, and *Methanococcus voltae* (5, 44, 45). *M. thermautotrophicus* showed low levels of Ade activity and an active Hpt (5, 6), *M. vannielii* demonstrated use of adenine as the sole nitrogen source (44), and *M. voltae* was able to incorporate the purines into nucleic acids and demonstrated to have both hypoxanthine and guanine phosphoribosyltransferase activity (7, 45). The source of adenine in *M. jannaschii* remains unknown, but one possible source could be from exogenous adenine that is taken up by the cell and then salvaged. A second source could be from thermal decomposition of DNA under extreme heat or pressure conditions, which proved lethal for *M. jannaschii* when heat-shocked from 88 ^{o}C to 98 ^{o}C (46). Furthermore, adenine could be salvaged through DNA repair mechanisms occurring in *M. jannaschii* as there are genes that have been identified to be involved in these processes (47). Even though the source of adenine is unclear, the data presented indicate the presence of a purine salvage pathway for adenine in methanogens that primarily proceeds through deamination of adenine to hypoxanthine followed by condensation with PRPP to form IMP (Figure 1A). Additionally, hypoxanthine could be directly incorporated without the need to first deaminate adenine. *M. vannielii*, *M. thermoautotrophicum*, and *M. voltae* were all able to incorporate and utilize exogenously fed hypoxanthine (44, 48, 49).

Cloning, overexpression, and purification of the M. jannaschii Ade (Wt and C127S/A) and Hpt. In order to increase the thermal stability of Ade and to produce more soluble protein, the expression of Wt, C127S, and C127A Ade was conducted in growth medium supplemented with 1 mM Mn(II). The addition of Mn(II) to the media was previously reported for expressing *E. coli* Ade (21). After sonication of cells suspended in extraction buffer and centrifugation (14,000 $\times g$, 5 min), about an equal amount of the expressed protein (Wt Ade) was found to be in the soluble fraction and in the insoluble pellet. C127S Ade and Hpt were found to be completely soluble as judged by SDS-PAGE. Heating the soluble sample for 10 min at

different temperatures followed by centrifugation (14,000 $\times g$, 5 min) indicated that a small band in the soluble protein fraction, possibly Wt Ade, was stable at temperatures above 90 ^{o}C, C127S Ade was only stable to 60 ^{o}C, and Hpt was stable up to 80 ^{o}C based on SDS-PAGE analysis. The low levels of expression and high thermal stability of Wt Ade have been previously observed in *M. jannaschii* during gene expression analyses during temperature and pressure stress response (46). The first step in the purification was heating of the Wt Ade sonicated cell extract to 90 °C for 10 min, C127S Ade cell extract to 60 ^{o}C for 10 min, and Hpt cell extracts to 80 ^{o}C for 10 min prior to separation of the heated cell extracts on MonoQ. The desired protein eluted at 0.36 M NaCl for Wt Ade, 0.56 M NaCl for C127S Ade, and 0.54 M NaCl for Hpt. MALDI analysis of the SDS-PAGE purified bands showed that the Wt Ade *M. jannaschii* was confirmed by the presence of four unique peptides and Hpt was confirmed by the presence of seven unique peptides identified from the tryptic digest of the excised bands at ~66 and ~20 kDa.

Unfortunately, the recombinantly expressed C127A Ade had extremely low expression levels and was unable to be observed on the SDS-PAGE gel (Figure S2). In this case the crude extract of the recombinantly produced C127A Ade was tested in comparison to the crude extract of the *E. coli* overexpressing the MJ0100 gene product (referred to as *E. coli* control), which was found to be completely insoluble (Figure S2C). This allowed us to determine which fractions contained *E. coli* Ade activity or *M. jannaschii* C127A Ade activity (Table S2). The results demonstrated deaminase activity that was greater than the *E. coli* control, indicating that C127A Ade was expressed, but the expression level was too low to be detected by SDS-PAGE (Figure S2A). The extracts heated at 60 ^{o}C were assayed for activity and these extracts containing C127A Ade also were more active than the *E. coli* control (Table S2). Purification of the 60 ^{o}C extracts resulted in a peak of C127A Ade activity at 0.39 M NaCl, where the activity of the *E. coli* control showed 7.5-fold less activity (Table S2).

Kinetic and physical characterization of Ade and Hpt. Recombinant Wt Ade (MJ1459 gene product) from *M. jannaschii* was found to be equally active after the addition of either Fe(II) or Mn(II) (Table 1), and size exclusion chromatography indicated a molecular mass of 80 kDa, indicating Ade was a monomer. Though Fe(II) is likely the in vivo metal as has been described previously (21), Mn(II) was used because it is stable to air oxidation and demonstrated the same activity as Fe(II) (Table 1). Metal analysis of the Wt Ade was found to contain 1.5 mole of Fe, 1.1 mole of Zn and 14 mole of Mn per mole of Wt Ade. These results indicate that

the Wt Ade contains Fe and Mn in the protein, which is what has been reported previously for the Ade from *A. tumefaciens* (21). The excess Mn is likely due to the presence of 1 mM Mn(II) in the media during overexpression of the recombinant protein. Ade was demonstrated to efficiently (k_{cat}/K_M) use adenine even though it has a relatively low binding affinity for adenine (Table 2). The K_M of the *E. coli* Ade with two irons was demonstrated to be 0.33 mM, which is a 2.5-fold higher affinity for adenine than the *M. jannaschii* Ade (21).

The recombinant Hpt from *M. jannaschii* (MJ1655 gene product) was tested for its ability to combine adenine, guanine, or hypoxanthine with PRPP; it was demonstrated to be specific for hypoxanthine and guanine, but not adenine (Table 3), further supporting the salvage pathway to first proceed through deamination of adenine to hypoxanthine (Figure 1A). Hpt exhibited a linear dependence of product formation up to 20 min at 70 ^{o}C. The *M. jannaschii* Hpt demonstrates approximately equal specificity (k_{cat}/K_M) for either hypoxanthine or guanine (Table 3). Interestingly, the *M. jannaschii* Hpt shares low sequence identity (less than 50%) with the characterized Hpt from *M. thermautrophicum* (6) and *M. voltae* (7) and even less with bacterial homologues (less than 20% identity).

Purine salvage in *M. jannaschii*. Characterization of the *M. jannaschii* Ade and Hpt demonstrates that purine salvage in *M. jannaschii* proceeds first through deamination of adenine to hypoxanthine by Ade. Hpt then transfers the phosphoribosyl-moiety of PRPP to N9 of hypoxanthine to form IMP, which can be readily transformed to either AMP through the *de novo* purine biosynthetic enzymes, adenylosuccinate synthetase (50) and adenylosuccinate lyase (51) (Figure 1A). Alternatively, IMP can be dehydrogenated at C2 of the purine ring to form xanthine monophosphate (XMP) by an IMP dehydrogenase, followed by conversion to GMP by a GMP synthase (Figure 1B) (5). These two routes suggest that hypoxanthine and IMP serve as the central purine nucleobase and nucleotide, respectively, in purine salvage for the production of AMP and GMP (Figure 1). Inosine is not directly salvaged, but is first phosphorolyzed to hypoxanthine and ribose 1-phosphate by a purine nucleoside phosphorylase family enzyme present in *M. jannaschii* (Miller unpublished). Furthermore, there is no identifiable inosine kinase homologue in the *M. jannaschii* genome to suggest the direct formation of IMP from inosine and ATP for purine salvage by this route. Collectively, these data imply that hypoxanthine and IMP are essential intermediates required for re-generation of AMP and GMP for general metabolism.

Characterization of C127A and C127S Ade. C127A Ade had no detectable activity when the same amount (1 μg) of enzyme was included in the standard assay; however, activity was detectable with 10 μg of C127A Ade in the assay. Activity of C127A was found to be greater with added Fe(II) than Mn(II) (Table 1). Interestingly, the C127S Ade demonstrated no detectable activity even with 1000-fold more enzyme than the Wt and was deemed inactive (Table 1). Kinetic analysis of the C127A and Wt Ade indicate that the binding affinity for adenine decreased more than 2.5-fold, the turnover of Ade decreased 10-fold, and the catalytic efficiency (k_{cat}/K_M) decreased over 25-fold (Table 2). This change in catalytic efficiency suggests that the thiol moiety of C127 plays a critical role in active site construction even if it is initially too distant (>10 Å) from the active site to be directly involved in catalysis.

Several bacterial homologues were found to have an amino acid other than cysteine at position 127 (*M. jannaschii* numbering). For example, the *Bacillus subtilis* and *Enterococcus faecalis* enzymes (Figure 2) have never been demonstrated to have Ade activity and lack a cysteine at this position. The *B. subtilis* enzyme was demonstrated to produce an Ade as determined through gene complementation studies; however, purified Ade from *B. subtilis* was unable to be studied because the authors were unable to purify active Ade (52). The predicted Ade from *Enterococcus faecalis* (Figure 2) was demonstrated to not be an adenine deaminase but instead to hydrolyze acetyl-(R)-mandelate (53). Therefore, given the two species that contain an alternative amino acid at position 127 instead of a Cys and do not demonstrate Ade activity, it can be suggested that the presence of Cys at that position is essential for Ade activity. Our site-directed mutagenesis and MD studies further support this claim.

Generation of Wt, C127A, and C127S Ade homology models. To better understand the structure and active site of *M. jannaschii*, homology models of Wt, C127S, and C127A Ade were generated by homology modeling and evaluated by several methods. The Verify 3D server (26, 27) indicated that the structural features of the models were generally favorable, though all structures had regions (residues ~380 to 395) that did not evaluate well. Because this region is distant from the active site, it was decided that the models were acceptable for our other modeling studies. In addition, Ramachandran plots were generated from ProCheck (25) analysis of the Wt, C127A, and C127S Ade homology models (Figure S3A - C). The results showed that the Wt Ade model had only 0.6% of the residues in disallowed regions, the C127A Ade model had only 0.6% of the residues in disallowed regions, and the C127S Ade model had only 0.8% of

residues in disallowed regions. None of the residues found in the disallowed regions of the Ramachandran plots were the same as those determined not to be modeled well based on the Verify 3D analysis. The residues identified in these regions were checked individually and determined to be sufficiently distant from the active site and not directly involved in catalysis. Overlays of the Wt Ade model with the template structure (PDB 3NQB), C127S, and C127A Ade are shown in Figure S5 A-C, respectively, and C127A Ade overlaid with C127S Ade, in Figure S5 D.

Molecular docking of Wt, C127A, and C127S Ade with adenine. Molecular docking to the Wt, C127S, and C127A models was employed to discover if the thiol moiety of cysteine helps maintain the proper active site environment for adenine binding. A possible orientation of adenine in the active site was previously described for Ade from *A. tumefaciens* (21), where it was shown to interact with several amino acids involved in coordinating the bound active site metals including H97, E98, E212, D260, D261, and the α metal (*M. jannaschii* numbering) (Figure 4A). Considering the importance of metals to the activity of Ade, we included Mn(II) at the α, β, and γ metal binding positions for our docking studies. The addition of the γ metal in our docking studies showed H97 and E98 maintained interactions with N3 of the adenine ring, comparable to the results described for the Ade of *A. tumefaciens* (21), which did not include the γ metal in the structure. To score the docking results, we developed a knowledge-based scoring function based on the interactions in the catalytically competent position described by Kamat et al. (21). When multiple poses contained all of the important interactions, calculated free energy scores were used to select the best pose of adenine generated from that docking run.

Docking of adenine to Wt Ade demonstrated a docked pose that was close to the previously published result (21) (Figure 4A) and further supported our structure models, but docking into C127A and C127S Ade was not as successful as compared to the Wt Ade (Figure 4B and 4C). The best pose from the C127A Ade docking studies positioned the amino group of adenine at 4.0 Å from the α-metal, which was the closest of the nine generated poses. The relative position of the adenine in all poses in C127A was very different than the position of adenine docked into the Wt structure, and the active site in C127A showed some slight rearrangements compared with the Wt Ade (Figure 4B). The replacement of C127 with alanine shifted D260 into a bridging position similar to E159 in Wt Ade, altering D260 into a position too distant to interact with adenine. The carboxyl moiety of D261, instead of D260, in the

C127A Ade docked model is 4.6 Å from the amino group of adenine. This positions D261 into the active site 1.6 Å from the α Mn and hinders the binding of adenine compared to Wt D261 (>6 Å from the α Mn) (Figure 4B). However, the position of the adenine amine moiety being 4.0 Å from the α-metal would position it close enough for the nucleophilic water to attack the C6 position of the adenine ring to form hypoxanthine albeit, at a slower rate, which is represented by the lower k_{cat} of C127A Ade as compared to Wt (Table 2).

Only one pose of adenine docked into C127S Ade positioned the adenine similarly to the pose in Wt Ade (Figure 4C). The remaining docked poses positioned adenine at distances greater than 6 Å away from the α and β metals, which would not allow the nucleophilic water to attack the C6 position of the adenine ring for catalysis. The inability of adenine to correctly "sit" in the active site suggests that the C127S mutation has a larger effect on the binding cavity than initially believed and corresponds with experimental results.

It was observed that D261 in the Wt Ade structure is ~5.9 Å from the amino group of adenine, whereas in C127S Ade the distance is 3.2 Å. In C127S Ade, adenine is more distant from the α and β metals (5.3 Å), such that it is not in close proximity to the correct location and residues for catalysis to occur with the bridging substrate water (Figure 4C, water not shown) (21). This difference in positioning, as compared to Wt Ade, can be attributed to rotation of D261 towards the β metal, in such a way that it blocks the adenine from binding into the pocket (Figure 4C, Table S4). Ultimately, molecular docking suggested that replacement of Cys with Ala and Ser had an effect on adenine binding into the active site, where C127A retained some activity through retention of the amino group within 4 Å of the α-metal for catalysis and C127S prevented adenine binding due to the greater re-structuring of the active site that prohibited catalysis.

MD studies of Ade, C127A, and C127S Ade. MD simulations were performed to determine if the C127A and C127S mutations influenced structural features of the active site. AMBER99SB-ILDN was selected as the force field for simulations because it is specifically optimized for Ile, Asp, Asn, and Gln (34). Given that there is a ligating Asp in the active site and GAFF parameters for Mn(II) were utilized, this choice in force fields was appropriate. Simulations were extended until no systematic conformational change occurred for a period of 50 ns, as shown by backbone RMSD (Figure S4) and RMSD clustering results (Table S3). Secondary structure analysis was also performed to confirm convergence and to determine any

differences between Wt, C127A, and C127S simulations (Table 4). A measurable increase in coil formation and decrease in ordered structure (α helices and β strand) was observed in C127A and C127S, as compared to Wt Ade (Table 4). The slight increase in coil formation and the decrease of ordered structure is especially apparent in residues 153-169, 178-190, 260-273, and 452-460 in C127S compared to the Wt Ade. Residues 153-169, 178-190, and 260-273 are in areas that surround the active site of the Ade and include several of the metal binding residues. Of specific interest are residues E159, D260, and H190, which are important residues involved in coordinating the α and β metals. The fourth region, residues 452-460, is more coiled and is near the C-terminus of Ade in an area over the γ-metal binding site. Thus, secondary structure analysis supports that there is slight rearrangement in the active site when C127 is replaced by Ala and Ser. This rearrangement in the active site provides context for correlating with molecular docking results, which show the change in the position of D260 and D261 influences adenine binding.

Analysis of the solvent-accessible surface area (SASA) of the total protein and specific active site residues was performed to determine how the C127A and C127S mutations influenced the exposure of the overall protein and those side-chain atoms in the active site to water. There was an overall increase in total SASA in C127A and C127S (Table 5). By comparing the whole protein and the side chain atoms of specific active site residues, we were able to pinpoint slight, but significant, changes in the SASA of the active site residues (H97, E98, H447, D448, D260, D261, H190, E159, H67, H69, E212, and H211). The total SASA of the side chain atoms of these residues remained similar to the Wt Ade for the C127A Ade (Table 5). However, there was an increase in the total SASA of the active site residues in C127S Ade (Table 5). The change in the SASA of these residues suggests that the environment of the active site is indeed influenced by the change of a hydrophobic amino acid (cysteine) to hydrophilic (serine) (Figure 4). When cysteine was replaced by alanine, the overall environment in regards to SASA was maintained and similar to the Wt, indicating the hydrophobicity of cysteine and alanine is important in maintaining active site composition. However, the decrease in activity of C127A and the slight rearrangement of amino acids in the active site as shown by torsional angle rearrangement, indicate that the thiol moiety is essential for maximum activity.

Analysis of the χ1 torsional angles of D260, D261, and C/S 127 was performed in order to quantitatively assess their position and influence in the active site. In Wt, C127A, and C127S

Ade, D260 samples similar positions indicating that the residue is occupying the same space in both enzymes and not related to any changes in activity. However, distinct differences are apparent when comparing D261 in Wt, C127A, and C127S Ade. In Wt Ade, the χ1 torsional angle of D261 samples several positions indicating that it is able to move as necessary for adenine binding and mostly occupies the gauche- position, away from the active site for adenine binding. Wt Ade also shows that it can sample the gauche+ position, indicating residue flexibility. In C127A, the χ1 torsional angel of D261 samples only one position that is gauche- and facing into the active site, which allows adenine to partially bind into the active site, but prevents interaction with the β metal. Also, since D261 in C127A only samples the gauche- position, it appears to lack some of the flexibility as demonstrated by D261 in Wt Ade. The opposite trend is observed with the C127S; the χ1 torsional angle of D261 samples only one position that is gauche+ and facing into the active site, ultimately preventing adenine from being able to interact with the α and β metals. Finally, C/S127 χ1 torsional angles showed that both sampled similar positions, with S127 sampling more gauche+ angles and pointing into the active site, which is supported by other data and ultimately influences the dynamics of the active site.

By combining SASA data, the change of position of D261 in the molecular docking, χ1 torsional angles of D260, D261, and C/S 127, and minimum distance measurements (Table S4), we were able to determine subtle movements in the active site that could be influencing adenine binding and enzyme catalysis in the C127A and C127S mutants. Table S4 shows that the D261 moves closer to the α Mn(II) when Cys is replaced with Ala and to the β Mn(II) when the Cys is replaced with either Ala or Ser. These changes in distance suggest that the character of the Cys thiol moiety may play a role in maintaining the hydrophobicity of the active site even though it is greater than 10 Å from active site (Table 5 and Figure 4). Removal of the thiol moiety by replacement with the methyl moiety of Ala generates a more hydrophobic active site that allows adenine to interact with the α metal, with restructuring of the active site so that D260 bridges both the α and β metals (Figure 4B) and D261 rotates into the position originally held by D260 in the Wt active site (Figure 4). Therefore, there is not as much rearrangement of the aspartate residues to completely abolish activity, as seen with C127S. When the hydroxyl moiety of the Ser is introduced into the place of C127, the hydrophobicity of the active site is influenced and a slight rearrangement of the active site residues occurs, with D261 rotating into the active site

towards the β Mn(II). When D261 rotates into the active site, it occupies the space in the active site into which adenine would normally bind (Figure 4).

Many of the residues in an enzyme are essential for maintaining structural integrity and conformation of the active site, whereupon mutation of these residues can alter enzymatic activity. In a glycosynthase from *Agrobacterium sp*., two amino acid mutations not in the active site caused a conformational change in the active site making it better suited to stabilize the transition state intermediates, thus improving the activity of the enzyme with alternate substrates (54). In an aspartate aminotransferase from *E. coli*, mutations in regions distant from the active site (greater than 10 Å) were shown to have a large effect on the activity and substrate specificity (55). The authors attribute this change to the charge distribution throughout the entire enzyme that is responsible for substrate binding and that mutations to amino acids outside of the active site can play a large role in substrate binding (55). Both of these examples demonstrate that mutations of amino acids outside the active site can influence enzymatic activity through maintenance of the active site conformation. This information supports our hypothesized role for C127 in Ade, specifically in defining the structure of the active site to allow adenine binding. When C127 is mutated to Ser, the structure and general characteristics of the active site are altered and become more hydrophilic. This influences the rotation of D261 into the active site, preventing adenine from binding properly and leading to a loss in activity. Mutation of C127 to Ala does increase the hydrophobicity of the active site, however slight rearrangements prevent adenine from binding as needed for full catalysis (Figure 4).

Conclusions. The route of purine salvage in *M. jannaschii* and other methanogens has been further elucidated through characterization of Ade and Hpt. Hpt was demonstrated to be specific for hypoxanthine and guanine, and not adenine, as substrates, further proving that hypoxanthine and IMP are the central metabolites of purine salvage in *M. jannaschii*. These results also indicate that an active Ade must be present, which was confirmed by this work to be Fe(II) and/or Mn(II) dependent. Without an Ade present, Hpt was unable to directly salvage adenine into AMP, instead relying on an active Ade for the production of hypoxanthine in the purine salvage pathway. Detailed analysis of Ade identified a conserved cysteine found in archaeal and bacterial Ade's that is essential in maintaining the active site architecture to allow adenine binding and for catalysis. This research represents the first step in defining an

alternative role for cysteine residues in proteins that is not associated with the formation of disulfide bonds, binding of iron-sulfur clusters, or direct involvement in catalysis.

Acknowledgements. The authors thank Dr. W. Keith Ray for performing the mass spectrometry experiments, Doctors Laura Grochowski, Justin Lemkul, and Nikki Lewis for help and mentorship on the outset of this project, and Advanced Research Computing at Virginia Tech for computing time and resources on the HokieOne supercomputer. The mass spectrometry resources are maintained by the Virginia Tech Mass Spectrometry Incubator, a facility operated in part through funding by the Fralin Life Science Institute at Virginia Tech and by the Agricultural Experiment Station Hatch Program (CRIS Project Number: VA-135981). This work was supported by the National Science Foundation Grant MCB0722787. Funding for this work was also provided in part, by the Virginia Agricultural Experiment Station and the Hatch Program of the National Institute of Food and Agriculture, U.S. Department of Agriculture.

References

1. **Armenta-Medina D, Segovia L, Perez-Rueda E.** 2014. Comparative genomics of nucleotide metabolism: a tour to the past of the three cellular domains of life. BMC Genomics **15:**1-16.

2. **Pospisilova H, Frebort I.** 2007. Aminohydrolases acting on adenine, adenosine and their derivatives. Biomed Pap Med Fac Univ Palacky Olomouc Czech Repub **151:**3-10.

3. **Holm L, Sander C.** 1997. An evolutionary treasure: unification of a broad set of amidohydrolases related to urease. Proteins **28:**72-82.

4. **Seibert CM, Raushel FM.** 2005. Structural and catalytic diversity within the amidohydrolase superfamily. Biochemistry **44:**6383-6391.

5. **Worrell VE, David P. Nagle J.** 1990. Genetic and Physiological Characterization of the Purine Salvage Pathway in the Archaebacterium *Methanobacterium thermoautotrophicum* Marburg. J Bacteriol **172:**3328-3334.

6. **Sauer J, Nygaard P.** 1999. Expression of the *Methanobacterium thermoautotrophicum hpt* Gene, Encoding Hxypoxanthine (Guanine) Phosphoribosyltransferase, in *Escherchia coli*. J Bacteriol **181:**1958-1962.

7. **Bowen TL, Lin WC, Whitman WB.** 1996. Characterization of Guanine and Hypoxanthine Phosphoribosyltransferase in *Methanococcus voltae*. J Bacteriol **178:**2521-2526.

8. **Creighton TE.** 1993. Proteins: Structures and Molecular Properties, second ed. W.H. Freeman and Company, New York.

9. **Ladenstein R, Ren B.** 2008. Reconsideration of an early dogma, saying "there is no evidence for disulfide bonds in proteins from archaea". Extremphiles **12:**29-38.

10. **Major TA, Burd H, Whitman WB.** 2004. Abundance of 4Fe-4S motifs in the genomes of methanogens and other prokaryotes. FEMS Microbiol Lett **239:**117-123.

11. **Heinemann J, Hamerly T, Maaty WS, Movahed N, Steffens JD, Reeves BD, Hilmer JK, Therien J, Grieco PA, Peters JW, Bothner B.** 2014. Expanding the paradigm of thiol redox in the thermophilic root of life. Biochem Biophys Acta **1840:**80-85.

12. **Grzonka Z, Jankowska E, Kasprzykowski F, Kasprzykoska R, Lankiewicz L, Wiczk W, Wieczerzak E, Ciarkowski J, Drabik P, Janowski R, Kozak M, Jaskolski M, Grubb A.** 2001. Structural studies of cysteine proteases and their inhibitors. Acta Biochim Pol **48:**1-20.

13. **Graham DE, Xu H, White RH.** 2002. Identification of coenzyme M biosynthetic phosphosulfolactate synthase: a new family of sulfonate biosynthesizing enzymes. J Biol Chem **277:**13421-13429.

14. **Bradford MM.** 1976. A rapid and sensitive method for the quantitation of microgram quantities of protein utilizing the principle of protein-dye binding. Anal Biochem **72:**248-254.

15. **Miller D, O'Brien K, Xu H, White RH.** 2014. Identification of a 5′-Deoxyadenosine Deaminase in *Methanocaldococcus jannaschii* and its Possible Role in Recycling the Radical SAM Enzyme Reaction Product 5′-Deoxyadenosine. J Bacteriol **196:**1064-1072.

16. **Allen KD, Miller DV, Rauch BJ, Perona JJ, White RH.** 2015. Homocysteine is biosynthesized from aspartate semialdehyde and hydrogen sulfide in methanogenic archaea. Biochemistry **54:**3129-3132.

17. **Bradford MM.** 1976. A rapid and sensitive method for the quantitation of microgram quantities of protein utilizing the principle of protein dye-binding. Anal Biochem **72:**248-257.

18. **Volkin E, Cohn WE.** 1954. Estimation of nucleic acids, vol I.

19. **Miller DV, Xu H, White RH.** 2012. A new subfamily of agmatinases in methanogenic Archaea is Fe(II) dependent. Biochemistry **51:**3067-3078.

20. **Sali A, Blundell TL.** 1993. Comparative Protein Modelling by Statisfaction of Spatial Restraints. J Mol Biol **234:**779-815.

21. **Kamat SS, Bagaria A, Kumaran D, Holmes-Hampton GP, Fan H, Sali A, Sauder JM, Burley SK, Lindahl PA, Swaminathan S, Raushel FM.** 2011. Cataytic Mechanism and Three- Dimensional Structure of Adenine Deaminase. Biochemistry **50:**1917-1927.

22. **Melo F, Feytmans E.** 1998. Assessing Protein Structures with a Non-local Atomic Interaction Energy. J Mol Biol **277:**1141-1152.

23. **Melo F, Sali A.** 2007. Fold assessment for comparative protein structure modeling. Prot Sci **16:**2412-2426.

24. **Benkert P, Tosatto SCE, Schomburg D.** 2007. QMEAN: A comprehensive scoring function for model quality assessment. Proteins: Struct, Funct, Bioinf **71:**261-277.

25. **Laskowski RA, W. MM, Moss D, Thornton JM.** 1996. PROCHECK: a program to check the stereochemical quality of protein structures. J Appl Crsytallogr **26:**283-291.

26. **Bowie JU, Luthy R, Eisenberg D.** 1991. A method to identify protein sequences that fold into a known three deminsional structure. Science **253:**164-170.

27. **Luthy R, Bowie JU, Eisenberg D.** 1992. Asssessment of protein models with three-dimensional profiles. Nature **356:**83-85.

28. **Anonymous.** 2013. Molecular Operating Enviroment (MOE), 2013.08, 1010 Sherbooke St. West, Suite#910, Montreal, QC, Canada, H3A 2R7.

29. **Kaminski GA, Friesner RA, Tirado-Rives J, Jorgensen WL.** 2001. Evaluation and Reparametrization of the OPLS-AA Force Field for Proteins via Comparison with Accurate Quantum Chemical Calculations on Peptides. J Phys Chem B **105:**6474-6487.

30. **Morris GM, Huey R, Lindstrom W, Sanner MF, Belew RK, Goodsell DS, Olson AJ.** 2009. AutoDock 4 and AutoDock Tools 4: automated docking with selective receptor flexibility. J Comput Chem **16:**2785-2791.

31. **Trott O, Olson AJ.** 2010. AutoDock Vina: Improving the Speed and Accuracy of Docking with a New Scoring Function, Efficient Optimization, and Multithreading. J Comput Chem **31:**455-461.

32. **Hess B, Kutzner C, van der Spoel D, Lindahl E.** 2008. GROMACS 4: Algorithms for Highly Efficient, Load-Balanced, and Scalable Molecular Simulation. J Chem Theory Comput **4:**435-447.

33. **Pronk S, Páll S, Schulz R, Larsson P, Bjelkmar P, Apostolov R, Shirts MR, Smith JC, Kasson PM, van der Spoel D, Hess B, Lindahl E.** 2013. GROMACS 4.5: a high-throughput and highly parallel open source molecular simulation toolkit. Bioinformatics **29:**845-854.

34. **Lindorff-Larsen K, Piana S, Palmo K, Maragakis P, Klepeis JL, Dror RO, Shaw DE.** 2010. Improved side-chain torsion potentials for the Amber ff99SB protein force field. Proteins: Struct, Funct, Bioinf **78:**1950-1958.

35. **Jorgensen WL, Chandrasekhar J, Madura JD, Impey RW, Klein ML.** 1983. Comparison of simple potential functions for simulating liquid water. J Chem Phys **79:**926-935.

36. **M. Bradbrook G, Gleichmann T, J. Harrop S, Habash J, Raftery J, Kalb J, Yariv J, H. Hillier I, R. Helliwell J.** 1998. X-Ray and molecular dynamics studies of concanavalin-A glucoside and mannoside complexes Relating structure to thermodynamics of binding. J Chem Soc Faraday **94:**1603-1611.

37. **Berendsen HJC, Postma JPM, van Gunsteren WF, DiNola A, Haak JR.** 1984. Molecular dynamics with coupling to an external bath. J Chem Phys **81:**3684-3690.

38. **Hess B.** 2007. P-LINCS: A Parallel Linear Constraint Solver for Molecular Simulation. J Chem Theory Comput **4:**116-122.

39. **Darden T, York D, Pedersen L.** 1993. Particle mesh Ewald: An N log(N) method for Ewald sums in large systems. J Chem Phys **98:**10089-10092.

40. **Essmann U, Perera L, Berkowitz ML, Darden T, Lee H, Pedersen LG.** 1995. A smooth particle mesh Ewald method. J Chem Phys **103:**8577-8593.

41. **Daura X, Gademann K, Jaun B, Seebach D, van Gunsteren WF, Mark AE.** 1999. Peptide Folding: When Simulation Meets Experiment. Angew Chem Int Ed **38:**236-240.

42. **Kabsch W, Sander C.** 1983. Dictionary of protein secondary structure: Pattern recognition of hydrogen-bonded and geometrical features. Biopolymers **22:**2577-2637.

43. **Albers E.** 2009. Metabolic characteristics and importance of the universal methionine salvage pathway recycling methionine from 5'-methylthioadenosine. IUBMB Life **61:**1132-1142.

44. **DeMoll E, Tsai L.** 1986. Conversion of Purines to Xanthine by *Methanococcus vannielii*. Arch Biochem Biophys **250:**440-445.

45. **Bowen TL, Whitman WB.** 1987. Incorporation of Exogenous Purines and Pyrimidines by *Methanococcus voltae* and Isolation of Analog-Resistant Mutants. Appl Environ Microbiol **53:**1822-1826.

46. **Boonyaratanakornkit BB, Miao LY, Clark DS.** 2007. Transcriptional responses of the deep-sea hyperthermophile *Methanocaldococcus jannaschii* under shifting extremes of temperature and pressure. Extremophiles **11:**495-503.

47. **Bult CJ, White O, Olsen GJ, Zhou L, Fleischmann RD, Sutton GG, Blake JA, FitzGerald LM, Clayton RA, Gocayne JD, Kerlavage AR, Dougherty BA, Tomb J-F, Adams MD, Reich CI, Overbeek R, Kirkness EF, Weinstock KG, Merrick JM, Glodek A, Scott JL, Geoghagen NSM, Weidman JF, Fuhrmann JL, Nguyen D, Utterback TR, Kelley JM, Peterson JD, Sadow PW, Hanna MC, Cotton MD, Roberts KM, Hurst MA, Kaine BP, Borodovsky M, Klenk H-P, Fraser CM, Smith HO, Woese CR, Venter JC.** 1996. Complete Genome Sequence of the Methanogenic Archaeon, *Methanococcus jannaschii*. Science **273:**1058-1073.

48. **DeMoll E, Tsai L.** 1986. Utilization of Purines or Pyrimidines as the Sole Nitrogen Source by *Methanococcus vannielii*. J Bacteriol **167:**681-684.

49. **Veronica E. Worrell and David P. Nagle J.** 1990. Genetic and Physiological Characterization of the Purine Salvage Pathway in the Archaebacterium *Methanobacterium thermoautotrophicum* Marburg. J Bacteriol **172:**3328-3334.

50. **Mehrotra S, Balaram H.** 2007. Kinetic characterization of adenylosuccinate synthetase from the thermophilic archaea *Methanocaldococcus jannaschii*. Biochemistry **46:**12821-12832.

51. **Toth EA, Worby C, Dixon JE, Goedken ER, Marqusee S, Yeates TO.** 2000. The crystal structure of adenylosuccinate lyase from *Pyrobaculum aerophilum* reveals an intracelluar protein with three disulfide bonds. J Mol Biol **301:**433-450.

52. **Per Nygaard PD, and Hans Henrik Saxild.** 1996. Role of Adenine Deaminase in Purine Salvage and Nitrogen Metabolism and Characterization of the ade Gene in *Bacillus subtilis*. J Bacteriol **178:**846-853.

53. **Ornelas A, Korczynska M, Ragumani S, Kumaran D, Narindoshvili T, Shoichet BK, Swaminathan S, Raushel FM.** 2012. Functional Annotation and Three-Dimensional

Structure of an Incorrectly Annotated Dihydroorotase from cog3964 in the Amidohydrolase Superfamily. Biochemistry **52:**228-238.

54. **Kim Y-W, Lee SS, Warren RAJ, Withers SG.** 2004. Directed Evolution of a Glycosynthase from *Agrobacterium* sp. Increases Its Catalytic Activity Dramatically and Expands Its Substrate Repertoire. J Biol Chem **279:**42787-42793.

55. **Oue S, Okamoto A, Yano T, Kagamiyama H.** 1999. Redesigning the Substrate Specificity of an Enzyme by Cumulative Effects on the Mutations of Non-active Site Residues. J Biol Chem **274:**2344-2349.

Tables

Table 1. Comparison of Wt, C127S, and C127A Ade activity with no metal, Mn(II), and Fe(II)

	Specific activity (μmol min^{-1} mg^{-1})		
	No Metal	Mn(II)[e]	Fe(II)[e]
Wt Ade[a]	1.4	5.8	5.3
C127S Ade	nd[b]	nd[b]	nd[b]
C127A Ade[c]	0.032	0.043	0.070
E. coli Control[d]	nd[f]	nd[f]	nd[f]

[a]1 μg of Wt Ade was used
[b]no detectable activity was observed even when 1000-fold excess enzyme was present in the standard assay of 1 mM adenine and 0.5 mM metal (Mn or Fe).
[c]10 μg of C127A Ade was used, no detectable activity was observed with 1 μg of enzyme
[d]Background for Ade activity from *E. coli*
[e]0.5 mM Mn(II) or Fe(II)
[f]no detectable activity under the same conditions as C127A Ade assays

Table 2. Kinetic parameters of Wt and C127A Ade

	K_M ± SD (mM)	k_{cat} (s^{-1})	k_{cat}/K_M ($s^{-1}M^{-1}$)
Wt Ade	0.92 ± 0.4	221	2.4×10^5
C127A Ade[b]	2.4 ± 1.6	22	9.0×10^3
E. coli Control[b]	nd[a]		

[a]no detectable activity under the conditions used (5.5 μg enzyme with 0.5 mM Mn(II))
[b]these are apparent values

Table 3. Kinetic parameters of Hpt.

Substrate	K_M ± SD (mM)	k_{cat} (s^{-1})	k_{cat}/K_M ($s^{-1}M^{-1}$)
Adenine[a]	nd[c]		
Hypoxanthine[a]	0.11 ± 0.07	3.6×10^3	3.2×10^7
Guanine[a]	0.28 ± 0.07	8.5×10^3	3.0×10^7
PRPP[b]	2.2 ± 0.9	1.8×10^4	8.1×10^6

[a] determined with PRPP in excess (0.5 mM)
[b] determined with guanine in excess (0.4 mM)
[c] no detectable activity was observed from 0.1 to 0.4 mM adenine

Table 4. Average secondary structure content (shown in %) of Wt and C127S Ade[a].

	Wt	C127S	C127A
Total Coil	52 ± 1	55 ± 1	56 ± 1
Total β-strand	24 ± 1	22 ± 2	22 ± 1
Total α-helix	24 ± 1	23 ± 1	22 ± 1

[a]Averages are shown over the last 50 ns of simulation time, with corresponding standard deviations.

Table 5. Average solvent-accessible surface area (SASA) (nm^2) for Ade (full protein) and specific side chain atoms of active site residues (ASR)[a,b,c]

	Wt		C127S		C127A	
	Ade	ASR	Ade	ASR	Ade	ASR
Hydrophilic	201 ± 4	11.5 ± 0.4*	207 ± 2	12.9 ± 0.5*	205 ± 1	11.3 ± 0.4
Hydrophobic	120 ± 3	5.3 ± 0.1*	123 ± 3	6.3 ± 0.1*	125 ± 2	5.4 ± 0.1
Total	321 ± 6	16.8 ± 0.3*	330 ± 5	19.2 ± 0.5*	330 ± 4	16.7 ± 0.3

[a]Averages are shown over the last 50 ns of simulation time, with corresponding standard deviations. Results were determined to be significant if $p < 0.05$ and are denoted by an asterisk.
[b]Active site residues (ASR) defined as: H97, E98, H447, D448, D260, D261, H190, E159, H67, H69, E212, H211.
[c]An atom is determined to be hydrophilic if $|q| > 0.2$

Figures

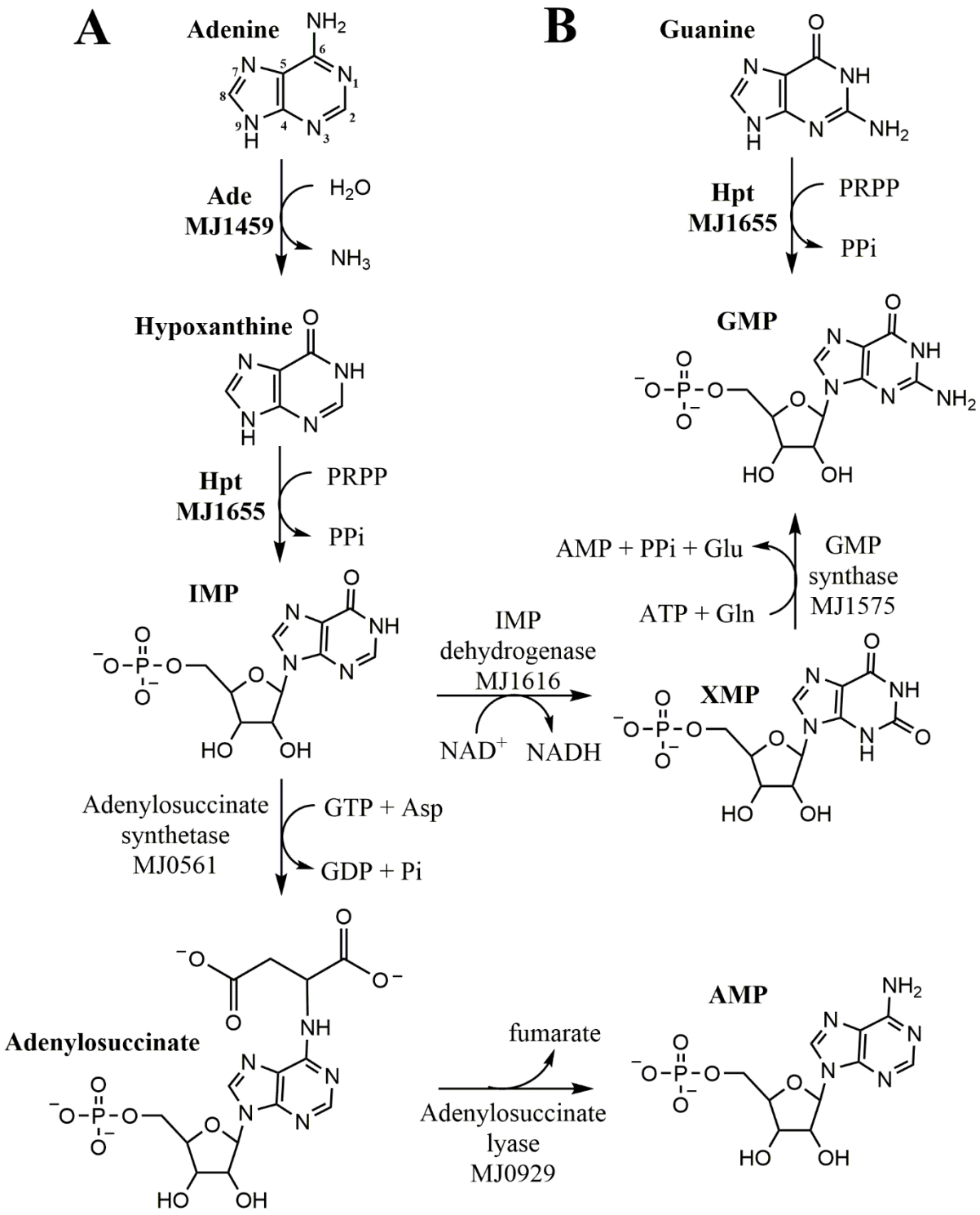

Figure 1. Purine salvage in *M. jannaschii* from adenine (A) and guanine (B).

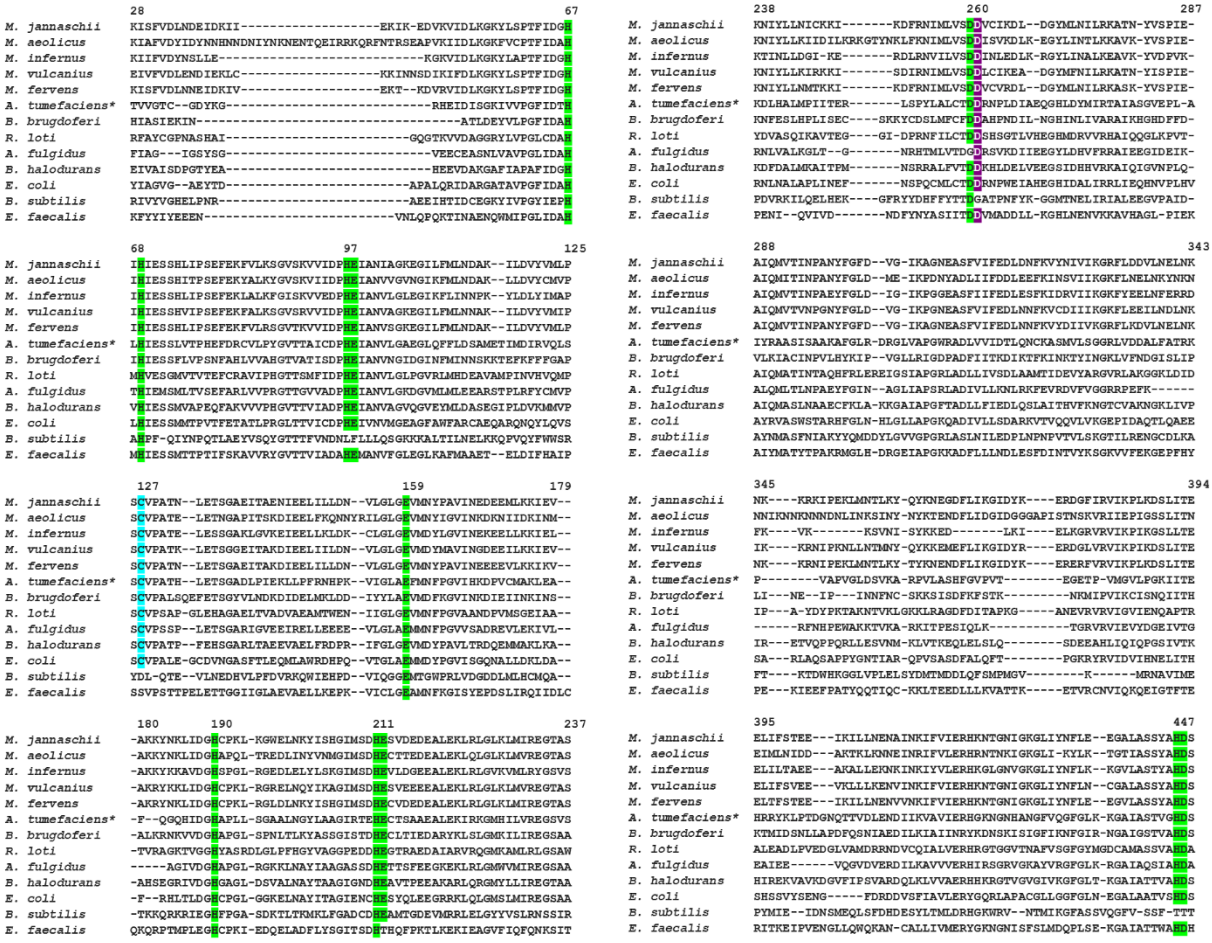

Figure 2. Truncated sequence alignment of adenine deaminases. Green highlighted residues represent the metal binding ligands, blue represents the conserved cysteine proposed to be involved in the control of active site environment, and purple with white lettering is D261. The asterisk indicates the amino acid sequence of the template structure (3NQB) used for modeling the Wt, C127S, and C127A Ade structures. Accession numbers for the organisms and pdb ID (if applicable) are as follows: *M. jannaschii* Q58854, *Methanocaldococcus aeolicus* A6UVJ0, *Methanococcoccus infernus* D5VSD3, *Methanococcoccus vulcanius* C9RH79, *Methanocaldococcus fervens* C7P5Y7, *Agrobacterium tumefaciens** Q7CXF0 (pdb 3NQB), *Borrelia burgdoferi* O50821, *Rhizobium loti* Q98NF9, *Archeaglobus fulgidus* O29999, *Bacillus halodurans* Q9KF46, *Escherichia coli* P31441, *Bacillus subtilus* PO34909, and *Enterococcus faecalis* Q835Z6.

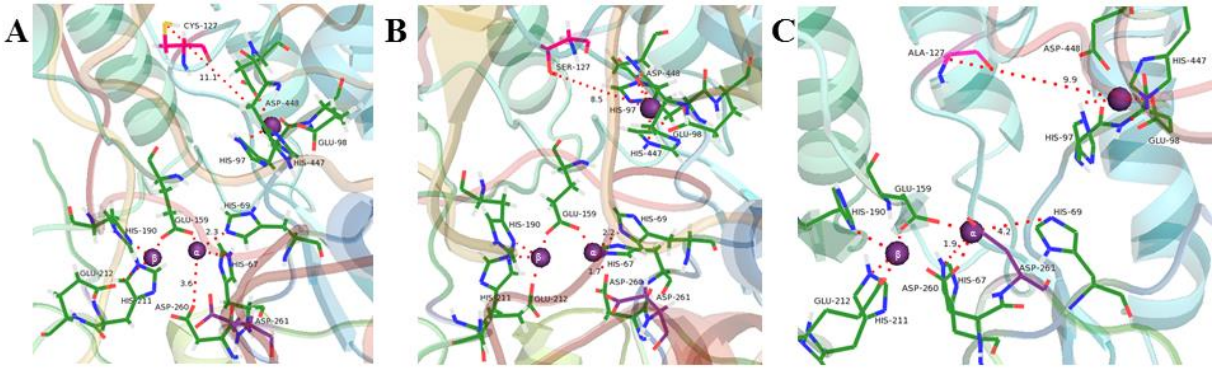

Figure 3. Comparison of representative replicates of Wt (A), C127S (B), and C127A (C) Ade from molecular dynamics simulations. Dominant structures from RMSD clustering, with the central structure of the first cluster, are shown. Metal ions are shown as purple spheres. Metal binding residues are shown with green carbon atoms, Cys, Ser, or Ala 127 is shown with pink, and D261 is shown with purple. Measured distances are shown with a red dotted line with the measured distance in Å between the heavy atoms. All nitrogen atoms are shown as blue, oxygen atoms as red, and sulfur atoms as yellow.

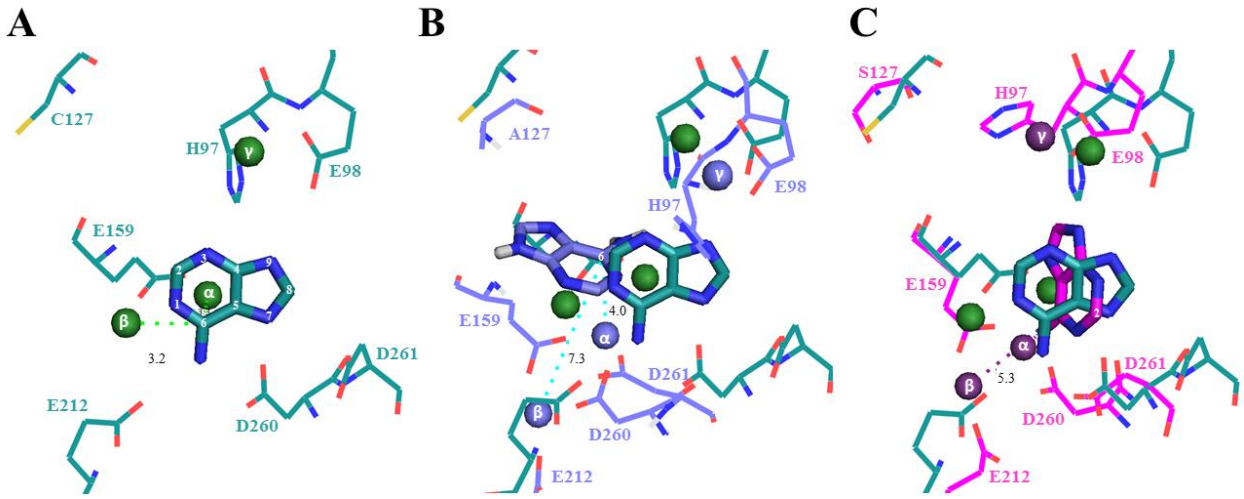

Figure 4. Molecular docking of adenine into Wt, C127A, and C127S Ade. A) Adenine docked into active site of Wt Ade (cyan carbon backbone). B) Overlay of C127A Ade (blue carbon backbone) docking results to Wt docking results. C) Overlay of C127S Ade (pink carbon backbone) and Wt docking results. Metal ions are shown as spheres and are labeled α, β, or γ, the measured distances are shown as dotted lines with the measured distance in Å between the heavy atoms. All nitrogen atoms are shown as blue, oxygen atoms as red, and sulfur atoms as yellow.

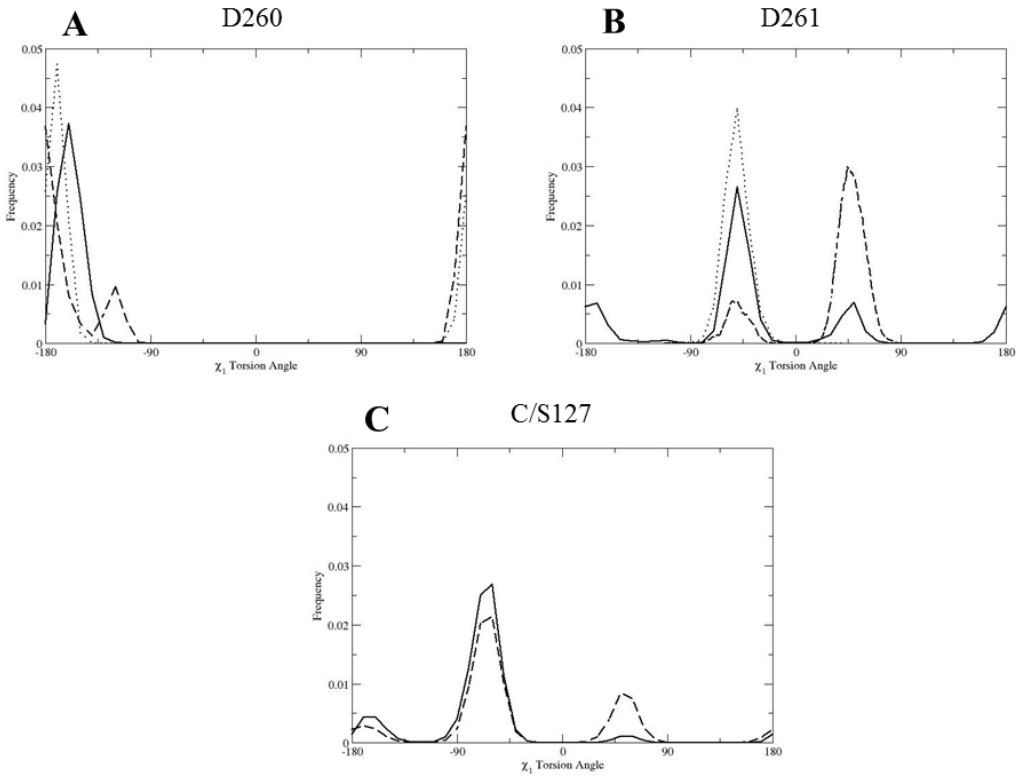

Figure 5. χ1 torsional angle analysis of D260 (A), D261 (B), and C/S 127 (C). Average frequency of χ1 torsional angle for all 3 replicates sampled for the respective residue over the last 50 ns of simulation time is shown (Wt-solid line, C127S-dashed line, and C127A-dotted line).

Supporting Information for Purine Salvage in *Methanocaldococcus jannaschii*: Elucidating the Role of the Conserved Cysteine in Adenine Deaminase

Danielle V. Miller, Anne M. Brown, Huimin Xu, David R. Bevan, and Robert H. White*
Department of Biochemistry, Virginia Polytechnic Institute and State University, Blacksburg, Virginia, USA, 24061

*To whom correspondence should be addressed:
Department of Biochemistry,
Virginia Polytechnic Institute and State University,
Blacksburg, Virginia, USA 24061
Telephone: +1 (540) 231-6605
Fax: +1 (540) 231-9070
e-mail: rhwhite@vt.edu

Tables

Table S1. Primers used for overexpression of MJ1459 Wt and the C127A/S mutants and MJ1655 gene products.

Gene	Primer	
Wt MJ1459	Fwd	5’-GGTCATATGATTGTCTTCAAAAATAC-3’
	Rev	5’-GCTGGATCC-CTAAATAAATAAATC-3’
C127A MJ1459	Fwd	5'- GTTATGCTTCCTTCCGCTGTTCCAGCTACAAAC-3'
	Rev	5'- GTTTGTAGCTGGAACAGCGGAAGGAAGCATAAC-3’
C127S MJ1459	Fwd	5'-GTTATGCTTCCTTCCAGTGTTCCAGCTACAAAC-3'
	Rev	5'-GTTTGTAGCTGGAACACTGGAAGGAAGCATAAC-3’
MJ1655	Fwd	5’-CATGCATATGTTATTAGAAGAAACATTAAA-3’
	Rev	5’- GATCGGATCCTAAAATAACAACCTTTCC-3’

Table S2. Purification of recombinant C127A Ade from *M. jannaschii* expressed in *E. coli*

Protein	Purification Step	Protein (mg)	Specific Activity (nmol min^{-1} mg^{-1} of protein)	Total Activity (nmol min^{-1})	Fold Purification	Yield (%)
C127Aa	Crude extract	2.3	70	4.7	1	100
	60 ºC Heating	1.0	214	4.3	3.1	91
	MonoQ[b]	0.23	235	1.6	3.4	34
E. coli c	Crude extract	6.9	10	2.1	1	100
	60 ºC Heating	1.6	24	0.75	2.4	36
	MonoQ	0.2	31	0.18	3.1	9

[a] C127A Ade
[b] Anion exchange chromatography by MonoQ with fraction at 0.39 M NaCl
[c] *E. coli* control cells were an *E. coli* cells overexpressing the MJ0100 gene product, which was only found in the insoluble pellet of *E. coli* and does not contain the C127A Ade.

Table S3. Percentage of number of frames during the last 50 ns of simulation that differ by no more than 0.2 nm RMSD from the central structure.

	WT	C127S	C127A
Replicate 1	91.6	89.7	24.2
Replicate 2	80.0	49.1	57.3
Replicate 3	45.8	42.2	56.6

Table S4. Influence of D261 in the active site as observed in MD simulations. Minimum distance (nm) of closest heavy atoms between D261 and C127/S127 and Asp261 and Mn^{2+} ions (α, β, and γ).

	WT	C127S	C127A
D261-C/A/S127	1.6 ± 0.1	1.4 ± 0.1	1.1 ± 0.1
D261-D260	0.38 ± 0.03	0.29 ± 0.03	0.3 ± 0.05
D261-α-Mn(II)	0.49 ± 0.04	0.50 ± 0.01	0.4 ± 0.1
D261-β-Mn(II)	0.61 ± 0.02	0.3 ± 0.1	0.3 ± 0.1
D261-γ-Mn(II)	1.00 ± 0.06	1.00 ± 0.03	0.9 ± 0.1

[a]Averages are shown over the last 50 ns of simulation time, with corresponding standard deviations.

Figures

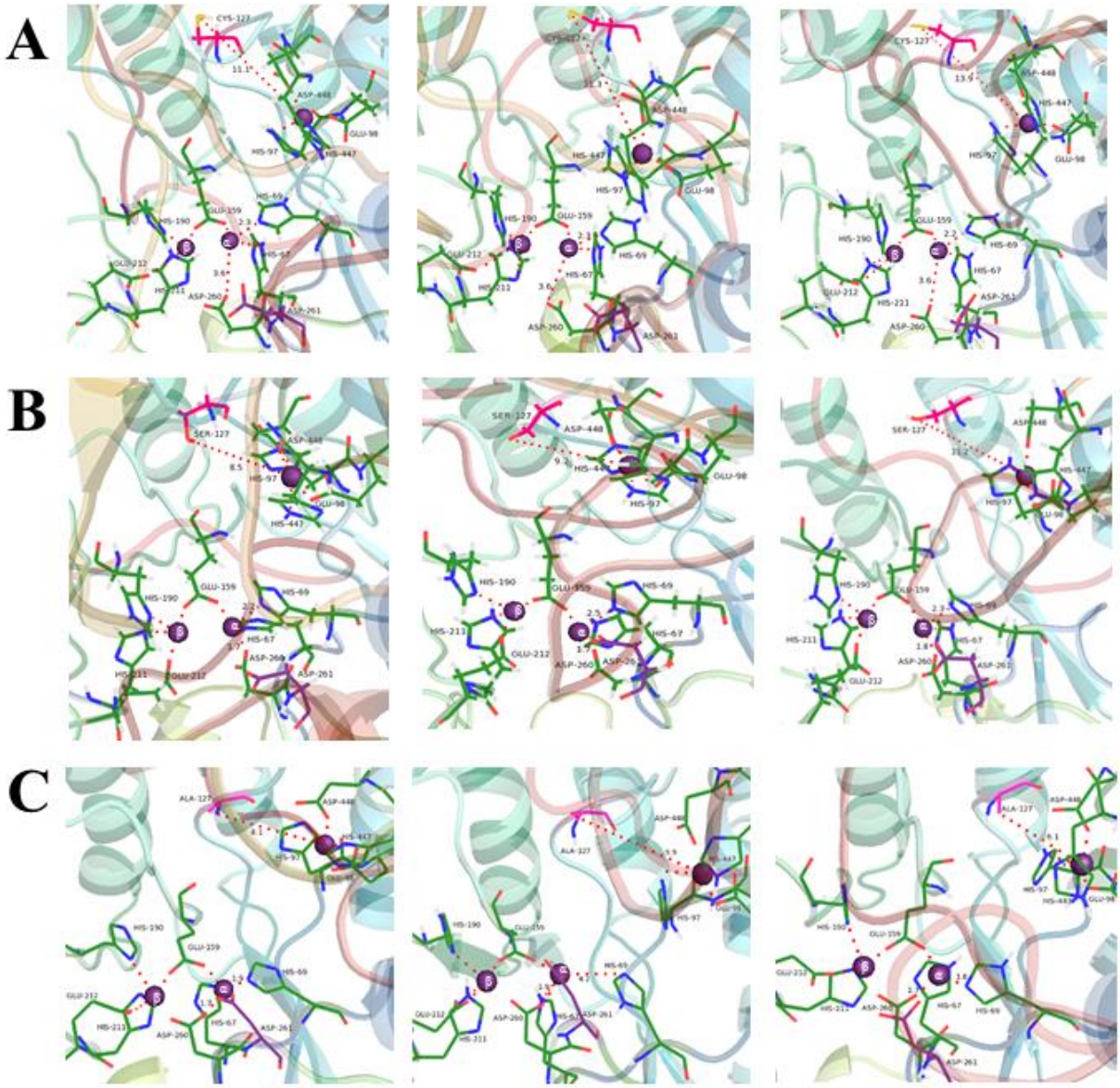

Figure S1. Comparison of three replicates each of Wt (A), C127S (B), and C127A (C). Ade from molecular dynamics simulations highlighting the active site of each replicate. Dominant structures from RMSD clustering, with the central structure of the first cluster, are shown. Metal ions are shown as purple spheres. Metal binding residues are shown with green carbon atoms, Cys, Ser, or Ala 127 is shown with pink, and D261 is shown with purple. Measured distances are shown with a red dotted line with the measured distance in Å between the heavy atoms. All nitrogen atoms are shown as blue, oxygen atoms as red, and sulfur atoms as yellow.

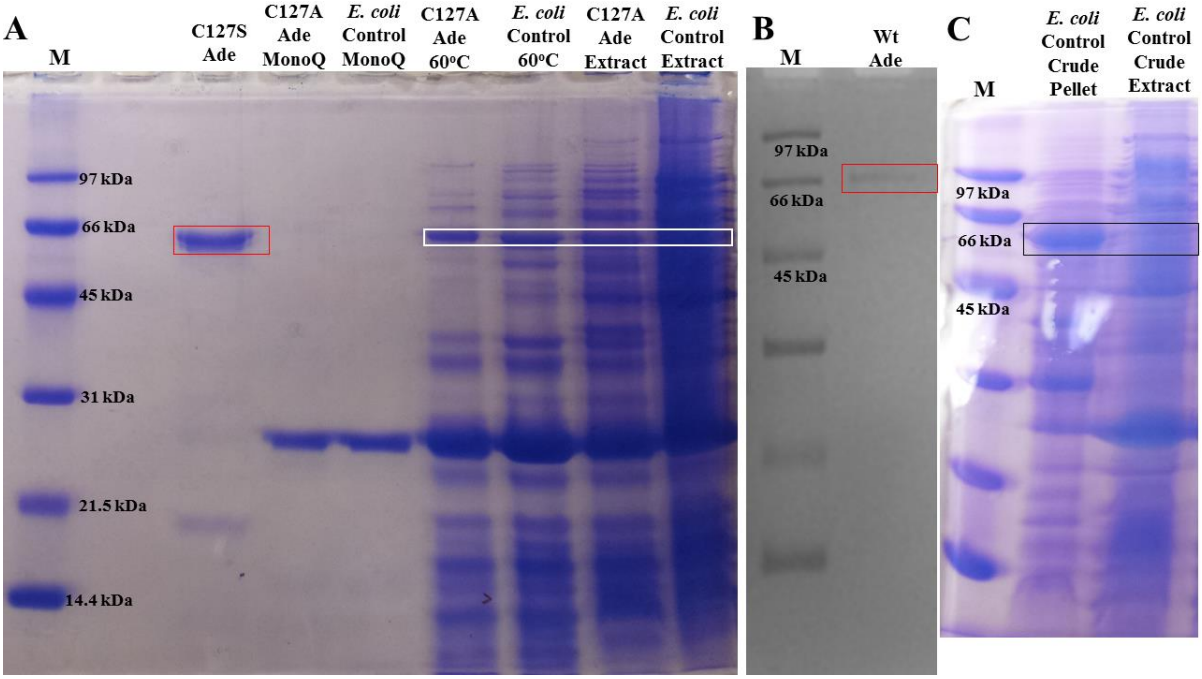

Figure S2. Picture of SDS-PAGE analysis of Wt, C127S, C127A Ade, and *E. coli* control. A) The red box indicates identified purified C127S Ade, the white box indicates where C127A Ade should be, but sequencing data of the excised bands found no Ade. The bands are labeled left to right as: M - marker, C127S Ade - purified fraction, C127A Ade MonoQ - purified fraction, *E. coli* control MonoQ - same purified fraction as C127A Ade, C127A Ade 60 °C - C127A Ade crude extract heated at 60 °C for 20 min, *E. coli* control 60 °C - *E. coli* control crude extract heated at 60 °C for 20 min, C127A Ade extract - crude extract of C127A Ade following recombinant overexpression in *E. coli*, and *E. coli* control extract - *E. coli* control crude extract following recombinant overexpression of MJ0100 gene product. B) Purified Wt Ade in the purified fraction indicated by red box. C) *E. coli* control cell extract pellet and soluble fractions overexpression MJ0100. The black box indicates where the MJ0100 gene product was identified by MALDI-MS sequencing to be in the pellet but not soluble extract.

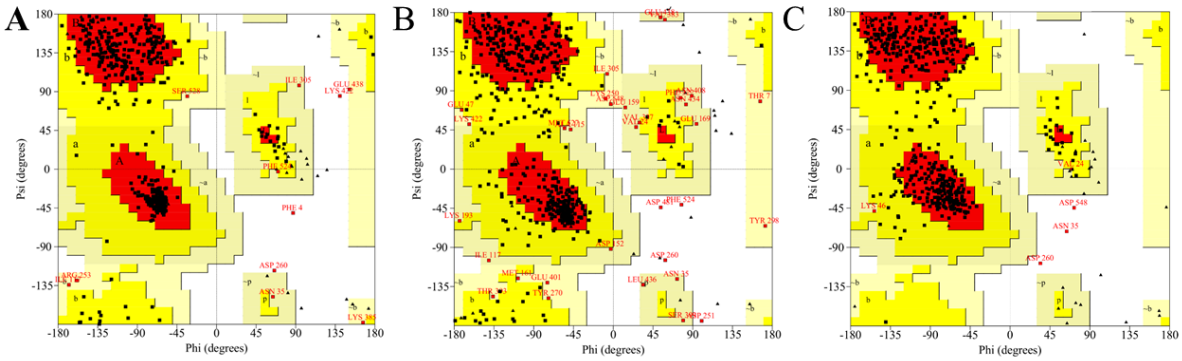

Figure S3. Ramachandran plots of Wt Ade (A), C127S Ade (B), and C127A (C) homology models.

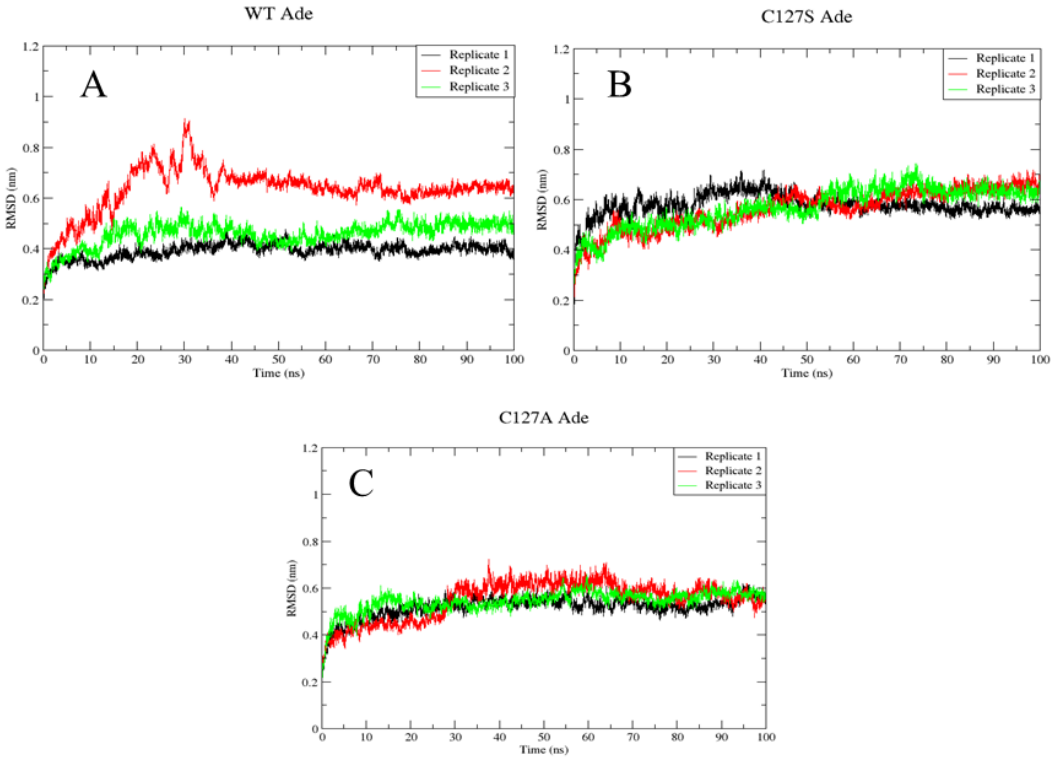

Figure S4. Cα-RMSD of Wt (A), C127S (B), and C127A (C) Ade as a function of time. Replicates are shown in black (1), red (2), and green lines (3).

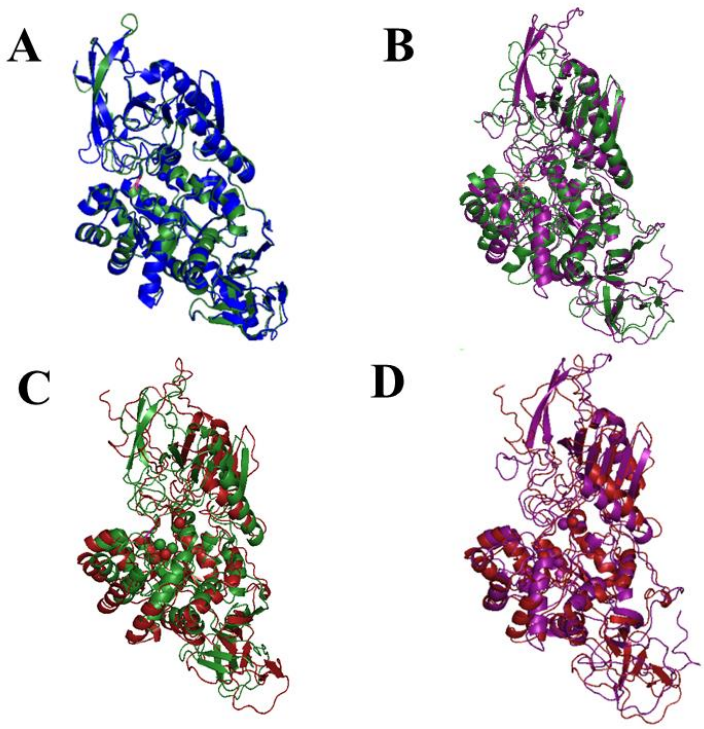

Figure S5. Overlay of Wt Ade with PDB 3NQB (A), with C127S Ade (B), with C127A (C), and overlay of C127S Ade with C127A Ade (D). Wt Ade is shown as green in (A), (B), and (C). PDB 3NQB is blue (A), C127S is purple in (B) and (D), and C127A is maroon in (C) and (D). The conserved cysteine is shown as stick (pink) to give relative position in the overall structure.

Conclusions

Due to the prevalence of S-adenosyl-L-methionine (SAM) dependent enzymes in *Methanocaldococcus jannaschii* the pathways involved in recycling the ribose and nucleobase moieties of SAM were investigated. The results of this work demonstrate that the canonical pathways are modified and additional unique pathways exist in the autotrophic methanogenic organism *M. jannaschii* for the recycling of SAM. SAM recycling pathways are essential to prevent feedback inhibition of SAM dependent enzymes, many of which have essential functions.(1, 2) The three major metabolites to arise from SAM dependent enzymes are *S*-adenosylhomocysteine (SAH), and methylthioadenosine (MTA), and 5'-deoxyadenosine (5'-dA) (Figure 1).

The first metabolite that was investigated was SAH. Since the 5'-deoxyadenosine deaminase (DadD) is able to deaminate SAH to *S*-inosylhomocysteine (SIH)(3), it was postulated that the annotated SAH hydrolase would utilize SIH instead of SAH.(4) In the canonical pathway, SAH is hydrolyzed to homocysteine and adenosine (Figure 2A) and homocysteine is methylated to methionine via a methionine synthase.(5–7) The results demonstrated that the annotated SAH hydrolase was indeed specific for SIH (Table 1) over SAH and had no activity with SAH.(4) These results prompted the renaming of the enzyme as an *S*-inosylhomocysteine hydrolase (SIHH) and this is the first report of an enzyme using SIH as a substrate.(4) Additionally, the results show that the SAH is recycled by a modified route where first SAH is deaminated to SIH followed by hydrolysis to homocysteine and inosine (Figure 2B).(4)

The SIHH was further characterized and the recombinant enzyme purified with bound NAD^+, which is required for both the hydrolysis and synthesis of SIH. These results are consistent with the mechanism of the homologous SAH hydrolase, which shares greater than 45% sequence identity with SIHH.(4) The presence of SIHH highlights that in *M. jannaschii* purine salvage in which hypoxanthine (HX), not adenine, is the central metabolite. These results were further supported by characterization of the adenine deaminase (Ade) and hypoxanthine/guanine phosphoribosyl transferase (Hpt) from *M. jannaschii*. Once adenine is deaminated by Ade to HX, HX can be condensed with 5-phospho-α-D-ribosyl-1-pyrophosphate (PRPP) to form IMP.(8) The Hpt from *M. jannaschii* was specific only for HX and guanine

(Table 2), which supports HX as the central metabolite in the salvage of purines instead of adenine (Figure 3).

The second metabolite of interest was methylthioadenosine (MTA). Like SAH, MTA is deaminated by DadD to methylthioinosine (MTI).(3) Prior to this work, only one other enzyme has been demonstrated to use MTI as a substrate, a methylthioinosine phosphorylase (MTIP) from *Pseudomonas aeruginosa*.(9) However, contrary to the *M. jannaschii* MTIP, the *P. aeruginosa* MTIP was active with MTA in addition to MTI and inosine.(9) The combined results are consistent with the two proteins belonging to the purine nucleoside phosphorylase superfamily which has been demonstrated to have a broad substrate range.(10) The *M. jannaschii* MTIP is known to use six different purine nucleosides that contain either hypoxanthine or guanine moieties (Table 3). These results along with the lack of a general purine nucleoside phosphorylase in the *M. jannaschii* proteome would suggest that MTIP is functioning as a general purine nucleoside phosphorylase in *M. jannaschii*, and plays a role in the salvage of purines (Figure 4) and of MTA to methionine (Figure 5).

The methionine salvage pathway in anaerobic organisms is still in need of further investigation. In *M. jannaschii* more than half of the known enzymes of the methionine salvage pathway are not present in the genome based on homology with the known enzymes (Figure 5, black). Recently, the anaerobic methionine salvage pathway (AnMSP) has been identified in the falcultative anaerobic bacteria *Rhodospirillum rubrum* (Figure 5, green).(11) However, the proposed pathway AnMSP in *R. rubrum* is unlikely to occur in *M. jannaschii* due to several differences. First, no homologues to the two proposed enzymes, methylthioribulose 1-phosphate (MTRu 1P) isomerase and methylthioxylulose 5-phosphate (MTXu 5P) sulfurylase, are present in *M. jannaschii* (Figure 5, green). Second, *M. jannaschii* uses the mevalonate pathway for the biosynthesis of isoprenoides(12) not the alternative route that uses 1-deoxy-D-xylulose 5-phospahte pathway (DXP). Lastly, the canonical enzymes for methionine biosynthesis are absent in *M. jannaschii* and are replaced by a single enzyme that is able to combine aspartate semialdehyde and hydrogen sulfide directly to form homocysteine.(13)

As shown in Figure 5 (red) the anaerobic methionine salvage pathway in *M. jannaschii* proceeds through a unique route, where many of the remaining steps remain unknown. Currently, three enzymes have been found to be involved. First, MTA is deaminated by DadD to MTI which is then phosphorolysized to hyoxanthine and methylthioribose 1-phosphate (MTR

1P). MTR 1P is then isomerized to methylthioribulose 1-phosphate (MTRu 1P) by a methylthioribose 1-phosphate isomerase (MTRI) (Table 4). MTRI is the only other enzyme that is annotated to be involved in the methionine salvage pathway in *M. jannaschii* in addition to MTIP. In an effort to identify other intermediates in the anaerobic methionine salvage pathway a strain of *Methanosarcina acetivorans* that is auxotrophic for either homocysteine or methionine (HcyAux)(14) was used. I hypothesized that if a proposed compound was able to restore the growth of *M. acetivorans* HcyAux, then the fed compound is converted to methionine by *M. acetivorans,* implicating the proposed compound as an intermediate of the methionine salvage pathway. This process was used to successfully identify 2-keto-4-(methylthio)butyrate (KMTB) as a possible intermediate (Figure 5, red). Unfortunately, that was the only intermediate that was able to be identified and it is unclear if KMTB is a physiological intermediate or if it is non-specifically transaminated to methionine by any of the numerous aminotransferases encoded by *M. acetivorans* or *M. jannaschii*. In order to determine if KMTB is indeed a physiological substrate of one of the ten encoded aminotransferase from *M. jannaschii* is currently under investigation. As of now five of the ten encoded aminotransferases in *M. jannaschii* have shown to be active with KMTB as a substrate with glutamate as the amino donor.

Lastly, the recycling of 5'-deoxyadenosine (5'-dA) was investigated. The work described in this dissertation are the first reports of a recycling pathway for 5'-dA. 5'-dA is proposed here to be recycled into methylglyoxal (MG) (Figure 6). I identified a specific deaminase for 5'-dA, DadD, which supports its role in preventing the feedback inhibition of SAM dependent enzymes.(3) Following deamination of 5'-dA to 5'-dI the two enzymes annotated from the methionine salvage pathway, MTIP and MTRI, were demonstrated to use 5'-dI and 5-deoxyribose 1-phosphate (5-dR 1P). MTIP and MTRI showed near equal specificity for the 5-deoxysugars compared with the methylthio-sugars (Tables 3 and 4). Next, two enzymes annotated from the pentose phosphate pathway (Figure 7, red), the ribulose 5-phosphate 3-epimerase (RPE) and transketolase (TK) were analyzed for their involvement in the recycling of 5'-dA.

The involvement of RPE and TK are proposed due to the lack of an operating pentose phosphate pathway in *M. jannaschii* and other Arachea. Instead the pentose phosphate pathway is replaced by the ribulose monophosphate pathway.(15, 16) Thus, there is no clear role for RPE and TK in *M. jannaschii*. I proposed that the two enzymes are functioning in the recycling

pathway of 5'-dA (Figure 6). Analysis of the RPE for activity with the canonical substrate, ribulose 5-phosphate, and the proposed substrate, 5-deoxyribulose 1-phosphate, demonstrated that *M. jannaschii* RPE was active with both. Unfortunately, at this time the *M. jannaschii* RPE was unable to be further characterized with 5-deoxyribulose 1-phosphate at this time due to the inability to obtain it. It would be of interest in the future to better define the activity of *M. jannaschii* RPE with ribulose 5-phospahte and with 5-deoxyribulose 1-phosphate to determine if the proposed activity is feasible in vitro.

The *M. jannaschii* TK was of further interest to study because enzyme is encoded by two genes annotated for the N- and C-terminal halves of the full length TK. Thus, the first line of investigation was to determine if the two halves were active alone, in combination by mixing the two halves in vitro, or if an active enzyme was only achieved by co-expression of the two genes in vivo. The results of this analysis demonstrated that only when the two genes are co-expressed simultaneously (*in vivo*) was an active enzyme achieved. When the enzyme was included in a coupled enzyme assay with MTIP, MTRI, and RPE with 5'-dI as the substrate, the production of lactaldehyde was confirmed. These results suggest the involvement of the *M. jannaschii* TK enzyme in the recycling pathway of 5'-dA (Figure 6). The specific activity of the *M. jannaschii* TK was determined to be 0.23 μmol min^{-1} mg^{-1} protein with 5-deoxyxylulose 1-phosphate and erythrose as substrates. Together, these results suggest RPE and TK are involved in the proposed recycling pathway for 5'-dA (Figure 6).

The final reaction proposed to be involved in recycling of 5'-dA (Figure 6) is an enzyme able to oxidize lactaldehyde to MG. Previous analysis of *M. jannaschii* cell extracts showed that the reduction of MG to lactaldehyde does occurs and is likely F_{420} dependent via an unknown enzyme(17) MG is a well-known to be a toxic metabolite and there are established enzymes that have been demonstrated to be responsible for the metabolism of MG.(18) However, MG has been demonstrated to be a required for the biosynthesis of 6-deoxy-5-ketofructose 1-phosphate (Figure 6) in *M. jannaschii*.(19) Bioinformatic searches were unable to identify potential enzymes that would produce MG from lactaldehyde. In order to identify the enzyme, it was purified based on enzymatic activity from *M. jannaschii* cell extracts using NADPH as the reductant. *M. jannaschii* cell extracts showed that MG could be reduced to lactaldehyde with NADPH, but to a lesser extent than $F_{420}H_2$.(17) Using this approach a single enzyme was identified: N^5, N^{10}-methylenetetrahydromethanopterin reductase (Mer). Mer was recombinantly

overexpressed and purified from *Escherichia coli* and analyzed for activity. The results demonstrate that Mer was able to successfully reduce methylglyoxal to lactaldehyde with NADPH as the reductant. Mer is an F_{420} dependent enzyme that is well known to be involved in methanogensis.(20–22) Unfortunately, due to the instability of the recombinant Mer, a more detailed analysis of the promiscuous activity was not able to be fully elucidated at this time.

In conclusion, this dissertation describes the elucidation of several unique pathways that are involved in the recycling of SAM. In each of these pathways there is an intersection of recycling pathways involving nucleobase, hypoxanthine, which is released by phosphorolysis of the 5'-dI, MTI, and inosine. Hypoxanthine is then incorporated into IMP by combination with PRPP (Figure 4). Furthermore, I have demonstrated that the canonical methionine salvage pathways proceeds through modified routes (Figures 2 and 5). Lastly, I have proposed a novel route for recycling 5'-dA into methylglyoxal for aromatic amino acid biosynthesis (Figure 6). Ultimately, this work helps shed light on how an organism, such as *M. jannaschii*, can maintain a small proteome, (~1800 encoded proteins), but sustain many diverse pathways. The enzymes described here have been demonstrated to utilize multiple substrates and are involved in numerous pathways. Through the identification of the pathways and enzymes involved in the unique pathways occurring in the methanogens, we will gain insight into the biochemical reactions that were occurring when life originated.

References

1. **Fontecave M**, **Atta M**, **Mulliez E**. 2004. S-adenosylmethionine: Nothing goes to waste. Trends Biochem Sci **29**:243–249.
2. **Challand MR**, **Ziegert T**, **Douglas P**, **Douglas P**, **Wood RJ**, **Kriek M**, **Shaw NM**, **Roach PL**. 2009. Product inhibition in the radical S-adenosylmethionine family. FEBS Lett **583**:1358–1362.
3. **Miller D**, **O'Brien K**, **Xu H**, **White RH**. 2014. Identification of a 5′-Deoxyadenosine Deaminase in Methanocaldococcus jannaschii and its Possible Role in Recycling the Radical SAM Enzyme Reaction Product 5′-Deoxyadenosine. J Bacteriol **196**:1064–1072.
4. **Miller D V**, **Xu H**, **White RH**. 2015. S-Inosylhomocysteine Hydrolase: A novel enzyme involved in SAM recycling. J Bacteriol **197**:1-8 JB – 00080.
5. **Weissbach H**, **Peterkofsky A**, **Redfield BG**, **Dickerman H**. 1963. Studies on the Terminal Reaction in the Biosynthesis of Methionine. J Biol Chem **238**:3318–3324.
6. **Rosenthal S**, **Smith LC**, **Buchanan JM**. 1965. Enzymatic Synthesis of the Methyl Group of Methionine. J Biol Chem **240**:836–843.
7. **Schroder I**, **Thauer RK**. 1999. Methylcobalamin:homocysteine methyltransferase from Methanobacterium thermoautotrophicum. Eur J Biochem **263**:789–796.
8. **Miller D V**, **Brown AM**, **Xu H**, **Bevan DR**, **White RH**. 2016. Purine salvage in Methanocaldococcus jannaschii: Elucidating the role of a conserved cysteine in adenine deaminase. Proteins Struct Funct Bioinforma **84**:828–840.
9. **Guan R**, **Ho M-C**, **Almo SC**, **Schramm VL**. 2011. Methylthioinosine Phosphorylase from Pseudomonas aeruginosa. Structure and Annotation of a Novel Enzyme in Quorum Sensing. Biochemistry **50**:1247–1254.
10. **Erion MD**, **Takabayashi K**, **Smith HB**, **Kessi J**, **Wagner S**, **Honger S**, **Shames SL**, **Ealick SE**. 1997. Purine Nucleoside Phosphoylase 1. Structure- Function Studies. Biochemistry **36**:11725–11734.
11. **North JA**, **Sriram J**, **Chourey K**, **Ecker CD**, **Sharma R**, **Wildenthal JA**, **Hettich RL**, **Tabita FR**. 2016. Metabolic Regulation as a Consequence of Anaerobic 5-Methylthioadenosine Recycling in Rhodospirillum rubrum. MBio **7**:e00855-16.
12. **Grochowski LL**, **Xu H**, **White RH**. 2006. Methanocaldococcus jannaschii uses a modified mevalonate pathway for biosynthesis of isopentenyl diphosphate. J Bacteriol

188:3192–3198.

13. **Allen KD**, **Miller DV**, **Rauch BJ**, **Perona JJ**, **White RH**. 2015. Homocysteine is biosynthesized from aspartate semialdehyde and hydrogen sulfide in methanogenic archaea. Biochemistry **54**:3129–3132.
14. **Rauch BJ**, **Gustafson A**, **Perona JJ**. 2014. Novel proteins for homocysteine biosynthesis in anaerobic microorganisms. Mol Microbiol2014/10/16. **94**:1330–1342.
15. **Orita I**, **Sato T**, **Yurimoto H**, **Kato N**, **Atomi H**, **Imanaka T**, **Sakai Y**. 2006. The Ribulose Monophosphate Pathway Substitutes for the Missing Pentose Phosphate Pathway in the Archaeon Thermococcus kodakaraensis. J Bacteriol **188**:4698–4704.
16. **Grochowski LL**, **Xu H**, **White RH**. 2005. Ribose-5-phosphate biosynthesis in Methanocaldococcus jannaschii occurs in the absence of a pentose-phosphate pathway. J Bacteriol **187**:7382–7389.
17. **White RH**. 2008. Biochemical Origins of Lactaldehyde and Hydroxyacetone in Methanocaldococcus jannaschii. Biochemistry **47**:5037–5046.
18. **Thornalley PJ**. 1996. Pharmacology of methyglyoxal: formation, modification of proteins and nucleic acids, and enzymatic detoxification--a role in pathogenesis and antiproliferative chemotherapy. Gen Pharmacol **27**:565–573.
19. **White RH**, **Xu H**. 2006. Methylglyoxal is an intermediate in the biosynthesis of 6-deoxy-5-ketofructose-1-phosphate: A precursor for aromatic amino acid biosynthesis in Methanocaldococcus jannaschii. Biochemistry **45**:12366–12379.
20. **MA K**, **THAUER RK**. 1990. Purification and properties of N5, N10-methylenetetrahydromethanopterin reductase from Methanobacterium thermoautotrophicum (strain Marburg). Eur J Biochem **191**:187–193.
21. **Kunow J**, **Schworer B**, **Setzke E**, **Thauer RK**. 1993. Si-face stereospecificity at C5 of coenzyme F420 for F420-dependent N5, N10-methylenetetrahydromethanopterin dehydrogenase, F420-dependent N5, N10-methylenetetrahydromethanopterin reductase and F420H2: dimethylnaphthoquinone oxidoreductase. Eur J Biochem **214**:641–646.
22. **Ma K**, **Thauer RK**. 1990. N5, N10-Methylenetetrahydromethanopterin reductase from Methanosarcina barkeri. FEMS Microbiol Lett **70**:119–124.

Tables

Table 1. Kinetic Parameters of SIHH

Substrate	K_M ± SD (mM)	k_{cat} ± SD (s^{-1})	k_{cat}/K_M ($s^{-1}M^{-1}$)
Inosine[a]	0.64 ± 0.4	0.83 ± 0.21	1.3×10^3
Hcy[a]	5.4×10^{-3} ± 0.006		1.52×10^5
SIH[b]	0.22 ± 0.11	0.42 ± 0.06	1.9×10^3

[a]this was determined without the addition of NAD^+ in the assay
[b]this was determined in the presence of excess NAD^+

Table 2. Kinetic Parameters of Hpt.

Substrate	K_M ± SD (mM)	k_{cat} ± SD (s^{-1})	k_{cat}/K_M ($s^{-1}M^{-1}$)
Adenine[a]	nd[c]		
Hypoxanthine[a]	0.11 ± 0.07	3.6×10^3	3.2×10^7
Guanine[a]	0.28 ± 0.07	8.5×10^3	3.0×10^7
PRPP[b]	2.2 ± 0.9	1.8×10^4	8.1×10^6

[a]Determined with PRPP in excess (0.5 mM)
[b]Determined with guanine in excess (0.4 mM)
[c]No detectable activity was observed from 0.1 to 0.4 mM adenine

Table 3. Apparent kinetic parameters of MTIP at 37 °C

Substrate	K_M ± SD (mM)	k_{cat} ± SD (s^{-1})	k_{cat}/K_M ($s^{-1}M^{-1}$)
MTI	0.13 ± 0.08	1.5 ± 0.12	1.2×10^4
5'-dI	0.86 ± 0.17	6.6 ± 0.61	7.6×10^3
inosine	0.93 ± 0.75	1.30 ± 0.72	1.4×10^3
2'-deoxyinosine	0.86 ± 0.09	4.2 ± 0.8	4.9×10^3
guanosine	0.61 ± 0.50	0.92 ± 0.38	1.5×10^3
2'-deoxyguanosine	15 ± 5	64 ± 22	4.3×10^3
MTA	N.d[a]		
5'-dA	N.d[a]		
adenosine	N.d[a]		

[a]No detectable activity with 0.2 mM MTA, 5'-dA, or adenosine

Table 4. Apparent kinetic parameters of MTRI at 60 °C

Substrate	K_M ± SD (mM)	k_{cat} ± SD (s^{-1})	k_{cat}/K_M ($s^{-1}M^{-1}$)
MTR 1P[a]	0.53 ± 0.11	0.14 ± 0.021	2.5×10^2
5-dR 1P[a]	0.41 ± 0.09	0.067 ± 0.0037	1.7×10^2
5-dR[b]	1.6 ± 0.8	0.0043 ± 0.0013	2.6
Ribose 5P[b]	N.d.c		

[a]Coupled assay through MTIP
[b]Substrate added directly to MTIR
[c]No detectable activity with 0.2 mM ribose 5P and 5 µg MTRI

Figures

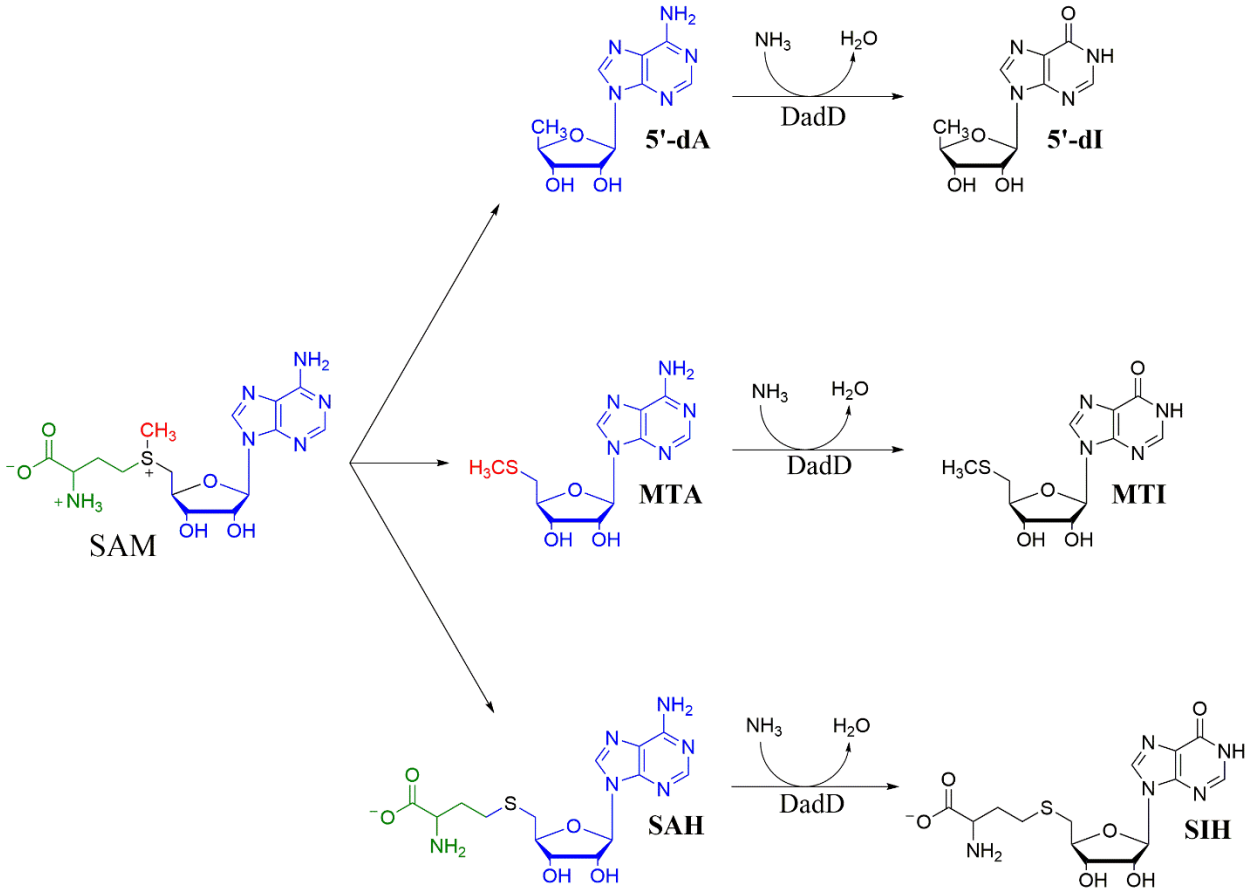

Figure 1. First step in the salvage of SAM via DadD.

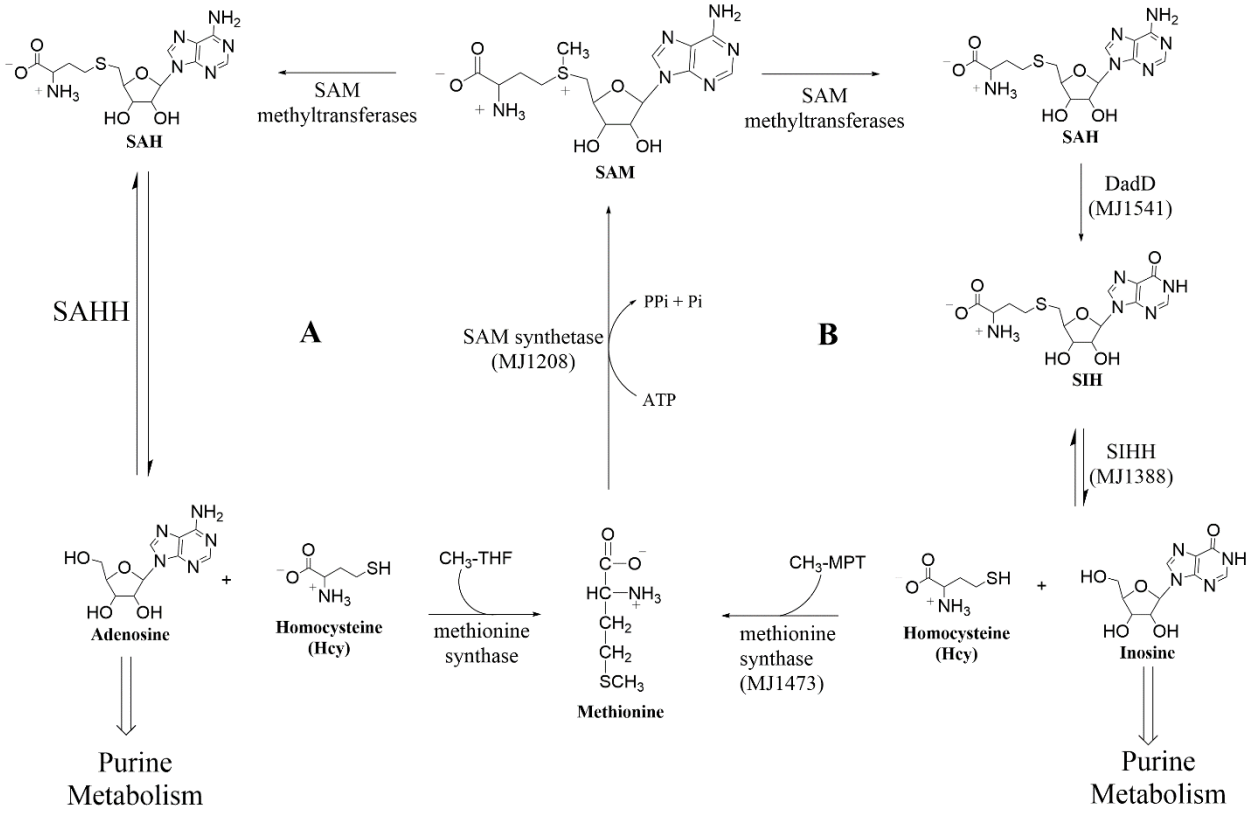

Figure 2. Canonical (A) versus methanogenic (B) pathways for the recycling of SAH to SAM.

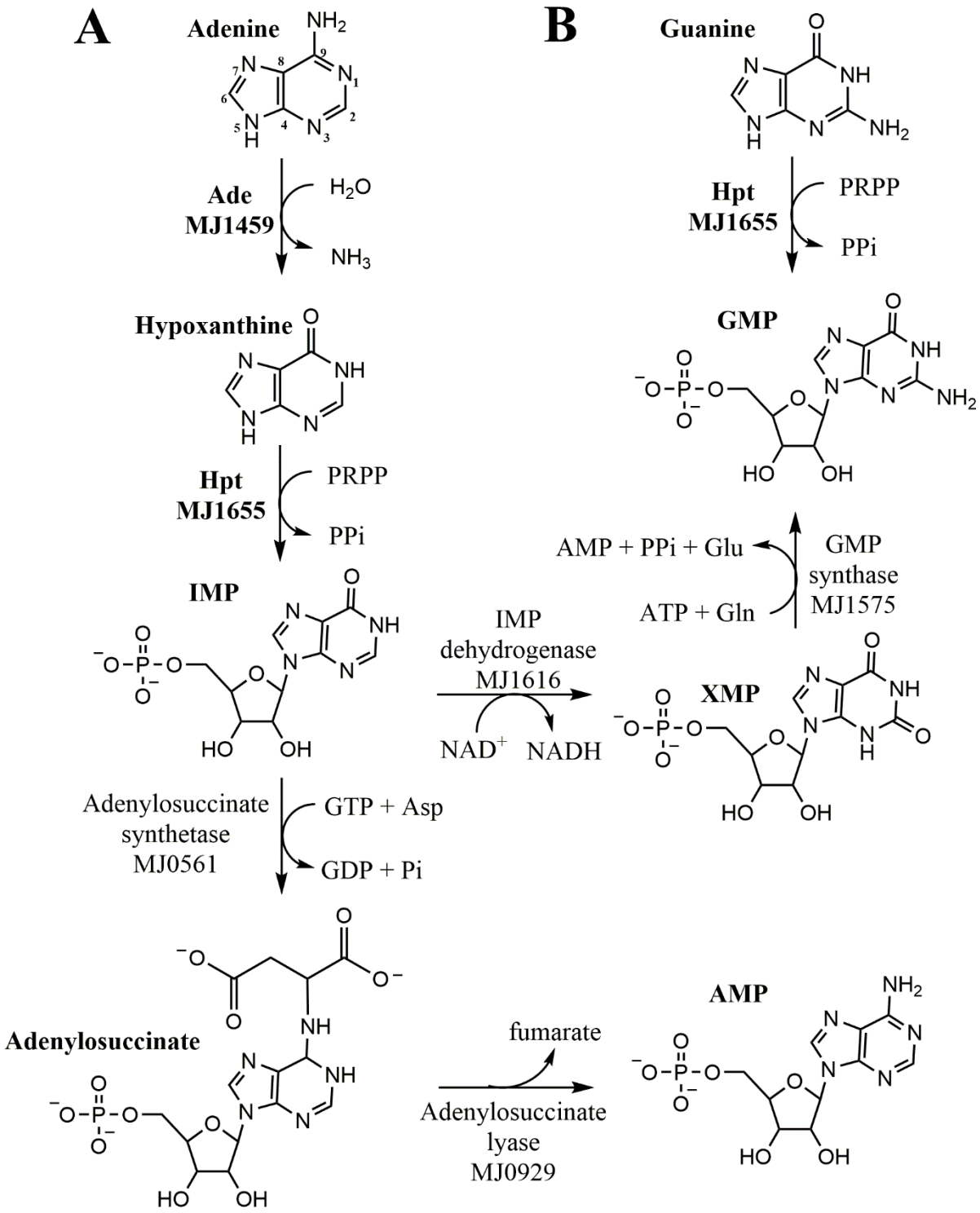

Figure 3. Purine Salvage in *M. jannaschii* from adenine (A) and guanine (B).

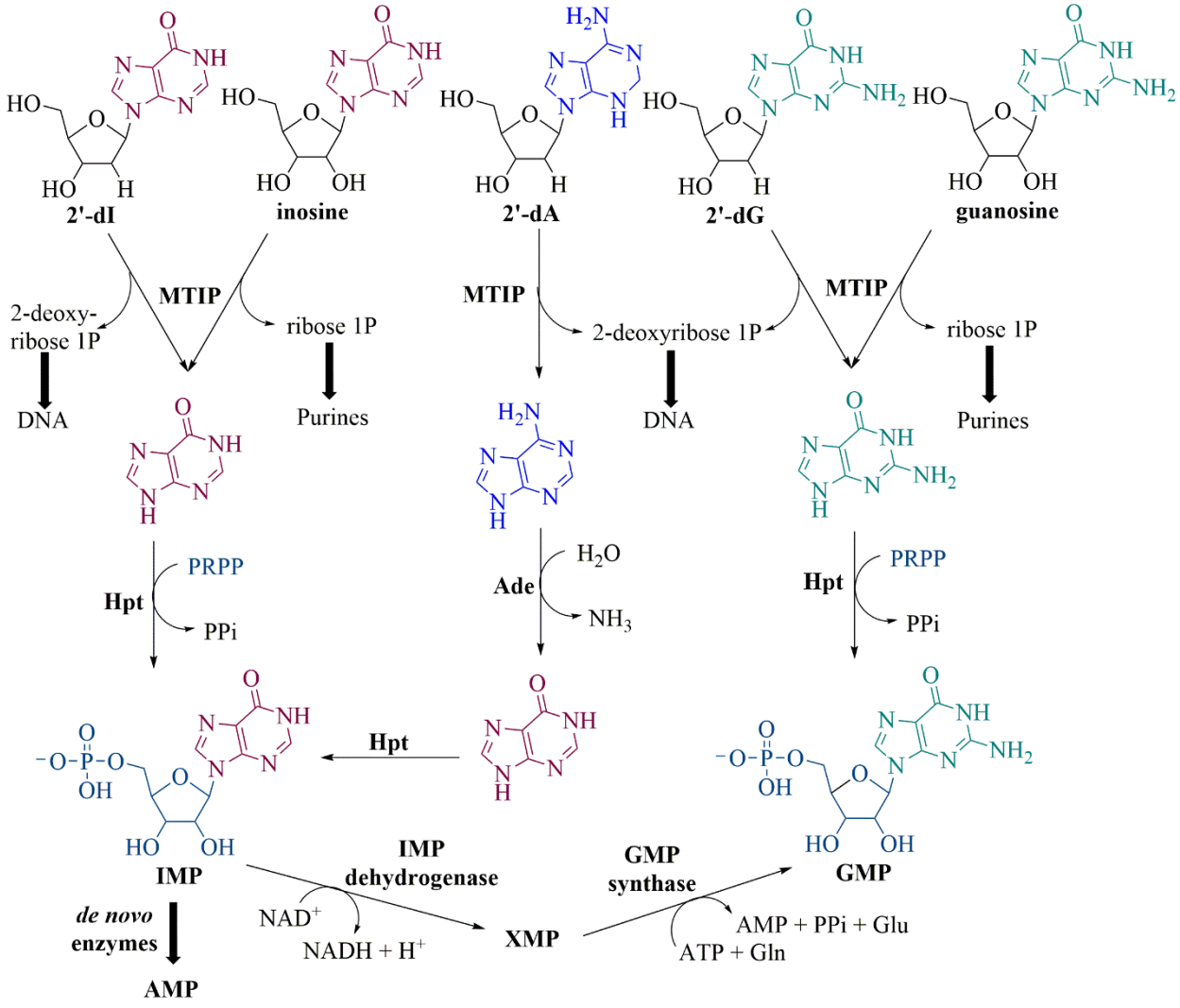

Figure 4. Interconversion of purines in *M. jannaschii*

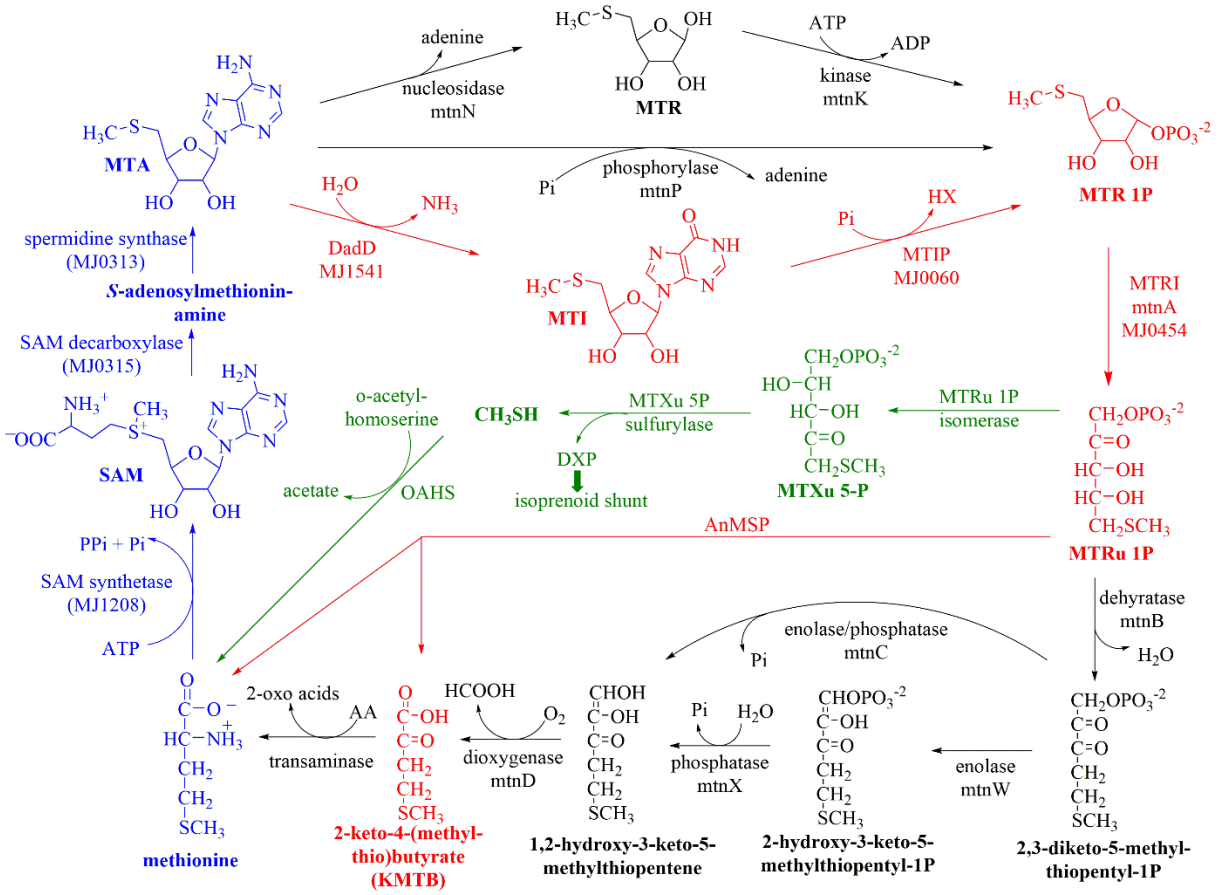

Figure 5. Different methionine salvage pathways. Highlighted in blue are the known intermediates shared in the canonical and proposed AnMSP, red is the AnMSP proposed in methanogens, green is the bacterial AnMSP, and shown in black are the intermediates and enzymes missing from the canonical pathway in anaerobic organisms.

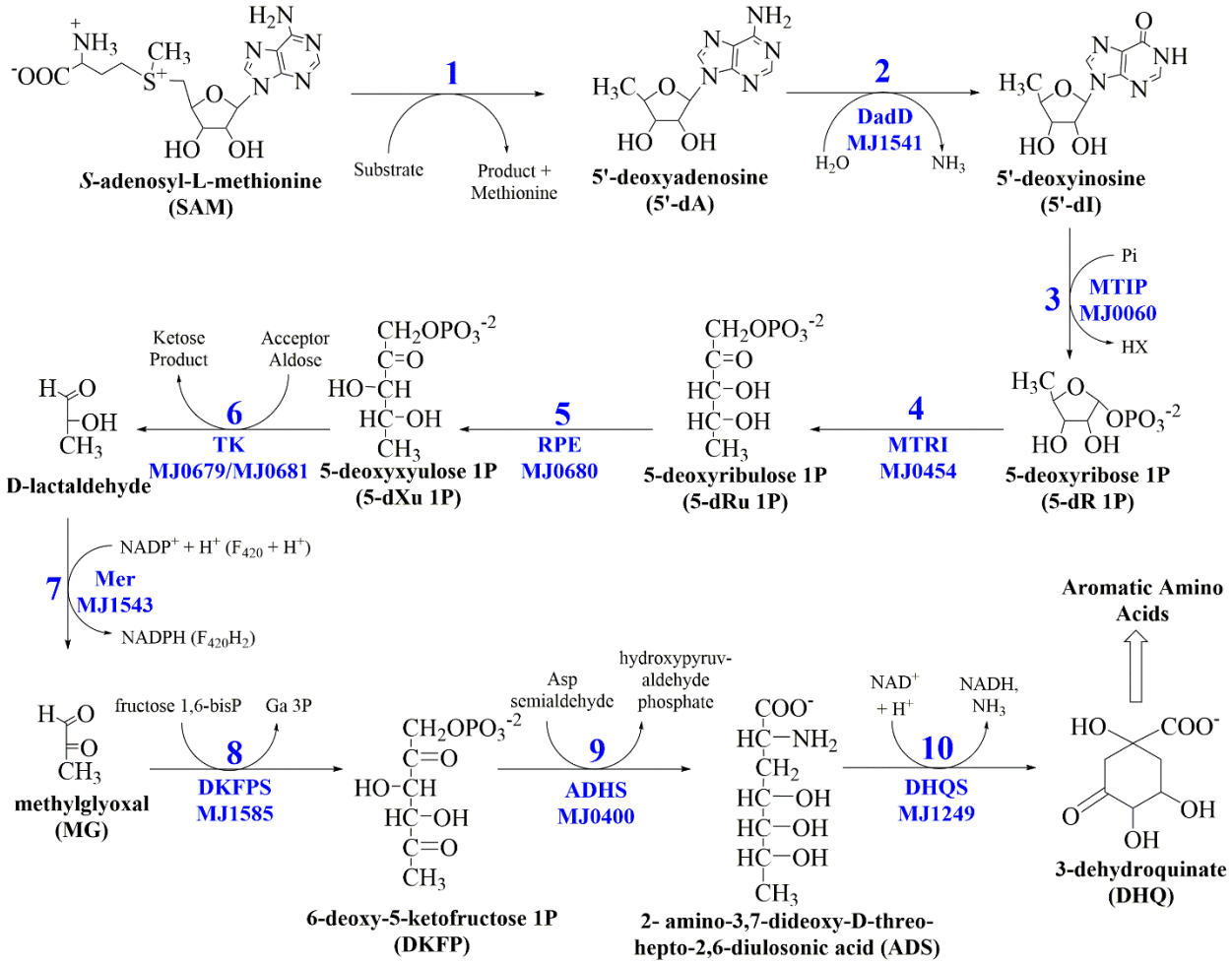

Figure 6. Complete biosynthetic route proposed for DHQ from SAM.

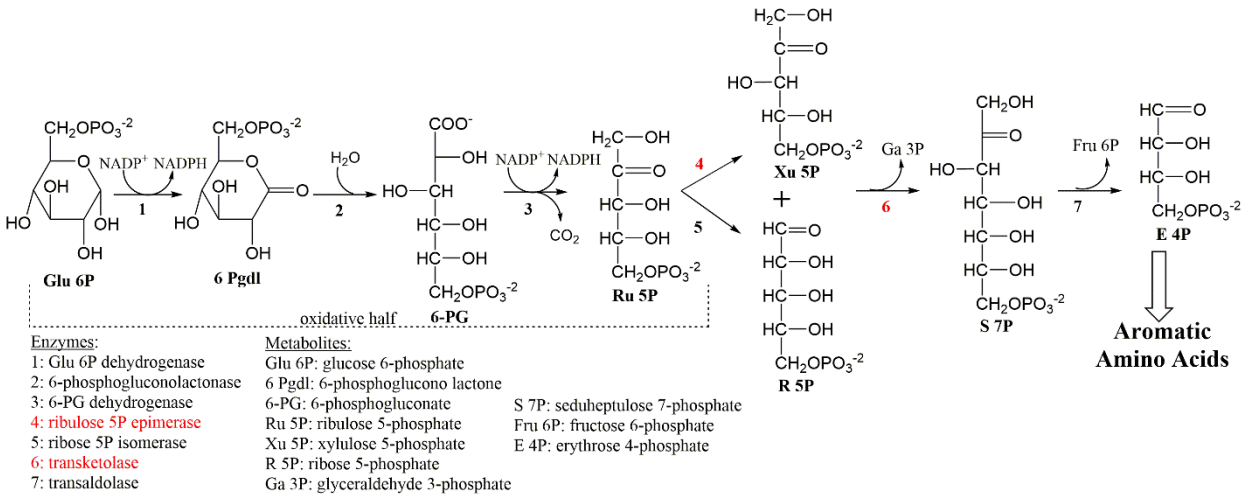

Figure 7. Pentose phosphate pathway

Appendices

Appendix A

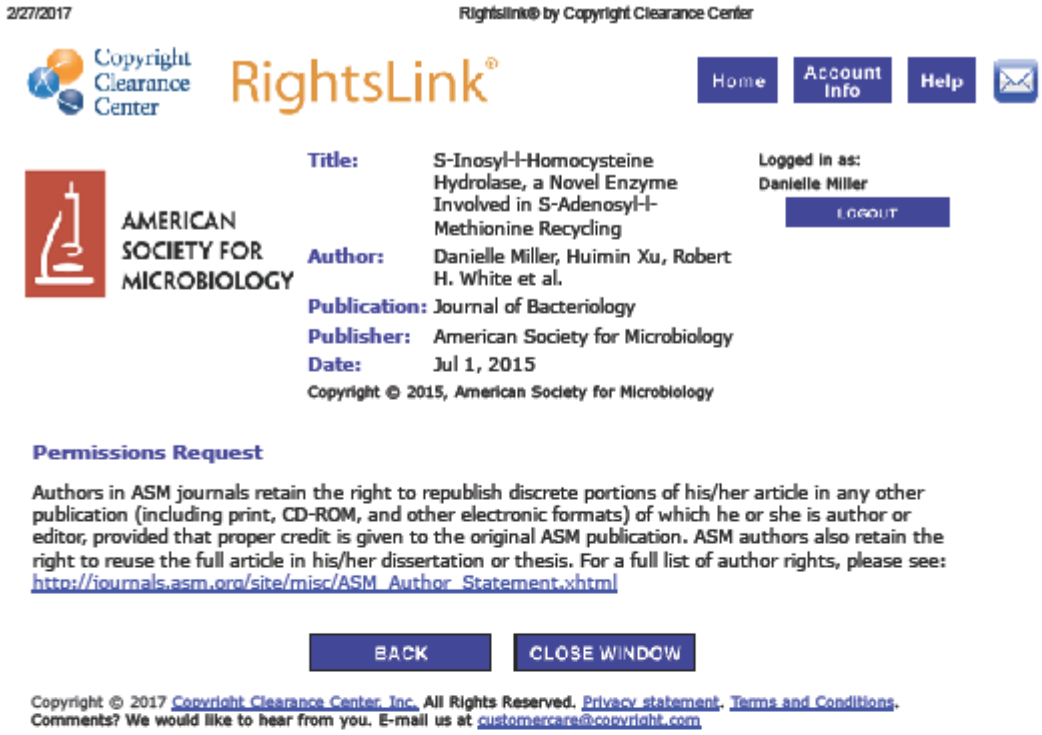

2/27/2017 RightsLink® by Copyright Clearance Center

Copyright Clearance Center RightsLink®

Home | Account Info | Help

AMERICAN SOCIETY FOR MICROBIOLOGY

Title: S-Inosyl-l-Homocysteine Hydrolase, a Novel Enzyme Involved in S-Adenosyl-l-Methionine Recycling

Author: Danielle Miller, Huimin Xu, Robert H. White et al.

Publication: Journal of Bacteriology

Publisher: American Society for Microbiology

Date: Jul 1, 2015

Copyright © 2015, American Society for Microbiology

Logged in as: Danielle Miller

LOGOUT

Permissions Request

Authors in ASM journals retain the right to republish discrete portions of his/her article in any other publication (including print, CD-ROM, and other electronic formats) of which he or she is author or editor, provided that proper credit is given to the original ASM publication. ASM authors also retain the right to reuse the full article in his/her dissertation or thesis. For a full list of author rights, please see: http://journals.asm.org/site/misc/ASM_Author_Statement.xhtml

BACK | CLOSE WINDOW

Copyright © 2017 Copyright Clearance Center, Inc. All Rights Reserved. Privacy statement. Terms and Conditions.
Comments? We would like to hear from you. E-mail us at customercare@copyright.com

https://s100.copyright.com/AppDispatchServlet#formTop 1/1

Appendix B

JOHN WILEY AND SONS LICENSE TERMS AND CONDITIONS

Feb 27, 2017

This Agreement between Danielle V Miller ("You") and John Wiley and Sons ("John Wiley and Sons") consists of your license details and the terms and conditions provided by John Wiley and Sons and Copyright Clearance Center.

License Number	4057111042792
License date	Feb 27, 2017
Licensed Content Publisher	John Wiley and Sons
Licensed Content Publication	Proteins: Structure, Function and Bioinformatics
Licensed Content Title	Purine salvage in Methanocaldococcus jannaschii: Elucidating the role of a conserved cysteine in adenine deaminase
Licensed Content Author	Danielle V. Miller,Anne M. Brown,Huimin Xu,David R. Bevan,Robert H. White
Licensed Content Date	Apr 1, 2016
Licensed Content Pages	13
Type of use	Dissertation/Thesis
Requestor type	Author of this Wiley article
Format	Electronic
Portion	Full article
Will you be translating?	No
Order reference number	02272017
Title of your thesis / dissertation	Methanocaldococcus jannaschii and the Recycling of S-adenosyl-L-methionine
Expected completion date	Mar 2017
Expected size (number of pages)	300
Requestor Location	Danielle V Miller 101 Engel Hall BLACKSBURG, VA 24061 United States Attn: Danielle V Miller
Publisher Tax ID	EU826007151
Billing Type	Invoice
Billing Address	Danielle V Miller 101 Engel Hall BLACKSBURG, VA 24061 United States Attn: Danielle V Miller
Total	0.00 USD
Terms and Conditions	